Natural Product Chemical Probe Discovery against Parkinson's Disease

Dongdong Wang

B. Sc., M. Sc.

School of Natural Sciences

Griffith Sciences

Griffith University

Submitted in fulfillment of the requirements of the degree of

Doctor of Philosophy

February 2016

In loving memory of my parents

Zhenqiang Wang and Yushuang Feng

为了不能忘却的回忆

谨以此论文深切缅怀我含辛茹苦的父母

Abstract

Parkinson's disease (PD) is the second most common neurodegenerative disease, affecting over five million patients worldwide. Like Alzheimer's disease (AD), it mostly affects the elderly and causes considerable disability and suffering. Unfortunately, the molecular mechanism of PD is still poorly understood, and there are no drugs available to treat the disease. Our overall aim was to identify natural products to probe PD by phenotypic assay using human olfactory neurosphere-derived (hONS) cells from PD patients. The research presented in this thesis exemplifies the importance of natural products as chemical probes for further investigation of PD as well as lead compounds for future PD-drug development.

The thesis begins with an introduction of PD and the chemotherapeutics for PD. It also covers a review on the natural origin anti-PD compounds and the analysis of their physicochemical properties using Lipinski's rule of five. As part of a research program aiming to identify anti-PD chemical probes, a high throughput screening assay was developed to screen 4224 fractions. Twenty fractions were confirmed to display neuroprotective effects of the PD cells against rotenone. Seven prioritized fractions, representing one Australian marine sponge *Jaspis splendens* (subject 1) and two Australian terrestrial plants *Gloriosa superba* (subject 2) and *Alangium villosum* (subject 3), were selected for large scale extraction and isolation. The results were presented in Chapter 2 to 5.

Chapter 2 describes the chemical and biological investigation of Australian marine sponge *Jaspis splendens*. Chemical investigation of 50 grams of biota sample resulted in the

isolation of three series and total of 22 compounds, of which three were new to science. The structures of the three new compounds were unambiguously elucidated on the basis of NMR and mass spectroscopic data. Phenotypic responses of the metabolites in hONS cell model of Parkinson's disease suggested that jaspamycin had significant effects on the cytological parameters associated with mitochondria, α-tubulin, LC3b and endosomes and could be used as a chemical probe to investigate the molecular mechanism underlying PD.

Chapter 3 describes the isolation of 39 compounds from 20 grams of an Australian plant *Gloriosa superba* L., and their cytological profiles against hONS cells. The 39 compounds, of which 7 were new, represented five structural classes: colchicines, lumicolchicines, nucleosides, phenolic glycosides, and flavones. The structures of the seven new compounds were unambiguously elucidated on the basis of NMR and mass spectroscopic data. Their absolute configurations were determined by Circular Dichroism (CD) measurements. Colchicines and lumicolchicines exhibited different perturbation on mitochondria/LC3b and α-tubulin related parameters, which could be used as chemical probes. There may be an alternative mechanism in neurodegeneration and, further investigation underlying Parkinson's disease is warranted.

In Chapter 4, chemical investigation of 20 grams of Australian plant *Alangium villosum* resulted in the isolation of eight new natural products and 36 known metabolites, representing six classes of natural products: benzoquinolizidines, tetrahydroisoquinoline monoterpene glycosides, iridoids, lignan glycosides, sesquiterpenoids and triterpenoids. The structures of the eight new compounds were unambiguously elucidated on the basis of NMR and mass

spectroscopic data. Their absolute configurations were determined by CD measurements. Tubulosine and its congeners displayed phenotypic profiles with major effects on α-tubulin and EEA-1-related cytological markers in the PD patient derived hONS cells. This group of compounds were identified as anti-PD chemical probes to further investigate the mechanism of PD.

The thesis concluded with an analysis of the physicochemical properties and ChemGPS of 103 isolated natural products. The results showed that the chemical probes identified in Chapters 2-4 all had favorable physical chemical properties and located within a biological relevant chemical space. By a combined strategy using cytological profiling, Ro5 and ChemGPS analysis, we were able to identify ideal chemical probes to further investigate Parkinson's disease. The chemical probes can also be potentially used as lead compounds for future PD-drug development.

Statement of Originality

This work has not previously been submitted for a degree or diploma in any university. To the best of my knowledge and belief, the thesis contains no material previously published or written by another person except where due reference is made in the thesis itself.

(Signed)_____
Dongdong Wang

Table of Contents

List of Figures

List of Tables

List of Abbreviations

$[\alpha]_d$	specific rotation
℃	degrees Celsius
μm	micrometre
1D	one dimensional
2D	two dimensional
3D	three dimensional
AD	Alzheimer's disease
amu	atomic mass units
anti-PD	anti-Parkinson's disease
br	broad
C_{18}	octadecyl bonded silica
CD	Circular dichroism
$CDCl_3$	deuterated chloroform
CE	Cotton effect
CH_2Cl_2	dichloromethane
CNS	central nervous system
CO_2	carbon dioxide
COSY	correlation spectroscopy
CsA	cyclosporine A
d	doublet
DAP1	4',6-diamidino-2-phenylinodole
DBS	deep brain stimulation
DCM	dichloromethane
DMPK	drug metabolism and pharmacokinetics
DMSO	dimethylsulfoxide
DMSO-d_6	deuterated DMSO
EGCG	(-)-epigallocatechin-3-gallate
equiv.	equivalent(s)
Et	ethyl
FBS	foetal bovine serum
FDA	Food and Drug Administration
g	gram(s)
GBA	glucocerebrosidase
GM1	ganglioside
h	hour(s)

H_2O	water
HBA	hydrogen bond acceptor
HBD	hydrogen bond donor
HCS	high content screening
HD	Huntington's disease
HLB	hydrophilic lipophilic balanced
HMBC	heteronuclear multiple-bond correlation spectroscopy
hONS	human olfactory neurosphere-derived
HPLC	high-pressure liquid chromatography
HRESIMS	high-resolution electron spray ionisation mass spectrometry or spectrum
HSQC	heteronuclear single-quantum coherence spectroscopy
HTS	high-throughput screening
Hz	Hertz
IC_{50}	half maximal inhibitory concentration
IR	infrared
J	coupling constant
LC-MS	liquid chromatography/mass spectrometry
L-dopa	levodopa
LLE	lead like enhanced
LLEE	lead like enhanced extract
LLEF	lead like enhanced fraction
LRESIMS	low-resolution electron spray ionization mass spectrometry or spectrum
LRMS	low resolution mass spectrometry or spectrum
LRRK-2	leucine rich repeat kinase 2
m	meter
m	multiplet
m/z	mass to charge ratio
MAO-A	type A monoamine oxidase
MAO-B	type B monoamine oxidase
MAOs	monoamine oxidases
MeOH	methanol
mg	milligram
MHz	mega Hertz
min	minute(s)
mL	millilitre
MPTP	1-methyl-4-phenyl-1,2,3,6-tetrahydropyridine
MS	mass spectrometry

MW	molecular weight (g/mol)
N	normal
N_2	nitrogen
(±)-NBP	(±)-3-n-butylphalide
NCI	National Cancer Institute
NMR	nuclear magnetic resonance
NPs	natural products
OMe	methoxyl
PBS	phosphate-buffered saline
PC	principle component
PCA	principle component analysis
PD	Parkinson's disease
ppm	parts per million
PSA	polar surface area
q	quartet
QCL	Queensland compound library
Ro5	rule-of-five
ROESY	rotational nuclear Overhauser effect spectroscopy
rt	room temperature
s	singlet
SD	standard deviation
sh	shoulder
sp	species
t	triplet
TDD	target-based drug discovery
TFA	trifluroacetic acid or trifluoroacetate
TOF	time of flight
t_R	retention time
UV	ultraviolet
UV/vis	ultraviolet-visible
wt	weight
δ	chemical shift
µg	microgram
µL	microlitre

Acknowledgements

I cannot find words to express my gratitude to Professor Ronald James Quinn and Dr Yunjiang Feng who gave me the opportunity to come to Australia and undertake my PhD under their supervision. They have provided invaluable guidance to me through their knowledge of science and their personal integrity whilst supervising my PhD studies. Many thanks to them for sharing their wisdom with me, allowing me enough independence to pursue my own research interests, and putting so much of their time and energy into developing this thesis.

I would like to thank Professor George D. Mellick, Associate Professor Stephen A. Wood for their assistance in the biological part of the collaborative project, Dr Jianguo Shan for the high throughput screening and Dr Mariyam Murtaza for the high content screening. I also thank Dr Jianguo Shan and Miss Marie-Laure Vial who spent some days teaching me tissue culture.

I am particularly grateful to Associate Professor Anthony R. Carroll, Dr Sue Boyd and Dr Tanja Grkovic, who have taught me an advanced NMR spectrometry lesson during my PhD studying. The acquisition of knowledge can be such a pleasurable experience when a truly inspirational individual is guiding me. Their wisdom and the ability to share it are second to none. Many, many thanks to Tony, Sue and Tanja, you have helped more than you may realise.

I am grateful to Dr Christoph Rohmann from the University of Queensland, Miss Chao Wang and Miss Yang Yang from Eskitis Institute for sharing their knowledge and teaching me the density function theory calculation.

I am truly grateful to the staff and students with in the School of Natural Sciences for their assistance on all things technical. Especially thanks to Associate Professor Andreas Hofmann for the suggestions on CD data processing, Emeritus Professor Ian Jenkins, Dr Rebecca Pouwer, Dr Stephan Boettcher and Dr Haifeng Sun for sharing their knowledge and giving me valuable suggestions for my synthesis questions, Mr Alan White with the GC-MS spectrometry, Miss Liliana Pedro and Dr Wendy Loa-Kum-Cheung with the HRESIMS spectrometry.

I would like to acknowledge all the past and present members of Eskitis Institute with whom I have had the opportunity to work with during my PhD studies. Thank you for being such good lab members, always willing to lend a hand and provide assistance. I am truly overwhelmed by the support and friendship that has come to me. I would like to especially thank Mrs Sheila Twilley and Dr Tanja Grkovic, who grow from the scariest people to the closest friends at Eskitis Institute, for always being so helpful in my life. They are instilling me with confidence and motivation for my second language improvement, especially listening and speaking in English. Many thanks to Dr Tanja Grkovic and Dr Catherine Roullier for making me feel comfortable in a chemistry lab and for their friendship; Dr Emma Barnes and Dr Liwen Tian for always being available to talk about any problems I have; Dr Karren Beattie and Miss Rachel Treers for being so helpful and kind to me; Dr Vanida Choomuenwai and Dr Michelle da Silva Liberio for being great friends. I will not name all of you here, it seems inappropriate to make a list, but you have all made the experience of learning and living truly enjoyable.

Thanks to Dr John N. A. Hooper from Queensland Museum for the collection, taxonomic identification and photographs of the marine sponge that I studied. Thanks to Paul I. Forster from Queensland Herbarium for the collection, taxonomic identification and photographs of the two territorial materials that I studied.

A very special thank you to my family and especially my parents who encouraged me to pursue my dream of traveling overseas to further my study. It was with great sadness that I lost both my parents within 17 months of each other. I am eternally grateful to my parents who supported me through my PhD study and encouraged me through my hardest moments and gave me their wisdom and love when I could not see the light at the end of the tunnel.

I am indebted to all my friends who supported me emotionally and helped me to stay focused and motivated, especially Martin Kuehn, Riki Leef, my landlords Myles Frost and Emma Frost. They become my family in Australia. Thanks also to Mr Ronald Quinn, Mrs Yun Feng, Mr David Pass, Mrs Sheila Twilley, Mr Christoph Rohmann, Mrs Tanja Grkovic, Mrs Chunping Tang, Mrs Chongyun Cheng, Mrs Bin Fan, Mr Haifeng Sun and Mr Ben Yang who helped me a lot at the hardest time after my parents' passed away. Your love and friendship is such an important part of me. I would be lost without it. Thank you.

This thesis would not have been possible without a GUIPRS scholarship support from Griffith University.

Publications

Journal articles

Wang D, Feng Y, Murtaza M., Wood S. A., Mellick G. D., Hooper J. N., and Quinn R. J.; A Grand Challenge: Unbiased Phenotypic Function of Metabolites from Jaspis splendens against Parkinson's Disease; *J. Nat. Prod*., **2016**, *79* (2), 353-361. DOI: 10.1021/acs.jnatprod.5b00987.

Oral presentations

Wang D. 2014. Natural product drug discovery targeting Parkinson's disease. **Eskitis/Sino International Conference 2014**, Shanghai, China, (17th October 2014).

Poster presentations

Wang D, Feng Y, Murtaza M., Wood S. A., Mellick G. D., Hooper J. N., and Quinn R. J.; New *β*- and *γ*-lumicolchicosides from an Australian plant *Gloriosa superba* L.; **2014 American Society of Pharmacognosy (ASP) Annual Meeting & the 14th Annual International Conference on the Science of Botanicals (ICSB)**, Oxford, Mississippi, America (2^{nd}-6^{th} August, 2014).

Wang D, Feng Y, Murtaza M., Wood S. A., Mellick G. D., Hooper J. N., and Quinn R. J.; New *β*- and *γ*-lumicolchicosides from an Australian plant *Gloriosa superba* L.; **28th International Symposium on the Chemistry of Natural Products and the 8th International Conference on Biodiversity,** Shanghai, China (20^{th}-24^{th} October, 2014).

ALL PAPERS INCLUDED ARE CO-AUTHORED

Acknowledgement of Papers included in this Thesis

Section 9.1 of the Griffith University Code for the Responsible Conduct of Research ("Criteria for Authorship"), in accordance with Section 5 of the Australian Code for the Responsible Conduct of Research, states:

> To be named as an author, a researcher must have made a substantial scholarly contribution to the creative or scholarly work that constitutes the research output, and be able to take public responsibility for at least that part of the work they contributed. Attribution of authorship depends to some extent on the discipline and publisher policies, but in all cases, authorship must be based on substantial contributions in a combination of one or more of:
>
> - conception and design of the research project
> - analysis and interpretation of research data
> - drafting or making significant parts of the creative or scholarly work or critically revising it so as to contribute significantly to the final output.

Section 9.3 of the Griffith University Code ("Responsibilities of Researchers"), in accordance with Section 5 of the Australian Code, states:

> Researchers are expected to:
>
> - Offer authorship to all people, including research trainees, who meet the criteria for authorship listed above, but only those people.
> - accept or decline offers of authorship promptly in writing.
> - Include in the list of authors only those who have accepted authorship
> - Appoint one author to be the executive author to record authorship and manage correspondence about the work with the publisher and other interested parties.
> - Acknowledge all those who have contributed to the research, facilities or materials but who do not qualify as authors, such as research assistants, technical staff, and advisors on cultural or community knowledge. Obtain written consent to name individuals.

Included in this thesis are papers in *Chapters 2, 3 and 4* which are co-authored with other researchers. My contribution to each co-authored paper is outlined at the front of the relevant chapter. The bibliographic details (if published or accepted for publication)/status (if prepared or submitted for publication) for these papers including all authors, are:

(Where a paper(s) has been published or accepted for publication, you must also include a statement regarding the copyright status of the paper(s).

Chapter 2: Dongdong Wang,[†] Yunjiang Feng,[†] Mariyam Murtaza,[†] Stephen A. Wood,[†] George D. Mellick,[†] John N. A. Hooper[‡] and Ronald J. Quinn[†,*]

[†]Eskitis Institute for Drug Discovery, Griffith University, Brisbane, QLD 4111, Australia

[‡]Queensland Museum, South Brisbane, QLD 4101, Australia

Chapter 3: Dongdong Wang,[†] Yunjiang Feng,[†] Mariyam Murtaza,[†] Stephen A. Wood,[†] George D. Mellick,[†] Paul I. Forster[‡] and Ronald J. Quinn[†,*]

[†] Eskitis Institute for Drug Discovery, Griffith University, Brisbane, QLD 4111, Australia

[‡] Queensland Herbarium, Brisbane Botanic Gardens, Brisbane, QLD 4066, Australia

Chapter 4: Dongdong Wang,[†] Yunjiang Feng,[†] Mariyam Murtaza,[†] Stephen A. Wood,[†] George D. Mellick,[†] Paul I. Forster[‡] and Ronald J. Quinn[†,*]

[†] Eskitis Institute for Drug Discovery, Griffith University, Brisbane, QLD 4111, Australia

[‡] Queensland Herbarium, Brisbane Botanic Gardens, Brisbane, QLD 4066, Australia

Appropriate acknowledgements of those who contributed to the research but did not qualify as authors are included in each paper.

(Signed) _____ (Date)_____

Dongdong Wang

(Countersigned) _____ (Date)_____

Supervisor: Ronald J. Quinn

Chapter One. Introduction

1.1 Parkinson's disease

Parkinson's disease (PD), also known as idiopathic Parkinsonism, is a common neurodegenerative disease of the central nervous system (CNS) that can be accurately diagnosed. It was first described as an unrecognized disorder in An Essay on the Shaking Palsy in 1817 by James Parkinson.[1,2] In acknowledgement of the English apothecary's detailed description, the syndrome was proposed by Jean Martin Charcot, the father of neurology, to be called as maladie de Parkinson (Parkinson's disease).

The prevalence of PD in Australia has been estimated by the Australian Institute of Health and Welfare as 200 per 100,000 based on two published European studies.[3-5] There are over five million people affected worldwide and this estimate is expected to increase substantially in the coming decades.[6] Like Alzheimer's disease (AD), PD mostly affects the elderly and causes considerable disability and suffering.[6] There are about 10% of PD patients younger than 45 years of age.[7] As a neurodegenerative disease, ageing is the major risk factor, with incidence rising from 17.4 in 100,000 person between 50 and 59 years of age to 93.1 in 100,000 person between 70 and 79 years old.[7] The lifetime risk of developing Parkinson's disease will rise steadily with the increasing life expectancy of the general population.[5,8] Besides ageing as the major risk factor of PD, environmental causes or triggers, such as tobacco smoke,[9,10] nicotine and caffeine,[11,12] have been identified to be related to the sporadic disorder

disease.[13-15] Weak associated causes, such as head injury, lack of exercise, environmental toxins, herbicide and insecticide exposure, have also been reported.[16-18]

Genetic predisposition has also been found in Parkinson's disease.[19,20] Genetic studies have revealed that several mutations in susceptibility genes, including leucine rich repeat kinase 2 (LRRK-2), parkin, *α*-synuclein, and glucocerebrosidase (GBA) are closely related to Parkinson's disease.[7] LRRK-2 is a kinase encoding the protein dardarin. The Gly2019Ser mutation, the most common of the six pathogenic mutations in LRRK-2, is frequently found in patients diagnosed with PD in different areas worldwide.[9,21] Loss-of-function mutations in the parkin gene are the second most common genetic cause of Parkinson's disease.[7] These PD patients respond well to dopaminergic drugs. Mutations and gene triplications of *α*-synuclein have been linked with levodopa (L-dopa) responsive Parkinson's disease.[22,23] Loss-of-function of GBA can cause Gaucher's disease and increase the risk of developing Parkinson's disease.[24] Severe GBA mutation carriers can increase the risk of getting PD by 13 times and drop the mean age of PD onset from 60 to 55 years of age.[19]

The most obvious symptoms in the early stage of PD are movement-related. PD commonly presents with impairment of dexterity, fatigue and stiffness, extreme slowing down, a flexion of one arm with lack of swing. These physical signs might be hardly noticed or misinterpreted for a long period and the changes are often ascribed to old age, misery, introspection, or rheumatism by mistake. The detection of unequivocal slow movement (bradykinesia) can help to make the diagnosis of PD.[25] PD is also characterized by a coarse, slow, pill rolling tremor of the hands, flexion of the limbs and trunk or transient fixed posturing

of a hand after completing a motor task. In most cases, the diagnosis of Parkinson's disease can be made on clinical grounds and no ancillary investigations are needed. Once it is confirmed, patients and their relatives often start to remember potentially relevant symptoms, such as early difficulties with coordination, early motor symptoms and writing changes. Careful checking of patient's family history can also help to diagnose other first-degree relatives. Many patients are unaware of early loss of smell or disturbed sleep until they are formally tested.[26,27] An alternative diagnosis can be referenced to some symptoms including falls, fainting, urinary incontinence, prominent speech, disturbed swallowing, amnesia, or delirium, which have been observed for the early stage of the disease.

Advanced PD is defined as the onset of motor complications, despite aggressive pharmacological and behavioral management.[28] Cognitive and behavioral problems, such as postural instability and falls, speech and swallowing difficulties, freezing of gait, move all in one piece with a rapid propulsive shuffle, and nonmotor symptoms, may arise in this stage of PD. Dementia commonly occurs in the advanced stage of the disease. Risk factor for dementia development increases with age, particularly in those patients who present with prominent gait and speech disorders, depression, and a poor response to L-dopa.[29,30] There are three invasive options to treat motor complications when oral medications cannot address motor complications adequately: continuous subcutaneous apomorphine infusion, continuous duodenal L-dopa carbidopa pump and deep brain stimulation (DBS).[28] Although DBS has the highest risk, it has been used widely in the late stages of PD with the largest amount of evidence to treat motor fluctuations, dyskinesia and tremor. In addition, interdisciplinary therapy may be helpful in advanced Parkinson's disease.

The causes of death for PD patients have not been clearly identified, however pneumonia is by far the most commonly certificated cause.[7] By the year 2040, neurodegenerative diseases, including Parkinson's disease, are projected to surpass cancer as the second most common cause of death among the elderly.[31]

1.2 Chemotherapeutics for Parkinson's disease

Although PD is still an incurable progressive disease, treatment substantially improves quality of life and functional capacity. The treatment of early PD focuses on improved and more consistent drug delivery systems, targeting alternate neurotransmitter systems and neuroprotective therapies.[32] The available drugs currently include L-dopa, carbidopa, dopamine agonists and type B monoamine oxidase (MAO-B) inhibitors.

Monoamine oxidases (MAOs) are flavoproteins which catalyze the oxidative deamination of a variety of neurotransmitters.[33] MAO-A and MAO-B are the two major neurotransmitter-degrading enzymes in the central nervous system and in peripheral tissues, and play important roles in the control of substrate availability and activity.[34,35] In humans, MAO-B activity increases with age and is especially elevated in certain neurodegenerative diseases, such as PD.[36,37] Therefore, inhibition of MAO-B activity can improve the quality of PD patients' lives.

L-dopa (**1**) relieves the symptoms and is usually the first treatment option for all stages of PD. It is the most effective drug for PD, regardless of the age of the patients (Figure 1.1). Most patients can be managed over the first 5 years on 300-600 mg/day L-dopa. However, it has been reported that the long-term use of high doses of L-dopa can lead to the development

of motor fluctuations and dyskinesia.[6] There are two main treatment strategies that have been developed for L-dopa in the early stage of PD. One is to administer L-dopa in combination with a dopamine agonist or MAO-B inhibitor. The other is to use a dopamine agonist or MAO-B inhibitor and add L-dopa later to manage symptoms, particularly in younger patients. Using L-dopa (**1**)/carbidopa (**2**) in combination with entacapone (**3**) has showed greater L-dopa dose equivalents and symptomatic benefit than L-dopa (**1**) /carbidopa (**2**) treated patients.[38,39]

Pramipexole (**4**), ropinirole (**5**) and rotigotine (**6**), the popular first-line non-ergoline dopamine agonists, are widely used in patients under 55 years of age. Pramipexole (**4**), either immediate or extended release, has better treatment outcomes than placebo.[40] Ropinirole can improve Unified Parkinson's Disease Rating Scale (UPDRS) motor scores for PD compared with placebo.[41,42] Ergoline alkaloids, such as bromocriptine (**7**), lisuride (**8**), pergolide (**9**) and cabergoline (**10**), are dopamine agonists and used to delay the onset of motor fluctuations and dyskinesia. Dopamine agonists do not provoke dyskinesias, however, they can cause psychiatric and gastrointestinal side effects, sleep attacks, ankle oedema and impulse control disorders. Combination of lower doses of L-dopa and dopamine agonist may be a good approach to reduce the risk of motor complications and achieve the desired efficacy.

Selegiline (**11**) and rasagiline (**12**), selective MAO-B inhibitors, are the third treatment option for early stage of PD. They can be administered once daily and are well tolerated. Although they are less efficacious than either L-dopa or dopamine agonists, they have shown significant symptomatic benefit compared with placebo,[43,44] which were proposed as disease-

modifying agents.[45,46] Research on new symptomatic and neuroprotective treatment options is ongoing to identify new dopaminergic and neuroprotective compounds for early stage of PD.

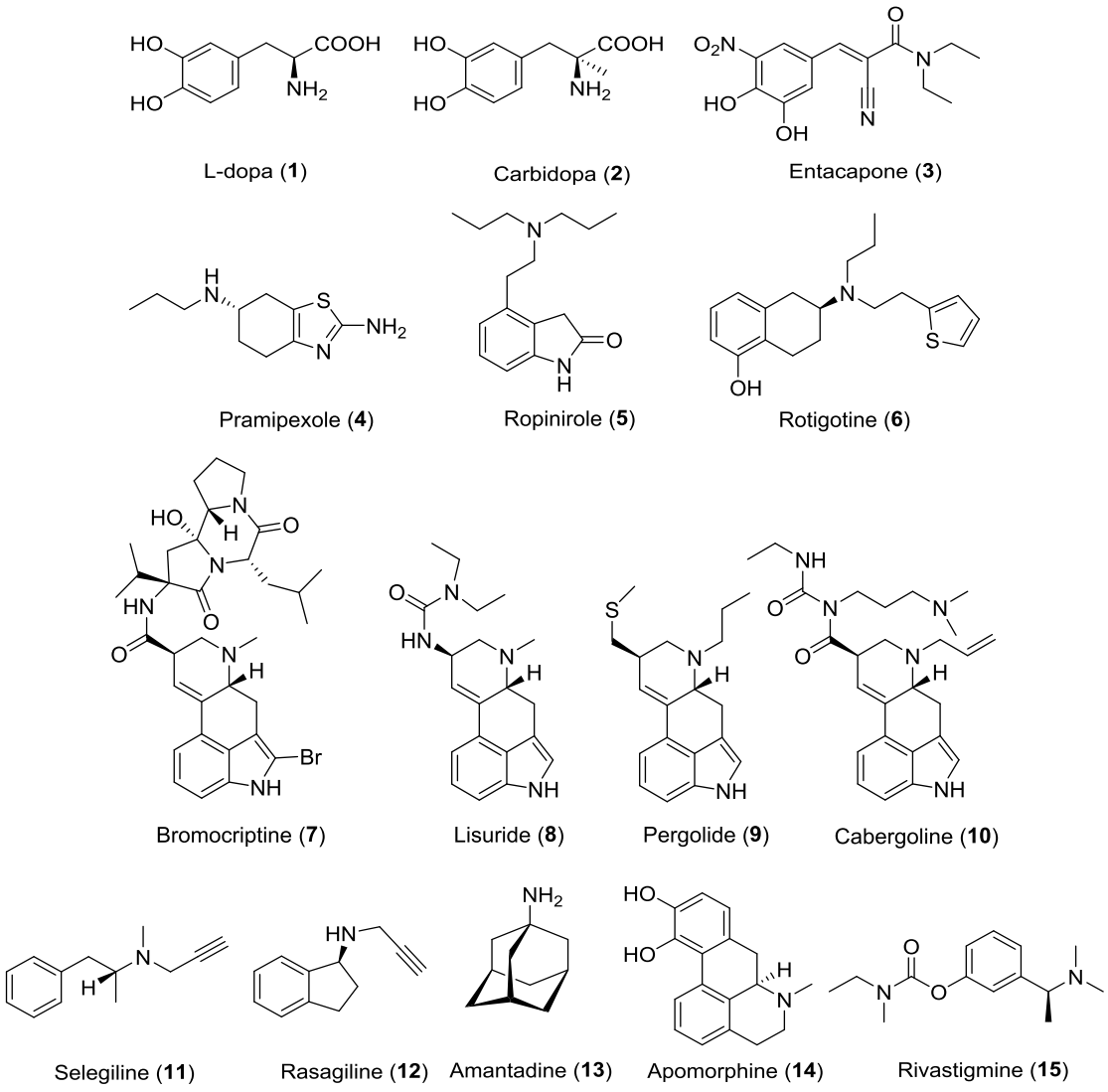

Figure 1.1 Chemical structures of drugs in the treatment of Parkinson's disease

For advanced PD where motor fluctuations are common,[47] sustained combination therapy has proven to be effective. IPX066, the oral extended-release capsule formulation of L-dopa (**1**) and cabidopa (**2**), has shown potential benefits including decreased off-time and reduced L-dopa dosing frequency in PD patients with motor fluctuations.[48] Rasagiline (**12**) in combination with L-dopa (**1**) can also improve motor fluctuations.[49] A dose of 100-400 mg/day

of amantadine (**13**), which has glutamate antagonist properties, can be used to manage L-dopa-induced dyskinesia and reduce painful dystonic phenomena in young onset cases.[50-52] As a dopamine agonist, subcutaneous apomorphine (**14**) has been used as fast-acting drug to help patients restore confidence. So far, rivastigmine (**15**) is the only FDA approved medication to treat dementia, which commonly occurs in advanced PD patients.[53]

1.3. Natural products and derivatives against Parkinson's disease

Natural products (NPs) are secondary metabolites displaying different ecological and biological functions, and are universally recognized as an important source of leads for the development of drugs.[54,55] They can be used as drug precursors, drug prototypes and pharmacological probes. Statistics suggested that about 50% of the best selling drugs today have been developed from natural sources and generated billions of dollars for the pharmaceutical industry.[56] Natural products have also played an important role in PD drug discovery. The potential for the development of natural origin chemical probes and drugs against Parkinson's disease is enormous. Here includes a summary of natural products which have been launched, in clinical trials or in preclinical research in the treatment of PD.

1.3.1 Phenylpropylamines

L-dopa (**1**) and related compounds (**16**-**22**) (Figure 1.2) are a class of natural products routinely used to treat PD. L-dopa was isolated from various species of bean, notably *Mucuna* spp.[57,58] The drug is now mainly obtained by synthesis. The drug L-dopa (**1**), often given in combination with carbidopa (**2**), can inhibit dopa-decarboxylase. Melevodopa (**16**) and etilevodopa (**17**), two ester forms of levodopa, have been clinically used as dopaminergic

agents for the treatment of PD (Figure 2.2).[59,60] Structurally similar phenylpropylamines, such as adrenaline (**18**) and noradrenaline (**19**), are important neurotransmitters that deliver dopamine across the blood brain barrier. Ephedrine (**20**) is the major naturally-occurring protoalkaloid obtained from some species of *Ephedra* (Ephedraceae) [61] and has been widely used in traditional Chinese medicine for many centuries. It is well known for its CNS-stimulant side effects, which may be due to its dopaminergic effect.[62] Chemically and pharmacologically similar to amphetamine (**21**), cathinone (**22**), the major natural product from *Catha edulis*,[63] was reported to reduce the PD-like tremors.[64]

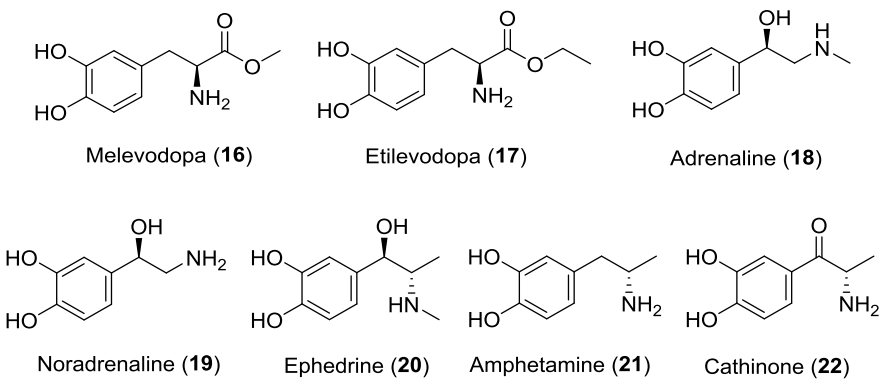

Figure 1.2 Chemical structures of dopamine related compounds **16-22**

1.3.2 Alkaloids

Ergot has a long history of poisoning animals and humans who eat cereal flour contaminated with ergot,[65] but has also been exploited in traditional medicine in some parts of Europe to aid childbirth. The ergot alkaloids, isolated from toxic fungus *Claviceps purpurea* Tulasne (Ergot),[66] have been well-documented for the effects on the CNS. Outbreaks of hallucinations were shown to correlate with heavy contamination of ergot in the communities affected.[67] The synthetic derivatives of ergot alkaloids, such as bromocriptine (**7**), lisuride (**8**),

pergolide (**9**) and cabergoline (**10**) (Figure 1), have been clinically used as dopamine agonists in the treatment of PD.[68,69] As the second most important group of compounds used for PD treatment, they are well-established drugs with numerous reviews on their clinical efficacy and applications.[70,71]

Hyoscine (**23**), a tropane alkaloid isolated from various genera of *Solanaceae*,[72] together with its synthetic analogues such as benzatropine (**24**), have been used to treat PD by inhibiting dopamine reuptake and increasing dopamine activity (Figure 1.3).[73] Phenyltropane derivatives, such as altropane (**25**) and ioflupane (**26**), have been reported as diagnostic tools for early detection of PD.[74] Altropane has shown potent dopamine reuptake inhibitory activity, while ioflupane has been used as a neuro-imaging radiopharmaceutical drug for differential diagnosis of Parkinson's disease over other disorders presenting similar symptoms.

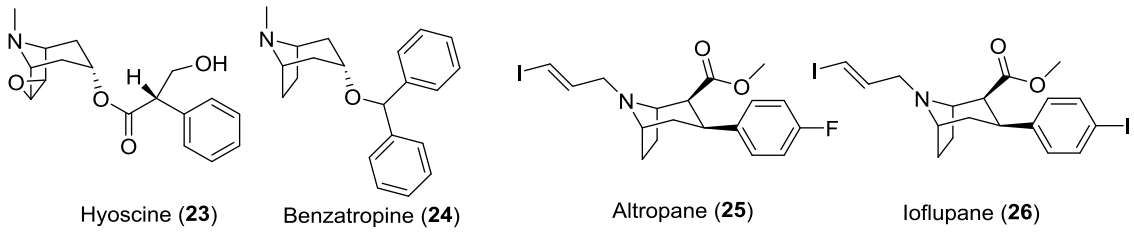

Figure 1.3 Chemical structures of tropane derivatives **23**-**26**

As a short-acting dopamine agonist, apomorphine (**14**), a semi-synthetic opium isoquinoline alkaloid, was approved by the FDA in 2004 as an injectable drug for the treatment of PD.[75] Salsolinol (**27**), another isoquinoline alkaloid isolated from the seeds of *Theobroma caca*,[76] is a dopaminergic agent and also had a protective effect against neurodegeneration (Figure 1.4).[77] It has been used as a protective substance to prevent or alleviate PD. Two *β*-carboline alkaloids harmane (**28**) and harmaline (**29**), isolated from *Banisteriopsis caapi* and

Morton (Malpighiaceae),[78,79] were reported to stimulate dopamine release from striatal cells, which may underlie the dopamine level improvement in PD patients.[80] Ibogaine (**30**), an indole alkaloid identified from *Tabernanthe iboga*,[81] increased dopamine release in isolated striatal tissue in mice, which preclude its effect in treating PD.[82]

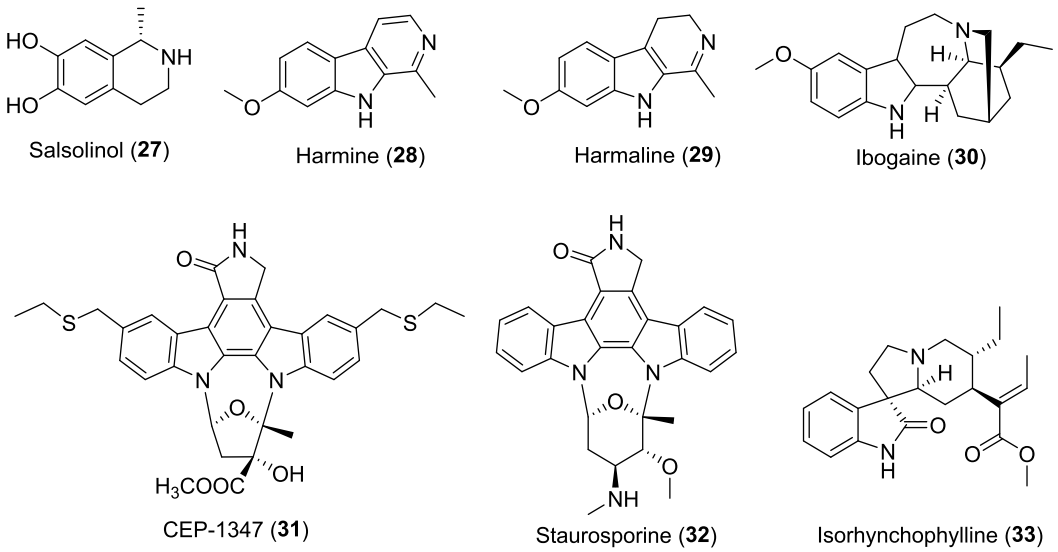

Figure 1.4 Chemical structures of alkaloids **27**-**33**

The indole alkaloid staurosporine (**32**), isolated from *Nocardiopsis sp.*,[83] and its semi-synthetic analogue CEP-1347 (**31**) showed inhibitory activity against lineage kinase, and have been clinically trialed to treat PD.[84,85] *Uncaria rhynchophylla* (known as Gouteng) was routinely used in traditional Chinese medicine prescriptions for the treatment of symptoms relevant to PD.[86,87] It was reported that the extract of *Uncaria rhynchophylla* exhibits MAO-B inhibitory activity which is relevant to neurological diseases including PD.[33] As a neuronal autophagy inducer, isorhynchophylline (**33**), a tetracyclic oxindole alkaloid isolated from Gouteng, stimulated autophagy in neuronal cells and exerted preventive and therapeutic values against PD.[88]

Nicotine (**34**) has been associated with a decreased risk of developing PD, and has shown a protective effect for neurons against neurotoxicity (Figure 1.5).[89] Caffeine (**35**) is an adenosine A2 receptor antagonist and can increase striatal dopamine release similar to nicotine.[90] As a caffeine analogue, istradefylline (**36**), a selective antagonist at the A_{2A} receptor, was found to be useful in the treatment of PD by reducing dyskinesia resulted from long-term treatment with L-dopa.[91,92]

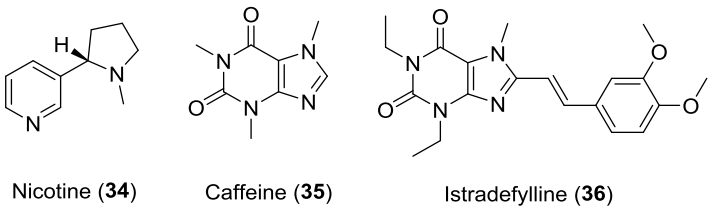

Figure 1.5 Chemical structures of alkaloids **34**-**36**

1.3.3 Flavonoids

Flavonoids are important antioxidants and have demonstrated neuroprotective properties.[93] Baicalcein (**37**), isolated from the roots of *Scutellaria baicalensis* and *Scutellaria lateriflora*,[94,95] has shown neuroprotective effect against 1-Methyl-4-phenyl-1,2,3,6-tetrahydropyridine (MPTP) induced damage of dopaminergic neurons in PD (Figure 1.6).[96] Kaempferol (**38**), a widely used herbal product isolated from the leaves of *Ginkgo biloba*,[97] has shown preventative properties against neurodegeneration.[97] Quercetin (**39**) has also shown MAO-B inhibitory activity and catalepsy reversing effects, which mimics the bradykinesia as seen in PD.[98,99] Tangeretin (**40**) might have therapeutic potential for PD by inhibiting MAO-B and consequently reducing dopamine depletion.[100] The flavanonol (-)-epigallocatechin-3-

gallate (EGCG, **41**), found in green tea,[101] has shown similar protective effect in PD and other conditions.[102]

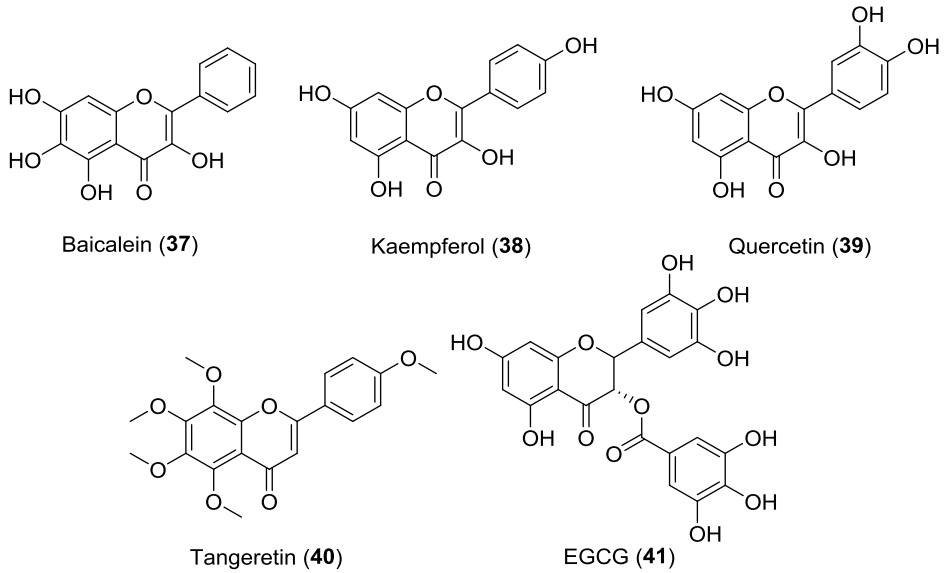

Figure 1.6 Chemical structures of flavonoids **37**-**41**

1.3.4 Other structural classes

Dl-3n-butylphthalide (dl-NBP, **42**), an antioxidant isolated from the seeds of *Apium graveolens*,[103] is used clinically to treat stroke in China (Figure 1.7).[104] It was also been found to have certain neuroprotective effects,[105] which could lead to a preventive medicine for PD. Ganglioside (GM1, **43**), isolated from ganglion cells of the brain,[106] was demonstrated to significantly reduce symptoms of PD in clinical trials and it is now an approved drug.[107] Preclinical studies on cyclosporine A (CsA, **44**), initially isolated from the fungus *Tolypocladium inflatum*,[108] showed that the compound had neuroprotective effect in stroke, traumatic brain injury and PD.[109]

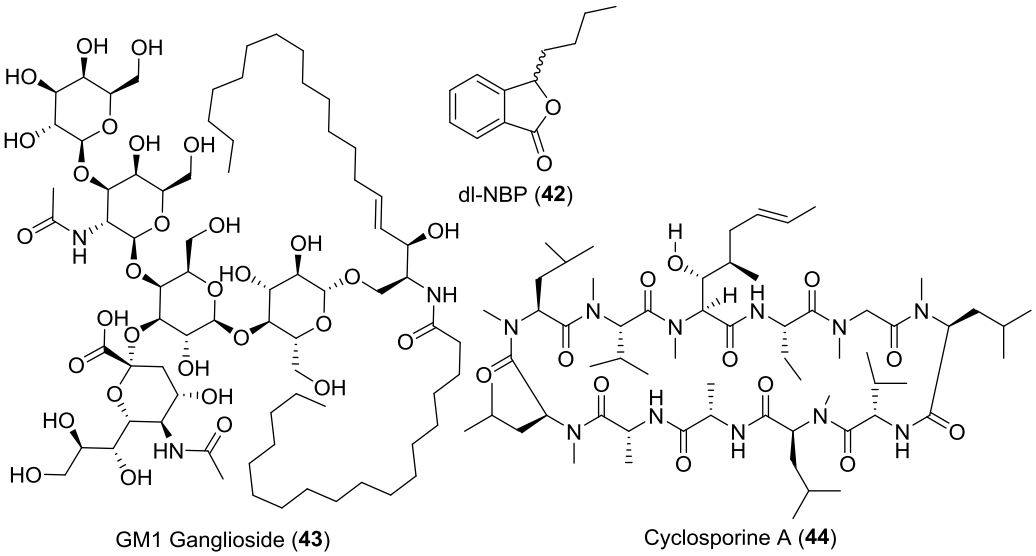

Figure 1.7 Chemical structures of natural products **42**-**44**

1.3.5 Physical chemical properties of anti-PD natural products

Natural products and their derivatives are indeed an important source for the development of anti-PD drugs.[110] The usefulness of a molecule as a lead is generally dependent upon the lead-like/drug-like properties. Lipinski's rule of five (Ro5) has been commonly used to assess the relationship between chemical structures and drug-like properties.[111,112] Although the rule cannot guarantee a molecule compliant with all criteria is druggable, it provides a guide for medicinal chemists for better design of compounds with satisfactory pharmacokinetics. Ro5 states that a small molecule is more likely to be orally active if its molecular weight is less than 500; its lipophilicity, expressed as a quantity known as log *P*, is less than 5; the number of hydrogen bond donors (HBD) is less than 5; the number of hydrogen bond acceptors (HBA) is less than 10.

Neurodegenerative diseases, such as PD, AD, HD and others, require drugs that penetrate the blood-brain barrier. Anti-PD natural products and their derivatives with

neuroprotective properties must possess certain physicochemical properties to allow brain penetration and exposure. We therefore calculated the physicochemical properties of these compounds for the evaluation of the likelihood as molecular probes and/or drugs.

Log *P* is considered one of the most important physicochemical parameter for drug discovery and development, since this value is directly related to a molecules' ability to permeate cells in order to modulate cellular signaling pathways or to have wider biology effects.[113,114] Other parameters have also been proposed to predict favorable drug metabolism and pharmacokinetics (DMPK) for lead compounds, such as rotatable bonds, polar surface area (PSA) and log $D_{5.5}$. Rules to predict "lead-likeness" are slightly more rigid than Lipinski's rules as the molecular weight of the leads should be less than 450 and also the log *P* should be less than 4. The selection criteria are stringent since drug molecules are usually derived from less complex lead compounds which usually have a smaller number of rings, less rotatable bonds, smaller molecular weight and are more hydrophilic. Both these rules have been designed so that the compounds can progress through traditional medicinal chemistry optimization.

The physicochemical properties of these 36 anti-PD natural products and their derivatives were calculated using Instant JChem 15.10.26.0 [ChemAxon Ltd. (http://www.chemaxon.com)].[115] The parameters including molecular weight (MW), log *P*, number of hydrogen bond acceptors (HBA) and number of hydrogen bond donors (HBD) were analysed against Lipinski's rule of five (Table 1.1 and Figure 1.8).

Table 1.1 Physicochemical Physicochemical properties of the 36 anti-PD natural products and their derivatives

compound	physicochemical parameters[a]				
	MW	log *P*	HBA	HBD	No. of Violations
34	162.24	1.16	2	0	0
21	167.21	0.40	3	3	0
19	169.18	-0.68	4	4	0
27	179.22	1.07	3	3	0
22	181.19	0.08	4	3	0
18	183.21	-0.43	4	4	0
42	190.24	3.36	1	0	0
35	194.19	-0.55	3	0	0
1	197.19	-1.79	5	4	0
20	197.23	-0.07	4	4	0
2	211.22	-1.36	5	4	0
16	211.22	0.62	4	3	0
28	212.25	1.85	2	1	0
29	214.27	1.67	2	1	0
17	225.24	0.97	4	3	0
14	267.33	2.88	3	2	0
37	286.24	2.46	6	4	0
38	286.24	2.46	6	4	0
39	302.24	2.16	7	5	0
23	303.36	0.89	4	1	0
24	307.44	4.19	2	0	0
30	312.46	3.01	3	1	0
9	312.48	4.04	1	1	0
8	338.46	2.17	2	2	0
33	368.48	3.47	3	1	0
40	372.37	2.18	7	0	0
36	384.44	2.42	5	0	0
25	429.27	3.95	2	0	0
10	449.60	2.39	4	2	0
32	466.54	3.97	4	2	0
41	472.36	3.10	11	8	2
26	537.18	4.74	2	0	1
31	615.76	5.73	4	2	2
7	652.63	3.67	5	3	1
44	1,202.64	3.64	12	5	3
43	1,546.84	1.98	31	20	3

[a]All physicochemical properties, including molecular weight (MW), log *P*, hydrogen bond acceptors (HBA) and hydrogen bond donors (HBD), were calculated using Instant JChem (version 15.10.26.0).

As shown in Table 1.1 and Figure 1.8, it is clear that most of the compounds had log *P* < 5 (97.2%), five compounds with molecular weight > 500, three compounds with HBA > 10 and two compounds with HBD > 5. In total 83.3% of these compounds obeyed Lipinski's Ro5. Excluding MW > 500 compounds will remove simultaneously the compounds with a high HBD or HBA count.

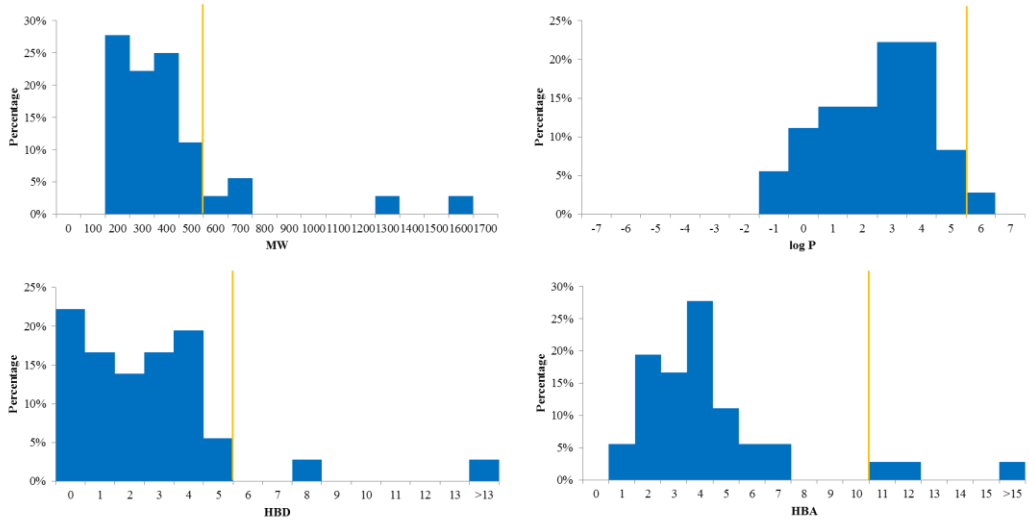

Figure 1.8 Analysis of physicochemical properties (MW, log P, HBA and HBD) of 36 anti-PD compounds. The orange line indicates the maximum desirable value for oral bioavailability defined by Lipinski's rule of five: MW < 500 Da; log P < 5, HBA < 10 and HBD < 5.

In summary, natural products are an important source of new and complex structures with small MW and lead- or drug-like properties.[116] They are also chemical probes for the mechanism research and targets identification.[117,118] The use of Ro5 guides the isolation and identification of anti-PD chemical probes more efficiently and facilitates the developing of leads and drugs for treatment of Parkinson's disease.

1.4. Discovery of natural product chemical probes against Parkinson's Disease

It is obvious that Parkinson disease is a complex neurodegenerative disease and thus far there is no clear understanding of the underlying causes of PD. There are many theories as to the causes and it is generally thought that multiple factors are responsible. Unfortunately, there is no effective drug available to cure this progressive disease. Medications, surgery and multidisciplinary management can only provide relief from the symptoms. Thus, there is an urgent need to develop new molecules to study the underlying mechanisms of PD, and to discover therapeutic agents.

In this project, two whole-cell based screening assays were developed using a human olfactory neurosphere-derived (hONS) cell model of PD. The initial screening of natural products fractions was conducted using a rotenone insult high-throughput screening (HTS) assay. During the course of my PhD research, a high content screening (HCS) assay on the same cell line was developed and used to cytologically profile the isolated natural products. The outcomes of this project may initiate further anti-PD research on the basis of the identified natural products chemical probes, which could subsequently lead to further development of new anti-PD lead compounds. Although drug discovery research is a serendipitous field, this work will contribute to the knowledge of anti-PD natural product chemical probes, their structures and biological activity.

1.4.1 Nature Bank Lead Like Enhanced Fractions

Nature Bank housed at the Eskitis Institute, Griffith University is a unique biodiversity resource and is the basis of the current bio-discovery project targeting PD. This unique

chemical biodiversity resource comprises over 45,000 biota samples, 18,453 lead-like enhanced extracts, 202,983 semi-purified fractions and more than 3,500 pure compounds. The Eskitis biota repository used to construct the LLE fraction library was collected from mega-diverse areas of tropical Queensland, Tasmania, Papua New Guinea and China. All samples have been collected in accordance with the UN Convention on Biological Diversity. Benefit-sharing agreements are in place to guarantee a fair return to the community and ensure that partner has no need to engage with Governments to arrange access.

A collection of 18,453 lead-like enhanced extracts (LLE extracts) from a representative subset of the biota library is far quicker and easier to screen than crude extracts, and increase the probability of quality hits.[119] These extracts have been optimized by removal of non-drug like components using a method to retain components with favorable log *P*. They were then used to prepare the lead-like enhanced fraction library (LLE fraction library) for screening. An example of an LLE fraction HPLC trace and the fractions collected for the screening library is shown below (Figure 1.9).[120] A small amount of biota (300 mg) was packed into a SPE cartridge (10 × 50 mm), washed with *n*-hexane (8 mL), and then extracted with DCM (8 mL), then MeOH (8 mL × 2). The *n*-hexane extract was discarded. The combined and dried DCM and MeOH extracts were reconstituted in MeOH (4 mL) before being loaded onto a hydrophilic lipophilic balanced (HLB) cartridge. It contains a universal polymeric reversed-phase sorbent that is developed for the extraction of a wide range of acidic, basic, and neutral compounds from various matrices using a simple, generic protocol and can sufficiently remove the non-lead-like components from the extraction, such as pigments.[121] The cartridge was washed with MeOH (8 mL) and the MeOH wash was dried to afford the crude extract. The crude extract

was re-dissolved in DMSO (600 μL). The DMSO solution (100 μL) was then fractionated by C_{18} analytical HPLC with solvent conditions consisting of a linear gradient from 90% H_2O (0.1% TFA)/10% MeOH (0.1% TFA) to 50% H_2O (0.1% TFA)/50% MeOH (0.1% TFA) in 3 min at a flow rate of 4 mL/min, followed by a convex gradient to MeOH (0.1% TFA) in 3.5 min at a flow rate of 3 mL/min. This was held at 100% MeOH (0.1% TFA) for 0.5 min at a flow rate of 3 mL/min and for further 1 min at a flow rate of 4 mL/min, then a linear gradient back to 90% H_2O (0.1% TFA)/10% MeOH (0.1% TFA) in 1 min at a flow rate of 4 mL/min was applied. Finally, the gradient was held at 90% H_2O (0.1% TFA)/10% MeOH (0.1% TFA) for 2 min at a flow rate of 4 mL/min, ready for the next injection. Total run time for each injection was 11 min, and 11 fractions were collected between 2.0 min and 7.0 min, these include: fraction 1 (time = 2.00 – 2.33 min), fraction 2 (time = 2.34 – 2.66 min), fraction 3 (time = 2.67 – 3.00 min), fraction 4 (3.01 – 3.50 min), fraction 5 (3.51 –4.00 min), fraction 6 (time = 4.01 – 4.50 min), fraction 7 (time = 4.51 – 5.00 min), fraction 8 (time = 5.01 – 5.50 min), fraction 9 (5.51 – 6.00 min), fraction 10 (time = 6.01 – 6.50 min) and fraction 11 (6.51 – 7.00 min). Only these fractions were collected because they are most likely to contain compounds with drug-like properties, the early eluting material consisting of media components and highly polar compounds was not collected nor was the late-eluting lipophilic portion. A standard containing uracil, methyl 4-hydroxy benzoate, ethyl 4-hydroxy benzoate, and benzophenone all at 0.125 mg/mL in DMSO was injected onto the C_{18} analytical column using the same gradient condition as this describe above. This standard injection was used as a quality control procedure.

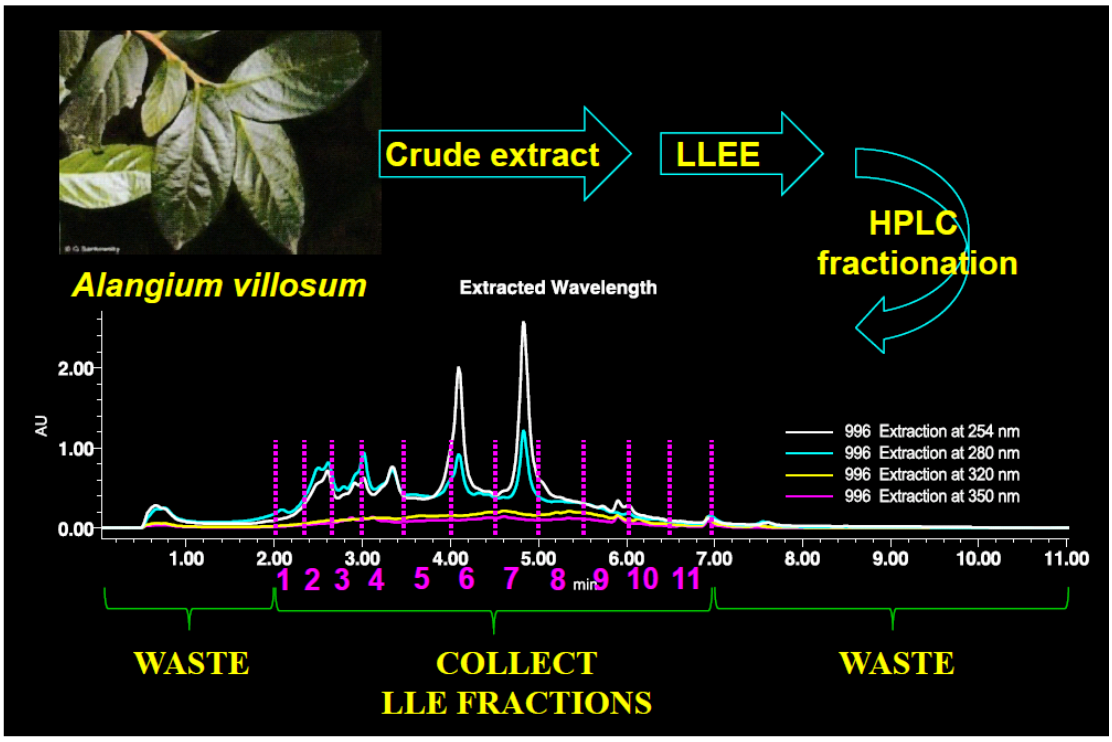

Figure 1.9 HPLC chromatogram depicting lead-like enhanced fractions

1.4.2 Initial High throughput screening (HTS) assay using rotenone

High throughput screening (HTS) is a relatively recent innovation especially used in drug discovery and relevant to the fields of biology and chemistry, largely made feasible through modern advances in robotics and high-speed computer technology. Compared to traditional drug development methods, application of HTS assays has significantly increased the availability of novel drug-like compounds as neuroprotective agents.[122] There is therefore a clear demand to develop this assay for more efficient screening.

An initial HTS assay was developed to screen a sub-set of the Eskitis Institute's pre-fractionated natural product library from Nature Bank using human olfactory neurosphere-derived (hONS) cell for neuroprotective agents that can reverse rotenone-induced cytotoxicity.[119] Much progress has been made in recent years in toxin-induced PD models,

based on the proposition that dopaminergic neurons have a common death cascade which can be mimicked by insults of small-molecule toxins.[123,124] Rotenone is a classic mitochondrial complex I inhibitor, which activates the apoptosis pathway through release of reactive oxygen species.[125] Selective degeneration of nigrostriatal dopaminergic neurons accompanied by α-synuclein-positive inclusions after administration to rats with low-dose intravenous rotenone has been reported.[126] Reports from other studies also demonstrated that rotenone inhibited complex I uniformly throughout the brain in rats with selective cell loss in the nigrostriatal dopaminergic system.[127,128] There have also been several reports in cell-based assays that linked α-synuclein aggregation to neuronal cell death.[129-131] Thus, rotenone induced cell death provides an excellent model system for drug discovery research for Parkinson's disease.

Neurological disease patient-derived stem cell models have the potential to elucidate cell biological aspects of brain diseases. Olfactory mucosa stem cells generated from Parkinson's disease patient have demonstrated PD associated characters, including disease-specific alterations in gene expression and cell functions, such as oxidative stress. Multiple genes of small effect can converge on shared cell signaling pathways to present as a disease-specific cellular phenotype.[132,133] Olfactory mucosa stem cells can be cultured to reveal patient-control differences in complex genetic diseases and maintained in homogeneous cultures, which allow robust and repeatable multi-well assays suitable for screening libraries of drug candidate molecules.[132]

hONS cell lines derived from sporadic PD patients and healthy donors were cultured at 37 ℃ in humidified atmosphere and 5% CO_2 in Dulbecco's modified Eagle's medium/F12

supplemented with 10% fetal bovine serum (FBS). The medium was refreshed every two days until the confluent of cells. Then the cells were harvested and resuspended in DMEM/F12 supplemented with 10% FBS and approximately 2,500 cells were placed into each well of a 96-well plate. After incubating at 37 ℃ in humidified atmosphere and 5% CO_2 for 12 h, the medium in each well were replaced with medium containing 50 nM rotenone and incubate at 37 ℃ in humidified atmosphere and 5% CO_2 for 24~120 h.

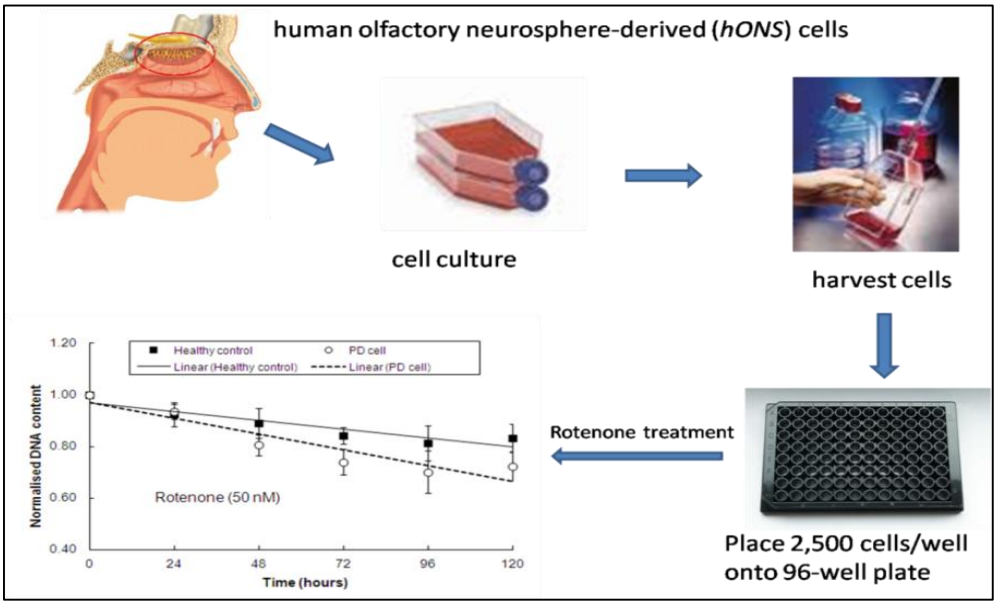

Figure 1.10 Optimization of rotenone treatment conditions in hONS cells

The CyQUANT assay is based on measurement of cellular DNA content via fluorescent dye binding to cellular DNA. Because cellular DNA content is highly regulated, it is closely proportional to cell number. Briefly, cells in a 96-well plate were washed twice with HBSS buffer and 50 μL of reaction mixture containing (1× CyQUANT dye reagent and 1× dye delivery reagent) was added in each well of a 96-well plate, respectively. Then the cells were incubated at 37 ℃ with cover for 90 min and the fluorescence intensity of each sample was measured using a fluorescence microplate reader with excitation at ~485 nm and emission

detection at ~530 nm. As shown by the CyQUANT assay results, the hONS cells from PD patients were more susceptible to rotenone than healthy controls (Figure 1.10). Finally, the HTS assay was optimized by using hONS cells from PD patients treated with rotenone (200 nM) for 96 hours.

1.4.3 HTS results

The initial HTS assay was developed to screen the fraction library using PD patient derived hONE cells for neuroprotective agents that can reverse rotenone-induced cytotoxicity. The fraction library screening was done via a robotic workstation by collaborators. Assays were assembled on 384-well plates, test fractions were added, and the completed assay mixtures were loaded into an automated multimodal plate reader where the readout was quantified. Briefly, hONS cells were harvested and re-suspended in DMEM/F12 supplemented with 10% fetal bovine serum and approximately 600 cells were placed into each well of a 384-well plate, which contained 0.5 µL of drug candidate (250 µge/uL, Compounds Australia) and 0.5 µL of DMSO. Column 23 of each plate was chosen as internal control, which contained 0.5 µL of distilled H_2O and 0.5 µL of DMSO. The plates were incubated at 37 ℃ in humidified atmosphere and 5% CO_2 for 96 hours before the CyQUANT assay. Raw data were normalized using the plate median method. Next, a *z*-score transformation was applied to center and scale the data across the experiment. Replicates for a given compound at a given dose (N = 2 for each dose/compound combination) were then mean summarized. A *z*-score threshold of ≥ 3 was chosen to identify potential hits.

To begin with, 4224 lead-like enhanced fractions from the LLE fraction library were randomly chosen and screened. In total, 108 hits by single dose screening showed activity. Twenty fractions were further confirmed as hits in triplicate experiments (Table 1.2).

Table 1.2 Twenty fractions and their associated biota identified by HTS assay. Seven fractions, representing 3 biota samples, were prioritized (in red) and they are the subject of this thesis.

Fraction_ID	Family	Genus	Species	Hits in DNP
QID016326-Fraction7	Colchicaceae	*Gloriosa*	*superba*	60
QID020164-Fraction 11	Balanopaceae	*Balanops*	na	4
QID020279- Fraction 10	Myrsinaceae	*Rapanea*	na	12
QID022416- Fraction 9	Betulaceae	*Alnus*	*trabeculosa*	113
QID031113- Fraction 1	Basellaceae	*Anredera*	na	2
QID2146928- Fraction 3				
QID2146928- Fraction 4				
QID2146928- Fraction 5	Alangiaceae	*Alangium*	*villosum*	194
QID2146928- Fraction 6				
QID2146928- Fraction 7				
QID2227096- Fraction 11	Agavaceae	*Furcraea*	na	17
QID5201865- Fraction 11	Solanaceae	*Cestrum*	none	66
QID5201869- Fraction 11	Aquifoliaceae	*Ilex*	none	317
QID5370277- Fraction 6	Balanophoraceae	*Balanophora*	none	53
QID6001527- Fraction 8	Cortinariaceae	*na*	na	
QID6005130- Fraction 11	Dictyonellidae	*Rhaphoxya*	3249	0
QID6007994- Fraction 2	Calthropellidae	*Jaspis*	*splendens*	157
QID6008543- Fraction 4	Suberitidae	*Aaptos*	*aaptos*	18
QID6009831- Fraction 9	Darwinellidae	*Dendrilla*	3106	40
QID5305633- Fraction 11	Theaceae	*Ternstroemia*	none	19

On the basis of the literature research, the results of chemical and biological analysis, as well as the amount of biota material available in Nature Bank, seven fractions, representing one Australian marine sponge *Jaspis splendens* (subject 1) and two Australian terrestrial plants *Gloriosa superba* (subject 2) and *Alangium villosum* (subject 3), were selected for large scale extraction and isolation. This is the subject of this thesis.

1.4.4. High content screening (HCS) and phenotypic profiling

A grand challenge in natural product chemistry is to determine the biological effects of all natural products. Target-based drug discovery (TDD) approaches provide efficient and high capacity in testing unprecedented numbers of compounds and molecular targets utilizing advances in automation, biochemistry, structural biology, and chemistry related technologies.[134] High throughput screening (HTS), however, has low hit rates. Target screening also heavily relies on knowledge of known therapeutic pathways. Other pathways or functional proteins affected by compounds may not be identified by target-based screening. In comparison, phenotypic screening has the advantage of the whole organism being exposed to compounds and interrogates all targets and biological pathways. When multiple parameters are examined, a multidimensional cytological profiling method can be used to cluster compounds. It is worth noting that new molecular entities identified by phenotypic screening approved by the FDA outnumbered target-based approaches during the time frame between 1999 and 2008 (37% versus 23%).[135]

Phenotypic screening is a strategy for the identification of molecules with particular biological effects in cell-based assays or animal models. For example, it can involve screening large libraries of chemical compounds in automated high throughput cellular assays that measure the levels of various proteins or effects on characteristics such as cell proliferation. It has been the basis for the discovery of new drugs in history. Recent statistical analysis reveals that phenotypic screening has led to the discovery of a number of first-in-class drugs with novel

mechanisms of action.[135] This has prompted interest in this screening method and has led to its resurgence in drug discovery.[136]

There are two major types of phenotypic screening: *in vitro* and *in vivo*. The simplest phenotypic screens are *in vitro* assays. Cell lines are employed and a single parameter such as cellular death or the production of a particular protein is monitored. High content screening (HCS) where changes in the expression of several proteins or cytological profiling of cellular parameters can be simultaneously monitored is also often used.[137] This has been specifically developed during the course of our research for the identification of anti-PD chemical probes isolated from the three biota samples chosen by the initial HTS screening.

Phenotypic screening in animal-based systems can utilize model organisms, such as the fruit fly, zebrafish and mice,[138] to evaluate the effects of drug candidates in fully assembled biological systems. The high content biological screening is best exemplified where drug candidates can be evaluated for potential therapeutic benefits across many different types of animal models representing different disease states.[139] It offers the advantage of interrogating test agents, or alterations in targets of interest, in the context of fully integrated, assembled, biological systems, providing insights that could not be obtained in cellular systems.[136,140] Some human disease processes involve many different cell types across many different organ systems, which can only be emulated in model organisms.[141,142] Cellular based systems are unable to adequately model this type of complexity. This notion is consistent with the productivity of drug discovery by phenotypic screening in model organisms.[135,143] The *in vivo* phenotypic screening can be also well utilized in evaluating already approved drugs or late

stage drug candidates for drug repositioning.[139] which has been specially used by a number of companies, such as Melior Discovery, Phylonix, and Sosei.

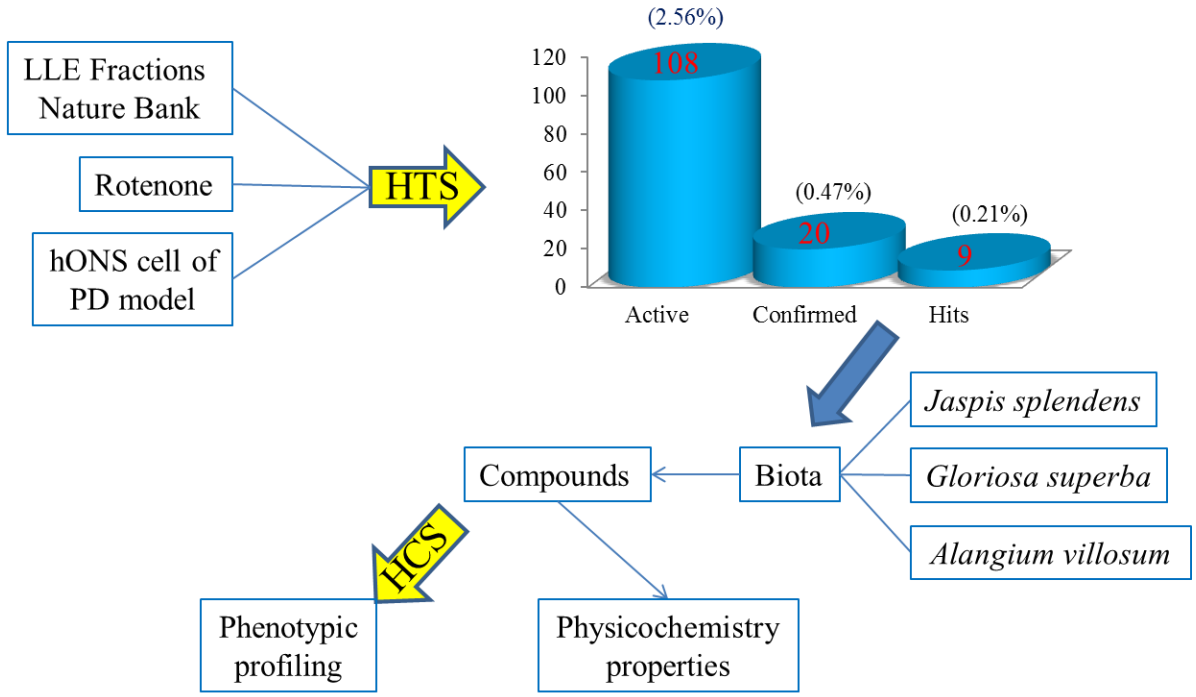

Figure 1.11 An overview of the project, including two cell-based assays (HTS and HCS), the fraction hits identified, the isolation of bioactive natural products from three prioritized biota samples, the physicochemical property analysis and phenotypic profiling of the isolated secondary metabolites.

Animal models may, however, not reflect the human situation. We used patient derived hONS cells in order to improve the chance to develop chemical probes, lead and drug candidates. An overview of this project is as shown in Figure 1.11. The whole cell based approaches to high content screening are amenable to screening libraries containing thousands of small molecules. The isolated secondary metabolites from the chosen biota can be examined to identify congeneric chemical series by coupling an unbiased multidimensional phenotype assay using nontransformed and nonimmortalized hONS cells, which are primary cells derived from a PD patient. The HCS assay we developed contains three steps: biological assay; cell

staining; imaging and image analysis. More details about the assay are discussed in Chapters Two, Three and Four.

As shown in Figure 1.11, this thesis describes the chemical investigation of one Australian marine organism and two Australian terrestrial plants. An overview of PD and natural products and derivatives against PD has been presented in Chapter One with an emphasis on the potential of natural products as a source of chemical probes and drugs targeting PD. Chapter Two, which has been published as a full paper in the *Journal of Natural Products*, describe the isolation and structure elucidation of three new natural products, two naturally-occurring new compounds, previously reported as synthetic products, together with 17 known natural products from the Australian marine sponge *Jaspis splendens* as well as the phenotypic profiles of these secondary metabolites. Chapter Three, which has been submitted to the *Journal of Natural Products*, outlines the isolation and structure elucidation of four new lumicolchicosides, one new nucleoside derivative and two new phenolic glycosides, together with 32 known natural products from the Australian plant *Gloriosa superba* L. as well as the phenotypic profiles of these secondary metabolites. In Chapter Four, which has been drafted for the *Journal of Natural Products*, the isolation and structure elucidation of four new benzoquinolizidine *N*-oxides and four new benzoquinolizidine alkaloids, together with 36 previously reported natural products from the Australian plant *Alangium villosum* is described and the phenotypic profiles of these compounds are discussed. Chapter Five provides a summary of the results obtained in this thesis. Three series of natural products were identified as ideal anti-PD chemical probes by a combine strategy using cytological profiling, Ro5 and ChemGPS analysis.

1.5 References

(1) Parkinson, J.; London, Macmillan: 1817.

(2) Kempster, P. A.; Hurwitz, B.; Lees, A. J. *Neurology* **2007**, *69*, 482-485.

(3) Mathers, C.; Vos, T.; Stevenson, C. *The burden of disease and injury in Australia*; Australian Institute of Health and Welfare, 1999.

(4) de Rijk, M. d.; Tzourio, C.; Breteler, M.; Dartigues, J.; Amaducci, L.; Lopez-Pousa, S.; Manubens-Bertran, J.; Alperovitch, A.; Rocca, W. *J. Neurol. Neurosurg. Psychiatry* **1997**, *62*, 10-15.

(5) De Rijk, M.; Breteler, M.; Graveland, G.; Ott, A.; Grobbee, D.; Van der Meche, F.; Hofman, A. *Neurology* **1995**, *45*, 2143-2146.

(6) Olanow, C. W.; Stern, M. B.; Sethi, K. *Neurology* **2009**, *72*, S1-S136.

(7) Lees, A. J.; Hardy, J.; Revesz, T. *Lancet* **2009**, *373*, 2055-2066.

(8) Bower, J. H.; Maraganore, D. M.; McDonnell, S. K.; Rocca, W. A. *Neurology* **1999**, *52*, 1214-1214.

(9) Paisán-Ruíz, C.; Jain, S.; Evans, E. W.; Gilks, W. P.; Simón, J.; van der Brug, M.; de Munain, A. L.; Aparicio, S.; Gil, A. M. n.; Khan, N. *Neuron* **2004**, *44*, 595-600.

(10) Hernán, M. A.; Zhang, S. M.; Rueda-DeCastro, A. M.; Colditz, G. A.; Speizer, F. E.; Ascherio, A. *Ann. Neurol.* **2001**, *50*, 780-786.

(11) Ascherio, A.; Weisskopf, M. G.; O'Reilly, E. J.; McCullough, M. L.; Calle, E. E.; Rodriguez, C.; Thun, M. J. *Am. J. Epidemiol.* **2004**, *160*, 977-984.

(12) Ascherio, A.; Chen, H.; Schwarzschild, M.; Zhang, S.; Colditz, G.; Speizer, F. *Neurology* **2003**, *60*, 790-795.

(13) Tanner, C. M. *Adv. Neurol.* **2003**, *91*, 133.

(14) Taylor, K.; Counsell, C.; Gordon, J.; Harris, C. *Age Ageing* **2005**, *34*, 501-504.

(15) Dick, F. D.; De Palma, G.; Ahmadi, A.; Scott, N.; Prescott, G.; Bennett, J.; Semple, S.; Dick, S.; Counsell, C.; Mozzoni, P. *Occup. Environ. Med.* **2007**, *64*, 666-672.

(16) Elbaz, A.; Tranchant, C. *J. Neurol. Sci.* **2007**, *262*, 37-44.

(17) Thacker, E. L.; Chen, H.; Patel, A. V.; McCullough, M. L.; Calle, E. E.; Thun, M. J.; Schwarzschild, M. A.; Ascherio, A. *Mov. Disord.* **2008**, *23*, 69-74.

(18) Tanner, C. M.; Aston, D. A. *Curr. Opin. Neurol.* **2000**, *13*, 427-430.

(19) Gan-Or, Z.; Giladi, N.; Rozovski, U.; Shifrin, C.; Rosner, S.; Gurevich, T.; Bar-Shira, A.; Orr-Urtreger, A. *Neurology* **2008**, *70*, 2277-2283.

(20) Aharon-Peretz, J.; Rosenbaum, H.; Gershoni-Baruch, R. *N. Engl. J. Med.* **2004**, *351*, 1972-1977.

(21) Healy, D. G.; Falchi, M.; O'Sullivan, S. S.; Bonifati, V.; Durr, A.; Bressman, S.; Brice, A.; Aasly, J.; Zabetian, C. P.; Goldwurm, S. *Lancet Neurol.* **2008**, *7*, 583-590.

(22) Polymeropoulos, M. H.; Lavedan, C.; Leroy, E.; Ide, S. E.; Dehejia, A.; Dutra, A.; Pike, B.; Root, H.; Rubenstein, J.; Boyer, R. *Science* **1997**, *276*, 2045-2047.

(23) Singleton, A.; Farrer, M.; Johnson, J.; Singleton, A.; Hague, S.; Kachergus, J.; Hulihan, M.; Peuralinna, T.; Dutra, A.; Nussbaum, R. *Science* **2003**, *302*, 841-841.

(24) Goker-Alpan, O.; Schiffmann, R.; LaMarca, M.; Nussbaum, R.; McInerney-Leo, A.; Sidransky, E. *J. Med. Genet.* **2004**, *41*, 937-940.

(25) Katzenschlager, R.; Cardozo, A.; Avila Cobo, M. R.; Tolosa, E.; Lees, A. J. *Mov. Disord.* **2003**, *18*, 1123-1131.

(26) Doty, R. L.; Bromley, S. M.; Stern, M. B. *Neurodegeneration* **1995**, *4*, 93-97.

(27) Iranzo, A.; Santamaria, J.; Rye, D.; Valldeoriola, F.; Marti, M.; Munoz, E.; Vilaseca, I.; Tolosa, E. *Neurology* **2005**, *65*, 247-252.

(28) Giugni, J. C.; Okun, M. S. *Curr. Opin. Neurol.* **2014**, *27*, 450-460.

(29) Levy, G. *Arch. Neurol.* **2007**, *64*, 1242-1246.

(30) Kempster, P.; Williams, D.; Selikhova, M.; Holton, J.; Revesz, T.; Lees, A. *Brain* **2007**, *130*, 2123-2128.

(31) Lilienfeld, D. E.; Perl, D. P. *Neuroepidemiology* **1993**, *12*, 219-228.

(32) Pahwa, R.; Lyons, K. E. *Curr. Opin. Neurol.* **2014**, *27*, 442-449.

(33) Lin, R.-D.; Hou, W.; Yen, K.; Lee, M. *Phytomedicine* **2003**, *10*, 650-656.

(34) Fernandes, M.; Soares-da-Silva, P. *Acta Physiol. Scand.* **1992**, *145*, 363-365.

(35) Saura, J.; Kettler, R.; Da Prada, M.; Richards, J. *J. Neurosci.* **1992**, *12*, 1977-1999.

(36) Saura, J.; Andres, N.; Andrade, C.; Ojuel, J.; Eriksson, K.; Mahy, N. *Neurobiol. Aging* **1997**, *18*, 497-507.

(37) Damier, P.; Kastner, A.; Agid, Y.; Hirsch, E. C. *Neurology* **1996**, *46*, 1262-1262.

(38) Hauser, R. A.; Panisset, M.; Abbruzzese, G.; Mancione, L.; Dronamraju, N.; Kakarieka, A. *Mov. Disord.* **2009**, *24*, 541-550.

(39) Stocchi, F.; Rascol, O.; Kieburtz, K.; Poewe, W.; Jankovic, J.; Tolosa, E.; Barone, P.; Lang, A. E.; Olanow, C. W. *Ann. Neurol.* **2010**, *68*, 18-27.

(40) Hauser, R. A.; Schapira, A. H.; Rascol, O.; Barone, P.; Mizuno, Y.; Salin, L.; Haaksma, M.; Juhel, N.; Poewe, W. *Mov. Disord.* **2010**, *25*, 2542-2549.

(41) Adler, C.; Sethi, K.; Hauser, R.; Davis, T.; Hammerstad, J.; Bertoni, J.; Taylor, R.; Sanchez-Ramos, J.; O'Brien, C. *Neurology* **1997**, *49*, 393-399.

(42) Group, P. S. *Arch. Neurol.* **2003**, *60*, 1721.

(43) Pålhagen, S.; Heinonen, E.; Hägglund, J.; Kaugesaar, T.; Kontants, H.; Mäki-Ikola, O.; Palm, R.; Turunen, J. *Neurology* **1998**, *51*, 520-525.

(44) Hauser, R. A.; Lew, M. F.; Hurtig, H. I.; Ondo, W. G.; Wojcieszek, J.; Fitzer-Attas, C. J. *Mov. Disord.* **2009**, *24*, 564-573.

(45) Group, P. S. *Arch. Neurol.* **2002**, *59*, 1937.

(46) Shoulson, I. *Acta Neurol. Scand.* **1989**, *80*, 171-175.

(47) Jankovic, J.; Stacy, M. *CNS drugs* **2007**, *21*, 677-692.

(48) Hauser, R. A.; Hsu, A.; Kell, S.; Espay, A. J.; Sethi, K.; Stacy, M.; Ondo, W.; O'Connell, M.; Gupta, S. *Lancet Neurol.* **2013**, *12*, 346-356.

(49) Fox, S. H.; Katzenschlager, R.; Lim, S. Y.; Ravina, B.; Seppi, K.; Coelho, M.; Poewe, W.; Rascol, O.; Goetz, C. G.; Sampaio, C. *Mov. Disord.* **2011**, *26*, S2-S41.

(50) Del Dotto, P.; Pavese, N.; Gambaccini, G.; Bernardini, S.; Metman, L. V.; Chase, T. N.; Bonuccelli, U. *Mov. Disord.* **2001**, *16*, 515-520.

(51) Poewe, W.; Lees, A.; Stern, G. *Ann. Neurol.* **1988**, *23*, 73-78.

(52) Rodnitzky, R. L.; Narayanan, N. S. *Neurology* **2014**, *82*, 288-289.

(53) Emre, M.; Aarsland, D.; Albanese, A.; Byrne, E. J.; Deuschl, G.; De Deyn, P. P.; Durif, F.; Kulisevsky, J.; van Laar, T.; Lees, A. *N. Engl. J. Med.* **2004**, *351*, 2509-2518.

(54) Pascolutti, M.; Campitelli, M.; Nguyen, B.; Pham, N.; Gorse, A. D.; Quinn, R. J. *PLoS One* **2015**, *10*, e0120942.

(55) Harvey, A. L. *Drug Discov. Today* **2008**, *13*, 894-901.

(56) Newman, D. J.; Cragg, G. M. *J. Nat. Prod.* **2012**, *75*, 311-335.

(57) Hussian, G.; Manyam, B. V. *Phytother. Res.* **1997**, *11*, 419-423.

(58) Manyam, B. V.; Dhanasekaran, M.; Hare, T. A. *Phytother. Res.* **2004**, *18*, 97-101.

(59) Hickey, P.; Stacy, M. *Drug Des. Devel. Ther.* **2011**, *5*, 241.

(60) Djaldetti, R.; Giladi, N.; Hassin-Baer, S.; Shabtai, H.; Melamed, E. *Clin. Neuropharmacol.* **2003**, *26*, 322-326.

(61) Robinson, T. In *The Biochemistry of Alkaloids*; Springer: 1981, p 20-34.

(62) Al-Motarreb, A.; Baker, K.; Broadley, K. J. *Phytother. Res.* **2002**, *16*, 403-413.

(63) Zelger, J.; Schorno, H. X.; Carlini, E. *Bull. Narc.* **1980**, *32*, 67-81.

(64) Pehek, E. A.; Schechter, M.; Yamamoto, B. *Neuropharmacology* **1990**, *29*, 1171-1176.

(65) Mann, J. *Murder, magic, and medicine*; Oxford University Press, USA, 2000.

(66) Tudzynski, P.; Hölter, K.; Correia, T.; Arntz, C.; Grammel, N.; Keller, U. *Mol. Gen. Genet.* **1999**, *261*, 133-141.

(67) Matossian, M. K. *Poisons of the past: molds, epidemics, and history*; Yale University Press, 1991.

(68) Van Camp, G.; Flamez, A.; Cosyns, B.; Weytjens, C.; Muyldermans, L.; Van Zandijcke, M.; De Sutter, J.; Santens, P.; Decoodt, P.; Moerman, C. *Lancet* **2004**, *363*, 1179-1183.

(69) Pastor, P.; Tolosa, E. *Neurologia (Barcelona, Spain)* **2003**, *18*, 202-209.

(70) Bonuccelli, U. *Curr. Opin. Neurol.* **2003**, *16*, S13-S19.

(71) Sit, S. *Curr. Pharm. Des.* **2000**, *6*, 1211-1248.

(72) Phillipson, J. D.; Handa, S. *Phytochemistry* **1975**, *14*, 999-1003.

(73) Hiranita, T.; Kohut, S. J.; Soto, P. L.; Tanda, G.; Kopajtic, T. A.; Katz, J. L. *J. Pharmacol. Exp. Ther.* **2014**, *348*, 174-191.

(74) Fischman, A. J.; Bonab, A. A.; Babich, J. W.; Palmer, E. P.; Alpert, N. M.; Elmaleh, D. R.; Callahan, R. J.; Barrow, S. A.; Graham, W.; Meltzer, P. C. *Synapse* **1998**, *29*, 128-141.

(75) Food, U.; Administration, D. *Further information available at: http://www. fda. gov/cder/rdmt/nmecy2004. htm (accessed November 2007)* **2008**.

(76) Melzig, M. F.; Putscher, I.; Henklein, P.; Haber, H. *J. Ethnopharmacol.* **2000**, *73*, 153-159.

(77) Antkiewicz-Michaluk, L.; Wardas, J.; Michaluk, J.; Romanska, I.; Bojarski, A.; Vetulani, J. *Int. J. Neuropsychopharmacol.* **2004**, *7*, 155-163.

(78) Kodani, S.; Imoto, A.; Mitsutani, A.; Murakami, M. *J. Appl. Phycol.* **2002**, *14*, 109-114.

(79) Li, S.; Teng, L.; Liu, W.; Cheng, X.; Jiang, B.; Wang, Z.; Wang, C.-h. *Pharm. Biol.* **2015**, 1-14.

(80) Schwarz, M.; Houghton, P.; Rose, S.; Jenner, P.; Lees, A. *Pharmacol. Biochem. Behav.* **2003**, *75*, 627-633.

(81) Bartlett, M.; Dickel, D.; Taylor, W. *J. Am. Chem. Soc.* **1958**, *80*, 126-136.

(82) Harsing Jr, L.; Sershen, H.; Lajtha, A. *J. Neural. Transm. Gen. Sect.* **1994**, *96*, 215-225.

(83) KASE, H.; IWAHASHI, K.; MATSUDA, Y. *J. Antibiot.* **1986**, *39*, 1059-1065.

(84) Saporito, M. S.; Hudkins, R. L.; Maroney, A. C. *Prog. Med. Chem.* **2002**, *40*, 23-62.

(85) Investigators, P. S. G. P. *Neurology* **2007**, *69*, 1480-1490.

(86) Kum, W. F.; Durairajan, S. S. K.; Bian, Z. X.; Man, S. C.; Lam, Y. C.; Xie, L. X.; Lu, J. H.; Wang, Y.; Huang, X. Z.; Li, M. *Evid. Based Complement. Alternat. Med.* **2011**, *2011*.

(87) De Caires, S.; Steenkamp, V. *Phytother. Res.* **2010**, *24*, 1265-1270.

(88) Lu, J.-H.; Tan, J.-Q.; Durairajan, S. S. K.; Liu, L.-F.; Zhang, Z.-H.; Ma, L.; Shen, H.-M.; Chan, H. E.; Li, M. *Autophagy* **2012**, *8*, 98-108.

(89) Elbaz, A.; Moisan, F. *Curr. Opin. Neurol.* **2008**, *21*, 454-460.

(90) Jankovic, J. *Ann. Neurol.* **2008**, *63*, 267-269.

(91) LeWitt, P. A.; Guttman, M.; Tetrud, J. W.; Tuite, P. J.; Mori, A.; Chaikin, P.; Sussman, N. M. *Ann. Neurol.* **2008**, *63*, 295-302.

(92) Fowler, J. S.; Volkow, N. D.; Wang, G.-J.; Pappas, N.; Logan, J.; Shea, C.; Alexoff, D.; MacGregor, R. R.; Schlyer, D. J.; Zezulkova, I. *Proc. Natl. Acad. Sci. U. S. A.* **1996**, *93*, 14065-14069.

(93) Bladt, S.; Wagner, H. *Nervenheilkunde* **1993**, *12*, 349-352.

(94) Gasiorowski, K.; Lamer-Zarawska, E.; Leszek, J.; Parvathaneni, K.; Bhushan Yendluri, B.; Blach-Olszewska, Z.; Aliev, G. *CNS Neurol. Disord. Drug Targets* **2011**, *10*, 184-191.

(95) Bergeron, C.; Gafner, S.; Clausen, E.; Carrier, D. J. *J. Agric. Food. Chem.* **2005**, *53*, 3076-3080.

(96) Cheng, Y.; He, G.; Mu, X.; Zhang, T.; Li, X.; Hu, J.; Xu, B.; Du, G. *Neurosci. Lett.* **2008**, *441*, 16-20.

(97) Sloley, B.; Urichuk, L.; Morley, P.; Durkin, J.; Shan, J.; Pang, P.; Coutts, R. *J. Pharm. Pharmacol.* **2000**, *52*, 451-459.

(98) Singh, A.; Naidu, P. S.; Kulkarni, S. K. *Pharmacology* **2003**, *68*, 81-88.

(99) Naidu, P.; Kulkarni, S. *Methods Find. Exp. Clin. Pharmacol.* **2004**, *26*, 323-326.

(100) Datla, K.; Christidou, M.; Widmer, W.; Rooparai, H.; Dexter, D. In *Br. J. Pharmacol.*; Nature Publishing Group Macmillan Building, 4 Crinan St, London N1 9XW, England: 2002; Vol. 135.

(101) Levites, Y.; Weinreb, O.; Maor, G.; Youdim, M. B.; Mandel, S. *J. Neurochem.* **2001**, *78*, 1073-1082.

(102) Mandel, S.; Weinreb, O.; Amit, T.; Youdim, M. B. *J. Neurochem.* **2004**, *88*, 1555-1569.

(103) Fazala, S. S.; Ansarib, M. M.; Singlac, R. K.; Khand, S. *Indo Glob. J. Pharm. Sci* **2012**, *2*, 258-261.

(104) Xiong, N.; Huang, J.; Chen, C.; Zhao, Y.; Zhang, Z.; Jia, M.; Zhang, Z.; Hou, L.; Yang, H.; Cao, X. *Neurobiol. Aging* **2012**, *33*, 1777-1791.

(105) He, W.; Zhou, W.; Hu, Z. *Neural Regener. Res.* **2011**, *6*.

(106) Eyres, L. *Food New Zealand* **2010**, *10*, 31.

(107) Schneider, J. S.; Sendek, S.; Daskalakis, C.; Cambi, F. *J. Neurol. Sci.* **2010**, *292*, 45-51.

(108) Wenger, R. M. *Helv. Chim. Acta* **1984**, *67*, 502-525.

(109) Kaminska, B.; Gaweda-Walerych, K.; Zawadzka, M. *J. Cell. Mol. Med.* **2004**, *8*, 45-58.

(110) Quinn, R. J.; Carroll, A. R.; Pham, N. B.; Baron, P.; Palframan, M. E.; Suraweera, L.; Pierens, G. K.; Muresan, S. *J. Nat. Prod.* **2008**, *71*, 464-468.

(111) Leeson, P. *Nature* **2012**, *481*, 455-456.

(112) Proudfoot, J. R. *Bioorg. Med. Chem. Lett.* **2002**, *12*, 1647-1650.

(113) Ganesan, A. *Curr. Opin. Chem. Biol.* **2008**, *12*, 306-317.

(114) Lipinski, C. A.; Lombardo, F.; Dominy, B. W.; Feeney, P. J. *Adv. Drug Deliv. Rev.* **2012**, *64*, 4-17.

(115) Instant JChem, version 15.10.26.10; ChemAxon Kft: Budapest, Hungary, 2015.

(116) Sarker, S.; Latif, Z.; Gray, A. In *Natural Products Isolation*; Sarker, S., Latif, Z., Gray, A., Eds.; Humana Press: 2005; Vol. 20, p 1-25.

(117) Hong, J. *Curr. Opin. Chem. Biol.* **2011**, *15*, 350-354.

(118) Carlson, E. E. *ACS Chem. Biol.* **2010**, *5*, 639-653.

(119) Harvey, A. L.; Edrada-Ebel, R.; Quinn, R. J. *Nat. Rev. Drug Discov.* **2015**, *14*, 111-129.

(120) Camp, D.; Davis, R. A.; Campitelli, M.; Ebdon, J.; Quinn, R. J. *J. Nat. Prod.* **2011**, *75*, 72-81.

(121) Tamura, M.; Takahashi, A.; Uyama, A.; Mochizuki, N. *Toxins (Basel)* **2012**, *4*, 476-486.

(122) Yoon, I. S.; Au, Q.; Barber, J. R.; Ng, S. C.; Zhang, B. *Anal. Biochem.* **2010**, *407*, 205-210.

(123) Dauer, W.; Przedborski, S. *Neuron* **2003**, *39*, 889-909.

(124) Sherer, T. B.; Betarbet, R.; Testa, C. M.; Seo, B. B.; Richardson, J. R.; Kim, J. H.; Miller, G. W.; Yagi, T.; Matsuno-Yagi, A.; Greenamyre, J. T. *J. Neurosci.* **2003**, *23*, 10756-10764.

(125) Ayala, A.; Venero, J. L.; Cano, J.; Machado, A. *Front. Biosci.* **2007**, *12*, 986-1007.

(126) Betarbet, R.; Sherer, T. B.; MacKenzie, G.; Garcia-Osuna, M.; Panov, A. V.; Greenamyre, J. T. *Nat. Neurosci.* **2000**, *3*, 1301-1306.

(127) Thiffault, C.; Langston, J. W.; Di Monte, D. A. *Brain Res.* **2000**, *885*, 283-288.

(128) Sherer, T. B.; Kim, J.-H.; Betarbet, R.; Greenamyre, J. T. *Exp. Neurol.* **2003**, *179*, 9-16.

(129) Uversky, V. N.; Li, J.; Fink, A. L. *FEBS Lett.* **2001**, *500*, 105-108.

(130) Lee, H.-J.; Shin, S. Y.; Choi, C.; Lee, Y. H.; Lee, S.-J. *J. Biol. Chem.* **2002**, *277*, 5411-5417.

(131) Sherer, T. B.; Betarbet, R.; Stout, A. K.; Lund, S.; Baptista, M.; Panov, A. V.; Cookson, M. R.; Greenamyre, J. T. *J. Neurosci.* **2002**, *22*, 7006-7015.

(132) Mackay-Sim, A. *Stem cells* **2012**, *30*, 2361-2365.

(133) Matigian, N.; Abrahamsen, G.; Sutharsan, R.; Cook, A. L.; Vitale, A. M.; Nouwens, A.; Bellette, B.; An, J.; Anderson, M.; Beckhouse, A. G. *Dis. Model. Mech.* **2010**, *3*, 785-798.

(134) Macarron, R.; Banks, M. N.; Bojanic, D.; Burns, D. J.; Cirovic, D. A.; Garyantes, T.; Green, D. V.; Hertzberg, R. P.; Janzen, W. P.; Paslay, J. W. *Nat. Rev. Drug Discov.* **2011**, *10*, 188-195.

(135) Swinney, D. C.; Anthony, J. *Nat. Rev. Drug Discov.* **2011**, *10*, 507-519.

(136) Kotz, J. *SciBX: Science-Business eXchange* **2012**, *5*.

(137) Haney, S. A. *High Content Screening: Science, Techniques and Applications*; John Wiley & Sons, 2008.

(138) Wheeler, G. N.; Field, R. A.; Tomlinson, M. L. *Chemical Genomics* **2012**, 121.

(139) Insa, R.; Wiley Online Library: 2013.

(140) Lee, J. A.; Uhlik, M. T.; Moxham, C. M.; Tomandl, D.; Sall, D. J. *J. Med. Chem.* **2012**, *55*, 4527-4538.

(141) Hellerstein, M. K. *Metab. Eng.* **2008**, *10*, 1-9.

(142) Lang, G.; Mayhudin, N. A.; Mitova, M. I.; Sun, L.; van der Sar, S.; Blunt, J. W.; Cole, A. L.; Ellis, G.; Laatsch, H.; Munro, M. H. *J. Nat. Prod.* **2008**, *71*, 1595-1599.

(143) Saporito, M. S.; Reaume, A. G. *Drug Discov. Today Ther. Strateg.* **2012**, *8*, 89-95.

Chapter Two. A Grand Challenge (I): Unbiased Phenotypic Function of Metabolites from *Jaspis splendens* against Parkinson's Disease

Dongdong Wang,[†] Yunjiang Feng,[†] Mariyam Murtaza,[†] Stephen A. Wood,[†] George D. Mellick,[†] John N. A. Hooper[‡] and Ronald J. Quinn[†,*]

[†]Eskitis Institute for Drug Discovery, Griffith University, Brisbane, QLD 4111, Australia

[‡]Queensland Museum, South Brisbane, QLD 4101, Australia

ABSTRACT

A grand challenge in natural product chemistry is to determine the biological effects of all natural products. A phenotypic approach is frequently used for determining the activity of a compound and its potential impact on a disease state. Chemical investigation of a specimen of *Jaspis splendens* collected from the Great Barrier Reef resulted in the isolation of a new pterin derivative, jaspterin (**1**), a new bisindole alkaloid, splendamide (**2**) and a new imidazole alkaloid, jaspnin A (**3**) TFA salt. Jaspamycin (**8**) and 6-bromo-1*H*-indole-3-amidine (**16**) are reported for the first time as naturally occurring metabolites. Known nucleosides (**4**-**7**, **9**, **10**), aglycones (**11**-**13**), indole alkaloids (**14**, **15**, **17**), and jaspamide peptides (**18**-**22**) were also isolated. The structures of the three new compounds **1-3** were unambiguously elucidated based on NMR and mass spectroscopic data. Jaspnin A (**3**) contained a rare thiomethylated imidazolinium unit. Jaspamycin (**8**) and 6-bromo-1*H*-indole-3-amidine (**16**) are reported for the first time as naturally occurring metabolites. Coupling an unbiased phenotypic assay using a human olfactory neurosphere-derived cell model of Parkinson's disease to all of the natural products from the species *J. splendens* allowed the phenotypic profiles of the metabolites to be investigated.

INTRODUCTION

A grand challenge in natural product chemistry is to determine the biological effects of all natural products. Target-based drug discovery approaches provide efficient and high capacity in testing unprecedented numbers of compounds and molecular targets utilizing advances in automation, biochemistry, structural biology, and chemistry related technologies.[1] High throughput screening (HTS), however, has lower hit rates. Target screening also heavily relies on knowledge of known therapeutic pathways. In addition, other pathways or functional proteins affected by compounds may not be identified by target based screening. New molecular entities identified by phenotypic screening approved by the FDA outnumbered target-based approaches during this time frame between 1999 and 2008 (37% versus 23%).[2] In comparison, phenotypic screening has the advantage of the whole organism being exposed to compounds and interrogates all targets and biological pathways. When multiple parameters are examined, a multidimensional cytological profiling method can be used to cluster compounds. Parkinson's disease is the second most common neurodegenerative disease, affecting over five million patients worldwide[3] and in the majority of cases has no clearly identifiable cause. Like Alzheimer's disease, it mostly affects the elderly and causes considerable disability and suffering. There is no effective drug available to cure this progressive disease. Thus, there is an urgent need to develop new therapeutic agents. Nontransformed and nonimmortalized human olfactory neurosphere-derived (hONS) cells, which are primary cells derived from Parkinson's disease patients, model functional aspects of Parkinson's disease.[4-6] Coupling an unbiased phenotypic assay using the hONS cell model of Parkinson's disease to an analysis of all natural products from one species could allow phenotypic profiles of all the metabolites to be investigated.

As part of a research program aiming to identify anti-Parkinson's disease lead

compounds, a marine sponge, *Jaspis splendens*, collected from the Great Barrier Reef was selected from Nature Bank.[7-9] Sponges of the genus *Jaspis* (family Ancorinidae) have been a rich source of structurally novel, biologically active natural products.[10] Over 150 natural products have been isolated from the genus including antifungal, anthelmintic, catatonic, insecticidal and ichthyotoxic jaspamide peptides,[11-13] antineoplastic and cytotoxic isomalabaricane triterpenes,[14-16] cytotoxic macrolides,[17] antifungal, antiparasitic and cytotoxic bengazoles,[18,19] antiparasitic, antimicrobial and cytotoxic bengamides,[20-22] cytotoxic bromotyrosine derivatives,[23,24] anticandidal and cytotoxic nucleosides[25] and a series of dihydroxystyrene sulphate derivatives.[26-28]

Chemical investigation of a specimen of *J. splendens* resulted in the isolation and characterization of 22 secondary metabolites, including a new pterin derivative, jaspterin (**1**), a new bisindole alkaloid, splendamide (**2**), a new methylthioimidazole containing alkaloid, jaspnin A (**3**) trifluoroacetic acid (TFA) salt and two naturally new products jaspamycin (**8**) and 6-bromo-1*H*-indole-3-amidine (**16**), previously reported as synthesis products,[29] together with 17 known natural products, namely guanosine (**4**),[30] 6-deoxyguanosine (**5**),[31] thymidine (**6**),[32] toyocamycin (**7**),[25] 5-(methoxycarbonyl)tubercidin (**9**),[25] sangivamycin (**10**),[33] 5-(methoxycarbonyl)tubercidin aglycone (**11**),[25] toyocamycin aglycone (**12**),[25] sangivamycin aglycone (**13**),[34] 6-bromotryptamine (**14**),[35] 6-bromo-1*H*-indole-3-carboxamide (**15**),[36] 6-bromo-1*H*-indole-3-carboxylic acid methyl ester (**17**),[37] jaspamide (**18**),[38] jasplakinolide B (**19**),[39] jaspamide Z_1 (**20**),[40] jasplakinolide F (**21**),[11] and pipestelide A (**22**).[41]

All compounds were subjected to an unbiased phenotypic assay on hONS cells followed by cluster analysis of cytological effects. Based on previous work, we had developed a theoretical framework that explains that all natural products interact with biologically relevant space.[42,43] Herein we report the isolation and structure elucidation of the five new

natural compounds (**1, 2**, **3**, **8** and **16**) as well as the phenotypic effects of all isolated natural products from *J. splendens*.

RESULTS AND DISCUSSION

The ground and freeze-dried *J. splendens* (50 g) was sequentially extracted with *n*-hexane, CH_2Cl_2 and MeOH. The CH_2Cl_2/MeOH extracts were combined and fractionated using a C_{18} bonded silica flash column and a stepwise H_2O/MeOH/0.1%TFA gradient. Five fractions were collected by eluting with H_2O, 90% H_2O/10% MeOH, 50% H_2O/50% MeOH, 10% H_2O/90% MeOH and MeOH, respectively (each containing 0.1% TFA). Further purification of the 90% H_2O/10% MeOH fraction by C_{18} bonded silica HPLC (gradient H_2O/MeOH with 0.1% TFA) resulted in the isolation of three new metabolites, namely jaspterin (**1**), jaspnin A (**3**) TFA salt and jaspamycin (**8**), together with nucleosides (**4**-**7**, **9**, **10**), and aglycones (**11**-**13**). Previous studies of indole alkaloids by our group have revealed that the exchangeable NH proton typically manifests between δ_H 10.0 and 12.0 in deuterated DMSO.[44,45] The ^{1}H NMR spectrum in DMSO-d_6 of the 50% H_2O/50% MeOH fraction displayed exchangeable NH proton signals between δ_H 10.00 and 12.00 together with aromatic signals between δ_H 7.00 and 8.50, indicating the presence of indole alkaloids. HPLC purification of the fraction yielded a new bisindole alkaloid, splendamide (**2**) and a new indole alkaloid 6-bromo-1*H*-indole-3-amidine (**16**), along with three known indole alkaloids (**14**, **15**, **17**). The ^{1}H-NMR spectrum of the 10% H_2O/90% MeOH fraction contained some intriguing signals indicative of peptidic type molecules. Further purification of the fraction led to the isolation of five jaspamide peptides (**18**-**22**). In total, 22 structurally diverse natural products were isolated from the prolific sponge *J. splendens*.

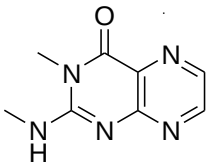

1

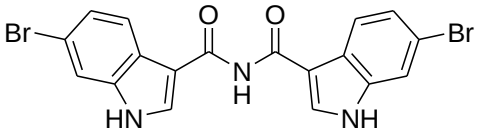

2

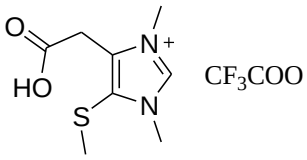

3

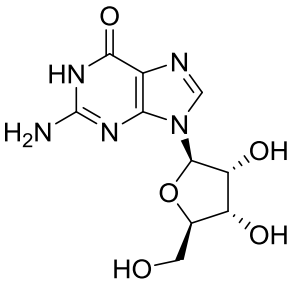

4

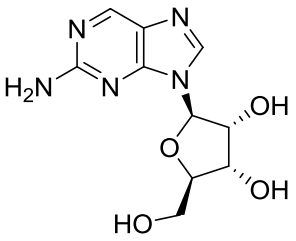

5

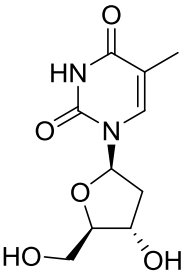

6

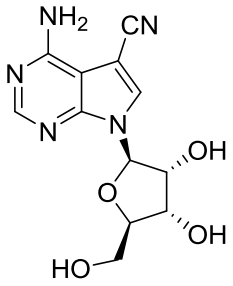

7

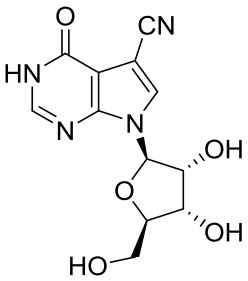

8

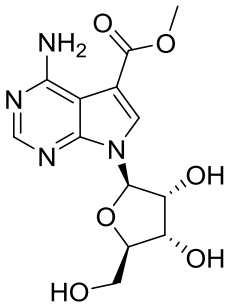

9

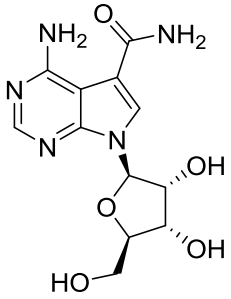

10

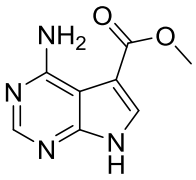

11

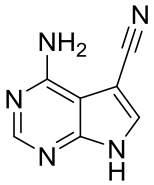

12

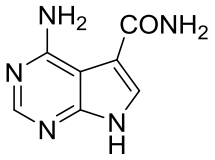

13

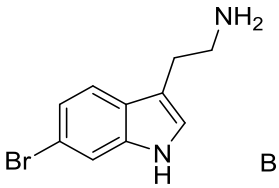

14

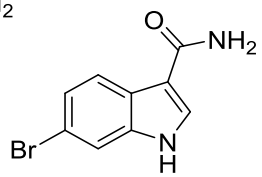

15

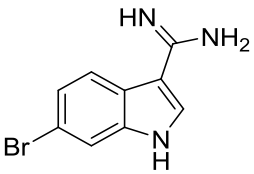

16

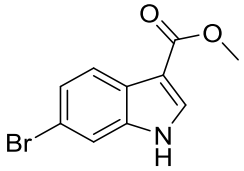

17

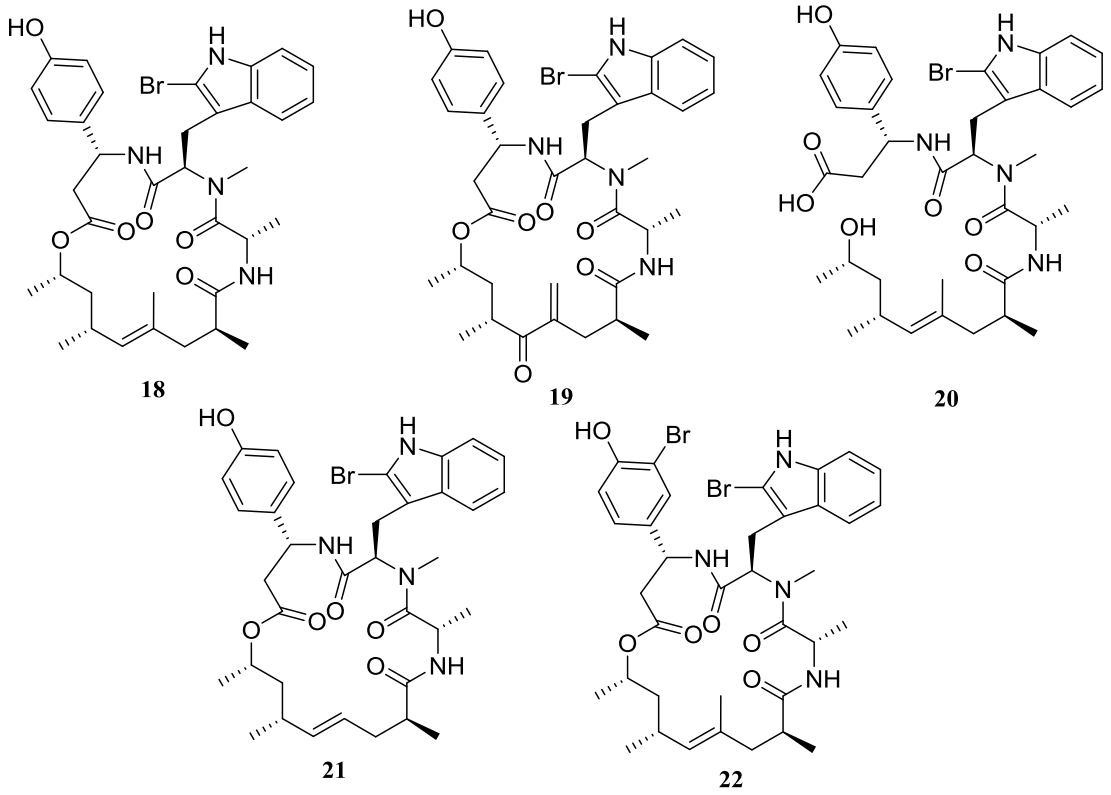

Jaspterin (**1**) was isolated as a white power. (+)-HRESIMS data gave a $[M+Na]^+$ ion at *m*/*z* 214.0670, which was consistent with a molecular formula of $C_8H_9N_5O$ with seven degrees of unsaturation. The IR spectrum had absorption bands at 1680 and 1630 cm^{-1}, suggesting carbonyl functionalities in the molecule. The ^1H NMR spectrum included two deshielded aromatic doublets (δ_H 8.68 and 8.40), one methyl singlet (δ_H 3.40), one methyl doublet (δ_H 2.96) and one broad exchangeable doublet (δ_H 7.54) (Table 1). Analysis of the HSQC and HMBC spectra indicated that the molecule contained one amide carbonyl signal (δ_C 160.7), five aromatic carbons (δ_C 155.2, 153.3, 149.5, 139.0, and128.1), and two methyl carbons (δ_C 28.5 and 28.2). The chemical shifts of the two methyls (δ_H 3.40 and δ_C 28.2, δ_H 2.96 and δ_C 28.5) indicated that they were both *N*-methyl groups.

The UV spectrum of **1** showed absorption maxima at 280 and 358 nm (broad), indicative of a pyrazine moiety. The small coupling constant (*J* 1.5 Hz) between the two methine doublets (δ_H 8.48 and 8.68) and their deshielded carbon chemical shifts (δ_C 139.0 and 149.5) suggested the two protons belonged to H-6 and H-7 in the pyrazine moiety. HMBC

correlations from H-6 (δ_H 8.48) to C-4a and C-7 (δ_C 128.1 and 149.5), and from H-7 (δ_H 8.68) to C-6 and C-8a (δ_C 139.0 and 155.2) confirmed the assignment. HMBC correlations were observed from the aminomethyl protons to the nonprotonated carbon (δ_C 153.3), suggesting the CH_3NH- functionality was attached at the C-2 position. Further HMBC correlations from the second *N*-methyl (δ_H 3.40) to the same nonprotonated carbon (δ_C 153.3) as well as an amide carbonyl carbon (δ_C 160.7) indicated an isocytosine moiety. With all the atoms accounted for and the degrees of unsaturation satisfied, the structure of **1** was established (Figure 1).

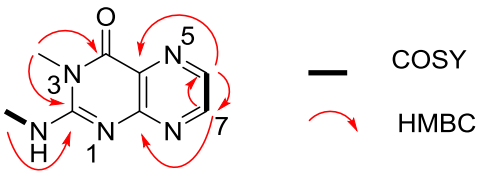

Figure 1. Key COSY and HMBC correlations for **1**

Jaspterin (**1**) closely resembles pterins, a class of naturally occurring compounds biosynthesized from guanosine triphosphate (GTP) in all living organisms.[46] Pterins were first discovered in the pigments of butterfly wings. Biopterin and neopterin were also reported from human urine.[46,47] This class of compounds plays an important role in amino acid hydroxylation and they also act as cofactors in enzyme catalysis. In the field of heterocyclic chemistry pterins owe their exceptional position mainly to their unusual chemical properties and their conspicuous fluorescence.

Table 1. NMR Spectroscopic Data (600 MHz for ^{1}H and 150MHz for ^{13}C, DMSO-d_6) for **1**

position	δ_C, type	δ_H, mult. (*J* in Hz)	COSY	HMBC[a]
2	153.3, C			
4	160.7, C			
4a	128.1, C			
6	139.0, CH	8.40, d (1.5)	H-7	4a, 7
7	149.5, CH	8.68, d (1.5)	H-6	6, 8a
8a	155.2, C			
9-NH		7.54, d (5.0)	H-10	
10	28.5, CH_3	2.96, d (5.0)	NH	2
11	28.2, CH_3	3.40, s		2, 4

[a] HMBC correlations are from proton(s) stated to the indicated carbon.

Splendamide (**2**) was isolated as a colorless gum. (+)-LRESIMS for **2** displayed an isotopic cluster of ions $[M+H]^+$ at *m/z* 459, 461, and 463 in the ratio of 1:2:1, indicating the presence of two bromines. The adduct ion in the (+)-HRESIMS spectrum at *m/z* 481.9116 $[M+Na]^+$ allowed the molecular formula to be assigned as $C_{18}H_{11}{}^{79}Br_2N_3O_2$, which was consistent with 14 degrees of unsaturation. The IR spectrum had absorption bands at 1683 cm^{-1} indicating an amide functionality in the molecule. The ^1H NMR data (Table 2) contained four aromatic methines (δ_H 8.40, 8.06, 7.69 and 7.32) and two sharp exchangeable protons (δ_H 11.99 and 10.34). Analysis of the HSQC and HMBC spectra indicated the molecule contained a carbonyl carbon (δ_C 167.8) and eight aromatic carbons (δ_C 137.3, 132.2, 125.8, 123.8, 122.3, 114.9, 114.5 and 110.0).

The UV spectrum had absorption maxima at 216 nm and a broad band around 272 nm, indicative of an indole moiety. HMBC correlations from the NH (δ_H 11.99) to the methine carbon C-7 (δ_C 114.5) and the nonprotonated carbon C-3 (δ_C 110.0), and from the methine proton H-2 (δ_H 8.40) to the nonprotonated carbons C-3a and C-7a (δ_C 125.8 and 137.3) established the presence of 6-substituted indole-3-yl moiety (Figure 2). The assignment was confirmed by HMBC correlations from the methine proton H-4 (δ_H 8.06) to the nonprotonated carbons C-3, C-6 and C-7a (δ_C 110.0, 114.9 and 137.3), and from the methine proton H-7 (δ_H 7.69) to the methine carbon C-5 (δ_C 123.8) and the nonprotonated carbon C-3a (δ_C 125.8). A bromine substitution at position 6 was confirmed due to its carbon chemical shift (δ_C 114.9). Further HMBC correlations were observed from a methine proton (δ_H 8.40) and the second exchangeable proton (δ_H 10.34) to a carbonyl carbon (δ_C 167.8), indicating an amide group at the C-3 position. So far only half of the molecular formula was accounted for. On the basis of the observation of a relatively deshielded chemical shift of the amide proton (δ_H 10.34) together with its integration as half a proton compared with other proton signals, and the requirement of 14 degrees of unsaturation, **2** was assigned as a dimeric imide structure (Figure 2).

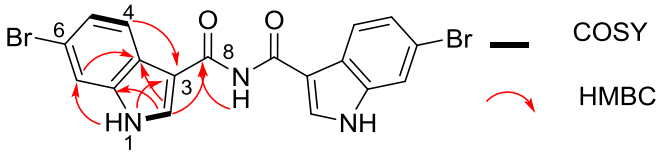

Figure 2. Key COSY and HMBC correlations for **2**.

Table 2. NMR Spectroscopic Data (600 MHz for ^{1}H and 150MHz for ^{13}C, DMSO-d_6) for **2**

position	δ_C, type	δ_H, mult. (*J* in Hz)	COSY	HMBC[a]
1, 1'		11.99, bs	H-2, H-2'	3a, 3a', 7, 7'
2, 2'	132.2, CH	8.40, d (3.0)	H-1, H-1'	3, 3', 3a, 3a', 7a, 7a', 8, 8'
3, 3'	110.0, C			
3a, 3a'	125.8, C			
4, 4'	122.3, CH	8.06, d (8.5)	H-5, H-5'	3, 3', 6, 6', 7a, 7a'
5, 5'	123.8, CH	7.32, dd (1.8, 8.5)	H-4, H-7, H-4', H-7'	3a, 3a', 7, 7', 7a, 7a'
6, 6'	114.9, C			
7, 7'	114.5, CH	7.69, d (1.8)	H-5, H-5'	3a, 3a', 5, 5', 7a, 7a'
7a, 7a'	137.3, C			
8, 8'	167.8, C			
9		10.34, s		8, 8'

[a] HMBC correlations are from proton(s) stated to the indicated carbon.

Indole-3-carboximidamides are rarely encountered in nature. Wuzhuyurutine A from *Evodia rutaecarpa* (Juss.) Benth. (Rutaceae),[48] and *N*-(aminocarbonyl)-1*H*-indole-3-carboxamide from the sponge *Zyzza massalis* [49] are the only natural products similar to splendamide (**2**). A number of more complex indole-3-carboximidamide containing natural products have been reported from marine sponges, including the cytotoxic and antifungal nortopsentins A-C (**23**-**25**) from *Spongosorites ruetzleri*,[50] and nortopsentin D (**26**) from a *Dragmacidon* sp.[51] (Figure 3)

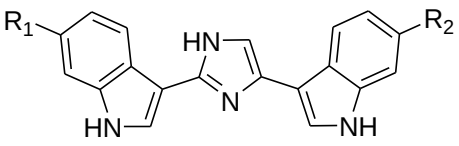

23. $R_1 = R_2 = Br$
24. $R_1 = Br$, $R_2 = H$
25. $R_1 = H$, $R_2 = Br$

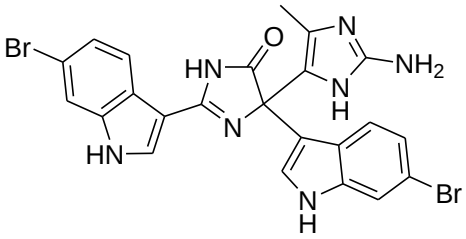

26

Figure 3. Chemical structures of nortopsentins A-D (**23**-**26**)

Jaspnin A (**3**) TFA salt was isolated as a white powder. (+)-HRESIMS measurement gave an adduct $[M+Na]^+$ ion at *m/z* 223.0511, consistent with a molecular formula of $C_8H_{12}N_2O_2S$ with four degrees of unsaturation. The IR spectrum had an absorption at 1660 cm^{-1}, suggesting a carbonyl functionality in the molecule. The UV spectrum had an absorption maximum at 208 nm and weak absorption at 244 nm, indicative of an imidazole moiety. The ^1H NMR data contained one aromatic singlet (δ_H 9.01), one methylene singlet (δ_H 4.01), and three methyl singlets (δ_H 3.97, 3.87 and 2.36) (Table 3). Five protonated carbons were identified in the HSQC and HMBC spectra. The chemical shifts of the two methyls (δ_H 3.97 and δ_C 33.0, δ_H 3.87 and δ_C 33.9) suggested that they were *N*-methyl groups. The third methyl singlet (δ_H 2.34 and δ_C 17.8) was either an aromatic, olefinic, or *S*-methyl. The chemical shifts of the methine functionality (δ_H 9.01 and δ_C 139.7) indicated a diheteroatom-substituted sp^2-hybridized methine.

HMBC correlations from the methine (δ_H 9.01) and the methylene (δ_H 4.01) protons to two aromatic nonprotonated carbons (δ_C 134.3 and 127.7) suggested the presence of a substituted imidazole moiety. Weak COSY correlations between the methine proton and two *N*-methyls indicated the presence of 1,3-dimethylimidazole. The assignment was confirmed by HMBC correlations from the two methyl singlets (δ_H 3.94 and 3.87) to the methine carbon (δ_C 139.7). An HMBC correlation from the methylene singlet (δ_H 4.01) to a carbonyl carbon (δ_C 170.7) suggested the presence of a carboxylic acid. The remaining elements were assigned a methyl thioether and its attachment at C-4 was established based on the HMBC correlation from the methyl singlet (δ_H 2.36) to carbon C-4 *(*δ_C 127.7). Jaspnin A was therefore assigned as **3** (Figure 4). Because TFA was used throughout the purification process, the counterion for jaspnin A (**3**) was trifluoroacetate.

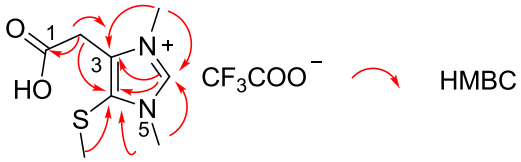

Figure 4. Key HMBC correlations for **3.**

Table 3. NMR Spectroscopic Data (600 MHz for ^{1}H and 150MHz for ^{13}C, CD_3OD) for **3**

position	δ_C, type	δ_H, mult. (*J* in Hz)	COSY	HMBC[a]
1	170.7, C			
2	28.9, CH_2	4.01, s		1, 3, 4
3	134.3, C			
4	127.7, C			
6	139.7, CH	9.01, s	N^5-CH_3, N^7-CH_3	3, 4
4-SCH_3	17.8, CH_3	2.36, s		4
5-NCH_3	33.0, CH_3	3.97, s	H_6	4, 6
7-NCH_3	33.9, CH_3	3.87, s	H_6	3, 6

[a] HMBC correlations are from proton(s) stated to the indicated carbon.

A number of methylthioimidazole containing natural products have been reported in the literature, including dysideanin A (**27**) from *Dysidea* sp.,[53] reticulatins A and B from *Hyrtios reticulatus*.,[52,53] leptoclinidamine C (**28**) from *Leptoclinides durus*,[54] didemnolines A-D from *Didemnum* sp.,[55] hyrtiomanzamine from *Hyrtios erecta*,[56] dragmacidonamines A and B from *Dragmacidon* sp.,[57] and gesashidine A from a *Thorectidae* sponge (Figure 5).[58]

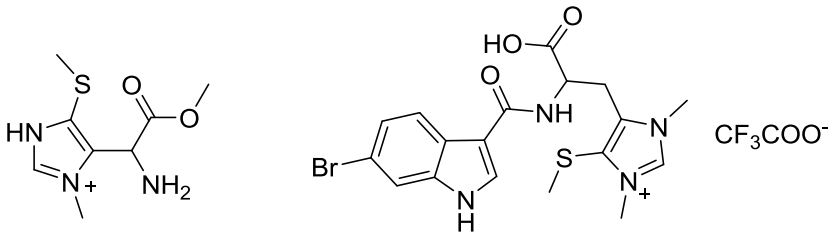

27 **28**

Figure 5. Chemical structures of dysideanin A (**27**) and leptoclinidamine C (**28**)

Jaspamycin (**8**) and 6-bromo-1*H*-indole-3-amidine (**16**) have been previously reported as synthetic products, the spectra were identical with the data in the literature.[29] 6-Bromo-1*H*-indole-3-amidine (**16**) is commercial source from Aurora Building Blocks. The 1D and 2D NMR data for **8** and **16** are given in the Supporting Information.

Consistent with the extraction and fractionation protocol developed in-house to prepare a Nature Bank fraction library targeting drug-like molecules, the isolated compounds were distributed within this lead-like space (five fractions in Figure 6).[8,59] The physicochemical property calculations using Instant JChem (version 15.7.27.0) are in the Supporting Information.[60]

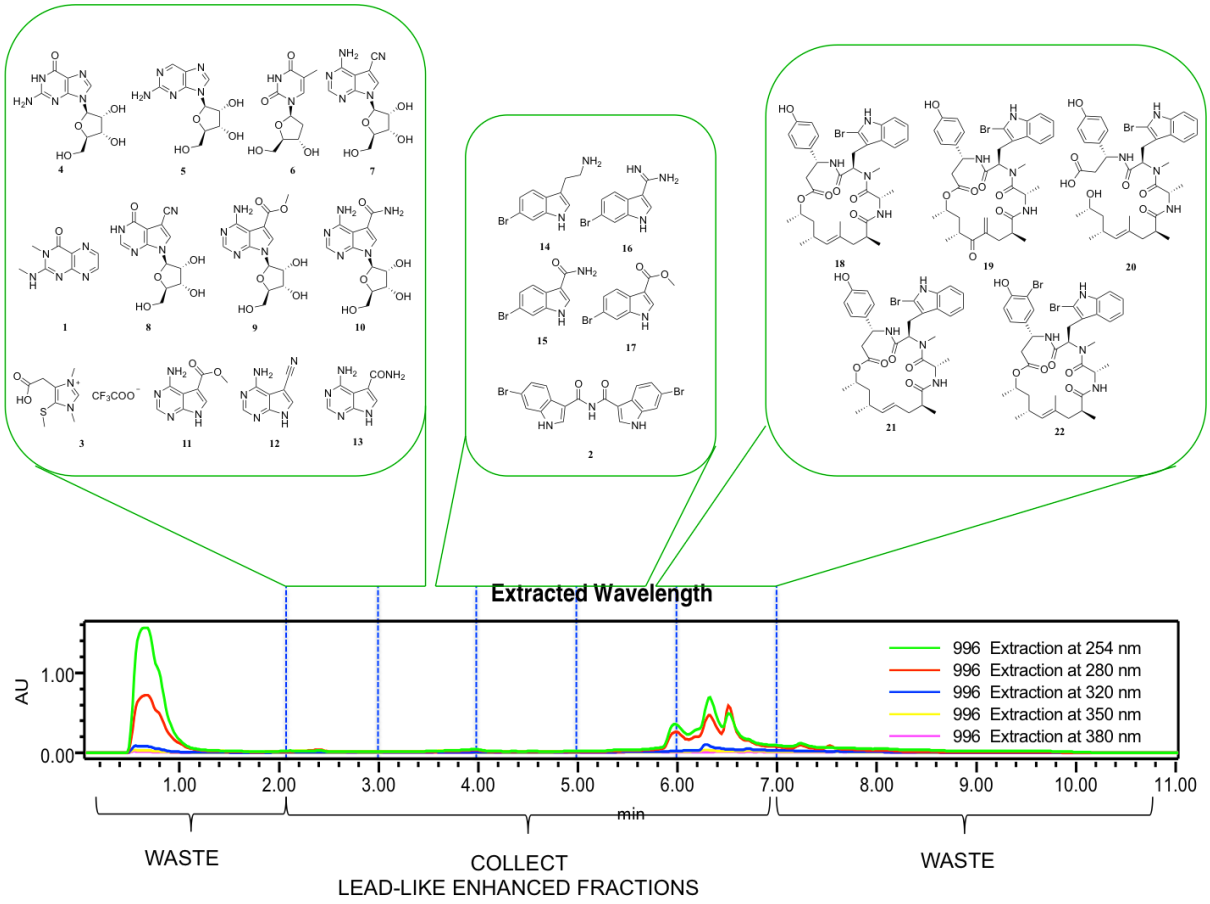

Figure 6. HPLC chromatogram of lead-like enhanced extract of the marine species *Jaspis splendens* and chemical structures isolated from different lead-like enhanced fractions.

The cytological profiles of the 22 metabolites from *J. splendens* were examined to identify congeneric chemical series by coupling an unbiased multidimensional phenotype assay using nontransformed and nonimmortalized hONS cells, which are primary cells derived from a Parkinson's disease patient. hONS cells were treated with 10 µM of each compound for 24 h. Cytological parameters were assessed by staining with fluorescent probes targeting various cellular pathways and organelles implicated in Parkinson's disease. These included

mitochondria, early endosomes, lysosomes, microtubule-based cytoskeleton, and autophagosomes. In total, 38 phenotypic features across the individual cell line were generated. The compounds were subsequently clustered based on their pairwise Pearson's correlation coefficient using Cluster 3.0 and visualized using Java TreeView (Figure 7). At the concentration of 10 µM, compounds **18**, **19**, **21** and **22** showed cytotoxicity, hence they were not included in the heat map.

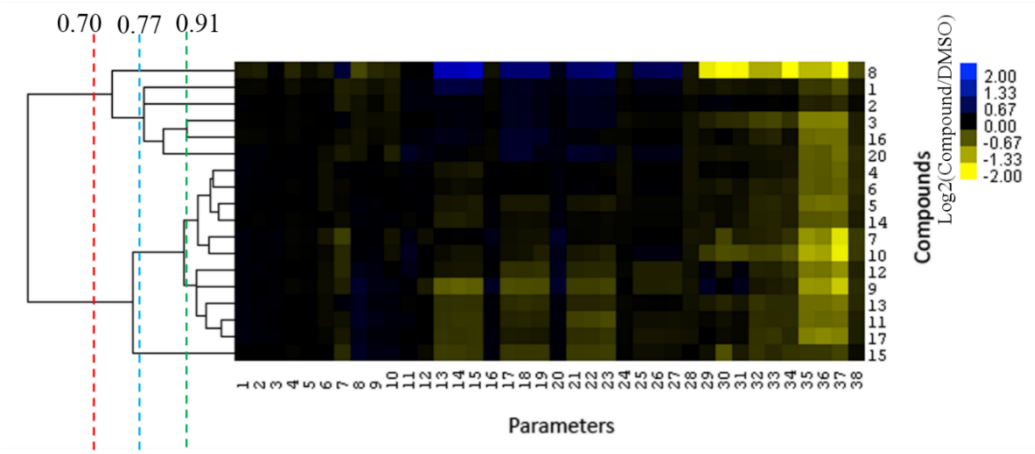

Figure 7. Heat map depicting the cytological profile of metabolites from *Jaspis splendens* at 10 µM on 38 parameters based on the $\log_2$ ratio of compound and vehicle (DMSO). Red shows a decrease versus vehicle and blue shows an increase versus vehicle. Individual compounds are presented on the y-axis with individual features on the x-axis. 1. Nucleus area (µm²) 2. Nucleus morphology width (µm) 3. Nucleus morphology length (µm) 4. Nucleus morphology ratio width to length 5. Nucleus morphology roundness 6. Nucleus marker texture index 7. Nucleus marker intensity 8. Cell area (µm²) 9. Cell width (µm) 10. Cell length (µm) 11. Cell ratio width to length 12. Cell roundness 13. *α*-Tubulin marker intensity in the cytoplasm 14. *α*-Tubulin marker intensity in outer region of cytoplasm 15. *α*-Tubulin marker intensity in inner region of cytoplasm 16. *α*-Tubulin marker texture index 17. Mitochondria marker intensity in the cytoplasm 18. Mitochondria marker intensity in outer region of cytoplasm 19. Mitochondria marker intensity in inner region of the cytoplasm 20. Mitochondria marker texture index 21. LC3b marker intensity in the cytoplasm 22. LC3b marker intensity in the outer region of the cytoplasm 23. LC3b marker intensity in inner region of cytoplasm 24. LC3b marker texture index 25. Lysosome marker intensity mean 26. Lysosome marker intensity outer region mean 27 Lysosome marker intensity inner region mean 28. Lysosome marker texture index. 29. Number of EEA1 marker spots in cytoplasm 30. Number of EEA1 marker spots in inner region of cytoplasm 31. Number of EEA1 marker spots in outer region of cytoplasm 32. Number of EEA1 marker spots per Area of cytoplasm 33. EEA1 marker intensity in outer region of cytoplasm 34 EEA1 marker intensity in inner region of cytoplasm 35. EEA1 marker intensity in the cytoplasm 36. Number of EEA1 marker spots per area of outer region 37 Number of EEA1 marker spots per Area of inner region of cytoplasm 38. EEA1 marker texture index.

On the basis of the similarity of their biological profile, two prominent clusters were obtained by a defined line across the dendrogram at a Pearson's correlation > 0.70. Under a Pearson's correlation of 0.77, there were four clusters A, B, C and D (Figures 7 and 8).

Jaspamycin **8** in cluster A showed the highest level of deviation from the control in the biological activity profile. Clustering of the 38 biological parameters resulted in a 3-modal effect. Nuclear and cytoplasmic markers were slightly affected compared to the DMSO control. Parameters associated with mitochondria, α-tubulin, LC3b and lysosome were moderately increased relative to DMSO control while an obvious decrease in the number of EEA1-associated early endosomes throughout the cytoplasm was evident with a corresponding increase in signal intensity. At a Pearson's correlation of 0.77, five compounds **1**-**3**, **16** and **20** in cluster B were similar in the biological activity profile to jaspamycin (**8**) in cluster A, with the main difference that cluster B showed a lower level of deviation from the control (Figures 7 and 8).

Compared to clusters A and B, compounds in clusters C and D showed negative deviation from the control for mitochondria, α-tubulin, LC3b and lysosome features. In cluster C, cytoplasmic, mitochondrial, and autophagy markers with compounds **4**-**7**, **10** and **14** were slightly decreased in comparison with compounds **9**, **11**-**13** and **17** under a Pearson's correlation at 0.91. The most striking and consistent alteration was the effect of these compounds on the early endosomal marker EEA1, which decreased in number and texture throughout the cytoplasm. Compound **15**, a singleton in cluster D, showed the lowest deviation from the DMSO control in its cytological profile.

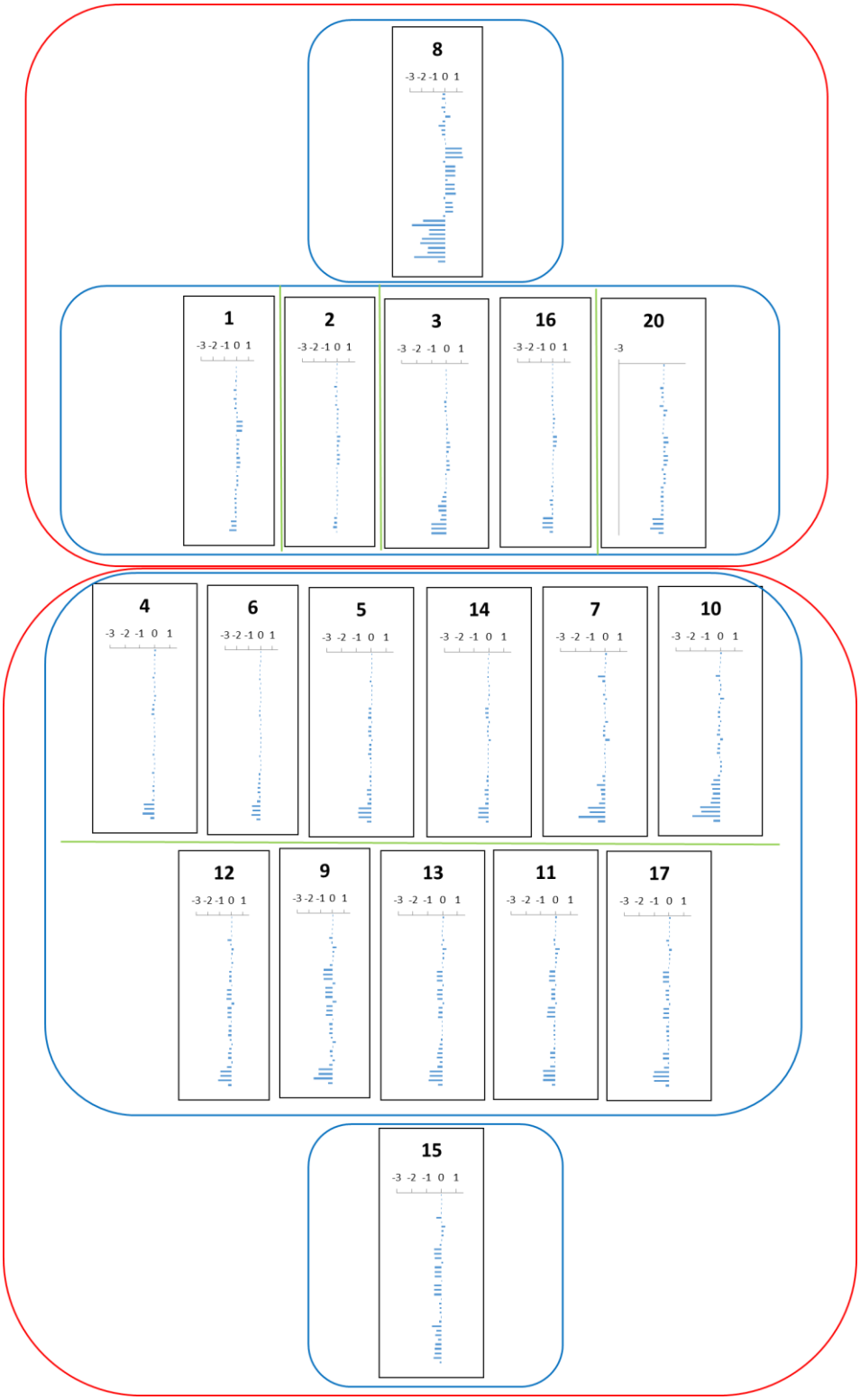

Figure 8. Clustered biological activity profile of metabolites from *Jaspis splendens*. The full description of all 38 cellular parameters and their response to natural products at 10 μM. (x-axis: log 2 ratio of metabolite (10 μM) vs control (DMSO); y-axis: 38 cellular parameters.) Two prominent clusters were shown in the red frames. Clusters A, B, C and D are shown in the light blue frames. The light green lines show a Pearson's correlation of 0.91.

Jaspamycin (**8**) in cluster A, had previously been synthesized and this is its first report as a natural product. As an analogue of toyocamycin (**7**), jaspamycin (**8**) had a very different cytological profile from the other six nucleosides (**4**-**7**, **9** and **10**) and three related aglycones (**11**-**13**) in cluster C. Further analogues of jaspamycin **8** at positions 4 and 5, and the sugar moiety would allow structure activity relationship to be developed (Figure 8). The four other new metabolites **1**-**3**, **16** plus **20** in cluster B presented a relatively lower activity than jaspamycin (**8**). All six of these chemically diverse compounds were clustered into one prominent cluster and displayed similar phenotypic profiles.

In contrast, the four chemically similar bromoindole alkaloids **14**-**17** (clusters B, C and D) were interestingly clustered into different groups, indicating that the substitutions for this scaffold played important roles in different therapeutic pathways or functional proteins.

In addition, the new bisindole alkaloid splendamide (**2**), with a carboxylic acid imide group and the monoindole alkaloid, 6-bromo-1*H*-indole-3-amidine (**16**), with a carboxamidine functionality, showed similar biological activity in cluster B. Under Pearson's correlation of 0.91, they were in different clusters revealing some structure-activity relationship.

Four of the five jaspamide peptides (**18**, **19**, **21** and **22**) exhibited an alteration of nuclear and cellular parameters at 10 μM suggesting that these cyclic jaspamide peptides are cytotoxic. Jaspamide Z_1 (**20**), the open-chain form of jaspamide (**18**), showed a lower cytotoxicity level.

A new neighbor correlation of the phenotype to compounds with known targets may identify possible biological targets. Jaspamycin (**8**) had significant phenotypic perturbation of Parkinson's disease patient-derived human olfactory neurosphere-derived cells on the markers. In previous research, iotrochotazine A, isolated from an Australian marine sponge *Iotrochota* sp., was used as a chemical probe and investigated in the phenotypic assay.[6] In comparison to iotrochotazine A, jaspamycin (**8**) moderately increased lysosomal staining and significantly

decreased the number of EEA-1-associated early endosomes, while iotrochotazine A decreased lysosomal staining and increased the number of EEA-1-associated early endosomes. In conclusion, we have isolated three new compounds and two natural products, previously reported as synthetic products, together with 17 known metabolites from *J. splendens*. Rather than any unique chemical feature, it was the phenotypic responses of the metabolites in a hONS cell model of Parkinson's disease that led us to identify jaspamycin (**8**) as having unique biologically relevant chemical space. Herein, the different phenotypic responses of jaspamycin (**8**) and iotrochotazine A offer useful probes to investigate the molecular mechanisms underlying Parkinson's disease.

EXPERIMENTAL SECTION

General Experimental Procedures. Optical rotations were recorded on a JASCO P-1020 polarimeter (10 cm cell). IR and UV spectra were recorded on a Bruker Tensor 27 spectrophotometer and a CAMSPEC M501 UV/vis spectrophotometer, respectively. NMR spectra were recorded in DMSO-d_6 (δ_H 2.50 and δ_C 39.5) or MeOH-d_4 (δ_H 3.31 and δ_C 49.0) at 30 ℃ on a Varian INOVA 600 MHz spectrometer equipped with a triple-resonance cold probe or at 25 ℃ on a Bruker Avance HDX 800 MHz spectrometer equipped with a TCI cryoprobe. The low-resolution mass spectra (LRESIMS) were recorded on a Mariner time-of-flight (TOF) spectrometer equipped with a Gilson 215 eight-probe injector and a Waters LCMS system equipped with a Luna C_{18} column (3 μm, 100 Å, 50 × 4.6 mm), a PDA detector, and a ZQ ESI mass spectrometer. The high-resolution mass spectra (HRESIMS) were recorded on a Bruker Daltonics SolariX 12 T Fourier transform mass spectrometer. An Edwards Instrument Company Bioline orbital shaker was used for extraction. The HPLC system included a Waters 600 pump fitted with a 996 photodiode array detector and Gilson FC204 fraction collector. A ThermoElectron Betasil C_{18} column (5 μm, 21.2 × 150 mm) and a Phenomenex Luna C_{18}

column (5 μm, 10 × 250 mm) were used for semipreparative HPLC. All solvents used for extraction, chromatography, $[\alpha]_D$, UV, IR, and MS were Lab-Scan HPLC grade, and the H_2O was Millipore Milli-Q PF filtered.

Animal Material. A specimen of *Jaspis splendens* was collected by scuba (-23 m) in Mid Reef (S 14.44813, E 144.88139), Great Barrier Reef, North Queensland, Australia on July 3, 2003. Sponge material was kept frozen prior to freeze-drying and extraction. Taxonomic identification of *J. splendens* was performed by Dr. J. N.A. Hooper. A voucher specimen, G320726, has been deposited at the Queensland Museum, South Brisbane, Australia.

Extraction and Purification of Compounds 1-22. The ground and freeze-dried *J. splendens* (50 g) was extracted with *n*-hexane (250 mL) for 2 h at room temperature (rt). The *n*-hexane extract was filtered under gravity and discarded. Then 250 mL CH_2Cl_2/MeOH (80:20) was added to the biota and extracted for 2 h. The CH_2Cl_2/MeOH extract was filtered, and the biota was further extracted with two lots of 250 mL of MeOH for 2 h and overnight, successively. Both MeOH extracts were combined with CH_2Cl_2/MeOH extract and dried to afford the crude extract. The crude extract was fractionated using a C_{18} bonded silica flash column. Five fractions were collected by eluting with gradients H_2O/MeOH containing 0.1% TFA (100% H_2O, 90% H_2O/10% MeOH, 50% H_2O/50% MeOH, 10% H_2O/90% MeOH, 100% MeOH, respectively). The 90% H_2O/10% MeOH fraction was chromatographed by HPLC (gradient H_2O/ MeOH with 0.1% TFA) using a semipreparative reversed-phase C_{18} Betasil column (21.2 mm × 150 mm). Initial isocratic conditions of 10% MeOH were used for 10 min then a linear gradient from 10 to 50% MeOH was performed over 40 min and continued isocratic for 10 min at a flow rate of 9 mL/min. Sixty fractions were collected by 1 min increments over 60 min to afford jaspterin (**1**) and jaspnin A (**3**) TFA salt, together with nucleosides (**4**-**10**), and aglycones (**11**-**13**). The 50% H_2O/50% MeOH fraction was

chromatographed by HPLC (gradient H_2O/ MeOH with 0.1% TFA) using the same semipreparative C_{18} column eluting with 70% H_2O/30% MeOH to 20% H_2O/80% MeOH. A new bisindole alkaloid, splendamide (**2**), along with four indole alkaloids (**14**-**17**) were isolated. In addition, five jaspamide pepitides (**18**-**22**) were also isolated from the 90% H_2O/10% MeOH fraction by the same semipreparative HPLC column eluting with gradient H_2O/ MeOH with 0.1% TFA from 40% H_2O/60% MeOH to 100% MeOH.

*Jaspterin (**1**):* white powder; UV (MeOH) λ_{max} (log ε), 238 (2.81), 252 (2.81), 280 (2.89), 358 (2.43) nm; ^{1}H NMR (600 MHz, DMSO-d_6) and ^{13}C NMR data (125 MHz, DMSO-d_6), Table 1; (+)-HRESIMS *m/z* 214.0670 $[M+Na]^+$ (calcd for $C_8H_9N_5NaO$, 214.0699).

*Splendamide (**2**):* colorless gum; UV (MeOH) λ_{max} (log ε), 216 (3.60), 275 (3.19), 304 (2.97) nm; ^{1}H NMR (600 MHz, DMSO-d_6) and ^{13}C NMR data (125 MHz, DMSO-d_6), Table 2; (+)-HRESIMS *m/z* 481.9116 $[M+Na]^+$ (calcd for $C_{18}H_{11}{}^{79}Br_2N_3NaO_2$, 481.9110).

*Jaspnin A (**3**) TFA salt:* white powder; UV (MeOH) λ_{max} (log ε), 208 (2.88), 244 (2.39) nm; ^{1}H NMR (600 MHz, MeOH-d_4) and ^{13}C NMR data (125 MHz, MeOH-d_4), Table 3; (+)-HRESIMS *m/z* 223.0511 $[M+Na]^+$ (calcd for $C_8H_{12}N_2NaO_2S$, 223.0511).

*Jaspamycin (**8**):* white solid; $[\alpha]_D^{26}$ = -25.0 (*c* 0.020, MeOH); UV (MeOH) λ_{max} (log ε), 208 (4.09), 265 (3.94) nm; ^{1}H NMR (600 MHz, DMSO-d_6): 12.48 (s, 1H), 8.33 (s, 1H), 8.08 (s, 1H), 6.02 (d, 5.5, 1H), 4.31 (dd, 5.5, 5.1, 1H), 4.09 (dd, 5.1, 3.9, 1H), 3.92 (m, 1H), 3.65(dd, 12.3, 2.9, 1H), 3.57(dd, 12.3, 3.2, 1H); (+)-HRESIMS *m/z* 315.0700 $[M+Na]^+$ (calcd for $C_{12}H_{12}N_4NaO_5$, 315.0700).

*6-Bromo-1H-indole-3-amidine (**16**) TFA salt:* white powder; UV (MeOH) λ_{max} (log ε), 235 (4.28), 290 (3.65) nm; ^{1}H NMR (600 MHz, DMSO-d_6): 12.38 (s, br, 1H), 8.79 (s, br, 2H),

8.50 (s, br, 2H), 8.22 (s, br, 1H), 7.79 (d, 1.8, 1H), 7.76 (d, 8.6, 1H), 7.41 (dd, 1.8, 8.6, 1H); (+)-HRESIMS *m/z* 237.9974 $[M+H]^+$ (calcd for $C_9H_8{}^{79}BrN_3$, 237.9980).

Biological Assay. Compounds were transferred into two optically clear bottom CellCarrie 384-well plates (PerkinElmer). hONS cells from the Parkinson's disease cell line C1 200 08 0013 were added to each well at a density of 1350 cells per well in 50 μL of growth medium (DMEM/F12, 10% FBS) leading to a final concentration of 10 μM (0.6% DMSO) for each compound. DMSO (0.6%) was used as negative control. The cells were incubated for 24 h at 37 ^oC under 5% CO_2.

Cell Staining. After 24 h of incubation, the medium was aspirated and one 384-well plate was treated with MitoTracker Orange CMTMRos (Invitrogen) (400 nM) for 30 min at 37 ^oC under 5% CO_2. The second 384-well plate was treated with LysoTracker Red DND-99 (Invitrogen) (100 nM) for 1 h at 37 ^oC under 5% CO_2. Cells were fixed in 4% paraformaldehyde for 5 min at room temperature (rt). Cells were washed twice with phosphate-buffered saline (PBS, Sigma-Aldrich) and treated with 3% goat serum (Sigma-Aldrich) and 0.2% Triton X-100 (Sigma-Aldrich) in PBS for 45 min at rt. Plates were incubated with primary antibodies. Mouse anti-*α*-tubulin 1/4000 (Sigma-Aldrich) and rabbit anti-LC3b 1/335 (Sigma-Aldrich) were added to the plate already treated with MitoTracker, and mouse anti-EEA1 1/200 (Sigma-Aldrich) was added to the plate previously treated with LysoTracker. Plates were incubated at rt for 1 h, then washed twice with PBS. Secondary antibodies goat anti-mouse Alexa-647 1/500 (Invitrogen) and goat anti-rabbit Alexa-488 1/500 (Invitrogen) were added to the first plate and goat anti-mouse Alexa-488 1/500 (Invitrogen) was added to the second plate for 30 min at rt. Cells were washed twice with PBS and stained with 4',6'-diamidino-2-phenylindole 1/5000 (Dapi, Invitrogen) and with CellMask Deep Red 1/5000 (Invitrogen) for the plate treated with

LysoTracker and incubated for 10 min at rt. Cells were washed twice with PBS and plates were stored in the dark at 4 ^{o}C with 25 μL of PBS/well.

Imaging and Image Analysis Plates were imaged automatically using Operetta (PerkinElmer), a high content imaging system using a 20× high numerical aperture objective lens. Six images per well for each wavelength were collected. Individual cell segmentation was done using the Harmony software and measurements for each cell were performed generating 38 parameters from six dyes: Dapi, *α*-tubulin staining, MitoTracker Orange CMTMRos, LC3b staining, LysoTracker Red DND-99 and EEA1 staining. The normality of the data was checked for each parameter and a $\log_2$ transform was made when required in order to perform a *t*-test to identify significant changes when compared to DMSO. The $\log_2$ compound/DMSO ratio was clustered using Cluster 3.0 software (uncentered correlation and centroid linkage) and analyzed using Java TreeView.

ASSOCIATED CONTENT

Supporting Information

The Supporting Information is available free of charge on the ACS Publications website at DOI: 10.1021/acs.jnatprod.5b00987.

1D and 2D NMR spectra for compounds **1**- **3**,.**8** and **16**.

AUTHOR INFORMATION

Corresponding Author

*Tel: +64 7 3735 6009. E-mail: r.quinn@griffith.edu.au.

Notes

The authors declare no competing financial interest.

ACKNOWLEDGMENTS

This research was supported by Australian Research Council *Discovery Projects* funding (project number DP130102400). D. W. thanks Griffith University for a GUIPRS scholarship.

REFERENCES

(1) Macarron, R.; Banks, M. N.; Bojanic, D.; Burns, D. J.; Cirovic, D. A.; Garyantes, T.; Green, D. V.; Hertzberg, R. P.; Janzen, W. P.; Paslay, J. W. *Nat. Rev. Drug Discov.* **2011**, *10*, 188-195.

(2) Swinney, D. C.; Anthony, J. *Nat. Rev. Drug Discov.* **2011**, *10*, 507-519.

(3) Olanow, C. W.; Stern, M. B.; Sethi, K. *Neurology* **2009**, *72*, S1-S136.

(4) Matigian, N.; Abrahamsen, G.; Sutharsan, R.; Cook, A. L.; Vitale, A. M.; Nouwens, A.; Bellette, B.; An, J.; Anderson, M.; Beckhouse, A. G. *Dis. Model. Mech.* **2010**, *3*, 785-798.

(5) Cook, A. L.; Vitale, A. M.; Ravishankar, S.; Matigian, N.; Sutherland, G. T.; Shan, J.; Sutharsan, R.; Perry, C.; Silburn, P. A.; Mellick, G. D. *PLoS One* **2011**, *6*, e21907.

(6) Grkovic, T.; Pouwer, R. H.; Vial, M. L.; Gambini, L.; Noel, A.; Hooper, J. N.; Wood, S. A.; Mellick, G. D.; Quinn, R. J. *Angew. Chem. Int. Ed.* **2014**, *53*, 6070-6074.

(7) Harvey, A. L.; Edrada-Ebel, R.; Quinn, R. J. *Nat. Rev. Drug Discov.* **2015**, *14*, 111-129.

(8) Camp, D.; Davis, R. A.; Campitelli, M.; Ebdon, J.; Quinn, R. J. *J. Nat. Prod.* **2012**, *75*, 72-81.

(9) Feng, Y.; Campitelli, M.; Davis, R. A.; Quinn, R. J. *Mar. Drugs* **2014**, *12*, 1169-1184.

(10) Ebada, S. S.; Wray, V.; de Voogd, N. J.; Deng, Z.; Lin, W.; Proksch, P. *Mar. Drugs* **2009**, *7*, 434-444.

(11) Gala, F.; D'Auria, M. V.; De Marino, S.; Zollo, F.; Smith, C. D.; Copper, J. E.; Zampella, A. *Tetrahedron* **2007**, *63*, 5212-5219.

(12) Gala, F.; D'Auria, M. V.; De Marino, S.; Sepe, V.; Zollo, F.; Smith, C. D.; Copper, J. E.; Zampella, A. *Tetrahedron* **2008**, *64*, 7127-7130.

(13) Gala, F.; D'Auria, M. V.; De Marino, S.; Sepe, V.; Zollo, F.; Smith, C. D.; Keller, S. N.; Zampella, A. *Tetrahedron* **2009**, *65*, 51-56.

(14) Ravi, B.; Wells, R. J.; Croft, K. D. *J. Org. Chem.* **1981**, *46*, 1998-2001.

(15) Tsuda, M.; Ishibashi, M.; Agemi, K.; Sasaki, T.; Kobayashi, J. i. *Tetrahedron* **1991**, *47*, 2181-2194.

(16) Kobayashi, J. i.; Yuasa, K.; Kobayashi, T.; Sasaki, T.; Tsuda, M. *Tetrahedron* **1996**, *52*, 5745-5750.

(17) Kobayashi, J. i.; Murata, O.; Shigemori, H.; Sasaki, T. *J. Nat. Prod.* **1993**, *56*, 787-791.

(18) Rodríguez, J.; Nieto, R. M.; Crews, P. *J. Nat. Prod.* **1993**, *56*, 2034-2040.

(19) Searle, P. A.; Richter, R. K.; Molinski, T. F. *J. Org. Chem.* **1996**, *61*, 4073-4079.

(20) D'Auria, M. V.; Giannini, C.; Minale, L.; Zampella, A.; Debitus, C.; Frostin, M. *J. Nat. Prod.* **1997**, *60*, 814-816.

(21) Groweiss, A.; Newcomer, J. J.; O'Keefe, B. R.; Blackman, A.; Boyd, M. R. *J. Nat. Prod.* **1999**, *62*, 1691-1693.

(22) Thale, Z.; Kinder, F. R.; Bair, K. W.; Bontempo, J.; Czuchta, A. M.; Versace, R. W.; Phillips, P. E.; Sanders, M. L.; Wattanasin, S.; Crews, P. *J. Org. Chem.* **2001**, *66*, 1733-1741.

(23) Park, Y.; Liu, Y.; Hong, J.; Lee, C.-O.; Cho, H.; Kim, D.-K.; Im, K. S.; Jung, J. H. *J. Nat. Prod.* **2003**, *66*, 1495-1498.

(24) Shinde, P. B.; Lee, Y. M.; Dang, H. T.; Hong, J.; Lee, C.-O.; Jung, J. H. *Bioorg. Med. Chem. Lett.* **2008**, *18*, 6414-6418.

(25) Zabriskie, T. M.; Ireland, C. M. *J. Nat. Prod.* **1989**, *52*, 1353-1356.

(26) Ohta, S.; Kobayashi, H.; Ikegami, S. *Tetrahedron Lett.* **1994**, *35*, 4579-4580.

(27) Ohta, S.; Kobayashi, H.; Ikegami, S. *Biosci. Biotechnol. Biochem.* **1994**, *58*, 1752-1753.

(28) Chang, Y. H.; Shin, D.; Na, Z.; Lee, H.-S.; Kim, D.-D.; Oh, K.-B.; Shin, J. *J. Nat. Prod.* **2008**, *71*, 779-783.

(29) Hinshaw, B. C.; Gerster, J. F.; Robins, R. K.; Townsend, L. B. *J. Org. Chem.* **1970**, *35*, 236-241.

(30) Broom, A. D.; Robins, R. K. *J. Org. Chem.* **1969**, *34*, 1025-1029.

(31) Nair, V.; Young, D. A.; DeSilvia Jr, R. *J. Org. Chem.* **1987**, *52*, 1344-1347.

(32) Fox, J.; Wempen, I. *Adv. Carbohydr. Chem.* **1959**, *14*, 283.

(33) Chenon, M. T.; Pugmire, R. J.; Grant, D. M.; Panzica, R. P.; Townsend, L. B. *J. Am. Chem. Soc.* **1975**, *97*, 4627-4636.

(34) Rao, K. V. *J. Med. Chem.* **1968**, *11*, 939-941.

(35) Fahy, E.; Potts, B. C.; Faulkner, D. J.; Smith, K. *J. Nat. Prod.* **1991**, *54*, 564-569.

(36) Wang, R.-P.; Lin, H.-W.; Li, L.-Z.; Gao, P.-Y.; Xu, Y.; Song, S.-J. *Biochem. Syst. Ecol.* **2012**, *43*, 210-213.

(37) Segraves, N. L.; Crews, P. *J. Nat. Prod.* **2005**, *68*, 1484-1488.

(38) Zabriskie, T. M.; Klocke, J. A.; Ireland, C. M.; Marcus, A. H.; Molinski, T. F.; Faulkner, D. J.; Xu, C.; Clardy, J. *J. Am. Chem. Soc.* **1986**, *108*, 3123-3124.

(39) Zampella, A.; Giannini, C.; Debitus, C.; Roussakis, C.; D'Auria, M. V. *J. Nat. Prod.* **1999**, *62*, 332-334.

(40) Watts, K. R.; Morinaka, B. I.; Amagata, T.; Robinson, S. J.; Tenney, K.; Bray, W. M.; Gassner, N. C.; Lokey, R. S.; Media, J.; Valeriote, F. A.; Crews, P. *J. Nat. Prod.* **2011**, *74*, 341-351.

(41) Sorres, J.; Martin, M. T.; Petek, S.; Levaique, H.; Cresteil, T.; Ramos, S.; Thoison, O.; Debitus, C.; Al-Mourabit, A. *J. Nat. Prod.* **2012**, *75*, 759-763.

(42) McArdle, B. M.; Campitelli, M. R.; Quinn, R. J. *J. Nat. Prod.* **2006**, *69*, 14-17.

(43) Kellenberger, E.; Hofmann, A.; Quinn, R. J. *Nat. Prod. Rep.* **2011**, *28*, 1483-1492.

(44) Feng, Y.; Davis, R. A.; Sykes, M. L.; Avery, V. M.; Quinn, R. J. *Bioorg. Med. Chem. Lett.* **2012**, *22*, 4873-4876.

(45) Feng, Y.; Carroll, A. R.; Pass, D. M.; Archbold, J. K.; Avery, V. M.; Quinn, R. J. *J. Nat. Prod.* **2008**, *71*, 8-11.

(46) Kim, S.; Kang, Y. *Bull. Korean Chem. Soc* **2011**, *32*, 3161-3163.

(47) Sakurai, A.; GOTO, M. *J. Biochem. (Tokyo)* **1967**, *61*, 142-145.

(48) Teng, J.; Yang, X. W. *Heterocycles* **2006**, *68*, 1691-1698.

(49) Mancini, I.; Guella, G.; Pietra, F.; Debitus, C.; Duhet, D. *Helv. Chim. Acta* **1994**, *77*, 1886-1894.

(50) Sakemi, S.; Sun, H. H. *J. Org. Chem.* **1991**, *56*, 4304-4307.

(51) Mancini, I.; Guella, G.; Pietra, F.; Debitus, C.; Waikedre, J. *Helv. Chim. Acta* **1996**, *79*, 2075-2082.

(52) Ren, S.; Ma, W.; Xu, T.; Lin, X.; Yin, H.; Yang, B.; Zhou, X.-F.; Yang, X.-W.; Long, L.; Lee, K. J. *J. Antibiot.* **2010**, *63*, 699-701.

(53) Imada, K.; Sakai, E.; Kato, H.; Kawabata, T.; Yoshinaga, S.; Nehira, T.; Terasawa, H.; Tsukamoto, S. *Tetrahedron* **2013**, *69*, 7051-7055.

(54) Carroll, A. R.; Avery, V. M. *J. Nat. Prod.* **2009**, *72*, 696-699.

(55) Schumacher, R. W.; Davidson, B. S. *Tetrahedron* **1995**, *51*, 10125-10130.

(56) Bourguet-Kondracki, M.; Martin, M.; Guyot, M. *Tetrahedron Lett.* **1996**, *37*, 3457-3460.

(57) Pedpradab, S.; Edrada, R.; Ebel, R.; Wray, V.; Proksch, P. *J. Nat. Prod.* **2004**, *67*, 2113-2116.

(58) Iinuma, Y.; Kozawa, S.; Ishiyama, H.; Tsuda, M.; Fukushi, E.; Kawabata, J.; Fromont, J.; Kobayashi, J. i. *J. Nat. Prod.* **2005**, *68*, 1109-1110.

(59) Quinn, R. J.; Carroll, A. R.; Pham, N. B.; Baron, P.; Palframan, M. E.; Suraweera, L.; Pierens, G. K.; Muresan, S. *J. Nat. Prod.* **2008**, *71*, 464-468.

(60) Instant JChem, version 15.16.29.10; ChemAxon Kft: Budapest, Hungary, 2015.

Supporting Information for Chapter Two

Supporting information for

A Grand Challenge: Unbiased Phenotypic Function of Metabolites from *Jaspis splendens* against Parkinson's Disease

Dongdong Wang,[†] Yunjiang Feng,[†] Mariyam Murtaza,[†] Stephen Wood,[†] George Mellick,[†] John N.A. Hooper[‡] and Ronald J. Quinn[†,*]

[†]Eskitis Institute for Drug Discovery, Griffith University, Brisbane, QLD 4111, Australia.

[‡]Queensland Museum, South Brisbane, QLD 4101, Australia.

List of supporting information

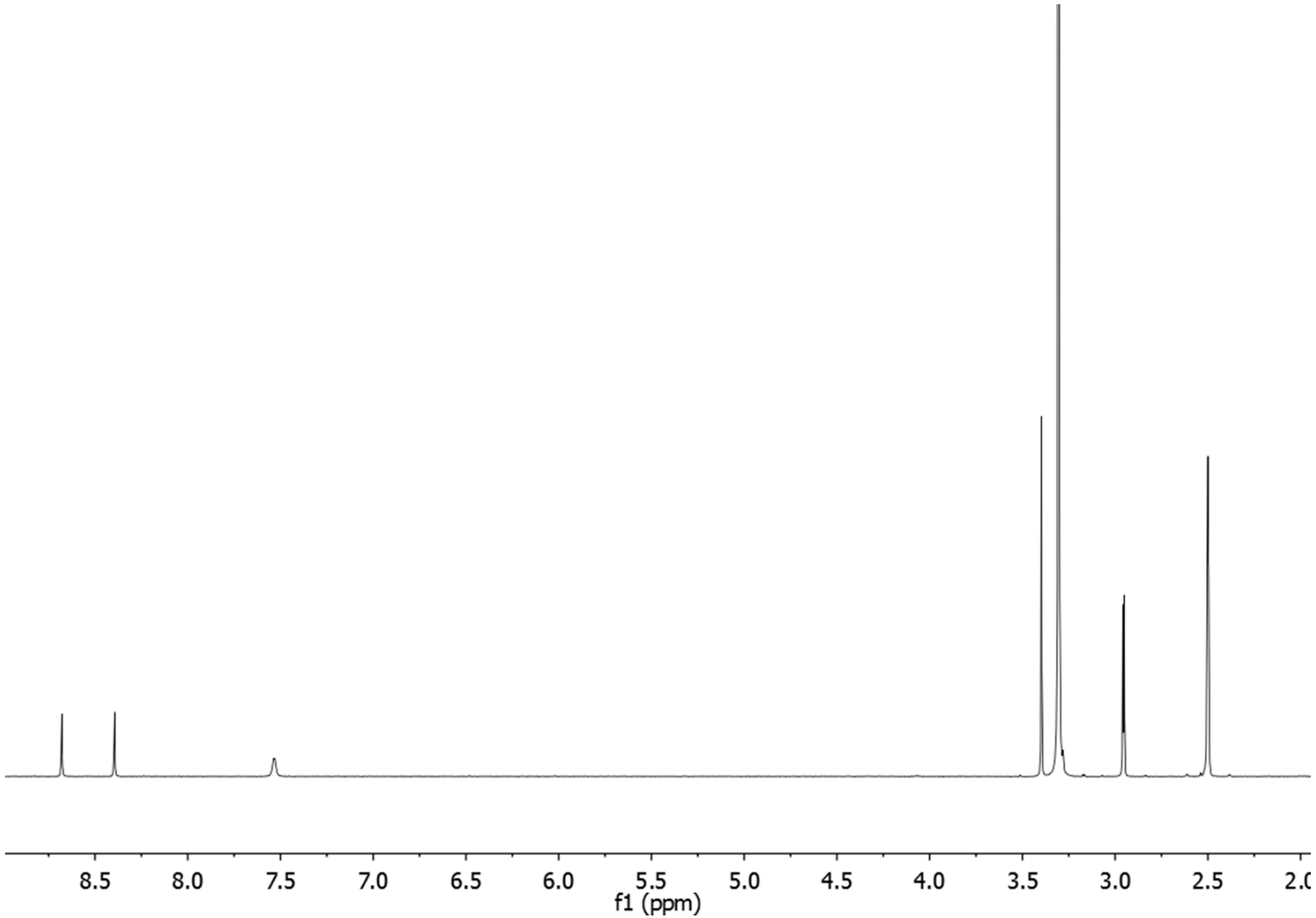

Figure S1. ^{1}HNMR spectrum of compound **1** in DMSO-d_6

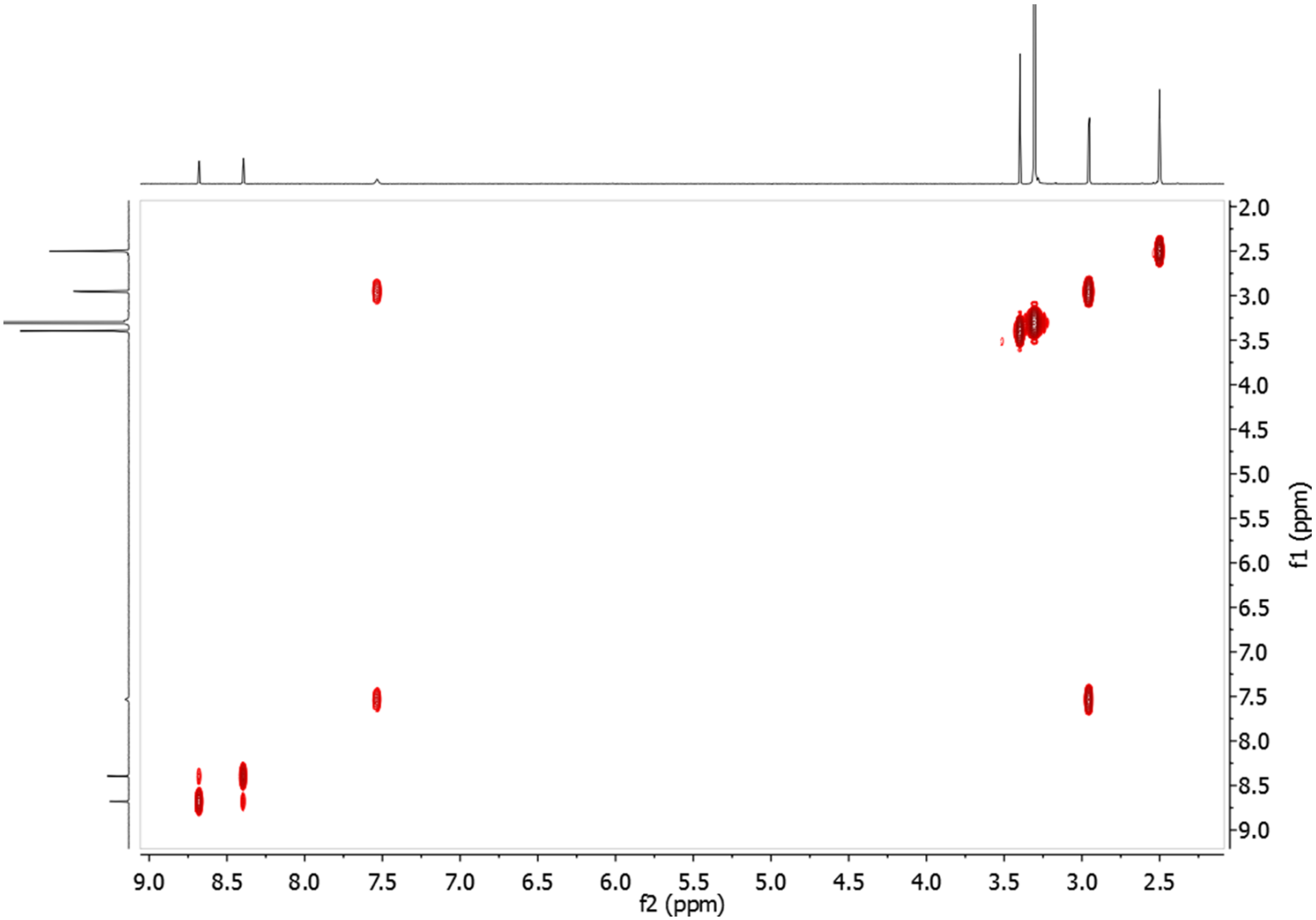

Figure S2. COSY spectrum of compound **1** in DMSO-d_6

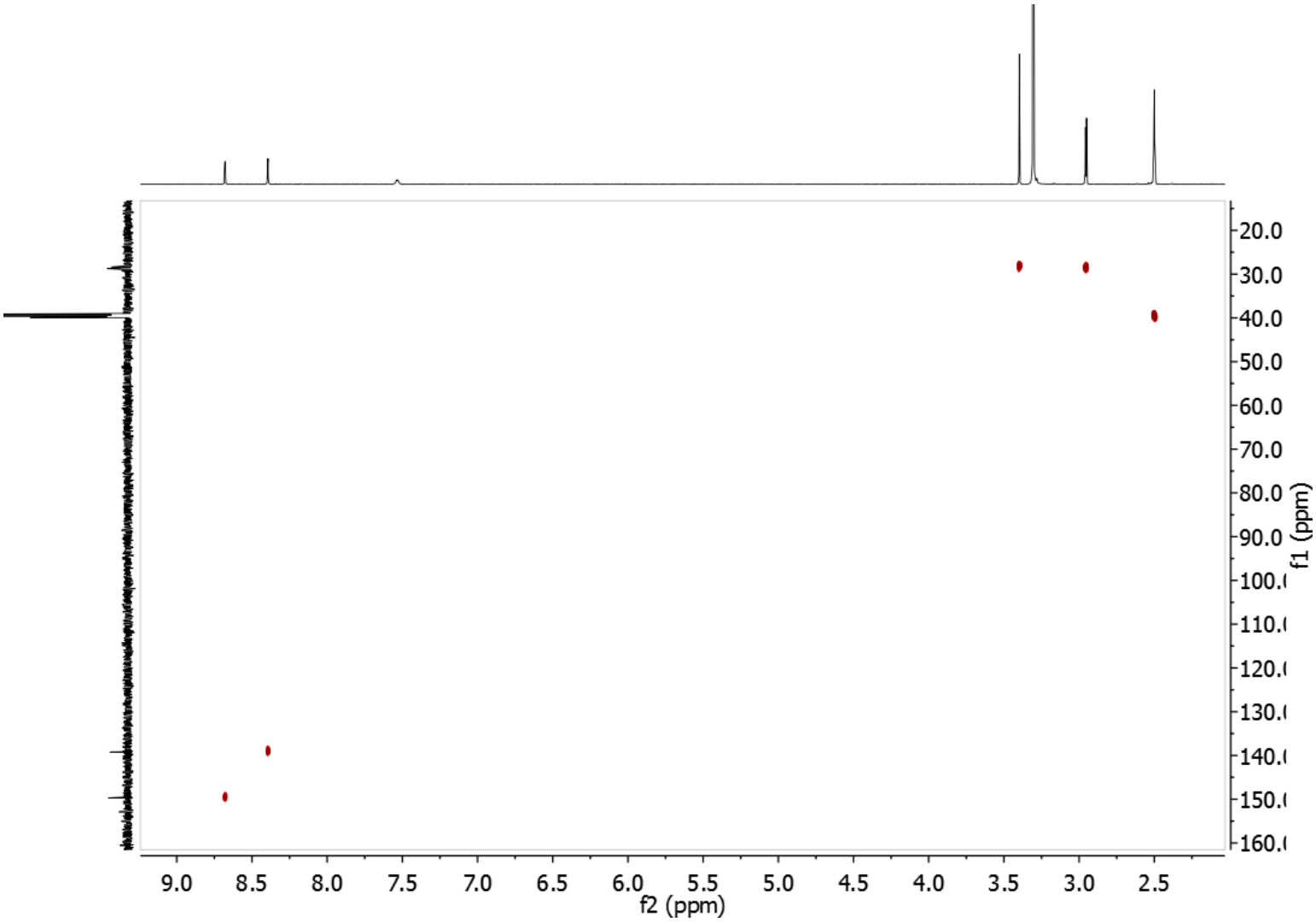

Figure S3. HSQC spectrum of compound **1** in DMSO-d_6

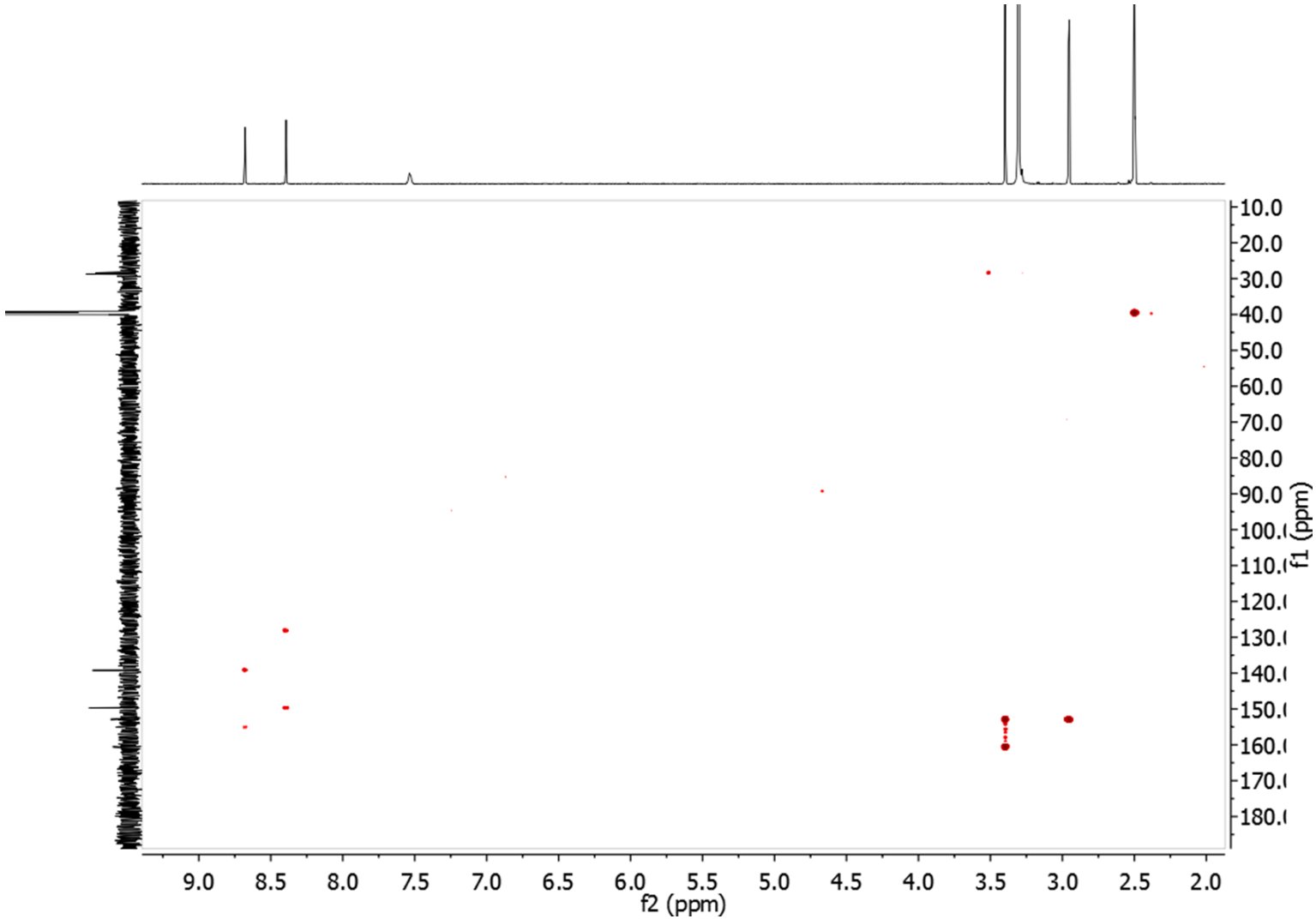

Figure S4. HMBC spectrum of compound **1** in DMSO-d_6

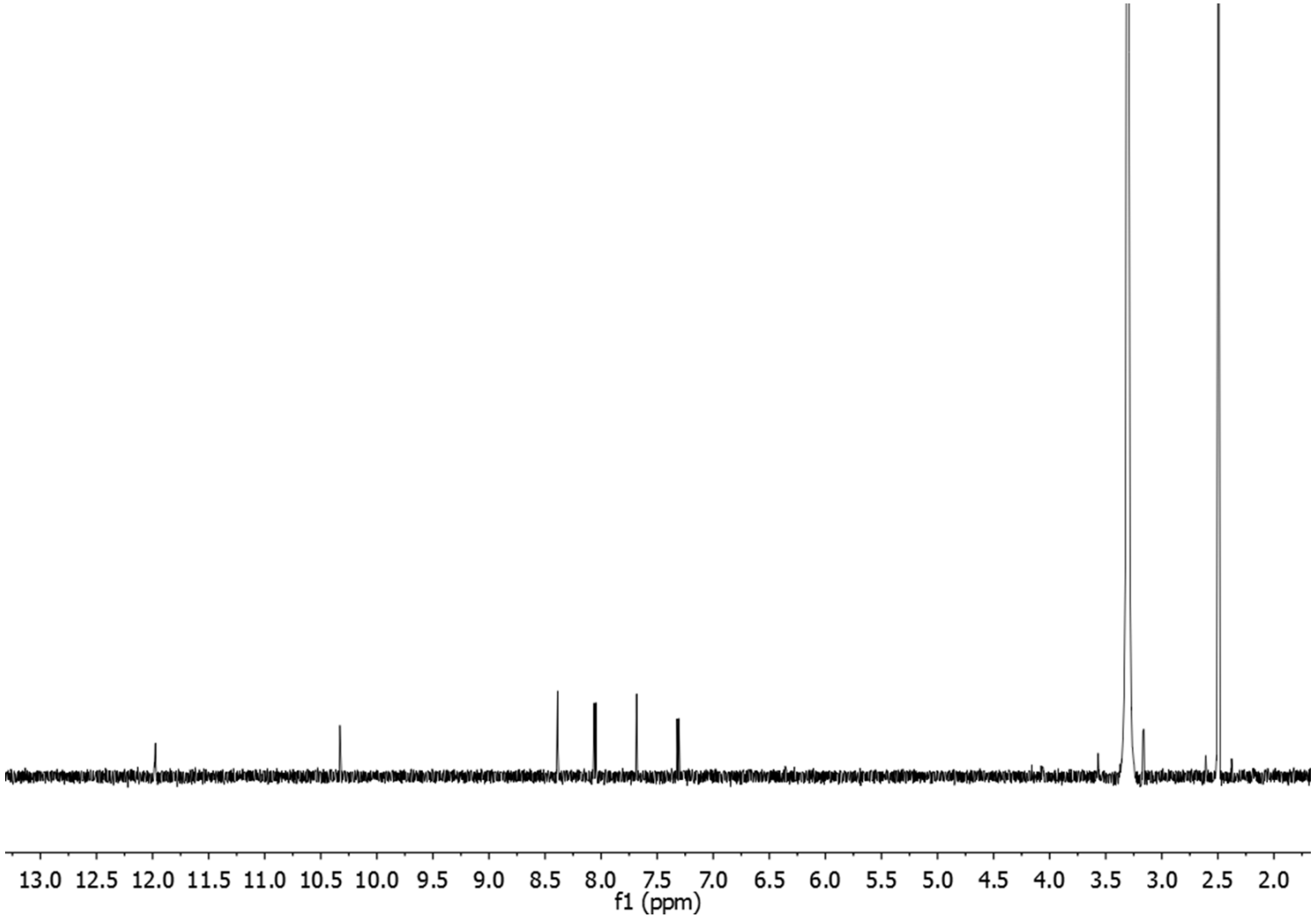

Figure S5. ^{1}HNMR spectrum of compound **2** in DMSO-d_6

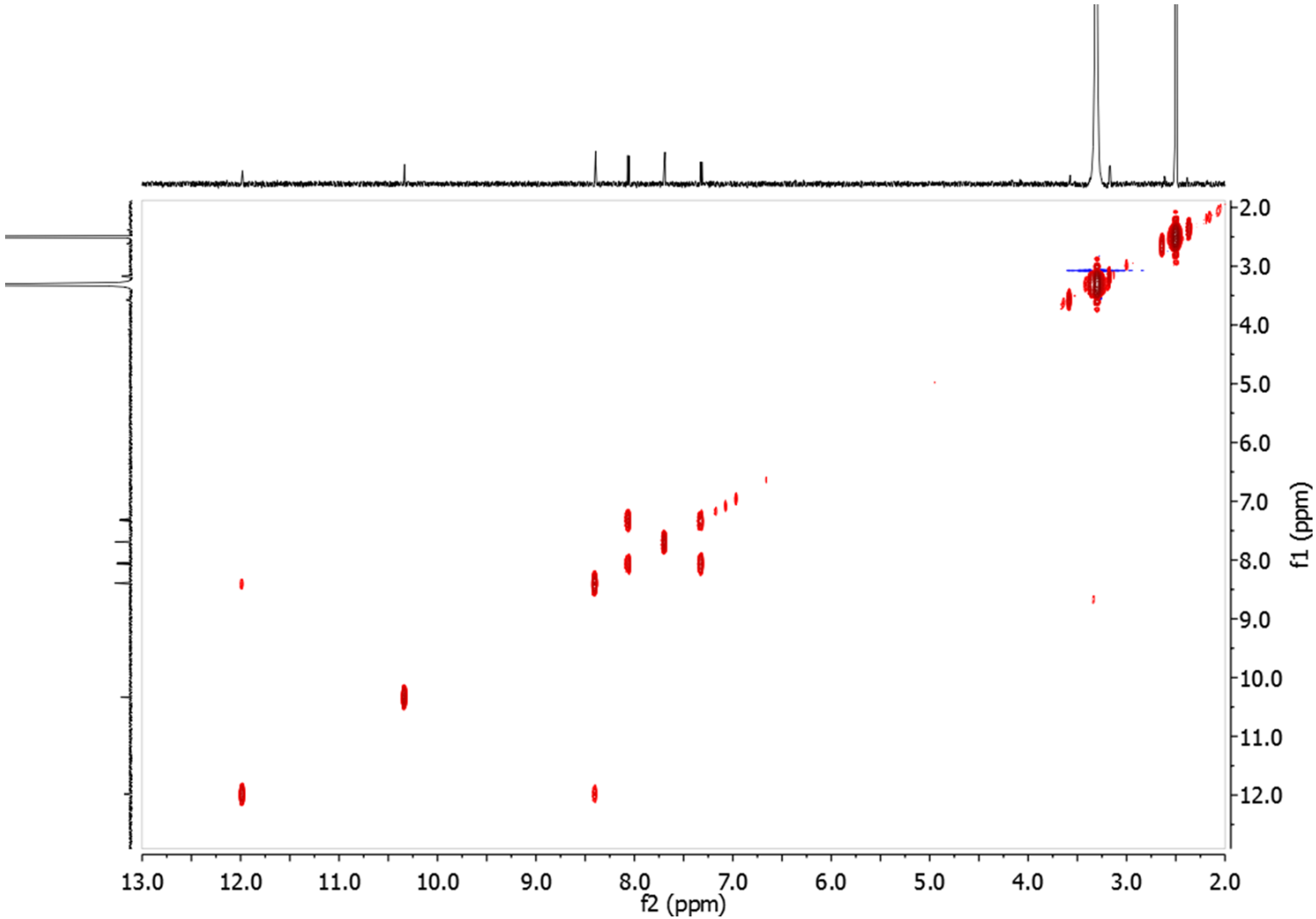

Figure S6. COSY spectrum of compound **2** in DMSO-d_6

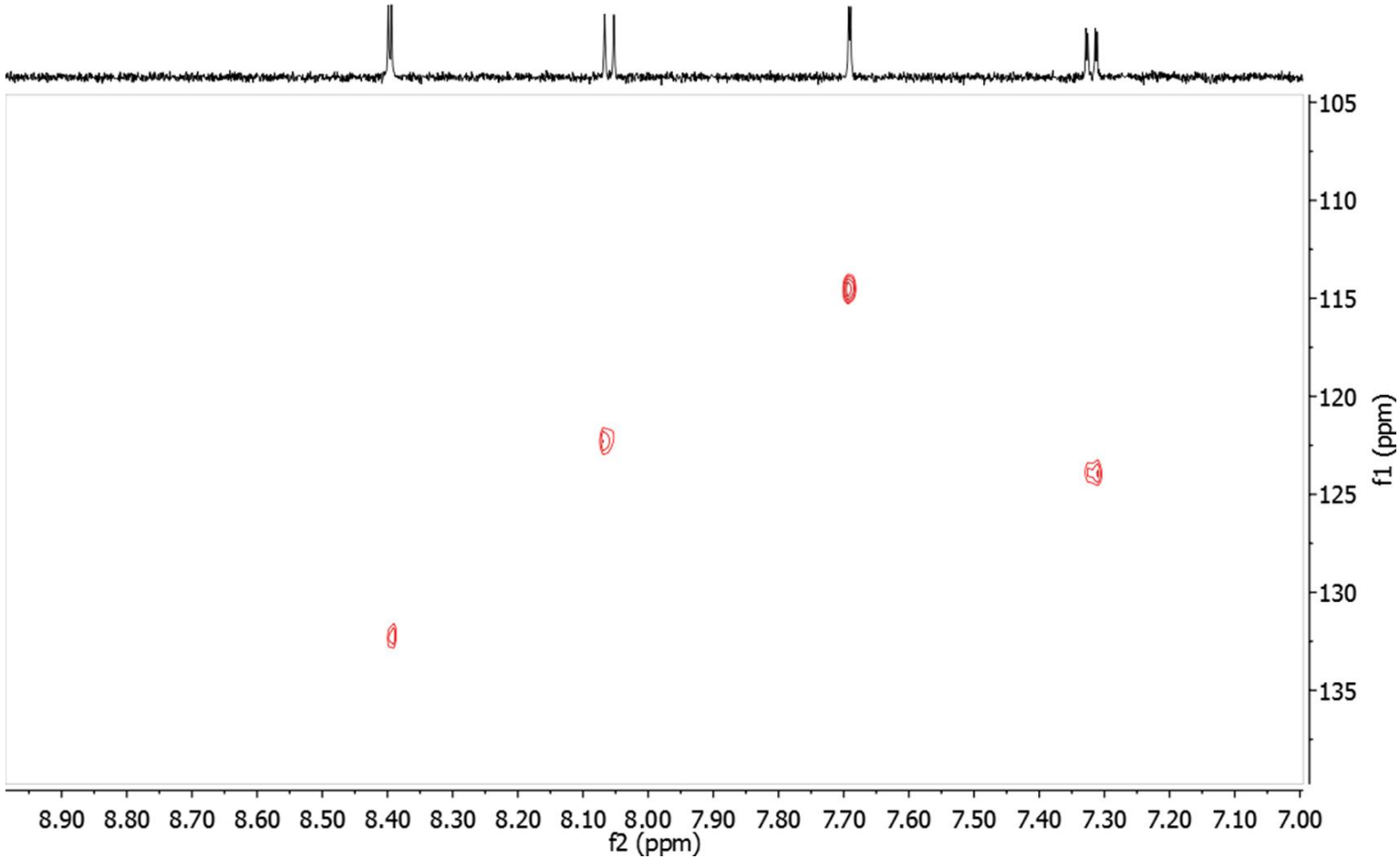

Figure S7. HSQC spectrum of compound **2** in DMSO-d_6

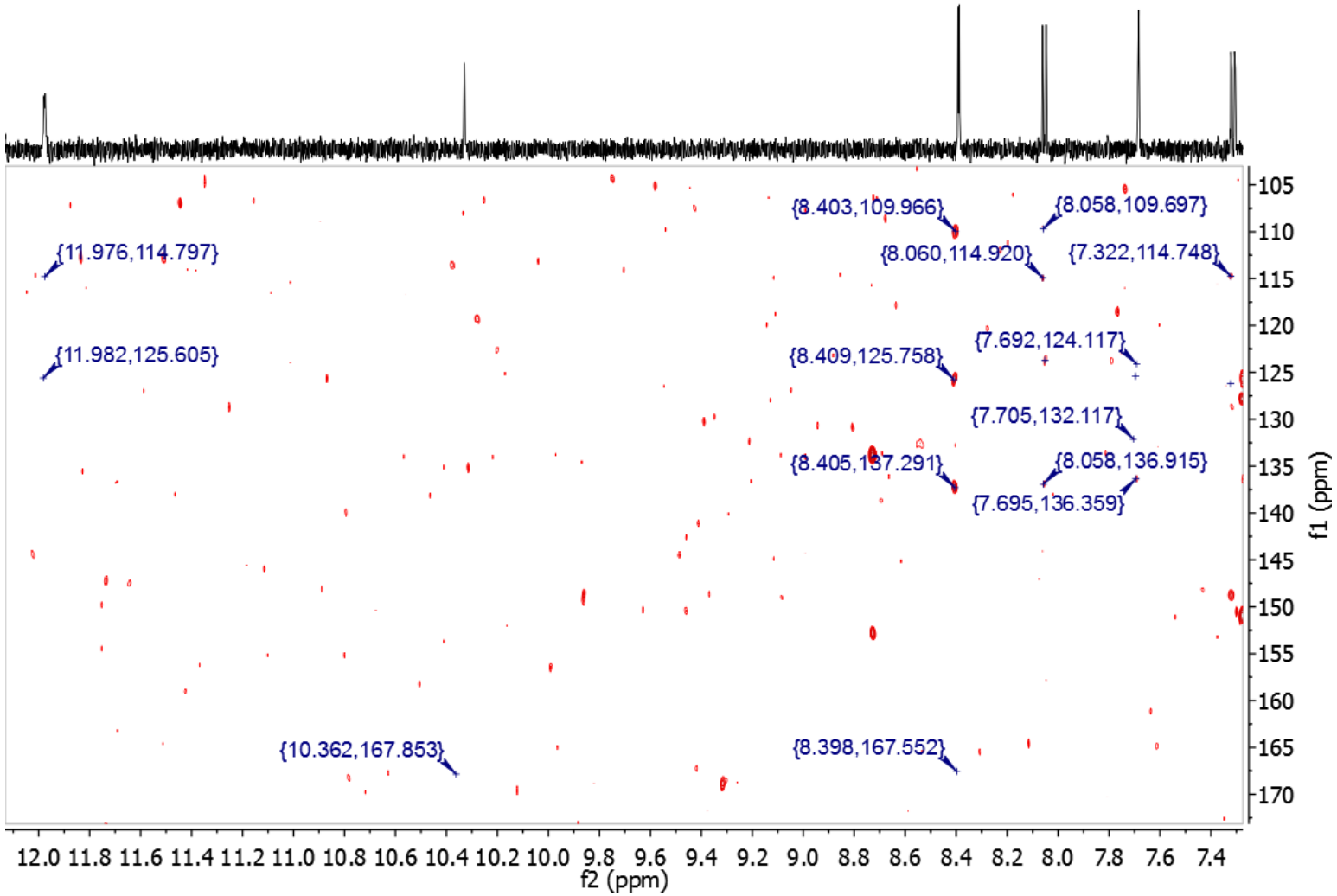

Figure S8. HMBC spectrum of compound **2** in DMSO-d_6

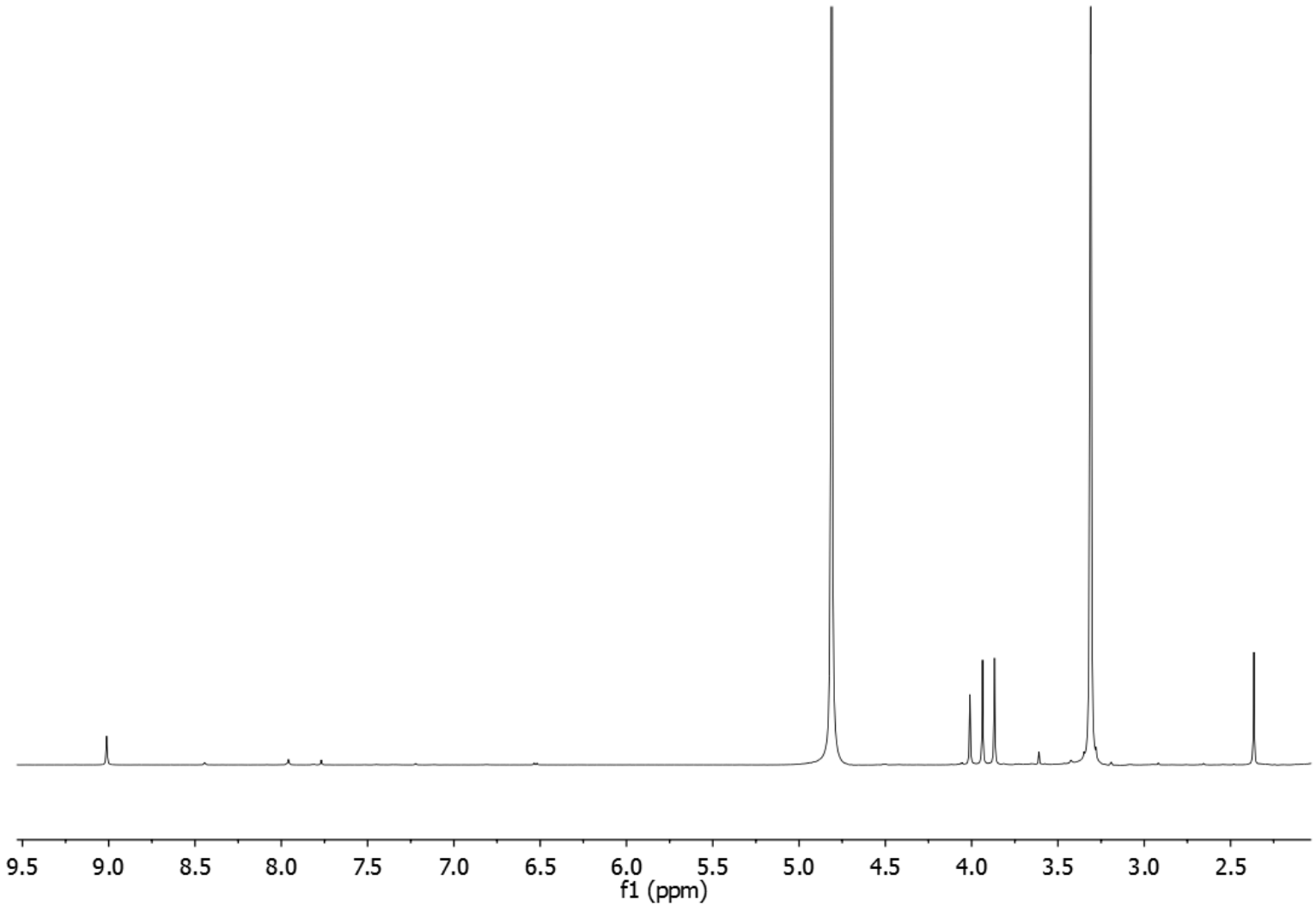

Figure S9. ^{1}HNMR spectrum of compound **3** in MeOH-d_4

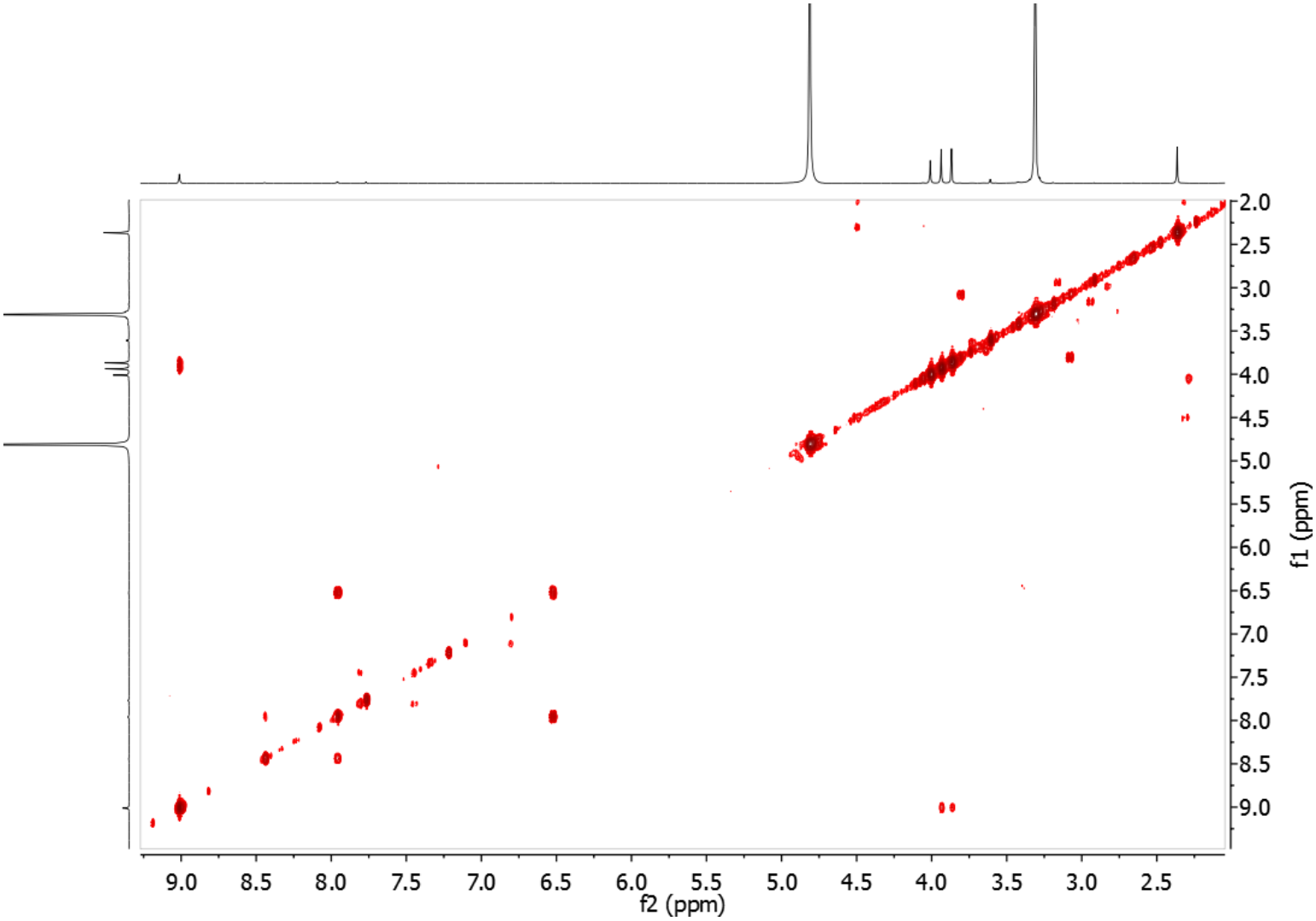

Figure S10. COSY spectrum of compound **3** in MeOH-d_4

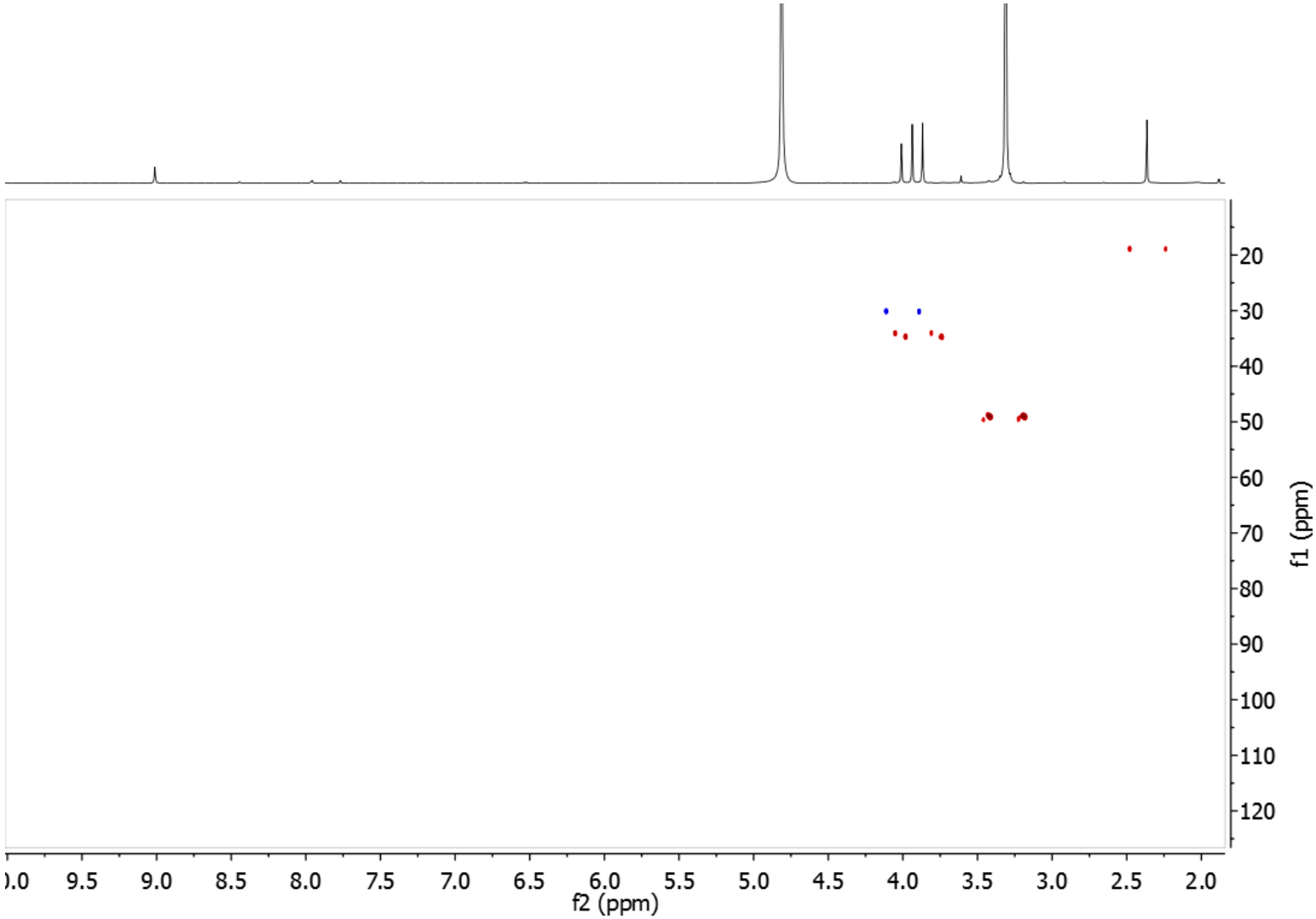

Figure S11. HSQC spectrum of compound **3** in MeOH-d_4

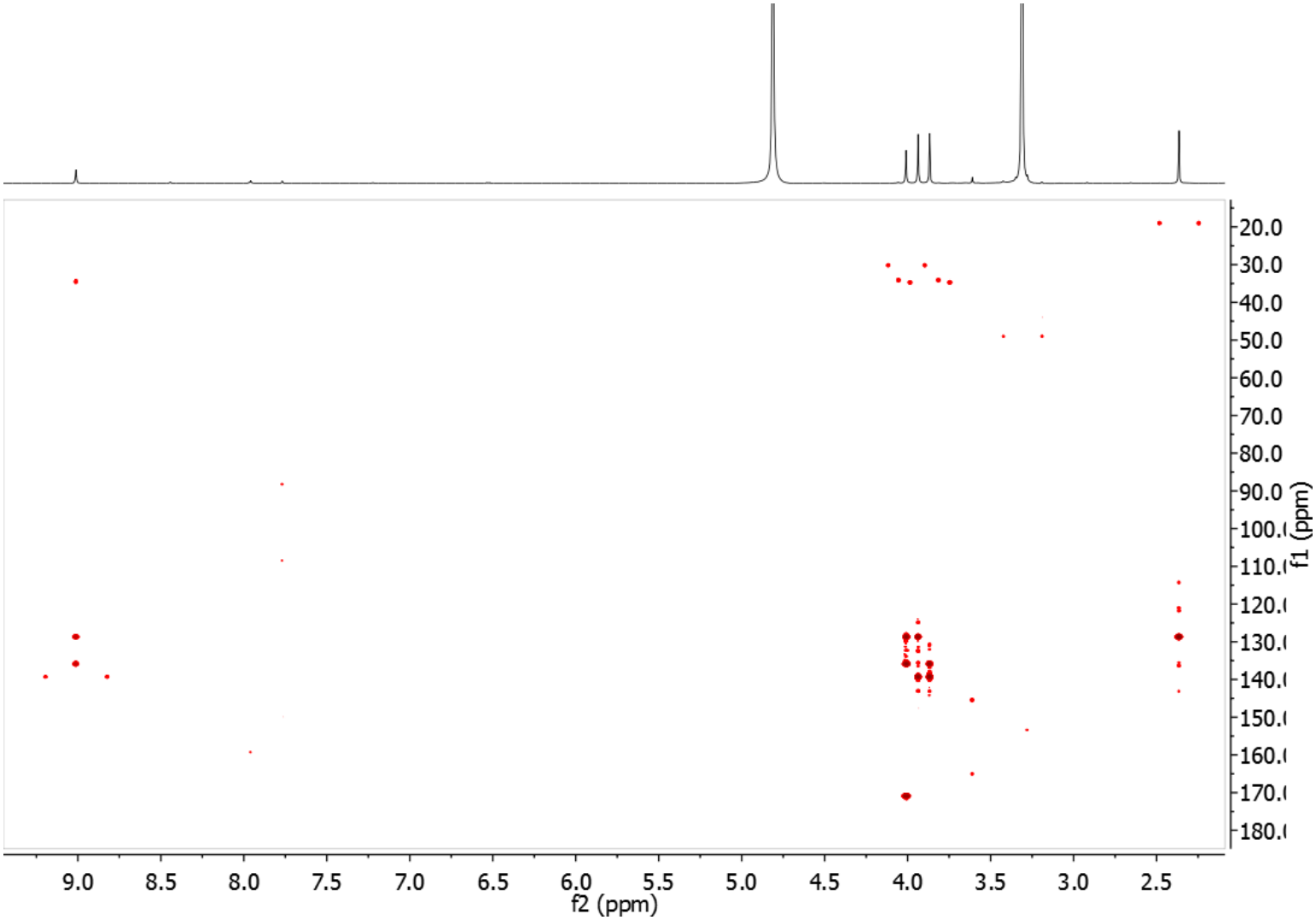

Figure S12. HMBC spectrum of compound **3** in MeOH-d_4

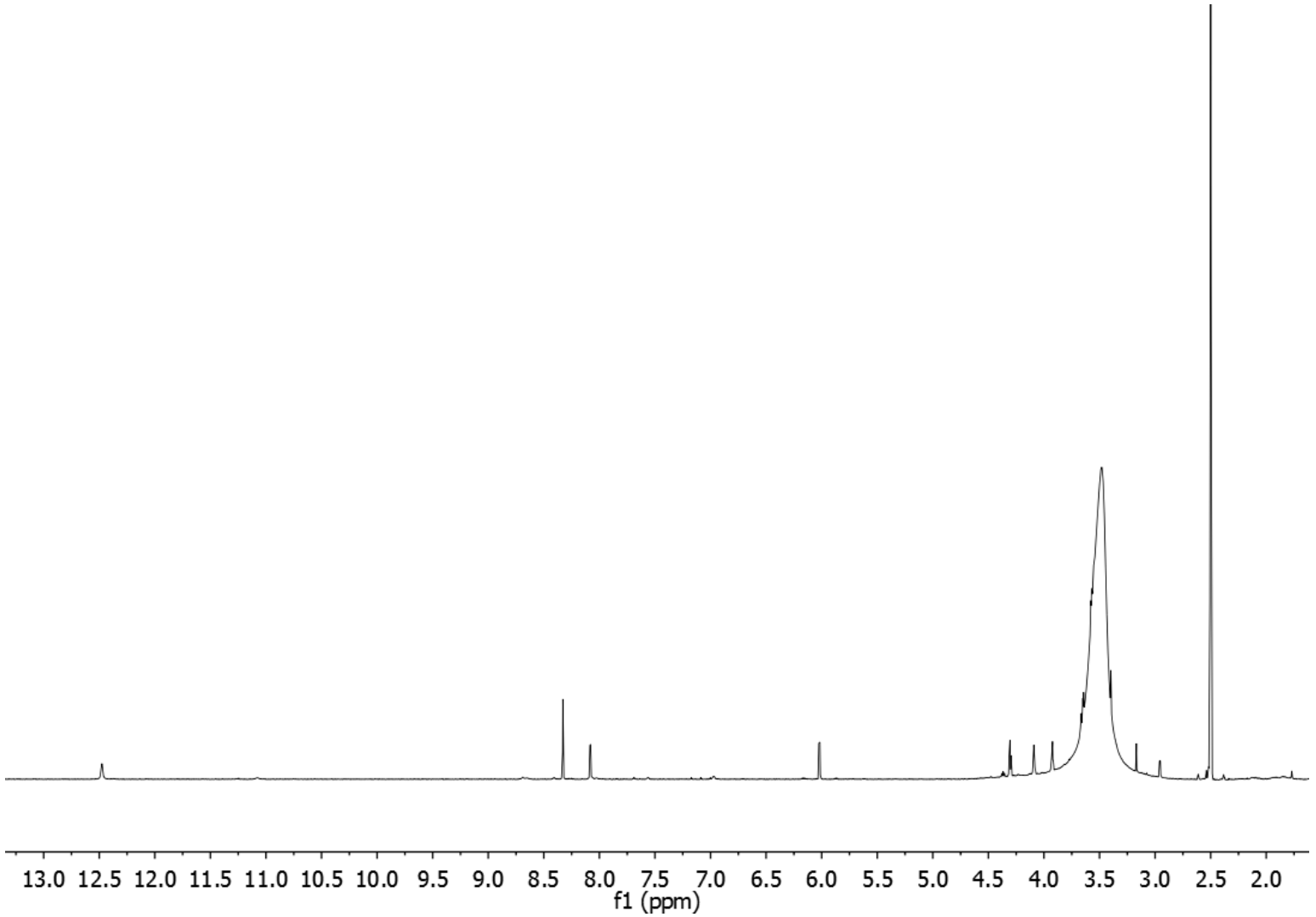

Figure S13. ^{1}HNMR spectrum of compound **8** in DMSO-d_6

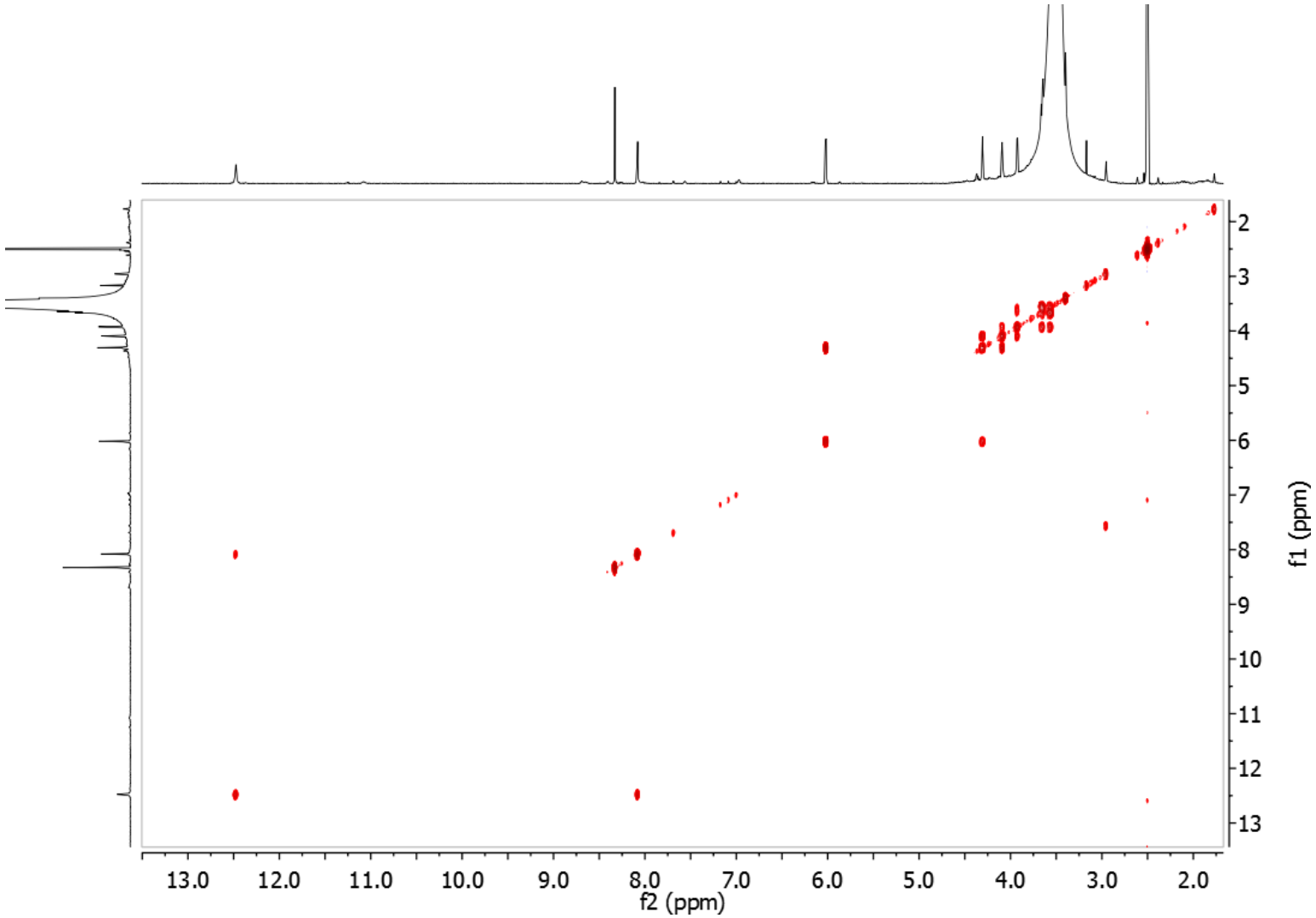

Figure S14. COSY spectrum of compound **8** in DMSO-d_6

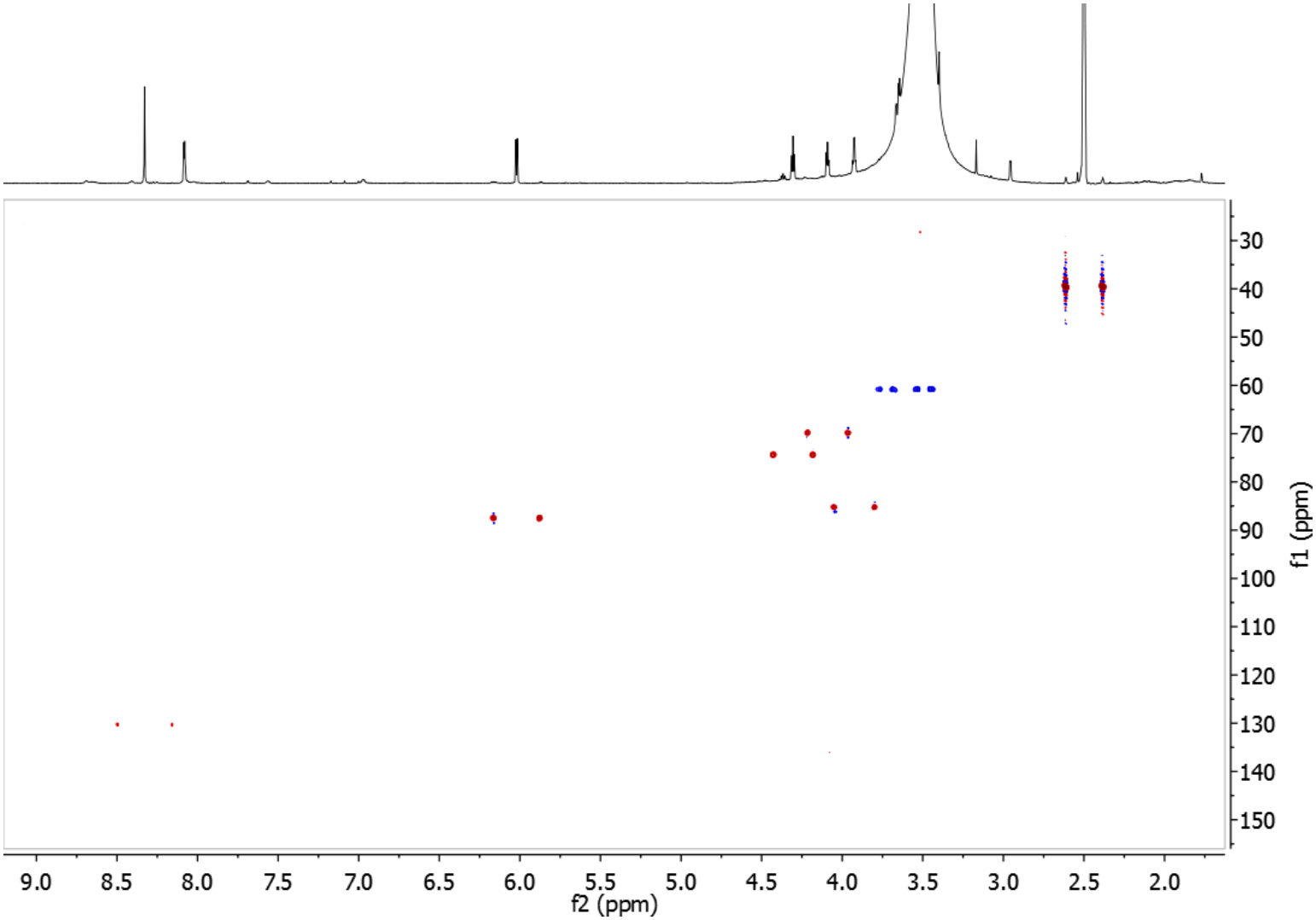

Figure S15. HSQC spectrum of compound **8** in DMSO-d_6

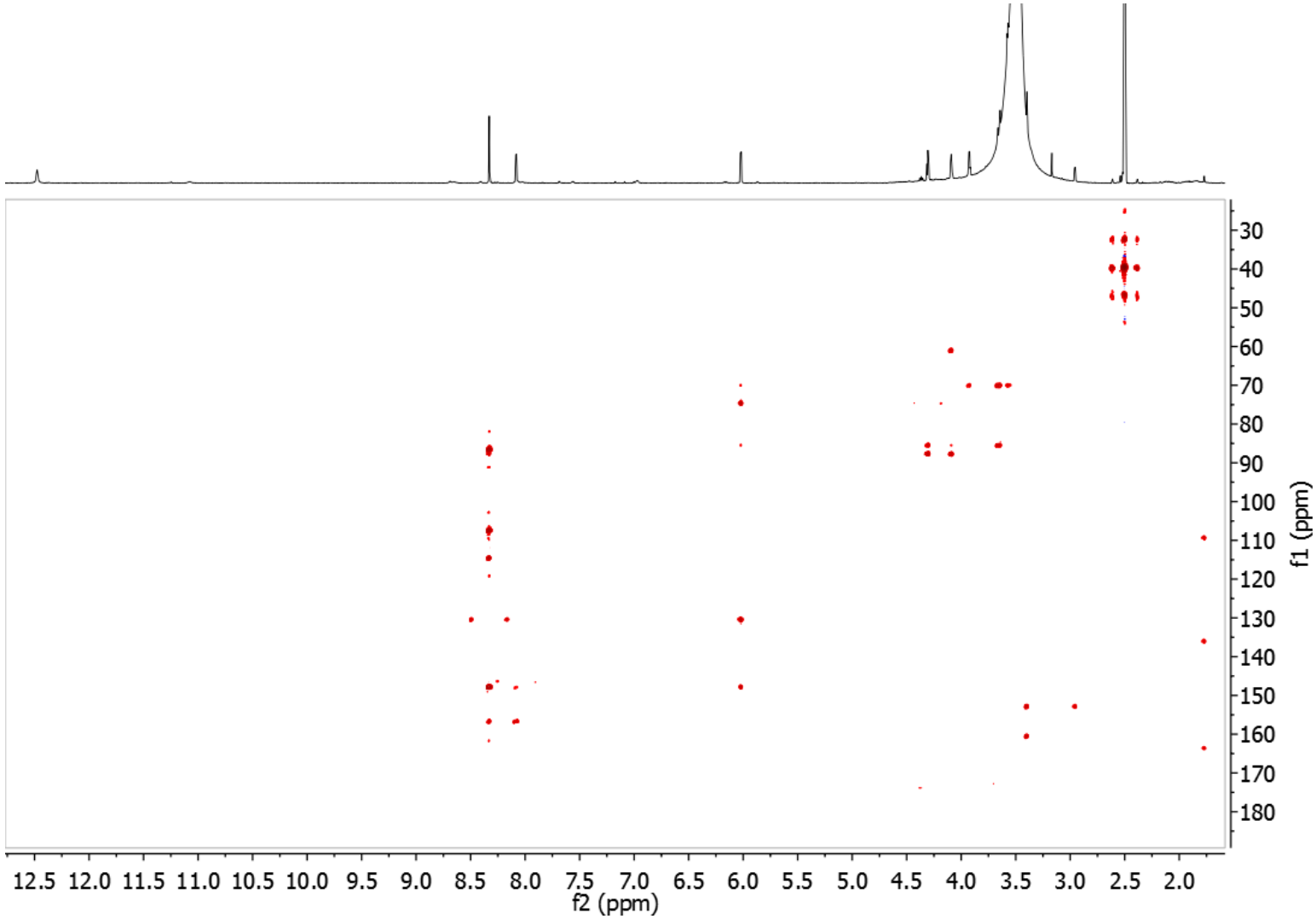

Figure S16. HMBC spectrum of compound **8** in DMSO-d_6

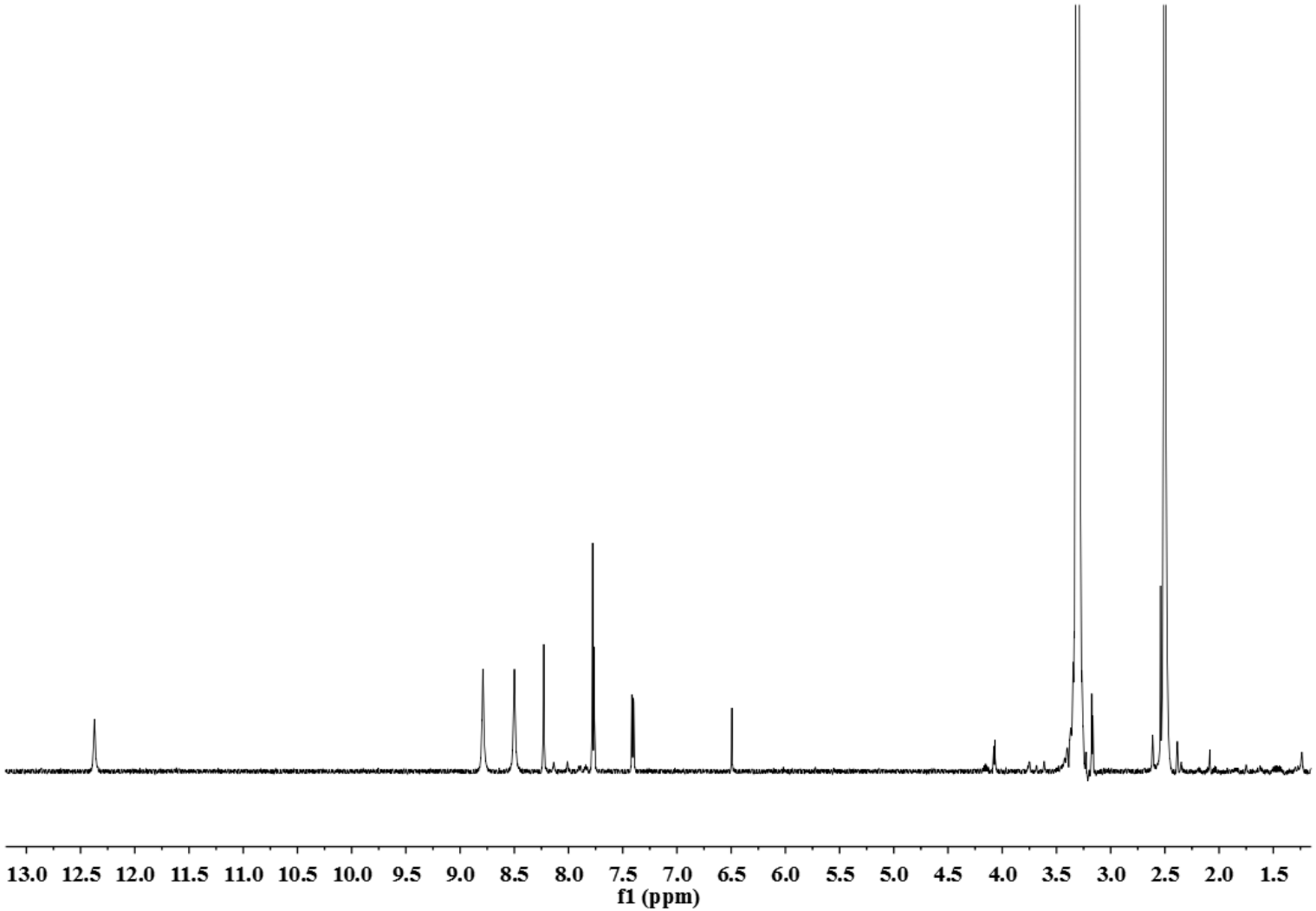

Figure S17. [1]HNMR spectrum of compound **16** in DMSO-d_6

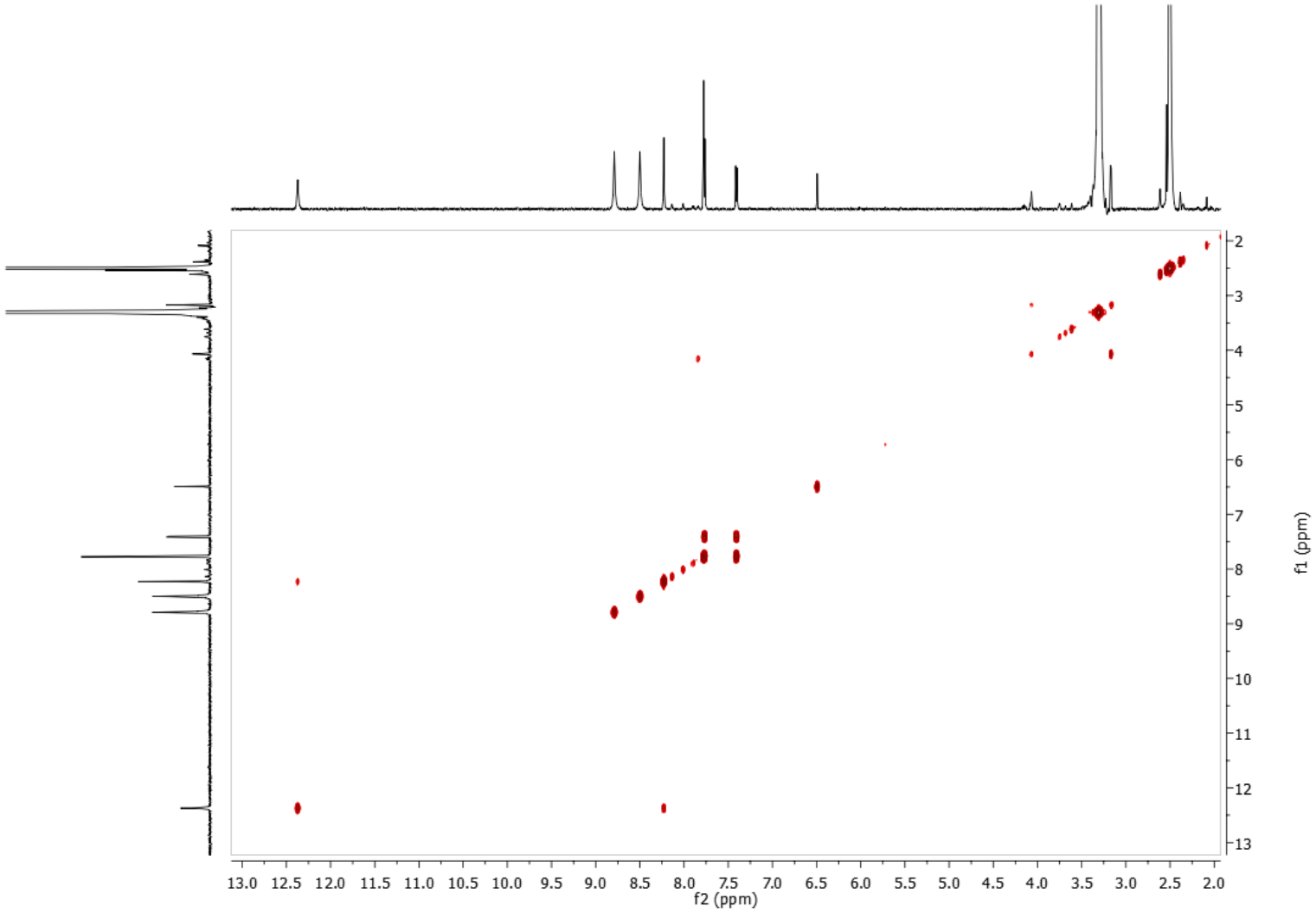

Figure S18. COSY spectrum of compound **16** in DMSO-d_6

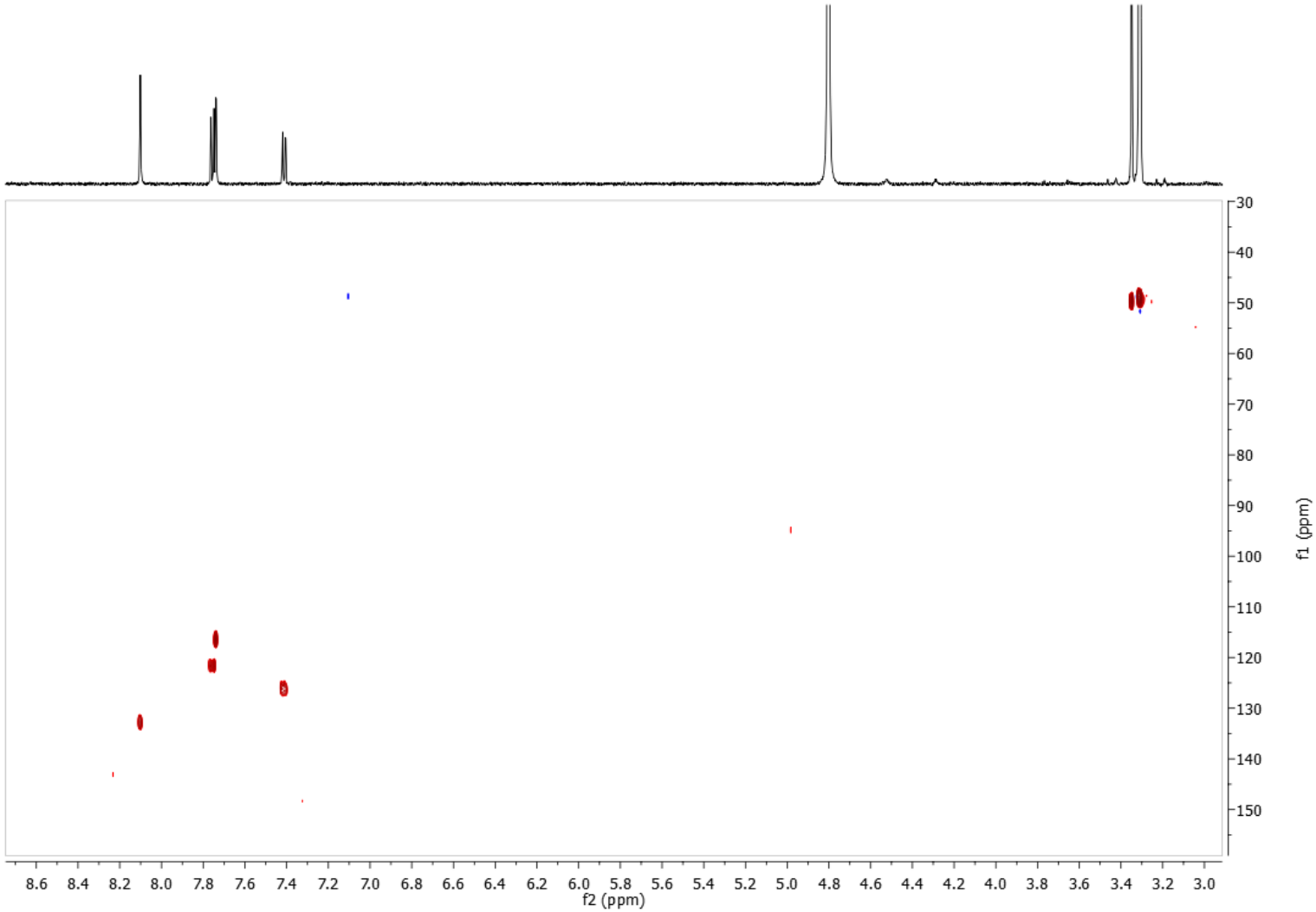

Figure S19. HSQC spectrum of compound **16** in MeOH-d_4

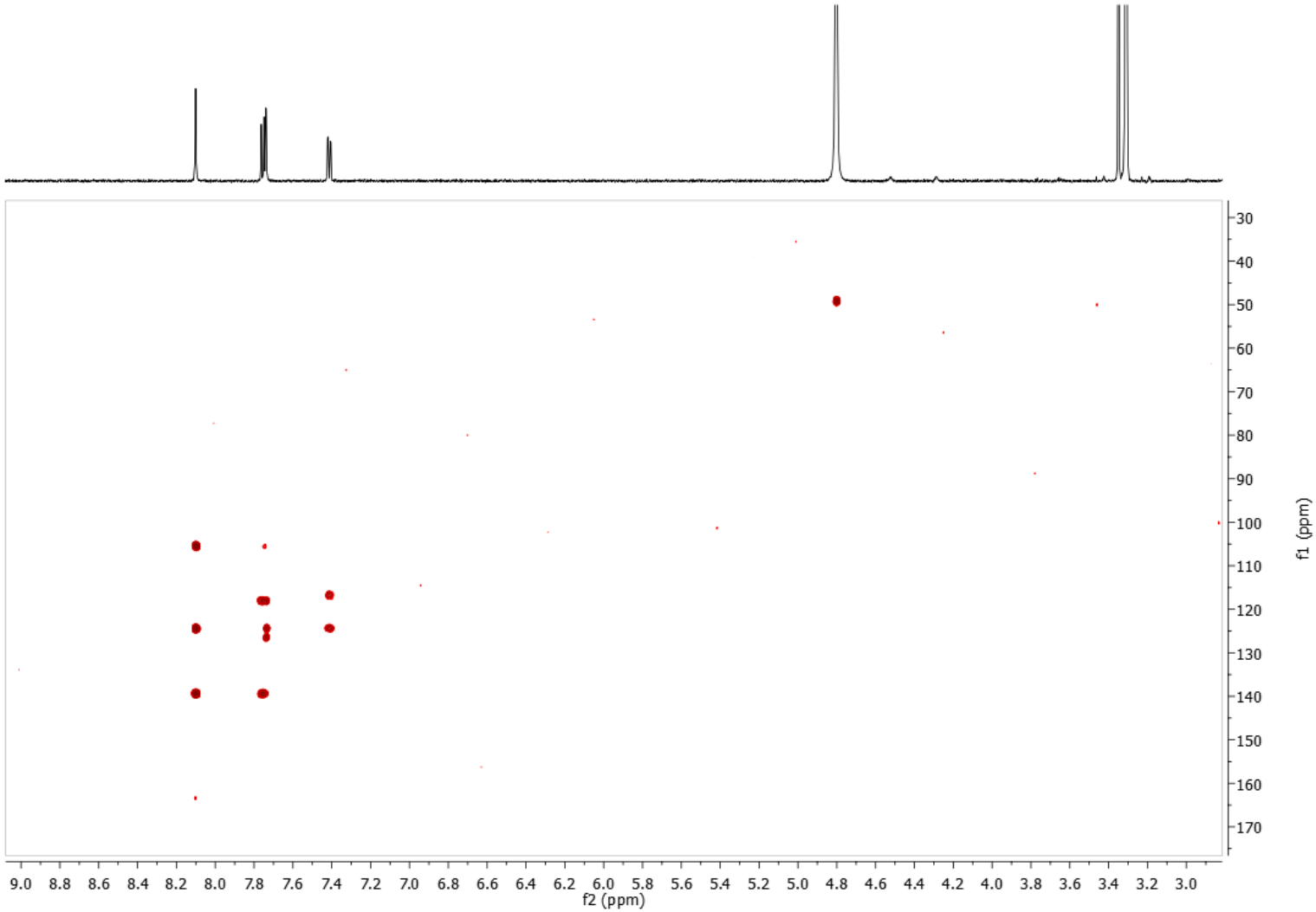

Figure S20. HMBC spectrum of compound **16** in MeOH-d_4

Table S1. The drug- and lead-like physicochemical properties

The drug- and lead-like physicochemical properties of these 22 natural products were calculated using Instant JChem (version 15.7.27.0). The parameters including molecular weight (MW), log P, number of hydrogen bond acceptors (HBA), and number of hydrogen bond donors (HBD) were analyzed against Lipinski's rule-of-five (Table **S1** and Figure **S21**).

Table **S1**. Physicochemical Profiling of Isolated Natural Products **1**-**22** from *Jaspis splendens*.

compound	physicochemical parameters[a]				
	MW	log *P*	HBA	HBD	No. of Violations
1	191.19	-0.46	5	1	0
2	461.11	4.40	2	3	0
3	201.26	-3.19	2	1	0
4	283.24	-2.71	8	5	0
5	267.25	-2.01	8	4	0
6	242.23	-1.12	5	3	0
7	291.27	-1.42	8	4	0
8	292.25	-1.81	7	4	0
9	324.29	-1.27	8	4	0
10	309.28	-2.43	8	5	0
11	192.18	0.28	4	2	0
12	159.15	0.14	4	2	0
13	177.17	-0.87	4	3	0
14	239.12	2.26	1	2	0
15	239.07	1.69	1	2	0
16	238.09	1.76	2	3	0
17	254.08	2.84	1	1	0
18	709.68	5.04	5	4	2
19	723.67	4.69	6	4	1
20	727.70	4.38	7	6	2
21	695.66	4.80	5	4	1
22	788.58	5.81	5	4	2

[a] All physicochemical properties, including molecular weight (MW), log P, hydrogen bond acceptors (HBA) and hydrogen bond donors (HBD), were calculated using Instant JChem (version 15.7.27.0).

The results (Table **S1** and Figure **S21**) suggested that the majority of isolated natural products obeyed Lipinski's rule-of-five in terms of log P < 5 (90.9%), MW < 500 Da (77.3%), HBA < 10 (100%) and HBD < 5 (95.5%).

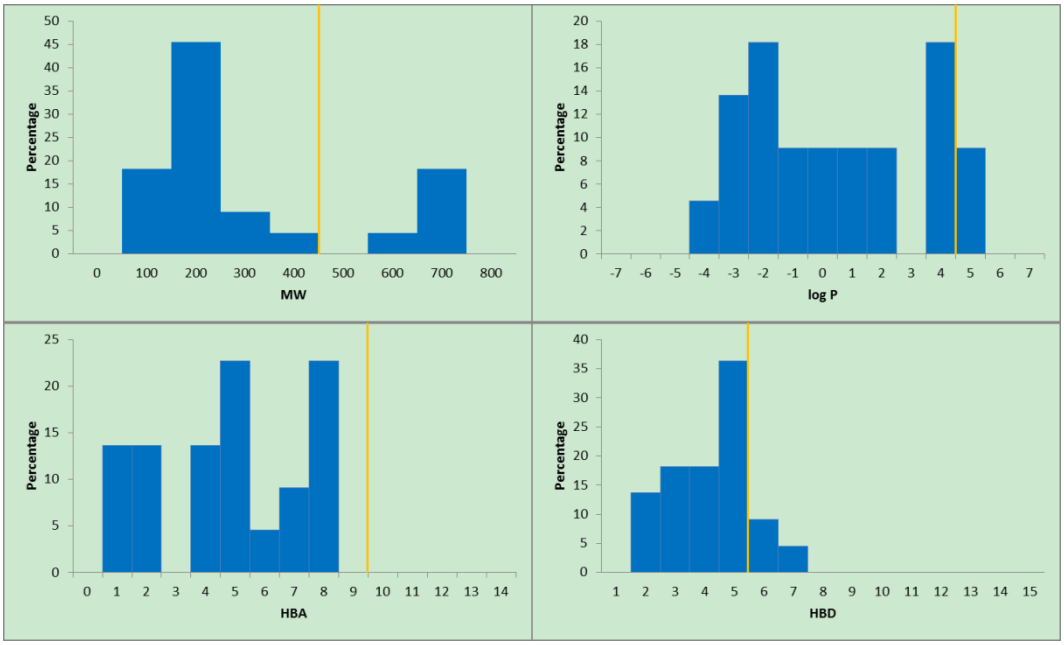

Figure **S21**. Physicochemical property histograms (MW, log P, HBD, and HBA) for compounds isolated from *Jaspis splendens*. In each case the orange line indicates the maximum desirable value for oral bioavailability defined by Lipinski's rule-of-five: MW < 500 Da; log P < 5, HBA < 10 and HBD < 5.

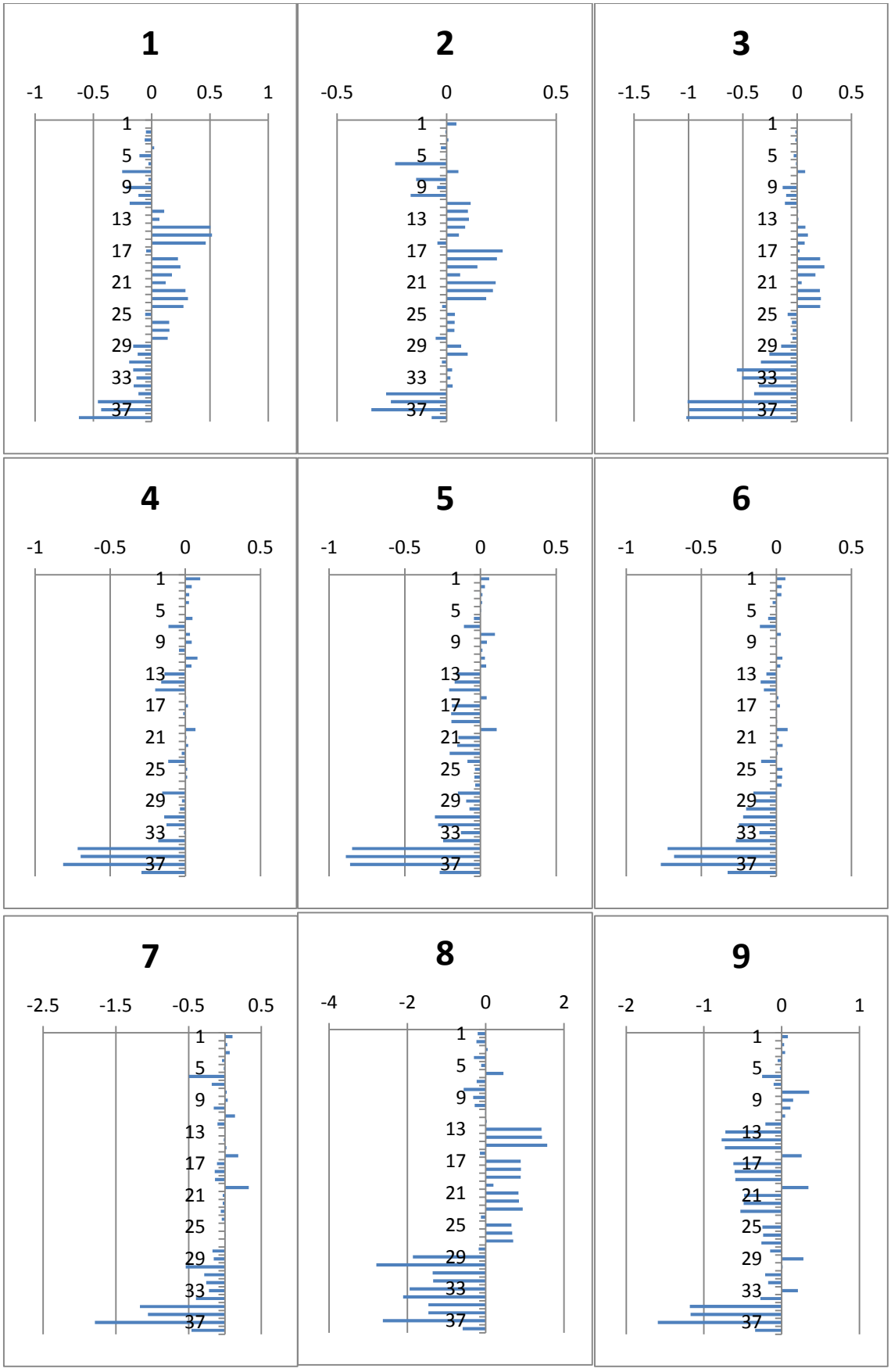

Figure S22. Biological activity profile of metabolites **1** to **9** from *Jaspis splendens*

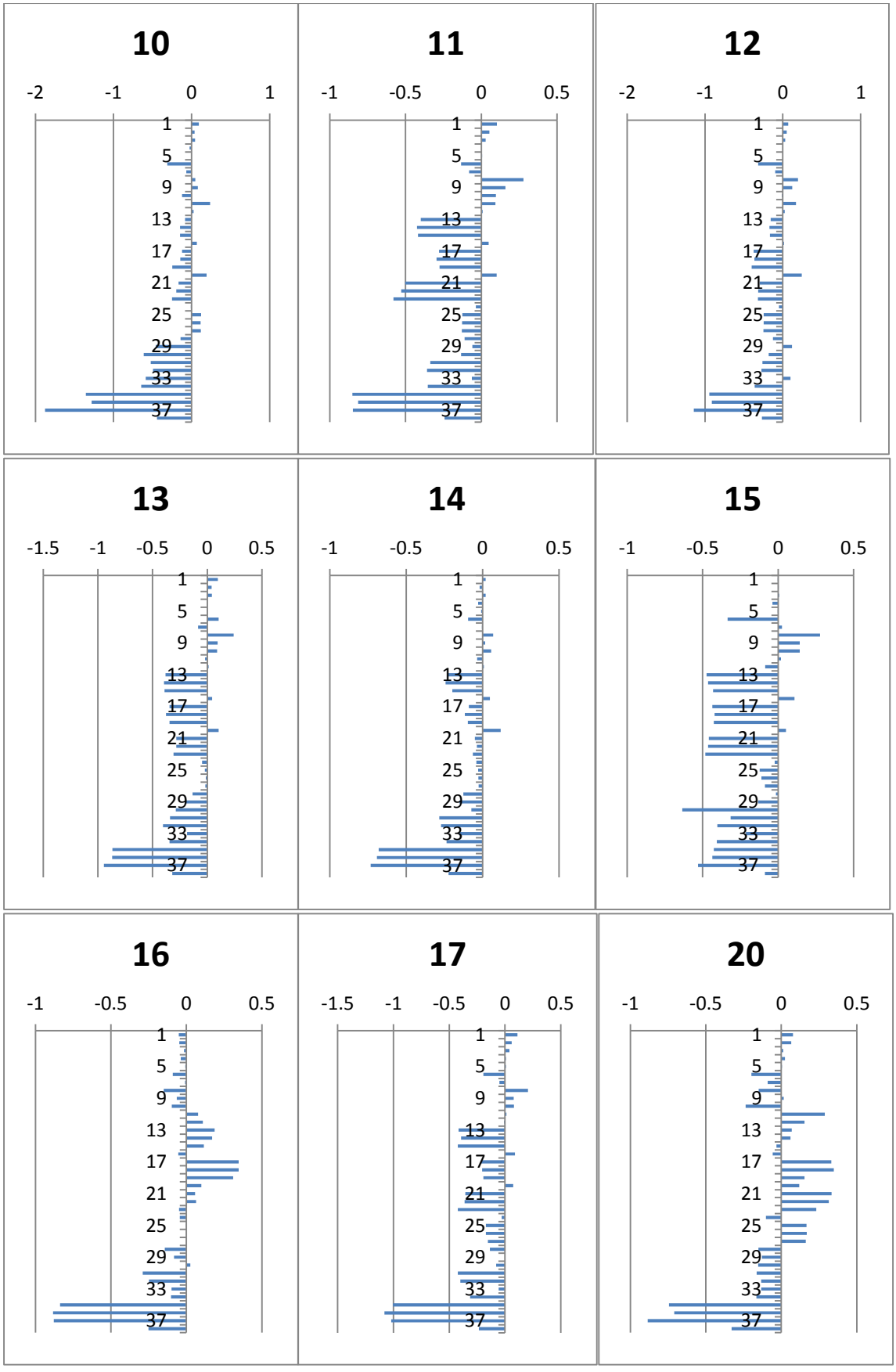

Figure S23. Biological activity profile of metabolites **10** to **17** and **20** from *Jaspis splendens*

Figure S24. Photograph of the marine sponge *Jaspis splendens* (G320726)

Chapter Three. A Grand Challenge (Ⅱ): Unbiased Phenotypic Function of Metabolites from *Gloriosa superba* L. against Parkinson's Disease

Dongdong Wang,[†] Yunjiang Feng,[†] Mariyam Murtaza,[†] Stephen A. Wood,[†] George D. Mellick,[†] Paul I. Forster[‡] and Ronald J. Quinn[†,*]

[†]Eskitis Institute for Drug Discovery, Griffith University, Brisbane, QLD 4111, Australia

[‡]Queensland Herbarium, Brisbane Botanic Gardens, Brisbane, QLD 4066, Australia

ABSTRACT

Following the footstep of the previous Grand Challenge paper, we chemically and biologically investigated the leaves of an Australian plant *Gloriosa superba* L. The chemical investigations resulted in the isolation of four new alkaloids *β*-lumicolchicosides A-C (**1**-**3**) and *γ*-lumicolchicoside A (**4**), one new nucleoside derivative N^3-2-hydroxybenzyluridine (**15**), two new phenolic glycosides gloriosides A and B (**19** and **22**), together with four lumicolchicine derivatives (**5**-**8**), six colchicine analogues (**9**-**14**), three nucleosides (**16**-**18**), eight phenolic glycosides (**19**, **20**, **23**-**28**), one coumarin (**29**), one ellagic acid glycoside (**30**), two flavones (**31**, **32**) and seven flavone glycosides (**33**-**39**). The chemical structures of the seven new compounds (**1**-**4**, **15**, **19** and **22**) were unambiguously characterized by extensive analyses of their NMR and mass spectroscopic data. An unbiased assay, using a human olfactory neurosphere-derived (hONS) cell model of Parkinson's disease (PD), examined the phenotypic profiles of all of the metabolites. The seven new compounds showed slight phenotypic perturbations of several markers in PD patient derived hONS cells. Colchicine and its congeners displayed phenotypic profiles with major effects on mitochondria and autophagy and modest effects on tubulin markers in patient derived PD cells.

INREODUCTION

As part of our continuing effort to identify chemical probes to interrogate Parkinson's disease using an unbiased phenotypic assay,[1] an Australian plant *Gloriosa superba* L. was chemically investigated.[2,3] Thirty-nine isolated natural products were cytologically profiled using the human olfactory neurosphere-derived (hONS) cells, from a Parkinson's disease patient, which models functional aspects of Parkinson's disease.[4]

Plants belonging to the genus *Gloriosa* (family Colchicaceae) have ten different species.[5-8] *G. superba* L. is a perennial climber and its alkaloid-rich tuber and seeds have long been used as traditional medicines in many cultures for the treatment of gout, rheumatism, ulcers, infertility, open wounds, and cancer.[9,10] However, there is no reported traditional medicinal use of *G. superba* L. for brain and neurological diseases.

The genus *Gloriosa* is the source of sixty characterized natural products,[11] of which the majority of compounds belong to the colchicine and lumicolchicine alkaloid structure classes.[11] Colchicine, the major poisonous alkaloid first isolated in 1820 by Pelletier and Caventou,[12] is a well-known secondary metabolite with a skewed phenyl-tropolone ring system.[13] Its complete structure was finally determined in the early 1950s.[14,15] Colchicine and its congeners have attracted a great amount of interest for many years due to their chemistry and biological activity. Colchicine was first used for the management of sore joints and acute gout.[16] It was approved by FDA in 2009 as a monotherapy for the treatment of familial Mediterranean fever,[17] acute gout flares, and prophylaxis of gout flares.[18] The compound has also been reported to possess antitumor and anti-inflammatory properties and is still used in the treatment of Behcet's syndrome,[19] cirrhosis, arthritis and

psoriasis.[20,21] Colchicine is an antimitotic drug that terminates cell division in such a manner that mitosis is arrested in metaphase.[22,23] Studies on the mechanism of action suggested that colchicine and its analogues inhibit mitosis and other cellular functions by specifically binding to tubulin and inhibiting its assembly into microtubule.[13,24] A series of cyclobutene containing colchicine derivatives, namely lumicolchicines, have been discovered within the last 60 years.[25] Chemically, colchicine alkaloids are unstable and in solution they can decompose under light and in high temperatures to *α*-, *β*- and *γ*-lumicolchicines.[26,27] There has also been reports of the isolation of colchicine and lumicolchicine glycosides from the genus *Gloriosa* and related genera.[28-31]

G. superba L. was collected from Hervey Bay, Australia. Chemical investigations of the leaves of *G. superba* L. resulted in the isolation and characterization of 39 secondary metabolites, including four new lumicolchicine glycosides *β*-lumicolchicoside A-C (**1**-**3**) and *γ*-lumicolchicoside A (**4**), one new nucleoside derivative N^3-2-hydroxybenzyluridine (**15**), two new phenolic glycosides gloriosides A and B (**19** and **22**), together with the previously reported natural products 2-*O*-demethyl-*β*-lumicolchicine (**5**),[32] 2-*O*-demethyl-*N*-deacetyl-*N*-formyl-*β*-lumicolchicine (**6**),[33] *N*-deacetyl-*N*-formyl-*β*-lumicolchicine (**7**),[34] *β*-lumicolchicine (**8**),[35] colchicine (**9**),[35] 3-*O*-demethylcolchicine (**10**),[36] 2-*O*-demethylcolchicine (**11**),[37] *N*-deacetyl-*N*-formylcolchicine (**12**),[38] 2-*O*-demethyl-*N*-deacetyl-formyl-colchicine (**13**),[37] cornigerine (**14**),[39] thymidine (**16**),[40] adenosine (**17**),[41] guanosine (**18**),[42] methyl 2-(*β*-D-glucopyranosyloxy-6-hydroxybenzoate (**20**),[43] jiamizioside C (**21**),[44] dodegranoside G (**23**),[45] 1-*O*-*β*-D-glucopyranosyl pyrocatechol (**24**),[45] salicin (**25**),[43] isosalicin (**26**),[46] 2'-*O*-*β*-D-glucopyranosylsalicin (**27**),[47] benzyl gentiobioside (**28**),[48] aesculetin (**29**),[49] 3,3'-di-*O*-methylellagic acid-4'-*O*-*β*-D-

glucopyranoside (**30**),[50] apigenin (**31**),[51] luteolin (**32**),[51] luteolin 3',7-diglucoside (**33**),[52] luteolin 4',7-diglucoside (**34**),[53] skolimoside (**35**),[54] neodiosmin (**36**),[55] luteolin-7-*O*-glucoside (**37**),[56] thermopsoside (**38**)[57] and dracocephaloside (**39**).[58] The chemical structures of the metabolites were elucidated using a series of spectrometric and spectroscopic techniques.

On the basis of previous work, we developed a theoretical framework that explains that all natural products interact with biologically relevant space.[59,60] All of the compounds were subjected to an unbiased phenotypic assay on human olfactory neurosphere-derived (hONS) cell line, followed by analysis of their cytological effects. Herein we report the isolation and structure elucidation of the seven new compounds (**1**-**4**, **15**, **19** and **22**) as well as the phenotypic effects of all of the isolated natural products from *G. superba* L.

RESULTS AND DISCUSSION

The air-dried and ground leaves of *G. superba* L. (20 g) were sequentially extracted with *n*-hexane, CH_2Cl_2, and MeOH. The CH_2Cl_2/MeOH extracts were combined and fractionated using a C_{18} bonded silica flash column. Subsequently four fractions were collected by eluting with stepwise MeOH/H_2O gradients (10% MeOH/90% H_2O, 50% MeOH/50% H_2O, 90% MeOH/10% H_2O and MeOH, respectively; each containing 0.1% trifluoroacetic acid (TFA)). Previous studies on colchicine analogues from the genus *Gloriosa* and its related genera have revealed that these type of alkaloids have typical methoxyl signals between δ_H 4.00 and 3.50 and acetamide signals between δ_H 8.20 and 7.50, 1.90 and 1.70 in their ^1H spectra.[35,39,61] The ^1H NMR spectrum in DMSO-d_6 of the 50% MeOH/50% H_2O fraction displayed signals characteristic of colchicine and

lumicolchicine alkaloids, including methoxyl singlets between δ_H 4.00 and 3.50, acetamidic proton doublets between δ_H 8.20 and 7.50, methyl singlets between δ_H 1.90 and 1.70, and aromatic signals between δ_H 8.50 and 7.00. Further purification of the fraction by C_{18} bonded silica HPLC (gradient MeOH/H_2O with 0.1% TFA) yielded four new lumicolchicine glycosides, namely *β*-lumicolchicosides A-C (**1**-**3**) and *γ*-lumicolchicoside A (**4**), along with known *β*-lumicolchicines (**5**-**8**), colchicines (**9**-**14**) and flavone glycosides (**33**-**39**). The ^{1}H NMR spectrum of the 10% MeOH/90% H_2O fraction contained signals indicative of nucleosides and phenolic glycoside type molecules. Further purification of the fraction led to the isolation of three new metabolites, namely N^3-2-hydroxybenzyluridine (**15**), gloriosides A and B (**19**, **22**), together with known nucleosides (**16**-**18**) and phenolic glycosides (**20**, **21** and **23**-**28**). Further purification of the 90% MeOH/10% H_2O fraction resulted in the isolation of four known natural products (**29**-**32**). In total, 39 structurally diverse secondary metabolites were isolated from the prolific Australian plant *G. superba* L.

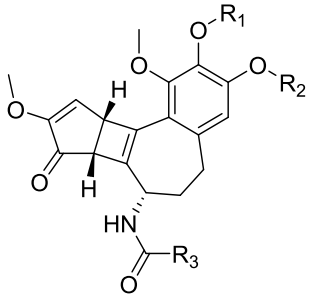

1 R_1=*β*-D-glucose, R_2=R_3=CH_3
2 R_1=*β*-D-glucose, R_2=CH_3, R_3=H
3 R_1=H, R_2=*β*-D-glucose, R_3=CH_3
5 R_1=H, R_2=R_3=CH_3
6 R_1=R_3=H, R_2=CH_3
7 R_1=R_2=CH_3, R_3=H
8 R_1=R_2=R_3=CH_3

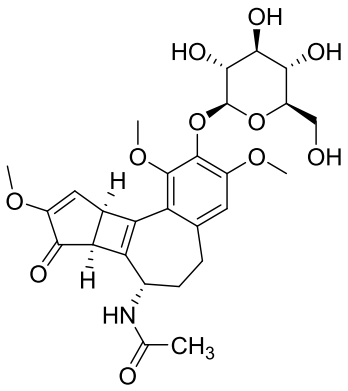

4

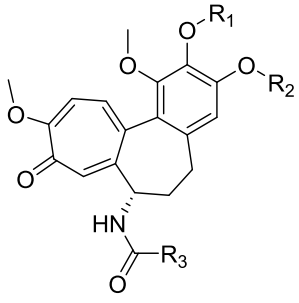

9 R_1=R_2=R_3=CH_3
10 R_1=R_3=CH_3, R_2=H
11 R_1=H, R_2=R_3=CH_3
12 R_1=R_2=CH_3, R_3=H
13 R_1=R_3=H, R_2=CH_3
14 R_1+R_2=CH_2, R_3=CH_3

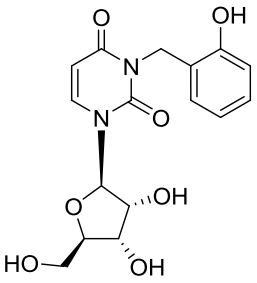

15

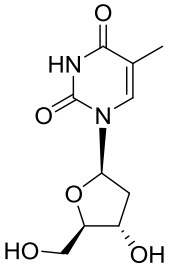

16

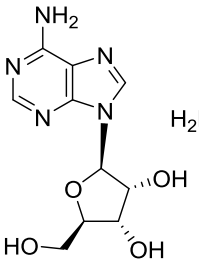

17

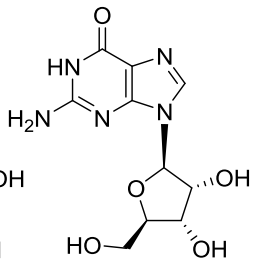

18

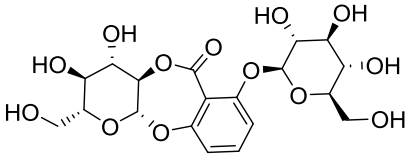

19

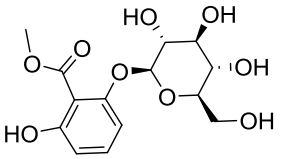

20

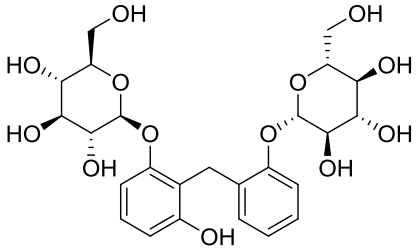

21

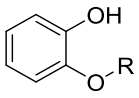

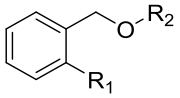

22 R=*β*-D-glucopyranosyl-(1→6)-*β*-D-glucopyranoside
23 R=*β*-D-glucopyranosyl-(1→2)-*β*-D-glucopyranoside
24 R=*β*-D-glucopyranoside

25 R_1=*O*-*β*-D-glucopyranoside, R_2=H
26 R_1=OH, R_2=*β*-D-glucopyranoside
27 R_1=*O*-*β*-D-glucopyranosyl-(1→2)-*β*-D-glucopyranoside, R_2=H
28 R_1=H, R_2=*β*-D-glucopyranosyl-(1→6)-*β*-D-glucopyranoside

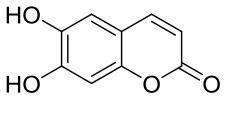

29

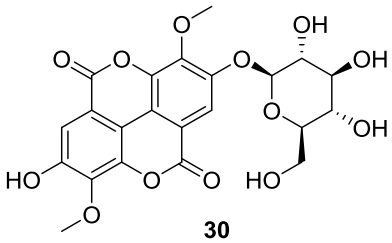

30

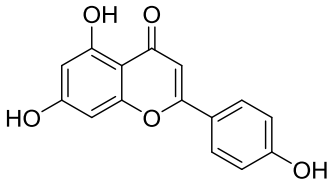

31

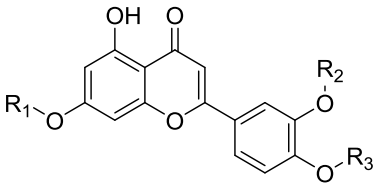

32 R_1=R_2=R_3=H
33 R_1=R_2=*β*-D-glucopyranoside, R_3=H
34 R_1=R_3=*β*-D-glucopyranoside, R_2=H
35 R_1=*α*-L-rhamnopyranosyl-(1→6)-*β*-D-glucopyranoside, R_2=R_3=H
36 R_1=*α*-L-rhamnopyranosyl-(1→6)-*β*-D-glucopyranoside, R_2=H, R_3=CH_3
37 R_1=*β*-D-glucopyranoside, R_2=R_3=H
38 R_1=*β*-D-glucopyranoside, R_2=CH_3, R_3=H
39 R_1=R_3=H, R_2=*β*-D-glucopyranoside

β-Lumicolchicoside A (**1**) was isolated as an optically active pale yellow powder with an $[\alpha]_D$ value of +41.4. HRESIMS data gave a $[M+Na]^+$ ion at *m*/*z* 570.1944, which was consistent with a molecular formula of $C_{27}H_{33}NO_{11}$, and implied twelve degrees of

unsaturation. The ^{1}H NMR spectrum contained one aromatic methine singlet (δ_H 6.68), one olefinic methine doublet (δ_H 6.61, d, J = 3.3 Hz), one anomeric methine doublet (δ_H 5.06, d, J = 7.2 Hz), seven deshielded methines (δ_H 4.72, 4.01, 3.45, 3.25, 3.24, 3.14 and 3.07), three methylene moieties (δ_H 3.62/3.40, 2.68 and 1.75), three methoxyl singlets (δ_H 3.89, 3.77 and 3.61), one methyl singlet (δ_H 1.78) and one exchangeable amino proton doublet (δ_H 7.78, d, J = 9.1 Hz) (Table 1). Analysis of the ^{13}C NMR spectrum indicated the molecule contained two carbonyl carbons (δ_C 199.1 and 168.1), ten sp^2 hybridized carbons (δ_C 157.6, 152.8, 151.2, 144.1, 139.6, 139.5, 136.8, 127.3, 118.5 and 109.9), three methoxyls (δ_C 61.5, 56.1 and 56.1), one methyl (δ_C 22.6), three methylenes (δ_C 60.8, 31.5 and 31.1) and eight sp^3 hybridized methines (δ_C 101.7, 76.8, 76.3, 74.1, 69.7, 51.1, 48.2 and 42.1), six of which were oxygen- or nitrogen-bearing (Table 2). Analysis of the COSY spectrum established three spin systems: CH-CH-CH, NH-CH-CH_2-CH_2 and a sugar moiety (Figure 1 in bold). The deshielded carbon chemical shift of C-1' (δ_C 101.7), the presence of four oxymethine ^{13}C resonances and a deshielded methylene (δ_H 3.62/3.40, δ_C 60.8) suggested a monosaccharide. The coupling constant of the anomeric proton ($J_{H\text{-}1', H\text{-}2'}$ = 7.2 Hz) and the chemical shift of the anomeric carbon ($\delta_{C\text{-}1'}$ 101.7) indicated *β-O*-glycosidic linkage of the glucopyranoside moiety in **1**.

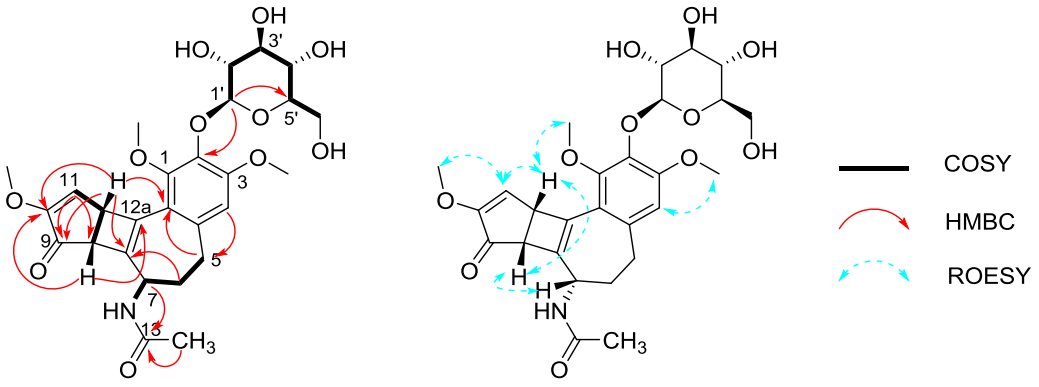

Figure 1. Key COSY, HMBC, and ROESY correlations for **1**

An HMBC correlation from the quadrupole broadened amidic proton doublet (δ_H 7.78, b d, J = 9.1 Hz), which was coupled to H-7 (δ_H 4.72), to a shielded carbonyl carbon C-13 (δ_C 168.1) suggested an acetamide moiety. It was confirmed by an HMBC correlation from the methyl singlet H-14 (δ_H 1.78) to C-13. HMBC correlations from the methine doublet H-11 (δ_H 6.61, d, J = 3.3 Hz) to a methine carbon C-8 (δ_C 51.1) and a carbonyl carbon C-9 (δ_C 199.1), and from the methine proton H-8 (δ_H 3.45) to a nonprotonated carbon C-10 (δ_C 157.6) suggested the presence of a five membered enone ring between CH-CH-CH and an enone. The presence of the cyclopentenone fragment was confirmed by additional HMBC correlations from the methine proton H-12 (δ_H 4.01) to the olefinic carbon C-10 (δ_C 157.6). Further HMBC correlations from the two methine protons H-8 and H-12 (δ_H 3.45 and 4.01) to two sp^2 hybridized carbons C-7a and C-12a (δ_C 139.5 and 144.1) established a cyclobutene ring system between CH-CH-CH and an ethenyl functionality; therefore, the presence of a bicycloheptadienone moiety was confirmed. HMBC correlations from H-7 (δ_H 4.72) to two sp^2 hybridized carbons C-7a and C-12a (δ_C 139.5 and 144.1) suggested the connectivity between NH-CH-CH_2-CH_2 and the bicycloheptadienone moiety. This assignment was confirmed by the HMBC correlation from the methylene proton H-6 (δ_H 1.75) to C-7a (δ_C 139.5). HMBC correlations from the bicycloheptadienone proton H-12 (δ_H 4.01) to the aromatic carbon C-12b (δ_C 118.5) and from the aromatic singlet H-4 (δ_H 6.68) to carbons C-5 and C-12b (δ_C 31.1 and 118.5) revealed the presence of a cycloheptene ring. The establishment was further confirmed by HMBC correlations from the methylene protons H-5 (δ_H 2.68) to two aromatic carbons C-4 and C-12b (δ_C 109.9 and 118.5). Three methoxyl singlets at δ_H 3.89, 3.77 and 3.61 were assigned to C-1, C-3 and C-10 positions (δ_C 151.2, 152.8, and 157.6) based on their HMBC

correlations to the respective carbon. These assignments were further confirmed by ROESY correlations between 1-OCH_3 (δ_H 3.89) and H-12 (δ_H 4.01), 3-OCH_3 (δ_H 3.77) and H-4 (δ_H 6.68), 10-OCH_3 (δ_H 3.61) and H-11 (δ_H 6.61), respectively. An HMBC correlation from the anomeric doublet H-1' (δ_H 5.06, d, J = 7.2 Hz) to C-2 (δ_C 136.8) established the connectivity between the *β-O*-glucopyranose and benzene ring. Thus, with all the atoms accounted for and the requirement to satisfy twelve degrees of unsaturation, the planar structure of *β*-lumicolchicoside A was assigned as **1**. The absolute configuration of the glucose moiety was determined by GC-MS of enantiomers as peracetylated thiazolidine derivatives.[62,63] Acid hydrolysis of **1** followed by derivatization with L-cysteine methyl ester hydrochloride and acetic anhydride gave a GC-MS peak at 18.18 min with a $[M+H]^+$ ion at *m/z* 550, while standard D-glucose derivative gave a retention time of 18.19 min and L-glucose derivative gave a peak at 20.52 min, indicating a D-glucose in the molecule.

Table 1. ^{1}H NMR Spectroscopic Data (600 MHz, DMSO-d_6) for *β*-lumicolchicosides A-C (**1**-**3**) and *γ*-lumicolchicoside A (**4**)

position	**1**	**2**	**3**	**4**
NH	7.78, d (9.1)	8.17, d (8.4)	7.77, d (9.2)	8.16, d (7.8)
4	6.68, s	6.68,s	6.77, s	6.67, s
5	2.68, m	2.70, 2.64, m	2.61, m	2.64, m
6	1.75, m	1.80, 1.75, m	1.72, m	1.74, m
7	4.72, m	4.79, m	4.73, m	4.44, m
8	3.45, d (2.7)	3.48, d (2.7)	3.45, d (2.8)	3.56, d (2.8)
11	6.61, d (3.3)	6.61, d (3.3)	6.64, d (3.2)	6.73, d (3.3)
12	4.01, dd (3.3, 2.7)	4.04, dd (3.3, 2.7)	4.01, dd (3.2, 2.8)	3.98, dd (3.3, 2.8)
13		7.95, s		
14	1.78		1.78	1.85
1-OCH_3	3.89, s	3.89, s	3.87, s	3.93, s
3-OCH_3	3.77, s	3.78, s		3.77, s
10-OCH_3	3.61, s	3.61, s	3.61, s	3.63, s
1'	5.06, d (7.2)	5.05, d (7.1)	4.65, d (7.5)	4.97, d (7.5)
2'	3.25, m	3.26, m	3.31, m	3.26, m
3'	3.24, m	3.25, m	3.26, m	3.21, m
4'	3.14, m	3.15, m	3.16, m	3.17, m
5'	3.07, m	3.06, m	3.31, m	3.07, m
6'a	3.62, m	3.62, m	3.72, dd (11.8, 2.0)	3.62, m
6'b	3.40, m	3.40, m	3.48, dd (11.8, 5.9)	3.41, m

Table 2. ^{13}C NMR Spectroscopic Data (150 MHz, DMSO-d_6) for β-lumicolchicosides A-C (**1**-**3**) and γ-lumicolchicoside A (**4**)

position	**1** ($^1J_{CH}$, Hz)	**2** ($^1J_{CH}$, Hz)	**3** ($^1J_{CH}$, Hz)	**4** ($^1J_{CH}$, Hz)
1	151.2, C	151.1, C	146.4, C	151.1, C
2	136.8, C	135.7, C	138.1, C	136.6, C
3	152.8, C	151.8, C	145.9, C	151.9, C
4	109.9, CH (160.3)	110.1, CH (160.7)	112.7, CH (161.1)	109.9, CH (159.1)
4a	139.6, C	138.2, C	132.8, C	139.5, C
5	31.1, CH_2 (*)	30.6, CH_2 (*)	31.1, CH_2 (*)	31.9, CH_2 (*)
6	31.5, CH_2 (*)	31.5, CH_2 (*)	31.7, CH_2 (*)	31.2, CH_2 (*)
7	48.2, CH (134.7)	46.4, CH (133.8)	48.5, CH (132.2)	47.3, CH (135.5)
7a	139.5, C	137.4, C	140.2, C	138.9, C
8	51.1, CH (148.0)	51.1, CH (147.9)	50.7, CH (146.2)	49.9, CH (147.7)
9	199.1, C	197.5, C	197.4, C	197.5, C
10	157.6, C	157.1, C	157.1, C	157.1, C
11	127.3, CH (168.7)	127.2, CH (169.7)	127.6, CH (170.9)	128.5, CH (171.3)
12	42.1, CH (152.8)	42.1, CH (153.2)	42.1, CH (153.4)	41.9, CH (151.7)
12a	144.1, C	144.5, C	143.2, C	145.6, C
12b	118.5, C	118.7, C	119.4, C	117.4, C
13	168.1, C	159.8, CH (195.5)	168.4, C	168.1, C
14	22.6, CH_3 (126.5)		22.6, CH_3 (124.7)	22.8, CH_3 (124.6)
1-OCH_3	61.5, CH_3 (143.7)	61.4, CH_3 (144.7)	59.9, CH_3 (145.8)	61.4, CH_3 (144.2)
3-OCH_3	56.1, CH_3 (143.7)	56.1, CH_3 (145.0)		56.1, CH_3 (143.3)
10-OCH_3	56.1, CH_3 (145.2)	55.9, CH_3 (144.7)	56.2, CH_3 (145.8)	56.6, CH_3 (145.0)
1'	101.7, CH (166.5)	101.3, CH (165.9)	102.3, CH (162.1)	102.1, CH (165.6)
2'	74.1, CH (140.3)	73.8, CH (140.7)	73.4, CH (139.2)	73.8, CH (141.1)
3'	76.3, CH (137.7)	76.1, CH (138.5)	75.6, CH (140.8)	76.4, CH (140.0)
4'	69.7, CH (138.9)	69.6, CH (137.3)	69.6, CH (137.3)	69.5, CH (137.5)
5'	76.8, CH (134.7)	76.9, CH (135.4)	77.1, CH (136.8)	77.2, CH (137.0)
6'	60.8, CH_2 (*)	60.6, CH_2 (*)	60.7, CH_2 (*)	60.9, CH_2 (*)

(*): signals not clear

β-Lumicolchicoside B (**2**) was assigned a molecular formula of $C_{26}H_{31}NO_{11}$, based on HRESIMS data for $[M-H]^-$ 532.1814, which was consistent with twelve degrees of unsaturation. Inspection of the ^1H and 2D NMR spectra for β-lumicolchicoside B (**2**) suggested that it was structurally related to β-lumicolchicoside A (**1**). However, the ^1H NMR spectrum for **2** lacked the acetamide methyl singlet H-14 at δ_H 1.78. Instead an additional proton singlet at δ_H 7.95 was evident, indicative of a formamide moiety with the

deshielded exchangeable amidic proton doublet (δ_H 8.17, d, J = 8.4 Hz). The assignment was confirmed by HMBC correlations from the formamide singlet H-13 (δ_H 7.95) to the sp^3 hybridized methine carbon C-7 (δ_C 46.4) and from the amido proton (δ_H 8.17) to the formamide carbon C-13 (δ_C 159.8). The coupling constant of the anomeric proton ($J_{H\text{-}1', H\text{-}2'}$ = 7.1 Hz) and the chemical shift of the anomeric carbon ($\delta_{C\text{-}1'}$ 101.3) indicated *β-O*-glycosidic linkage of the glucopyranoside moiety in **2**. Therefore, the planar structure of *β*-lumicolchicoside B was assigned as **2**. Acid hydrolysis of **2** followed by derivatization with L-cysteine methyl ester hydrochloride and acetic anhydride gave a GC-MS peak at 18.37 min with an adduct $[M+H]^+$ ion at *m/z* 550, while standard D-glucose derivative gave a retention time of 18.19 min and L-glucose derivative gave a peak at 20.52 min, indicating a D-glucose in the molecule.

The HRESIMS data ($[M+Na]^+$ *m/z* 556.1787) for *β*-lumicolchicoside C (**3**) supported a molecular formula of $C_{26}H_{31}NO_{11}$, for twelve degrees of unsaturation. The ^1H NMR spectrum for **3** was reminiscent of that for **1**. However, a careful comparison of the two spectra revealed the absence of a methoxyl singlet in **3**. HMBC correlations established the connectivity between 1-OCH_3 (δ_H 3.87) and C-1 (δ_C 146.4), 10-OCH_3 (δ_H 3.60) and C-10 (δ_C 157.1), respectively. These assignments were further confirmed by ROESY correlations between 1-OCH_3 (δ_H 3.87) and H-12a (δ_H 4.01), 10-OCH_3 (δ_H 3.60) and H-11 (δ_H 6.64), respectively. The coupling constant of the anomeric proton ($J_{H\text{-}1', H\text{-}2'}$ = 7.5 Hz) and the chemical shift of the anomeric carbon ($\delta_{C\text{-}1'}$ 102.3) indicated *β-O*-glycosidic linkage of the glucopyranoside moiety in **3**. An HMBC correlation from the anomeric proton doublet H-1' (δ_H 4.65, d, J = 7.5 Hz) to C-3 (δ_C 145.9) placed the monosaccharide at the C-3 position. It was further confirmed by the ROESY correlation between the anomeric

proton H-1' and H-4 (δ_H 6.68). Nonetheless, with all the atoms of **3** accounted for and the requirement to satisfy twelve degrees of unsaturation, the planar structure of *β*-lumicolchicoside C (**3**) was established. Acid hydrolysis of **3** followed by derivatization with L-cysteine methyl ester hydrochloride and acetic anhydride gave a GC-MS peak at 18.08 min with a $[M+H]^+$ ion at *m/z* 550, while standard D-glucose derivative gave a retention time of 18.19 min and L-glucose derivative gave a peak at 20.52 min, indicating a D-glucose in the molecule.

The fourth compound, *γ*-lumicolchicoside A (**4**) was assigned by HRESIMS ($[M+Na]^+$ 570.1944) as $C_{27}H_{33}NO_{11}$, implying twelve degrees of unsaturation. It was optically active with a negative $[\alpha]_D$ value of -26.9, which was different from those of **1**-**3** (+41.4, +38.2 and +32.7, respectively). Inspection of the ^1H and 2D NMR spectra for *γ*-lumicolchicoside A (**4**) suggested that it had the same planar structure to *β*-lumicolchicoside A (**1**). Major differences were noted in the chemical shifts of the diastereotopic protons NH, H-7 and H-8, which resonated at δ_H 8.16, 4.44 and 3.56 in compound **4** compared to δ_H 7.78, 4.72 and 3.45 in compound **1**. The coupling constant of the anomeric proton ($J_{H\text{-}1', H\text{-}2'}$ = 7.5 Hz) and the chemical shift of the anomeric carbon ($\delta_{C\text{-}1'}$ 102.1) indicated *β*-*O*-glycosidic linkage of the glucopyranoside moiety in **4**. Thus, considering its NMR and MS data, *γ*-lumicolchicoside (**4**) was a stereoisomer of **1**. Acid hydrolysis of **4** followed by derivatization with L-cysteine methyl ester hydrochloride and acetic anhydride gave a GC-MS peak at 17.93 min with an adduct $[M+H]^+$ ion at *m/z* 550, while standard D-glucose derivative gave a retention time of 18.19 min and L-glucose derivative gave a peak at 20.52 min, indicating a D-glucose in the molecule.

The relative configurations for **1**-**4** were determined by the comparison of the ^{1}H NMR data to the known lumicolchine analogues in the literature,[35] the ^{1}H-^{1}H coupling constants and ROSEY correlations. The ^{1}H-^{1}H coupling constant between H-8 and H-12 ($J_{H\text{-}8,H\text{-}12}$ = 2.7 Hz) in **1** supported a *cis* orientation of the two bridgehead protons. The ROESY correlation between H-7 and H-8 in **1** suggested that H-7 was on the same side of the ring system to H-8. Similar H-8 and H-12 coupling constants were observed in **2**-**4**, suggesting *cis* orientation of the bridgehead protons. ROESY correlations between H-7 and H-8 were observed in **2** and **3**, confirming the same relative configurations as in **1**.

The effects of the substituents and the basic skeleton on the chirality of lumicolchicine alkaloids have been discussed in the literature.[8] Two partial chromophores, a styrene and a cyclopentenone moiety, contributed to three major Cotton effects (CEs) at 350, 295 and 255 nm. In general, for β-lumicolchicines, where the absolute configuration defined as (7*S*,8*R*,12*S*), have a relatively strong positive CE at around 350 nm (due to an n→π* transition of the enone moiety), a strong negative exciton couplet at around 295 nm (related to the interaction of the electric dipole transition moments of the styrene and enone chromophores), and a strong positive CE at around 255 nm (ascribed to the conjugation band of the styrene in the ring system).[8] The bicycloheptadienone moieties of the γ-lumicolchicines are in enantiomeric relationship to the β forms. They have the opposite CEs at 350, 295 and 250 nm to those of the β forms and an absolute configuration of (7*S*,8*S*,12*R*).[8]

The CD spectra of compounds **1**-**3** showed positive CEs at 350 and 255 nm, negative CE at 295 nm (Figure 2b), indicating that the aglycones of compounds **1**-**3** had β absolute configuration as (7*S*,8*R*,12*S*). The new compound **4** had the opposite CEs at 350,

295 and 255 nm to the new compounds **1-3**, consistent with *γ* configuration of (7*S*,8*S*,12*R*). The absolute configurations of the four new alkaloids *β*-lumicolchicosides A-C (**1-3**) and *γ*-lumicolchicoside A (**4**) were therefore established. The CD spectra of compounds **5-8** were in agreement with the published data (Figure 2a),[8] indicating the absolute configurations of *β*-lumicolchicines (**5-8**) as (7*S*,8*R*,12*S*).

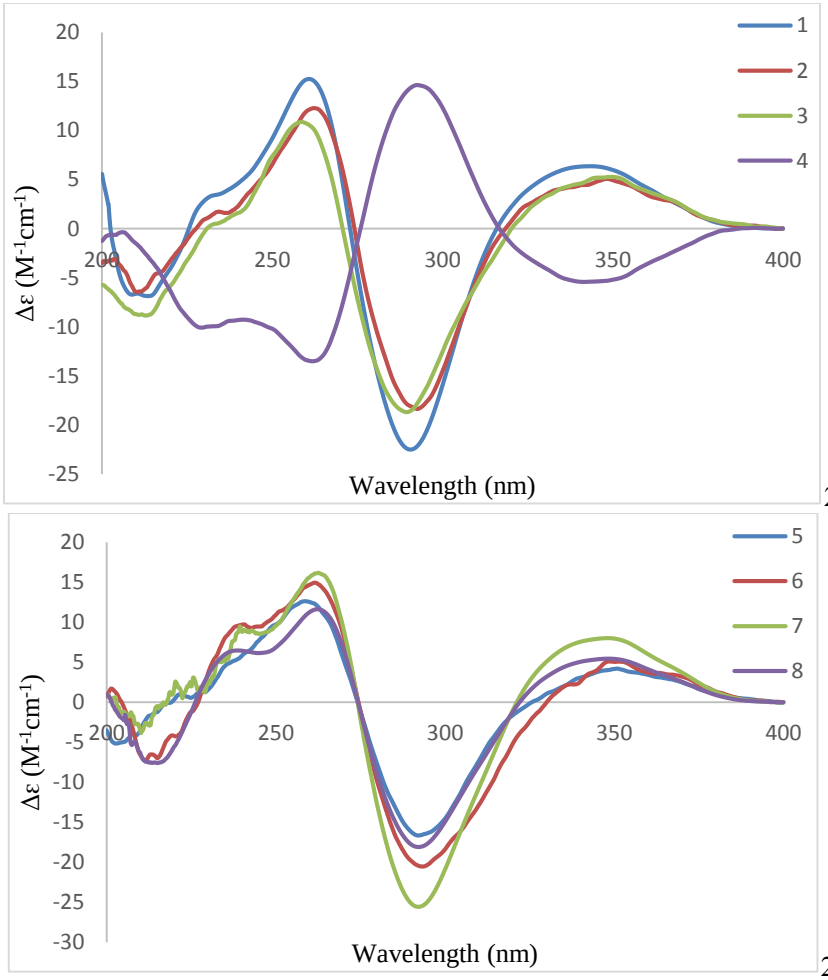

Figure 2. CD spectra of lumicolchicosides **1-4** (2b) and *β*-lumicolchicines **5-8** (2a) in MeOH

N^3-2-hydroxybenzyluridine (**15**) was obtained as an optically active colorless powder with an $[\alpha]_D$ value of +17.9. The HRESIMS data gave a $[M+Na]^+$ ion at *m*/*z* 373.1008, which was consistent with a molecular formula of $C_{16}H_{18}N_2O_7$, and implied nine degrees of unsaturation. The ^1H spectrum contained six aromatic methines (δ_H 8.04, 7.09,

7.09, 6.78, 6.75 and 5.85), one anomeric methine (δ_H 5.93), three deshielded methines (δ_H 4.18, 4.16 and 4.02), and two methylene moieties (δ_H 5.09 and 3.88/3.65) (Table 3). The ^{13}C NMR data which was extracted from the HSQC and HMBC spectra showed two carbonyl carbons (δ_C 165.1 and 152.6), eight sp^2 hybridized carbons (δ_C 156.6, 141.3, 130.3, 129.7, 123.4, 120.7, 115.6 and 101.9), one sp^3 hybridized carbon (δ_C 40.7), and five signals representing one terminal *N*-ribofuranose moiety (δ_C 91.7, 86.0, 75.8, 70.9 and 61.6). Analysis of the COSY spectrum established the presence of three spin systems: an vinyl group, a 1,2-disubstituted benzyl unit and a sugar moiety (Figure 3 in bold).

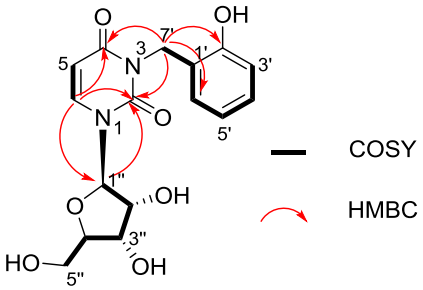

Figure 3. Selected COSY and HMBC correlations for **15**

Structure elucidation of the 1,2-disubstituted benzyl moiety was hindered by signal overlapping in the aromatic region. In particular, the chemical shifts of H-4′ and H-6′ in MeOH-d_4, or a pair of mutually coupled signals H-5′ and H-6′ in DMSO-d_6, were nearly coincident. The ^1H and COSY NMR spectra in mixed solvent DMSO-d_6/MeOH-d_4 (1:1) showed significant separation and splitting of the four aromatic protons H-3′, H-4′, H-5′ and H-6′, and was used for the unambiguous determination of the aromatic substitution pattern of the 1,2-disubstituted benzyl moiety (Figure 4).

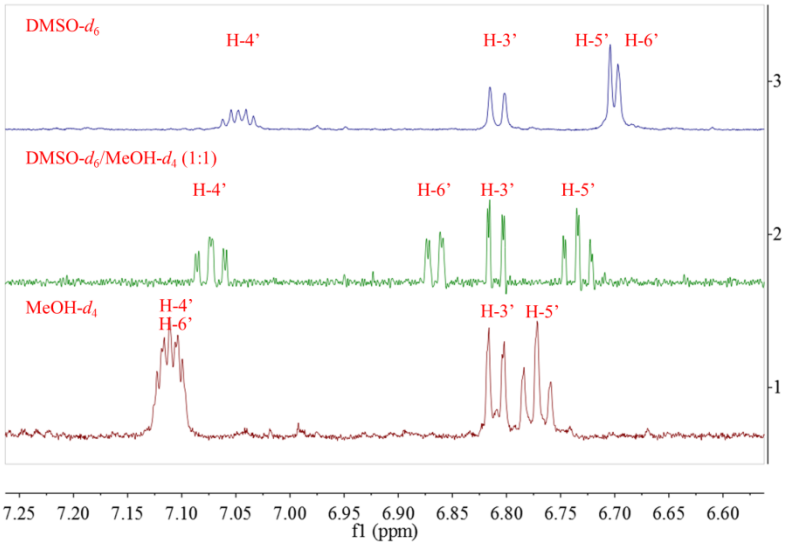

Figure 4. Determination of the aromatic substitution pattern of the 1,2-disubstituted benzyl moiety 1. The ^{1}H NMR spectrum of **15** in MeOH-d_4; 2. The ^{1}H NMR spectrum of **15** in DMSO-d_6/MeOH-d_4 (1:1); 3. The ^{1}H NMR spectrum of **15** in DMSO-d_6 (The chemical shifts of H-3′ in different solvents were all referenced at δ_H 6.81 in comparison)

HMBC correlations from the aromatic doublet H-6 (δ_H 8.04, d, J = 8.0 Hz) to the carbonyl carbons C-2 and C-4 (δ_C 152.6 and 165.1) and from H-5 (δ_H 5.85, d, J = 8.0 Hz) to C-6 (δ_C 141.3), together with the carbon chemical shifts of C-5 and C-6 (δ_C 101.9 and 141.3), suggested a uracil moiety,[64] which is consistent with the UV absorption maximum at 270 nm.[65] An HMBC correlation from H-6 (δ_H 8.11) to C-1″ (δ_C 91.7) established the connectivity between the ribofuranose and the uracil moiety. It was further confirmed by the observation of HMBC correlations from H-1″ (δ_H 5.93) to C-2 and C-6 (δ_C 152.6 and 141.3). HMBC correlations from the deshielded methylene doublet H-7′ (δ_H 5.09) to the carbonyl carbons C-2 and C-4 (δ_C 152.6 and 165.1) established the connectivity between the 1,2-disubstituted benzyl unit and uracil moiety. HMBC correlations from protons H-4′ and H-6′ (δ_H 7.09, 7.09) to the deshielded carbon C-2′ (δ_C 156.6) indicated that a hydroxyl

group was attached to C-2′. With all the atoms accounted for and the nine degrees of unsaturation satisfied, the structure of **15** was established.

Table 3. NMR Spectroscopic Data (600 MHz for ^{1}H and 150 MHz for ^{13}C, MeOH-d_4) for N^3-2-hydroxybenzyluridine (**15**)

position	δ_C, type ($^1J_{CH}$, Hz)	δ_H, mult. (J in Hz)	COSY	HMBC[a]
2	152.6, C			
4	165.1, C			
5	101.9, CH (180.7)	5.85, d (8.0)	H-6	6
6	141.3, CH (187.2)	8.11, d (8.0)	H-5	2, 4, 1"
1'	123.4,C			
2'	156.6, C			
3'	115.6, CH (160.3)	6.78, dd (8.4, 1.2)	H-4', H-5'	1', 5'
4'	130.3, CH (157.1)	7.09, m	H-3', H-5', H-6'	2', 6'
5'	120.7, CH (160.7)	6.75, ddd (7.6, 7.4, 1.2)	H-3', H-4', H-5'	1', 3'
6'	129.7, CH (157.1)	7.09, m	H-4', H-5', H-7'	4', 5'
7'	40.7,CH_2 ([b])	5.09, d (1.6)	H-6'	2, 4, 1', 2', 6'
1"	91.7, CH (166.5)	5.93, d (4.1)	H-2"	6
2"	75.8, CH (152.0)	4.18, dd (4.1, 5.4)	H-1", H-3"	3"
3"	70.9, CH (150.8)	4.16, dd (5.4, 5.5)	H-2", H-4"	1", 5"
4"	86.0, CH (150.1)	4.02, ddd (5.5, 3.1, 2.8)	H-3", H-5a", H-5b"	1"
5"	61.6, CH_2 ([b])	3.86, dd (12.3, 2.8) 3.74, dd (12.3, 3.1)	H-4", H-5b" H-4", H-5a"	3", 4"

[a] HMBC correlations are from proton(s) stated to the indicated carbon.

[b] signals not clear

The coupling constants in the sugar moiety ($J_{H\text{-}1'',\ H\text{-}2''}$ = 4.1 Hz, $J_{H\text{-}2'',\ H\text{-}3''}$ = 5.4 Hz and $J_{H\text{-}3'',\ H\text{-}4''}$ = 5.5 Hz) suggested a β-ribofuranose moiety.[66] Literature reports also suggested that strong positive Cotton effects at 270 nm are indicative of a β anomeric type pyrimidine derivatives, such as uridine, uridine-5'-fluro-5'-deoxy, cytidine, while the opposite signs observed for α-anomers.[67-71] The CD spectrum of compound **15** showed a strong positive Cotton effect at 270 nm (Figure 5), therefore the β anomer was confirmed. The attempt to determine the absolute configuration of ribofuranose moiety by GC-MS was hindered by the small quantity of compound **15** (0.2 mg). In the literature, N^3-benzyluridine, N^3-methyluridine and uridine, which contained a D-ribofuranose moiety in each molecule, had $[\alpha]_D$ value of +12.9,[72] +20.1[73] and +4.0,[74] respectively. In comparison,

compound **15** showed an $[\alpha]_D$ value of +17.9, indicating a D-ribofuranose moiety in the molecule. Therefore, the absolute configuration of N^3-2-hydroxybenzyluridine (**15**) was confirmed.

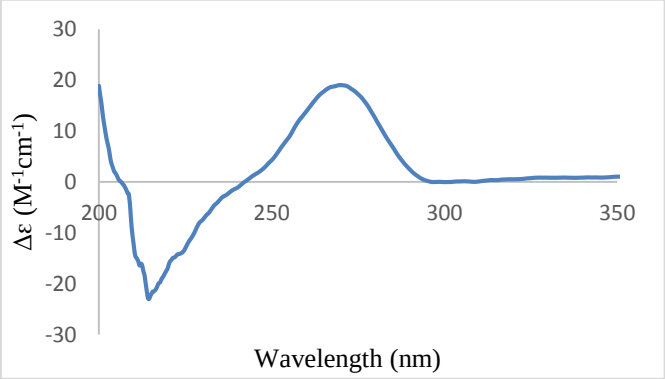

Figure 5. CD spectra of N^3-2-hydroxybenzyluridine (**15**) in MeOH

It is well established that uridine is one of the active components of a sleep-promoting and anti-epileptic substance to improve memory function and affect neuronal plasticity.[75,76] The class of N^3-benzyl-substituted uridines exhibited potent hypnotic activity as well as pentobarbital induced sleep effect on mice when administered by intracerebroventicular injection.[77,78] Uridine is the major form of pyrimidine nucleosides taken up by the brain. Pyrimidine nucleosides have been suggested for the treatment of epileptic and neurodegenerative diseases as neuroprotective agents.[76]

Glorioside A (**19**) was isolated as an optically active yellowish gum with an $[\alpha]_D$ value at -26.1. The HRESIMS data gave an adduct $[M+Na]^+$ ion at *m/z* 483.1109. This, in conjunction with NMR data (Table 4), enabled the establishment of a molecular formula of $C_{19}H_{24}O_{13}$, with eight degrees of unsaturation. The ^1H spectrum contained three aromatic methines (δ_H7.49, 7.17 and 6.84), two anomeric methines (δ_H 5.22 and 5.03,), eight sp^3 hybridized methines (δ_H 3.97, 3.82, 3.49, 3.46, 3.46, 3.46, 3.42 and 3.23), and two

methylene moieties (δ_H 3.88/3.72 and 3.88/3.65). The ^{13}C spectrum showed a carbonyl group (δ_C 166.7) and an aromatic ring (δ_C 158.1, 153.4, 135.3, 117.4, 115.9 and 113.8), with the remaining twelve signals representing two terminal *O*-glucose moieties (δ_C 102.6, 102.2, 79.8, 78.5, 78.1, 77.7, 74.8, 74.7, 72.0, 71.1, 62.6 and 62.6). Analysis of the COSY and HSQC spectra established the presence of three spin systems: two sugar moieties and a 1,2,3-trisubstituted benzene unit (Figure 6 in bold). The coupling constants of the two anomeric protons ($J_{H\text{-}1', H\text{-}2'}$ = 8.5 Hz and $J_{H\text{-}1'', H\text{-}2''}$ = 7.5 Hz) and the chemical shifts of the anomeric carbons ($\delta_{C\text{-}1'}$ 102.6 and $\delta_{C\text{-}1''}$ 102.2) indicated β-*O*-glycosidic linkages of the glucopyranoside moieties in **19**.

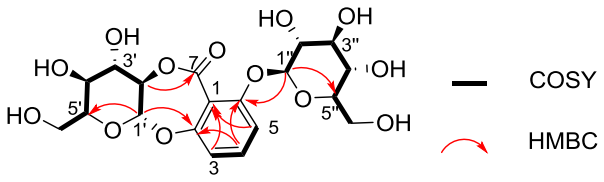

Figure 6. Selected COSY and HMBC correlations for **19**

HMBC correlations from the anomeric proton doublets H-1′ (δ 5.22) to C-2 (δ_C 153.4), and H-1″ (δ_H 5.03) to C-6 (δ_C 158.1), established the connectivity between the sugar moieties and the benzene moiety, respectively. The connectivity was further confirmed by additional HMBC correlations from the aromatic doublet of doublets H-4 (δ_H 7.49) to the deshielded nonprotonated carbons C-2 and C-6. Strong HMBC correlations from the two aromatic doublets H-3 and H-5 (δ_H 6.84 and 7.17) to the relatively shielded nonprotonated carbon C-1 (δ_C 115.9) and weak HMBC correlation from the aromatic proton H-4 (δ_H 7.49) to C-1 indicated that a carbonyl group was located at the C-1 position. An HMBC correlation from H-2′ (δ_H 3.97) to the carbonyl carbon C-7 (δ_C 166.7) established the connectivity between the glucopyranose and the carbonyl group, therefore a seven

membered lactone ring. The presence of lactone ring was further confirmed by the observation of deshielded protons H-2′, H-3′ (δ_H 3.97 and 3.82) and the carbon C-2′ (δ_C 77.7), and shielded C-3′ (δ_C 74.8) in the glucopyranoside moiety. With all the atoms accounted for and the degrees of unsaturation satisfied, the structure of **19** was established.

Table 4. NMR Spectroscopic Data (600 MHz for ^{1}H and 150 MHz for ^{13}C, CD_3OD) for glorioside A (**19**)

position	δ_C, type ($^1J_{CH}$, Hz)	δ_H, mult. (J in Hz)	COSY	HMBC[a]
1	115.9, C			
2	153.4, C			
3	117.4, CH (168.5)	6.84, d (8.1)	H-4	1, 2, 5, 7
4	135.3, CH (167.3)	7.49, dd (8.1, 8.5)	H-3, H-5	1, 2, 6
5	113.8, CH (170.0)	7.17, d (8.5)	H-4	1, 2, 3, 6, 7
6	158.1, C			
7	166.7, C			
2-OGlc				
1'	102.6,CH (162.2)	5.22, d (8.5)	H-2'	2, 3', 5'
2'	77.7, CH (140.3)	3.97, dd (8.5, 9.5)	H-1', H-3'	7, 1', 3'
3'	74.8, CH (143.6)	3.82, dd (9.5, 8.6)	H-2', H-4'	2', 4'
4'	72.0, CH (141.9)	3.23, dd (8.6, 9.0)	H-3', H-5'	3', 5', 6'
5'	79.8, CH (141.0)	3.46, m	H-4', H-6a', H-6b'	3', 4', 6'
6'	62.6, CH_2 ([b])	3.65, dd (5.8, 12.1)	H-5', H-6b'	4', 5'
		3.88, dd (2.2, 12.1)	H-5', H-6a'	4'
6-OGlc				
1"	102.2, CH (159.9)	5.03, d (7.3)	H-2"	6, 3", 5"
2"	74.7, CH (143.6)	3.49, m	H-1", H-3"	1", 3"
3"	78.1, CH (140.2)	3.46, m	H-2", H-4"	1", 2"
4"	71.1, CH (142.2)	3.42, m	H-3", H-5"	3", 5", 6"
5"	78.5, CH (139.3)	3.46, m	H-4", H-6a", H-6b"	4", 6"
6"	62.6, CH_2 ([b])	3.72, dd (5.5, 12.2)	H-5", H-6b"	4", 5"
		3.88, dd (2.3, 12.2)	H-5", H-6a"	4"

[a] HMBC correlations are from proton(s) stated to the indicated carbon.

[b] Signals not clear

The monosaccharide units of the hydrolysis product of **19** were established as D-glucose with the measurement of $[\alpha]_D^{25}$ +44.5 (c 0.10 MeOH) in comparison with the $[\alpha]_D$ data of commercially available standard D and L glucoses, which showed $[\alpha]_D^{25}$ +50.2 (c 0.10 MeOH) and $[\alpha]_D^{25}$ -48.6 (c 0.10 MeOH), respectively. GC-MS analysis of the peracetylated thiazolidine derivative of the hydrolysed **19** confirmed D-glucose moieties

with the retention time of 18.11 min, while standard D and L-glucose derivatives gave retention times at 18.19 min and 20.52 min, respectively. Consequently, the structure of the new phenolic glycoside was assigned as glorioside A (**19**).

The final molecule, glorioside B (**22**), was isolated as an optically active yellowish gum with an $[\alpha]_D$ value at -29.1. The HRESIMS measurement gave an adduct $[M+Na]^+$ ion at *m/z* 457.1318, in conjunction with NMR data (Table 5), corresponding to a molecular formula of $C_{18}H_{26}O_{12}$ with six degrees of unsaturation. The ^1H NMR spectrum contained four aromatic methines (δ_H7.23, 6.85, 6.79 and 6.76), two anomeric methines (δ_H 4.66 and 4.25), eight sp^3 hybridized methines (δ_H 3.57, 3.30, 3.27, 3.17, 3.12, 3.03, 3.03 and 2.98), two methylene moieties (δ_H 4.02/3.60 and 3.66/3.40) and seven exchangeable hydroxyl signals (δ_H 5.50, 5.16, 5.15, 4.94, 4.93, 4.89 and 4.48). The ^{13}C NMR data, derived from the HSQC and HMBC spectra, suggested the presence of an aromatic ring (δ_C 146.5, 145.2, 122.5, 119.4, 116.6 and 115.4), with the remaining twelve signals representing two sugar moieties (δ_C 103.1, 102.1, 76.4, 76.2, 75.8, 75.3, 73.4, 73.0, 69.8, 69.7, 68.2 and 61.0). Analysis of the COSY and HSQC spectra established the presence of three spin systems: a 1,2-disubstituted benzene moiety and two sugar moieties (Figure 7 in bold). The coupling constants of the two anomeric protons ($J_{H\text{-}1', H\text{-}2'}$ = 7.5 Hz and $J_{H\text{-}1'', H\text{-}2''}$ = 7.8 Hz) and the chemical shifts of the anomeric carbons ($\delta_{C\text{-}1'}$ 102.1 and $\delta_{C\text{-}1''}$ 103.1) indicated *β-O*-glycosidic linkages of the glucopyranoside moieties in **22**.

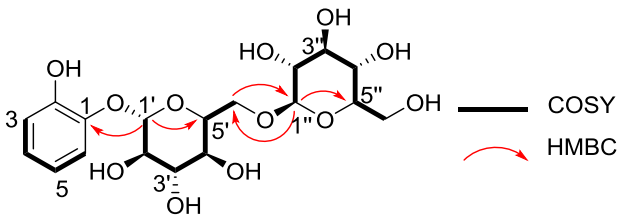

Figure 7. Selected COSY and HMBC correlations for glorioside B (**22**)

HMBC correlations from the anomeric proton doublet H-1′ (δ 4.66) to C-1 (δ_C 145.2), and from H-1″ (δ_H 4.25) to C-6′ (δ_C 68.2), established the connectivity among pyrocatechol and two sugar moieties, respectively. The connectivity between the two sugar moieties was further confirmed by additional HMBC correlations from the deshielded methylene protons H-6' (δ_H 4.02/3.60) to the anomeric carbon C-1″ (δ_C 103.1). With all the atoms accounted for and the degrees of unsaturation satisfied, the structure of **22** was established.

Table 5. NMR Spectroscopic Data (800 MHz for ^{1}H and 200 MHz for ^{13}C, DMSO-d_6) for glorioside B (**22**)

position	δ_C, type	δ_H, mult. (J in Hz)	COSY	HMBC[a]
1	145.2, C			
2	146.5, C			
3	115.4, CH	6.79, dd (7.9, 1.6)	H-4, H-5	1, 5
4	122.5, CH	6.85, ddd (7.9, 7.8, 1.5)	H-3, H-5, H-6	2, 6
5	119.4, CH	6.76, d (8.2, 7.8, 1.6)	H-3, H-4, H-6	1, 3
6	116.6, CH	7.13, dd (8.2, 1.5)	H-4, H-5	2,
1'	102.1,CH	4.66, d (7.5)	H-2'	1, 2', 5'
2'	73.0, CH	3.30, m	H-1', H-3', 2'-OH	1', 3'
3'	75.3, CH	3.27, m	H-2', H-4', 3'-OH	2', 4'
4'	69.7, CH	3.17, m	H-3', H-5', 4'-OH	3', 5', 6'
5'	75.8, CH	3.57, m	H-4', H-6a', H-6b'	1', 4', 6'
6'	68.2, CH_2	4.02, dd (5.8, 12.1)	H-5', H-6b'	4', 5', 1"
		3.60, dd (2.2, 12.1)	H-5', H-6a'	4', 5', 1"
1"	103.1, CH	4.25, d (7.3)	H-2"	6', 2", 5"
2"	73.4, CH	2.98, m	H-1", H-3", 2"-OH	1", 3"
3"	76.2, CH	3.12, m	H-2", H-4", 3"-OH	2", 4"
4"	69.8, CH	3.03, m	H-3", H-5", 4"-OH	3", 5", 6"
5"	76.4, CH	3.03, m	H-4", H-6a", H-6b"	1", 4", 6"
6"	61.0, CH_2	3.66, m	H-5", H-6b", 6"-OH	4", 5"
		3.40, m	H-5", H-6a", 6"-OH	4", 5"
2-OH		8.48, s		1, 3
2'-OH		5.50, d (3.8)	H-2'	2', 3'
3'-OH		5.15, d (5.5)	H-3'	2', 4'
4'-OH		5.16, d (5.5)	H-4'	4', 5'
2"-OH		4.93, d (4.7)	H-2"	1", 2", 3"
3"-OH		4.94, d (4.8)	H-3"	2", 3", 4"
4"- OH		4.89, d (4.5)	H-4"	3", 4", 5"
6"-OH		4.48, t (5.9)	H-6a", H-6b"	5", 6"

[a] HMBC correlations are from proton(s) stated to the indicated carbon.

The monosaccharide units of the hydrolysis product of **22** were established as D-glucose with the measurement of $[\alpha]_D^{25}$ +40 (c 0.10 MeOH) in comparison with the $[\alpha]_D$ data of commercially available standard D and L glucoses, which showed $[\alpha]_D^{25}$ +50.2 (c 0.10 MeOH) and $[\alpha]_D^{25}$ -48.6 (c 0.10 MeOH), respectively. GC-MS analysis of the peracetylated thiazolidine derivative of the hydrolysed **22** confirmed D-glucose moieties with the retention time of 17.96 min, while standard D and L glucose derivatives gave retention times at 18.19 min and 20.52 min, respectively. Thus, the structure of glorioside B (**22**) was assigned as shown in Figure 7.

Consistent with the extraction and fractionation protocol developed in-house to prepare a Nature Bank fraction library targeting drug-like molecules, the isolated compounds were distributed within this lead-like space.[79,80] The physicochemical properties of isolated compounds were calculated using Instant JChem (version 15.10.26.0).[81] The data suggested that 55% of the isolated metabolites obeyed Linpinski's Rule of five in terms of log *P* < 5 (100%), MW < 500 Da (76.9%), HBA < 10 (53.8%) and HBD < 5 (64.1%). The full data set is provided in the Supporting Information.

The cytological profiles of the 39 secondary metabolites from the Australian plant *G. superba* L. were examined to identify congeneric chemical series by coupling an unbiased multidimensional phenotype assay using nontransformed and nonimmortalized hONS cells, which are primary cells derived from a Parkinson's disease patient. hONS cells were treated with 10 μM of each compound for 24 h. Cytological parameters were assessed by staining with fluorescent probes targeting various cellular pathways and organelles implicated in Parkinson's disease. These included mitochondria, early

endosomes, lysosomes, microtubule-based cytoskeleton, and autophagosomes. The bar chart depicting the effects of all metabolites to the hONS cells is as shown in Figure 8.

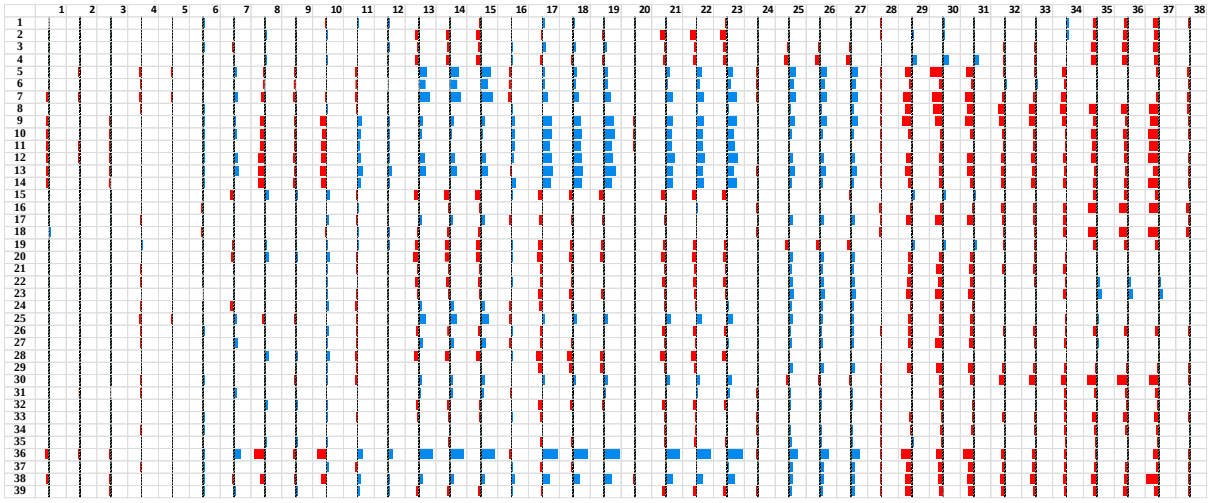

Figure 8. Bar chart depicting the cytological profile of metablites from *Gloriosa superba* L. at 10 µM on 38 parameters based on the $\log_2$ ratio of compound and vehicle (DMSO). Red shows a decrease versus vehicle and blue shows an increase versus vehicle. Individual compounds are presented on the y-axis with individual features on the x-axis. 1. Nucleus area (µm²) 2. Nucleus morphology width (µm) 3. Nucleus morphology length (µm) 4. Nucleus morphology ratio width to length 5. Nucleus morphology roundness 6. Nucleus marker texture index 7. Nucleus marker intensity 8. Cell area (µm²) 9. Cell width (µm) 10. Cell length (µm) 11. Cell ratio width to length 12. Cell roundness 13. *α*-Tubulin marker intensity in the cytoplasm 14. *α*-Tubulin marker intensity in outer region of cytoplasm 15. *α*-Tubulin marker intensity in inner region of cytoplasm 16. *α*-Tubulin marker texture index 17. Mitochondria marker intensity in the cytoplasm 18. Mitochondria marker intensity in outer region of cytoplasm 19. Mitochondria marker intensity in inner region of the cytoplasm 20. Mitochondria marker texture index 21. LC3b marker intensity in the cytoplasm 22. LC3b marker intensity in the outer region of the cytoplasm 23. LC3b marker intensity in inner region of cytoplasm 24. LC3b marker texture index 25. Lysosome marker intensity mean 26. Lysosome marker intensity outer region mean 27 Lysosome marker intensity inner region mean 28. Lysosome marker texture index. 29. Number of EEA1 marker spots in cytoplasm 30. Number of EEA1 marker spots in inner region of cytoplasm 31. Number of EEA1 marker spots in outer region of cytoplasm 32. Number of EEA1 marker spots per Area of cytoplasm 33. EEA1 marker intensity in outer region of cytoplasm 34 EEA1 marker intensity in inner region of cytoplasm 35. EEA1 marker intensity in the cytoplasm 36. Number of EEA1 marker spots per area of outer region 37 Number of EEA1 marker spots per Area of inner region of cytoplasm 38. EEA1 marker texture index.

The compounds were subsequently clustered using 38 phenotypic features across the individual cell line based on their pairwise Pearson's correlation coefficient using Cluster 3.0 and visualized using Java TreeView. The heat map depicting the cytological profile of metabolites from *G. superba* L. at 10 μM on 38 parameters is provided in the Supporting Information.

All the metabolites from *G. superba* L. exhibit minimal alterations to nuclear and cellular functions (parameters 1-12) at 10 μM suggesting that these natural products are not cytotoxic to the hONS cell model of Parkinson's disease. Mitochondrial dysfunction has long been implicated as a major contributing factor to the progression of Parkinson's disease. Colchicine and its analogues specifically bind to tubulin and inhibit its assembly into microtubule. In our assay, colchicine (**9**) and its congeners **10**-**14** displayed moderate phenotypic perturbation of Parkinson's disease patient-derived hONS cells on the mitochondria and LC3b (autophagosome) related parameters while only having slight effects the α-tubulin related parameters (Figure 9). The lumicolchicine analogues **5**-**8** showed moderate effects on α-tubulin related parameters and much weaker perturbation on the mitochondria and LC3b related cytological parameters compared to the colchicine compounds (Figure 9). None of the four new β- and γ-lumicolchicine glycosides **1**-**4**, showed similar phenotypic profile to colchicine and lumicolchicine analogues, indicating the extra sugar moiety in the molecules abolished the phenotypic effects (Figure 10). As shown in Figure 9c, it was straightforward to observe the significant different effects of the three groups of compounds to the patient derived PD cells.

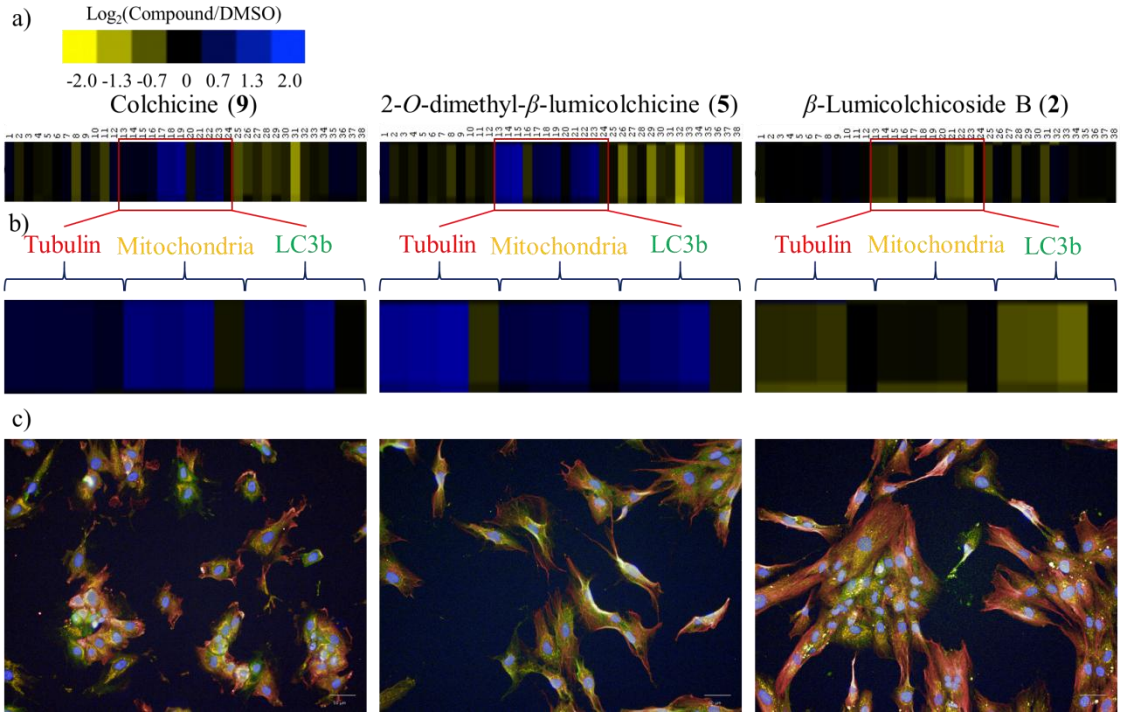

Figure 9. Representative profiles and images of compounds **2**, **5** and **9** affecting the α-Tubulin marker, Mitochondria marker and LC3b marker. a) Heat map depicting the cytological profile of compounds **2**, **5** and **9** at 10 µM on 38 parameters based on the $\log_2$ ratio of compound and DMSO. The effects of compounds were plotted as $\log_2$ ratio to the DMSO control. Yellow shows a decrease versus control and blue shows an increase versus control. Individual 38 features are presented on the x-axis as the same as shown in Figure 9. b) Expansion heat map depicting of the cytological profile on α-tubulin, mitochondria and LC3b markers. c) Biological signature and representative image of compounds **2**, **5** and **9** at 10 µM. Cells were seeded at 1350 cells/well in growth medium and treated for 24 h. Cells were stained for α-tubulin marker (red), mitochondria marker (orange) and LC3b marker (blue) and imaged with a 20x high numerical aperture objective on the Operetta™ (PerkinElmer). Scale bars = 50 µm.

Compound **36**, the flavone glycoside, showed moderate biological activity against Parkinson's disease patient-derived human olfactory neurosphere-derived cells on the α-tubulin, mitochondria, LC3b and lysosome related parameters. Compound **38**, with a different methoxy substitution in the ring C moiety of the flavone and only one sugar moiety, showed lower deviation on these same cytological parameters. The rest of the flavones and the related glycosides (**31**-**35**, **37** and **39**) had little effect on these parameters,

indicative of some structure activity relationship. The new nucleoside derivative **15** and the two new phenolic glycosides (**19** and **22**) induced slight phenotype profiles on the hONS cell model of Parkinson's disease.

In our previous research, the different phenotypic responses of iotrochotazine A, isolated from an Australian marine sponge *Iotrochota sp.* and jaspamycin, isolated from *Jaspis splendens* collected in the Great Barrier Reef (Australia), offer useful probes to investigate the molecular mechanisms underlying Parkinson's disease. In this research, colchicines and lumicolchicines exhibited moderate perturbation on mitochondria/LC3b and α-tubulin related parameters while the four new lumicolchicine glycosides (**1**-**4**) had diminished effects in these parameters. Colchicine is a known α-tubulin binder. The phenotypic response inducts potential alternate targets in the PD patient derived hONS cell model. Colchicine and its congeners have effects on mitochondria and autophagy in cells from Parkinson's disease patients, indicating that there may be an alternative mechanism in neurodegeneration and, further investigation is warranted.

EXPERIMENTAL SECTION

General Experimental Procedures. Optical rotations were recorded on a JASCO P-1020 polarimeter (10 cm cell). IR, UV and circular dichroism spectra were required on a Bruker Tensor 27 spectrophotometer, a CAMSPEC M501 UV/vis spectrophotometer and a JASCO J-720 spectropolarimeter, respectively. A free and open source software SDAR was used for the analysis and processing of UV and CD data.[82] NMR spectra were recorded in DMSO-d_6 (δ_H 2.50 and δ_C 39.5) or MeOH-d_4 (δ_H 3.31 and δ_C 49.0) at 30 ℃ on a Varian INOVA 600 MHz spectrometer equipped with a triple-resonance cold probe or at 25 ℃ on

a Bruker Avance HDX 800 MHz spectrometer equipped with a TCI cryoprobe. The low-resolution mass spectrum (LRESIMS) was recorded on a Mariner time-of-flight (TOF) mass spectrometer equipped with a Gilson 215 eight probe injector and a Waters LCMS system equipped with a Luna C_{18} column (3 μm, 100 Å, 50 × 4.6 mm), a PDA detector, and a ZQ ESI mass spectrometer. The high-resolution mass spectra (HRESIMS) were recorded on a Bruker Daltonics SolariX 12 T Fourier transform mass spectrometer. An Edwards Instrument Company Bioline orbital shaker was used for extraction. The HPLC system included a Waters 600 pump fitted with a 996 photodiode array detector and Gilson FC204 fraction collector. A ThermoElectron Betasil C_{18} column (5 μm, 21.2 × 150 mm) and a Phenomenex Luna C_{18} column (5 μm, 10 × 250 mm) were used for semipreparative HPLC. All solvents used for extraction, chromatography, $[\alpha]_D$, UV, IR, and MS were Lab-Scan HPLC grade, and the H_2O was Millipore Milli-Q PF filtered.

Plant Material. The leaves of *Gloriosa superba* L. were collected from Cult Hibiscus Street, Urangan, Hervey Bay, Queensland, Australia. Collection and taxonomic identification were undertaken by P. I. Forster from the Queensland Herbarium. A voucher specimen (AQ604947) has been deposited at the Queensland Herbarium, Brisbane, Australia.

Extraction and Isolation of Compounds 1-39. The air-dried and ground leaves of *G. superba* (20 g) were sequentially extracted with *n*-hexane (250 mL) for 2 h at room temperature (rt). The hexane extract was filtered under gravity and discarded. Then 250 mL of CH_2Cl_2 was added to the biota and extracted for 2 h. The CH_2Cl_2 extract was filtered, and the biota was further extracted with two lots of 250 mL of MeOH for 2 h and overnight, successively. All CH_2Cl_2 and MeOH extracts were combined and dried to afford the crude

extract. The crude extract was fractionated using C_{18} bonded silica flash column. Four fractions were collected by eluting with stepwise gradients with 0.1% TFA (10% MeOH/90% H_2O, 50% MeOH /50% H_2O, 90% MeOH/10% H_2O and MeOH, respectively). A portion of 50% MeOH /50% H_2O fraction was pre-adsorbed onto cotton and packed dry into a stainless steel cartridge (10 × 30 mm). This cartridge was subsequently chromatographed by HPLC (gradient MeOH/H_2O with 0.1% TFA) using a semipreparative reversed-phase Betasil C_{18} column (21.2 mm × 150 mm). Initial isocratic conditions of 20% MeOH were used for 10 min then a linear gradient from 20 to 70% MeOH was performed over 40 min and continued isocratic for 10 min at a flow rate of 9 mL/min. Sixty fractions were collected by 1 min increments over 60 min to afford four new lumicolchicine glycosides *β*-lumicolchicosides A (**1**, 0.8 mg, 0.004% dry wt), B (**2**, 0.4 mg, 0.002% dry wt) and C (**3**, 0.4 mg, 0.002% dry wt) and *γ*-lumicolchicoside A (**4**, 0.6 mg, 0.003% dry wt), along with *β*-lumicolchicine analogues (**5**-**8**), colchicine analogues (**9**-**14**) and flavone glycosides (**33**-**39**). The 10% MeOH/90% H_2O fraction was chromatographed by HPLC (gradient MeOH/H_2O with 0.1% TFA) using the same semipreparative C_{18} column eluting with 10% MeOH/90% H_2O to 60% MeOH/40% H_2O. Three new metabolites, namely N^3-2-hydroxybenzyluridine (**15**, 0.3 mg, 0.002% dry wt), gloriosides A (**19**, 23.2 mg, 0.116% dry wt) and B (**22**, 1.0 mg, 0.005% dry wt), together with nucleosides (**16**-**18**) and phenolic glycosides (**20**, **21** and **23**-**28**) were isolated. In addition, four known natural products (**29**-**32**) were also isolated from MeOH fraction by the same semipreparative HPLC column eluting with gradient MeOH/H_2O with 0.1% TFA from 60% MeOH/40% H_2O to MeOH.

*β-Lumicolchicoside B (**1**):* yellowish powder; $[\alpha]_D^{25}$ +41.4 (c 0.076, CH_3OH); UV/Vis λ_{max}^{MeOH} nm (log ε): 224 (4.24), 268 (4.13), 348 (3.08) nm; IR (null): 3363, 2933,

1665, 1599, 1497, 1455, 1361, 1323, 1125, 1079 cm^{-1}; 1D and 2D NMR data (DMSO-d_6), Tables 1 and 2; (+)-LRESIMS m/z 570 (100) $[M+Na]^+$, 548 (100) $[M+H]^+$; (+)-HRESIMS *m/z* 570.1948 ($C_{27}H_{33}NO_{11}Na$ $[M+Na]^+$ requires 570.1946).

*β-Lumicolchicoside B (**2**):* yellowish powder; $[\alpha]_D^{25}$ +38.2 (c 0.018, CH_3OH); UV/Vis λ_{max}^{MeOH} nm (log ε): 228 (4.17), 268 (3.93), 335 (3.23) nm; IR (null): 3383, 2934, 1699, 1611, 1497, 1462, 1362, 1323, 1208, 1135, 1086 cm^{-1}; 1D and 2D NMR data (DMSO-d_6), Tables 1 and 2; (+)-LRESIMS *m/z* 556 (100) $[M+Na]^+$, 534 (100) $[M+H]^+$; (-)-HRESIMS *m/z* 532.1814 ($C_{26}H_{30}NO_{11}$ $[M-H]^-$ requires 532.1824.).

*β-Lumicolchicoside C (**3**):* yellowish powder; $[\alpha]_D^{25}$ +32.7 (c 0.019, CH_3OH); UV/Vis λ_{max}^{MeOH} nm (log ε): 228 (4.18), 267 (3.91), 342 (3.14) nm; IR (null): 3381, 2931, 1611, 1515, 1323, 1210, 1081 cm^{-1}; 1D and 2D NMR data (DMSO-d_6), Tables 1 and 2; (+)-LRESIMS *m/z* 556 (100) $[M+Na]^+$, 534 (100) $[M+H]^+$; (+)-HRESIMS *m/z* 556.1787 ($C_{26}H_{31}NO_{11}Na$ $[M+Na]^+$ requires 556.1789).

*γ-Lumicolchicoside A (**4**):* yellowish powder; $[\alpha]_D^{25}$ -26.9 (c 0.033, CH_3OH); UV/Vis λ_{max}^{MeOH} nm (log ε): 226 (4.13), 271 (3.87), 336 (3.14) nm; IR (null): 3345, 2938, 1701, 1654, 1611, 1497, 1320, 1083 cm^{-1}; 1D and 2D NMR data (DMSO-d_6), Tables 1 and 2; (+)-LRESIMS *m/z* 570 (100) $[M+Na]^+$, 548 (100) $[M+H]^+$; (+)-HRESIMS *m/z* 570.1944 ($C_{27}H_{33}NO_{11}Na$ $[M+Na]^+$ requires 570.1946).

*N^3-2-hydroxybenzyluridine (**15**):* colorless powder; $[\alpha]_D^{25}$ +17.9 (c 0.017, CH_3OH); UV/Vis λ_{max}^{MeOH} nm (log ε): 270 (3.79), 334 (2.91) nm; IR (null): 3383, 2929, 1659, 1602, 1461, 1060, 1034 cm^{-1}; 1D and 2D NMR data (DMSO-d_6), Tables 3; (+)-

LRESIMS *m/z* 373 (100) $[M+Na]^+$, 351 (100) $[M+H]^+$; (+)-HRESIMS *m/z* 372.1008 ($C_{16}H_{18}N_2O_7Na$ $[M+Na]^+$ requires 373.1006).

*Glorioside A (**19**):* yellowish gum; $[\alpha]_D^{25}$ -26.1 (c 0.096, CH_3OH); UV/Vis λ_{max}^{MeOH} nm (log ε): 234 (4.20), 289 (4.02); IR (null): 3346, 1737, 1605, 1258, 1074, 1016 cm^{-1}; 1D and 2D NMR data (CD_3OD), Tables 4; (+)-LRESIMS *m/z* 483 $[M+Na]^+$, 461 $[M+H]^+$; (+)-HRESIMS *m/z* 483.1113 ($C_{19}H_{24}O_{13}Na$ $[M+Na]^+$ requires 483.1109).

*Glorioside B (**22**):* yellowish gum; $[\alpha]_D^{25}$ -29.1 (c 0.082, CH_3OH); UV/Vis λ_{max}^{MeOH} nm (log ε) 213 (3.68), 278 (3.06) nm; IR (null): 3373, 1603, 1279, 1076 cm^{-1}; 1D and 2D NMR data (DMSO-d_6), Tables 5; (+)-LRESIMS *m/z* 457 (100) $[M+Na]^+$, 435 (100) $[M+H]^+$; (+)-HRESIMS *m/z* 457.1318 ($C_{18}H_{26}O_{12}Na$ $[M+Na]^+$ requires 457.1316).

Sugar analysis. Acid hydrolysis of **1**-**4**, **15**, **19** and **22** (ranging 0.2-3 mg) was carried out by standard procedures (0.5 mL 2M HCl, 100 °C, 1.5 h).[83] After cooling, the monosaccharides were isolated using C_{18} bonded silica flash columns. The sugars obtained through acid hydrolysis of **1**-**4**, **15**, **19** and **22** were separately dissolved in pyridine (1 mL), added to L-cysteine methyl ester hydrochloride (0.1 M) in pyridine (1 mL), and the mixture was heated (60 °C, 1 h). An equal volume of acetic anhydride (ca.3 mL) was added and the heating continued (1 h). The absolute configurations of monosaccharides released by acid hydrolysis of compounds **1**-**4**, **19** and **22** were determined by comparing its optical rotation with standard D- and L-sugar samples,[83,84] and by GC-MS analysis of trimethylsilylated thiazolidine derivatives. The acetylated thiazolidine sugar derivatives were prepared using the standard method,[62,63] and subjected to GC-MS analysis. Conditions for GC were: capillary column, DB5-MS (30 m × 0.25 mm × 0.25 m), oven temperature programme,

180-300 °C at 6 °C /min; injection temp, 350 °C; carrier gas, He at 1 mL/min. The acetylated thiazolidine derivatives of authentic sugars (Sigma-Aldrich) gave following retention time: D-glucose, 18.19 min; L-glucose, 20.52 min. The acid hydrolysates of **1**-**4**, **19** and **22** each gave a retention time at 18.18 min, 18.37 min, 18.08 min, 17.93 min, 18.11 min and 17.96 min, respectively, consistent with D-glucose. Compound **15** did not show the hydrolysis product.

Biological Assay. Compounds were transferred into two optically clear bottom CellCarrier 384-well plates (PerkinElmer). hONS cells from the Parkinson's disease cell line C1 200 08 0013 were added to each well at a density of 1,350 cells per well in 50 μL of growth medium (DMEM/F12, 10% FBS) leading to a final concentration of 10 μM (0.6% DMSO) for each compound. 0.6% DMSO was used as negative control. The cells were incubated for 24 h at 37 °C under 5% CO_2.

Cell Staining. After 24 h of incubation, the medium was aspirated and one 384-well plate was treated with MitoTracker Orange CMTMRos (Invitrogen) (400 nM) for 30 min at 37 °C under 5% CO_2. The second 384-well plate was treated with LysoTracker Red DND-99 (Invitrogen) (100 nM) for 1 h at 37 °C under 5% CO_2. Cells were fixed in 4% paraformaldehyde for 5 min at room temperature (rt). Cells were washed twice with phosphate-buffered saline (PBS, Sigma-Aldrich) and treated with 3% goat serum (Sigma-Aldrich) and 0.2% Triton X-100 (Sigma-Aldrich) in PBS for 45 min at rt. Plates were incubated with primary antibodies. Mouse anti-α-tubulin 1/4000 (Sigma-Aldrich) and rabbit anti-LC3b 1/335 (Sigma-Aldrich) were added to the plate already treated with MitoTracker and mouse anti-EEA1 1/200 (Sigma-Aldrich) was added to the plate previously treated with LysoTracker. Plates were incubated at rt for 1 h then washed twice

with PBS. Secondary antibodies goat anti-mouse Alexa-647 1/500 (Invitrogen) and goat anti-rabbit Alexa-488 1/500 (Invitrogen) were added to the first plate and goat anti-mouse Alexa-488 1/500 (Invitrogen) was added to the second plate for 30 min at rt. Cells were washed twice with PBS and stained with 4',6'-diamidino-2-phenylindole 1/5000 (Dapi, Invitrogen) and with CellMask Deep Red 1/5000 (Invitrogen) for the plate treated with LysoTracker and incubated for 10 min at rt. Cells were washed twice with PBS and plates were stored in the dark at 4 ^{o}C with 25 μL of PBS/well.

Imaging and Image Analysis Plates were imaged automatically using Operetta (PerkinElmer), a high content imaging system using a 20X high numerical aperture objective lens. Five images per well for each wavelength were collected. Individual cell segmentation was done using the Harmony software and measurements for each cell were performed generating 38 parameters from six dyes: Dapi, α-tubulin staining, MitoTracker Orange CMTMRos, LC3b staining, LysoTracker Red DND-99 and EEA1 staining. The $\log_2$ compound/DMSO ratio was clustered using Cluster 3.0 software (uncentered correlation and centroid linkage) and visualized using Java TreeView.

ASSOCIATED CONTENT

Supporting Information

The Supporting Information is available free of charge on the ACS Publications website at DOI:

1D and 2D NMR spectra and the GC-MS data for compounds **1**-**4**, **15**, **19** and **22**.

AUTHOR INFORMATION

Corresponding Author

*Tel: +64 7 3735 6009. E-mail: r.quinn@griffith.edu.au.

Notes

The authors declare no competing financial interest.

ACKNOWLEDGMENTS

This research was supported by an Australian Research Council *Discovery Projects* funding (project number DP130102400). D. Wang thanks Griffith University for a GUIPRS scholarship.

REFERENCES

(1) Wang, D.; Feng, Y.; Murtaza, M.; Wood, S. A.; Mellick, G. D.; Quinn, R. J. *J. Nat. Prod.* **2016**, http://dx.doi.org/10.1021/acs.jnatprod.5b00987.

(2) Harvey, A. L.; Edrada-Ebel, R.; Quinn, R. J. *Nat. Rev. Drug Discov.* **2015**, *14*, 111-129.

(3) Grkovic, T.; Pouwer, R. H.; Vial, M. L.; Gambini, L.; Noel, A.; Hooper, J. N.; Wood, S. A.; Mellick, G. D.; Quinn, R. J. *Angew. Chem. Int. Ed.* **2014**, *53*, 6070-6074.

(4) Matigian, N.; Abrahamsen, G.; Sutharsan, R.; Cook, A. L.; Vitale, A. M.; Nouwens, A.; Bellette, B.; An, J.; Anderson, M.; Beckhouse, A. G. *Dis. Model. Mech.* **2010**, *3*, 785-798.

(5) Jana, S.; Shekhawat, G. S. *Fitoterapia* **2011**, *82*, 293-301.

(6) Smith, A. C. *Flora Vitiensis nova: A new flora of Fiji (spermatophytes only)*; Pacific Tropical Botanical Garden Lawai, Kauai, Hawaii,, USA, 1979; Vol. 1.

(7) Jayaweera, D. M. A. *Medicinal plants (Indigenous and Exotic) used in Ceylon. Part IV Magnoliaceae-Rubiaceae* **1982**, 9.

(8) Hrbek, J.; Hruban, L.; Simanek, V. *Chem. Pharm. Bull.* **1981**, *47*, 2258-2279.

(9) Alali, F. Q.; El-Elimat, T.; Li, C.; Qandil, A.; Alkofahi, A. *J. Nat. Prod.* **2005**, *68*, 173-178.

(10) Reinten, E.; Coetzee, J.; Van Wyk, B.-E. *S. Afr. J. Bot.* **2011**, *77*, 934-946.

(11) Dictionary of Natural Products; Chapman and Hall/CRC Press: London, UK, 2005 (http://www.crcpress.com).

(12) Pelletier, P. J.; Caventou, J.-B. *Examen chimique de plusieurs végétaux de la famille des Colchicées, et du principe actif qu'ils renferment [Cévadille (veratrum sabadilla); hellébore blanc (veratrum album); colchique commum (colchicum autumnale)]*, 1820.

(13) Yeh, H. J.; Chrzanowska, M.; Brossi, A. *FEBS Lett.* **1988**, *229*, 82-86.

(14) King, M. V.; De Vries, J.; Pepinsky, R. *Acta Crystallogr.* **1952**, *5*, 437-440.

(15) Corrodi, H.; Hardegger, E. *Helv. Chim. Acta* **1955**, *38*, 2030-2033.

(16) Nuki, G.; Simkin, P. A. *Arthritis Res. Ther.* **2006**, *8*, S1.

(17) Drenth, J. P.; Van Der Meer, J. W. *N. Engl. J. Med.* **2001**, *345*, 1748-1757.

(18) Yang, L. P. H. *Drugs Aging* **2010**, *27*, 855-857.

(19) Sakane, T.; Takeno, M. *Expert Opin. Invest. Drugs* **2000**, *9*, 1993-2005.

(20) Pirildar, S.; Sütlüpinar, N.; Atasever, B.; Erdem-Kuruca, S.; Papouskova, B.; Šimánek, V. *Pharm. Biol.* **2010**, *48*, 32-39.

(21) Gali-Muhtasib, H.; Hmadi, R.; Kareh, M.; Tohme, R.; Darwiche, N. *Apoptosis* **2015**, 1-32.

(22) Jordan, M. A.; Wilson, L. *Methods Cell Biol.* **1998**, *61*, 267-295.

(23) Sullivan, J. T.; Castro, L. *J. Invertebr. Pathol.* **2005**, *90*, 32-38.

(24) Biswas, B. B.; Sen, K.; Choudhury, G. G.; Bhattacharyya, B. *J. Biosci.* **1984**, *6*, 431-457.

(25) Dembitsky, V. M. *J. Nat. Med.* **2008**, *62*, 1-33.

(26) Capraro, H.-G.; Brossi, A. *The alkaloids* **1984**, *23*, 1-70.

(27) Körner, A.; Kohn, S. *J. Chromatogr. A* **2005**, *1089*, 148-157.

(28) uri, O. P.; Gupta, B. D.; Suri, K. A.; Sharma, A. K.; Satti, N. K. *Nat. Prod. Lett.* **2001**, *15*, 217-219.

(29) Yoshida, K.; Hayashi, T.; SANO, K. *Agric. Biol. Chem.* **1988**, *52*, 593-594.

(30) Šantavý, F. *Collect. Czech. Chem. Commun.* **1970**, *35*, 2857-2860.

(31) Potesilova, H.; Wiedermannova, J.; Santavy, F. *Collect. Czech. Chem. Commun.* **1969**, *34*, 3642-3645.

(32) He, H.-P.; Liu, F.-C.; Hu, U.; Zhu, H.-Y. *Acta Bot. Yunnanica* **1999**, *21*, 364-368.

(33) Thakur, R.; Potěsilová, H.; Santavý, F. *Planta Med.* **1975**, *28*, 201.

(34) Potěšilová, H.; Dolejš, L.; Sedmera, P.; Šantavý, F. *Collect. Czech. Chem. Commun.* **1977**, *42*, 1571-1580.

(35) Meksuriyen, D.; Lin, L.-j.; Cordell, G. A. *J. Nat. Prod.* **1988**, *51*, 88-93.

(36) Kiselev, V.; Yavich, P. *Chem. Nat. Compd.* **1990**, *26*, 502-509.

(37) Dumont, R.; Brossi, A.; Silverton, J. V. *J. Org. Chem.* **1986**, *51*, 2515-2521.

(38) Santavy, F.; Reichstein, T. *Helv. Chim. Acta* **1950**, *33*, 1606-1627.

(39) Roesner, M.; Hsu, F.-L.; Brossi, A. *J. Org. Chem.* **1981**, *46*, 3686-3688.

(40) Fox, J.; Wempen, I. *Adv. Carbohydr. Chem.* **1959**, *14*, 283.

(41) Johnson, L. F.; Jankowski, W. C.; Wiley-Interscience, New York: 1972.

(42) Broom, A. D.; Robins, R. K. *J. Org. Chem.* **1969**, *34*, 1025-1029.

(43) Jensen, S. R.; Nielsen, B. J.; Norn, V. *Phytochemistry* **1979**, *18*, 904-906.

(44) Wu, B.; Wu, S.; Qu, H.; Cheng, Y. *Helv. Chim. Acta* **2008**, *91*, 1863-1870.

(45) Kumar, M.; Rawat, P.; Khan, M. F.; Tamarkar, A. K.; Srivastava, A. K.; Arya, K. R.; Maurya, R. *Fitoterapia* **2010**, *81*, 475-479.

(46) Syahrani, A.; Widjaja, I.; Indrayanto, G.; Wilkins, A. L. *J. Asian Nat. Prod. Res.* **1998**, *1*, 111-117.

(47) Itoh, A.; Tanahashi, T.; Nagakura, N.; Inoue, K.; Kuwajima, H.; WU, H.-X. *Chem. Pharm. Bull.* **2001**, *49*, 1343-1345.

(48) De Rosa, S.; De Giulio, A.; Tommonaro, G. *Phytochemistry* **1996**, *42*, 1031-1034.

(49) Murray, R. D. H.; Méndez, J.; Brown, S. A. **1982**.

(50) Ye, G.; Peng, H.; Fan, M.; Huang, C.-G. *Chem. Nat. Compd.* **2007**, *43*, 125-127.

(51) Wawer, I.; Zielinska, A. *Magn. Reson. Chem.* **2001**, *39*, 374-380.

(52) Yuldashev, M.; Batirov, E. K.; Malikov, V.; Yuldashevaa, N. *Chem. Nat. Compd.* **1996**, *32*, 923-924.

(53) Mansour, R. M. A.; Ahmed, A. A.; Saleh, N. A. M. *Phytochemistry* **1983**, *22*, 2630-2631.

(54) Fu, H.-w.; Zhang, L.; Yi, T.; Feng, Y.-l.; Tian, J.-k. *Biochem. Syst. Ecol.* **2010**, *38*, 309-312.

(55) Del Rio, J. A.; Benavente, O.; Castillo, J.; Borrego, F. *Phytochemistry* **1992**, *31*, 723-724.

(56) Chiruvella, K. K.; Mohammed, A.; Dampuri, G.; Ghanta, R. G.; Raghavan, S. C. *Int. J. Biomed. Sci.* **2007**, *3*, 269.

(57) Shrestha, S.; Lee, D.-Y.; Park, J.-H.; Cho, J.-G.; Seo, W.-D.; Kang, H. C.; Jeon, Y.-J.; Yeon, S.-W.; Bang, M.-H.; Baek, N.-I. *J. Korean Soc. Appl. Bl.* **2012**, *55*, 689-693.

(58) Wang, Z.; Han, Z.; Cui, H.; Dai, H. *J. Trop. Subtrop. Bot.* **2007**, *15*, 359-362.

(59) McArdle, B. M.; Campitelli, M. R.; Quinn, R. J. *J. Nat. Prod.* **2006**, *69*, 14-17.

(60) Kellenberger, E.; Hofmann, A.; Quinn, R. J. *Nat. Prod. Rep.* **2011**, *28*, 1483-1492.

(61) Hufford, C. D.; Capraro, H. G.; Brossi, A. *Helv. Chim. Acta* **1980**, *63*, 50-56.

(62) Hara, S.; Okabe, H.; Mihashi, K. *Chem. Pharm. Bull.* **1987**, *35*, 501-506.

(63) Wang, H.; Zhao, W.; Choomuenwai, V.; Andrews, K. T.; Quinn, R. J.; Feng, Y. *Bioorg. Med. Chem. Lett.* **2013**, *23*, 5915-5918.

(64) Pretsch, E.; Bühlmann, P.; Badertscher, M. *Structure Determination of Organic Compounds: Tables of Spectral Data*; Springer Science & Business Media, 2009.

(65) Clark, L. B.; Tinoco, I. *J. Am. Chem. Soc.* **1965**, *87*, 11-15.

(66) Hruska, F. E.; Blonski, W. J. *Can. J. Chem.* **1982**, *60*, 3026-3032.

(67) Crabbé, P.; Klyne, W. *Tetrahedron* **1967**, *23*, 3449-3503.

(68) Ulbricht, T. L. V.; Jennings, J. P.; Scopes, P. M.; Klyne, W. *Tetrahedron Lett.* **1964**, *5*, 695-698.

(69) Frič, I.; Šmejkal, J.; Farkaš, J. *Tetrahedron Lett.* **1966**, *7*, 75-79.

(70) Ulbricht, T. L. V.; Emerson, T. R.; Swan, R. J. *Tetrahedron Lett.* **1966**, *7*, 1561-1567.

(71) Miyahara, T.; Nakatsuji, H.; Wada, T. *J. Phys. Chem. A* **2014**, *118*, 2931-2941.

(72) Nobumasa, I.; Takashi, T.; Tyunosin, U. *Chem. Pharm. Bull.* **1968**, *16*, 1105-1109.

(73) Todd Miles, H. *Biochim. Biophys. Acta* **1956**, *22*, 247-253.

(74) Levene, P.; Tipson, R. S. *J. Biol. Chem.* **1934**, *104*, 385-393.

(75) Yamamoto, I.; Kimura, T.; Tateoka, Y.; Watanabe, K.; Ho, I. K. *Chem. Pharm. Bull.* **1985**, *33*, 4088-4090.

(76) Dobolyi, A.; Juhász, G.; Kovács, Z.; Kardos, J. *Curr. Top. Med. Chem.* **2011**, *11*, 1058-1067.

(77) Yamamoto, I.; Kimura, T.; Tateoka, Y.; Watanabe, K.; Ho, I. K. *J. Med. Chem.* **1987**, *30*, 2227-2231.

(78) Kimura, T.; Ho, I.; Yamamoto, I. *Sleep* **2001**, *24*, 251-260.

(79) Camp, D.; Davis, R. A.; Campitelli, M.; Ebdon, J.; Quinn, R. J. *J. Nat. Prod.* **2012**, *75*, 72-81.

(80) Quinn, R. J.; Carroll, A. R.; Pham, N. B.; Baron, P.; Palframan, M. E.; Suraweera, L.; Pierens, G. K.; Muresan, S. *J. Nat. Prod.* **2008**, *71*, 464-468.

(81) Instant JChem, version 15.10.26.10; ChemAxon Kft: Budapest, Hungary, 2015.

(82) Weeratunga, S.; Hu, N.-J.; Simon, A.; Hofmann, A. *BMC Bioinformatics* **2012**, *13*, 201.

(83) Gupta, P.; Sharma, U.; Gupta, P.; Siripurapu, K. B.; Maurya, R. *Biorg. Med. Chem.* **2013**, *21*, 1116-1122.

(84) Du, L. C.; Wu, B. L.; Chen, J. M. *Chin. Chem. Lett.* **2008**, *19*, 1315-1318.

Supporting Information for Chapter Three

Supporting information for

A Grand Challenge (Ⅱ): Unbiased Phenotypic Function of Metabolites from *Gloriosa superba* L. against Parkinson's Disease

Dongdong Wang,[†] Yunjiang Feng,[†] Mariyam Murtaza,[†] Stephen A. Wood,[†] George D. Mellick,[†] Paul I. Froster[‡] and Ronald J. Quinn[†,*]

[†]Eskitis Institute for Drug Discovery, Griffith University, Brisbane, QLD 4111, Australia.

[‡]Queensland Herbarium, Brisbane Botanic Gardens, Brisbane, QLD 4066, Australia

Corresponding author contact details: Tel: +61-7-37356006. Fax: +61-7-37356001. E-mail: r.quinn@griffith.edu.au

List of supporting information

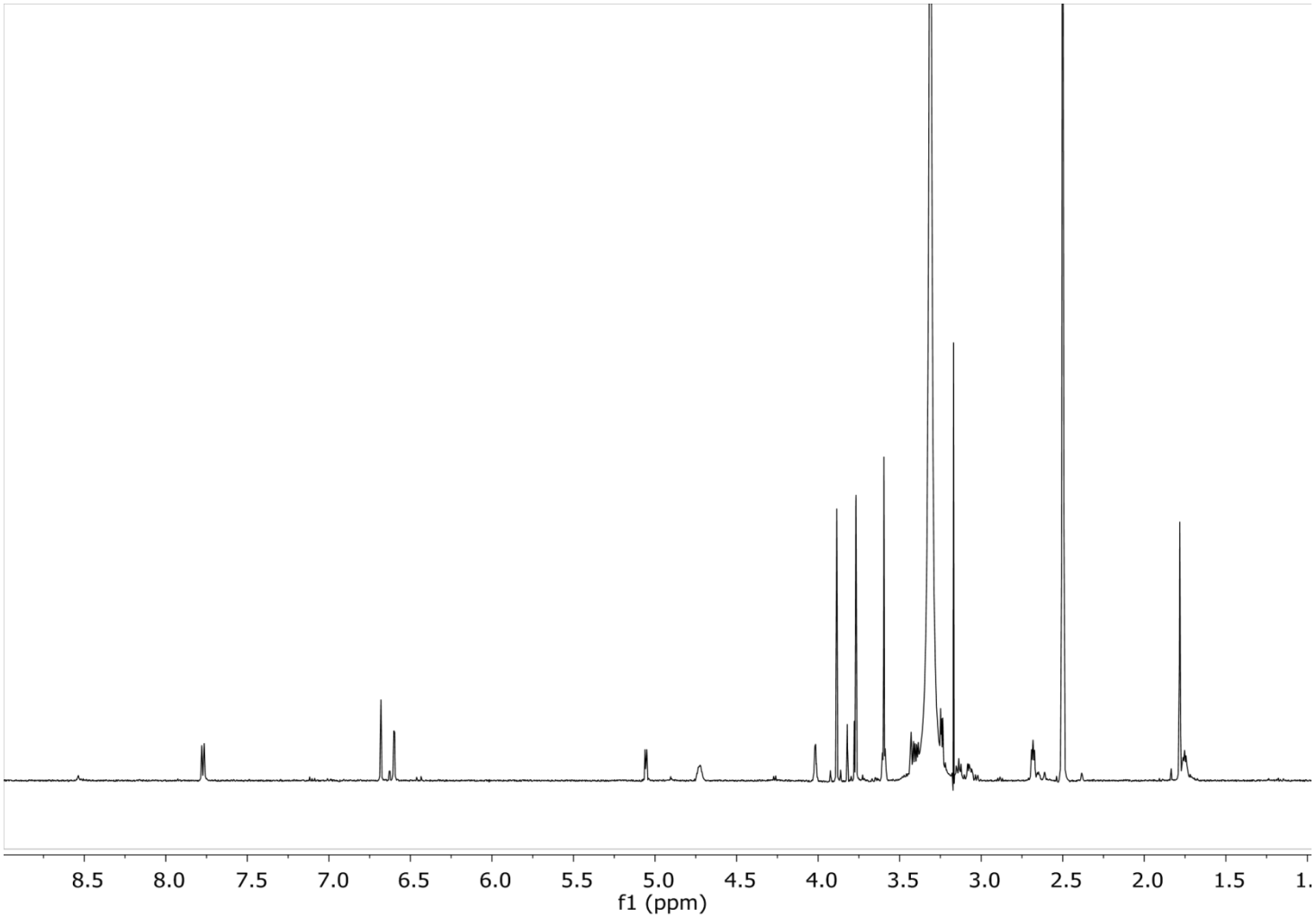

Figure S1. ^{1}H NMR spectrum of compound **1** in DMSO-d_6

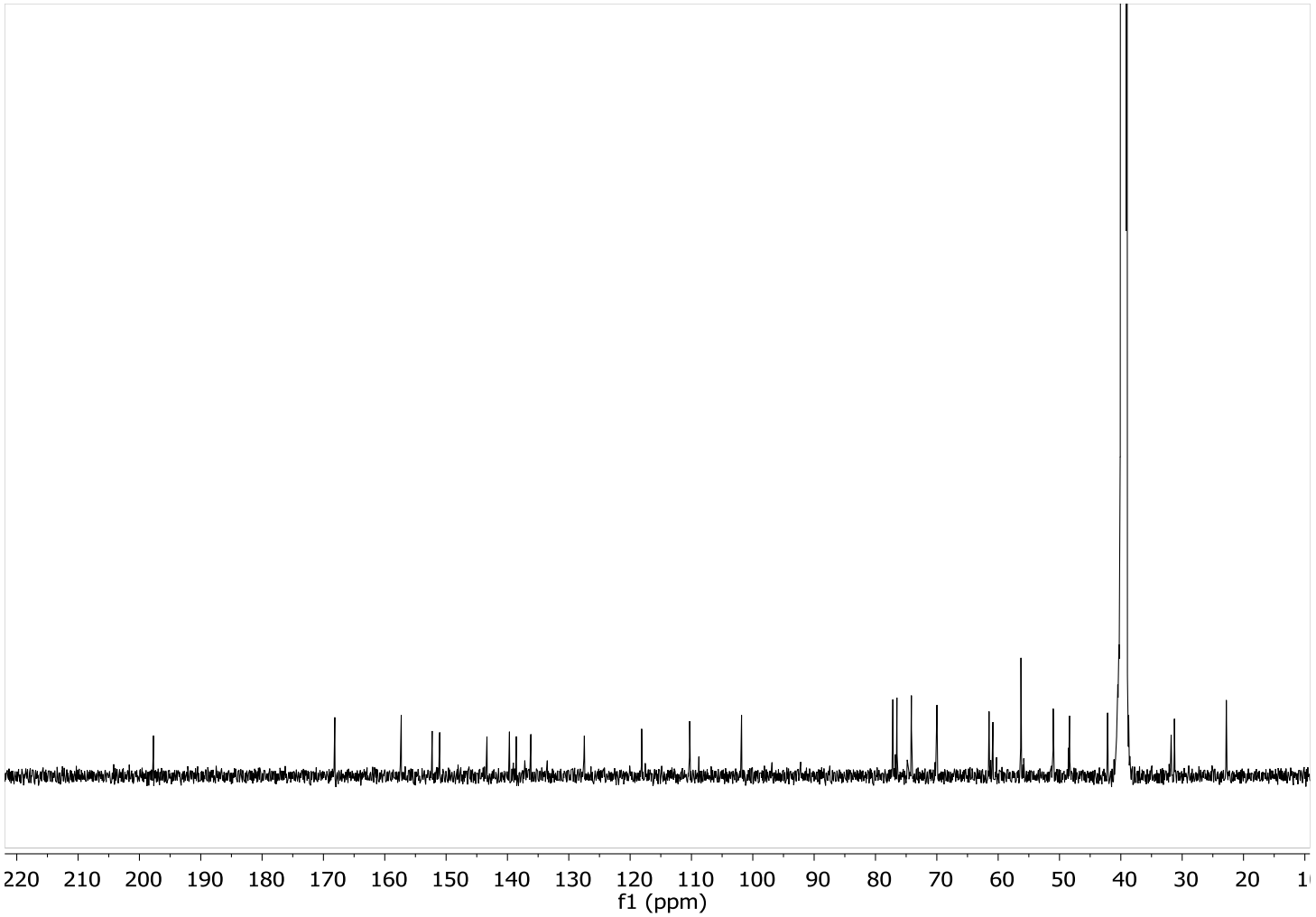

Figure S1. ^{13}C NMR spectrum of compound **1** in DMSO-d_6

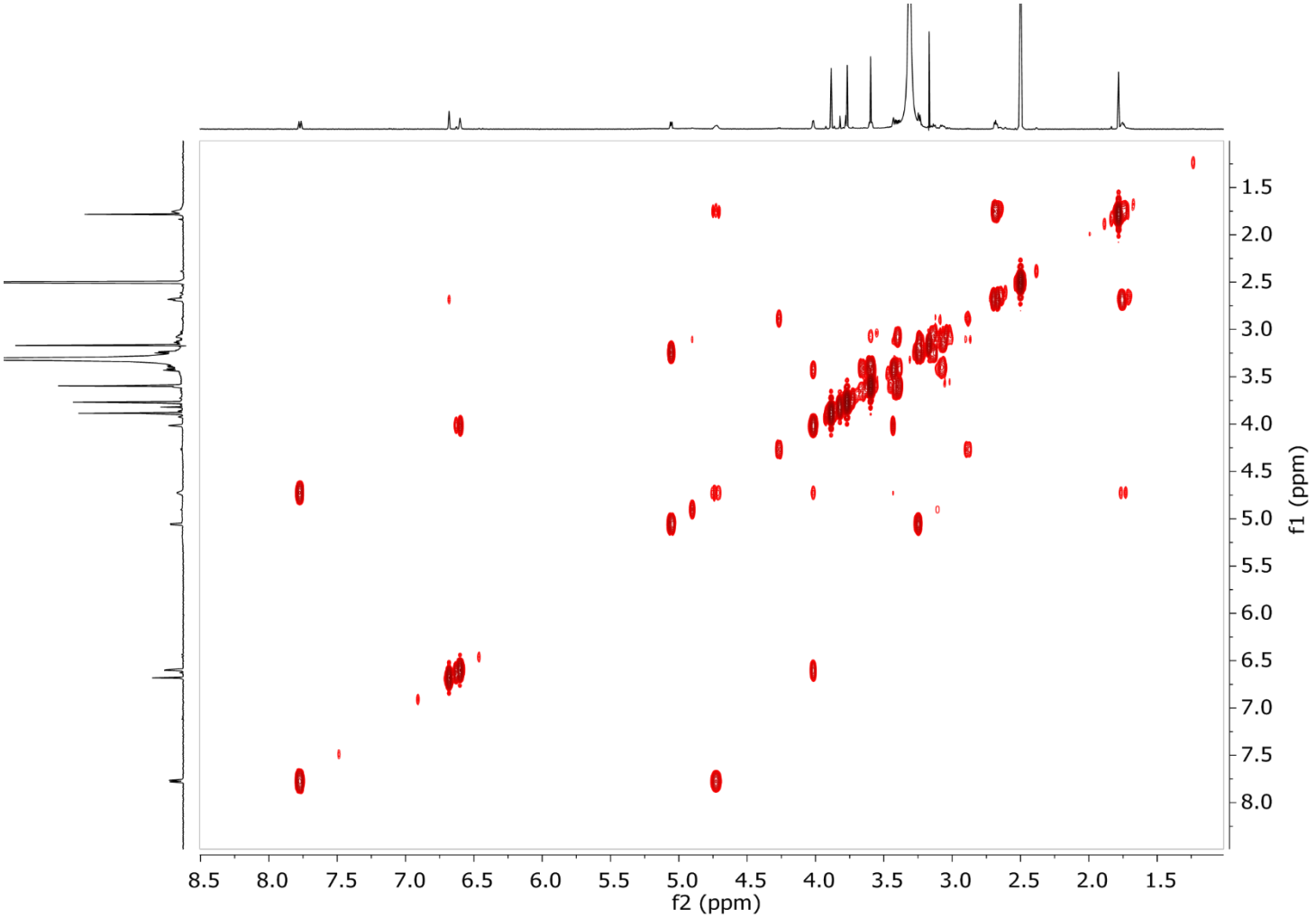

Figure S3. COSY spectrum of compound **1** in DMSO-d_6

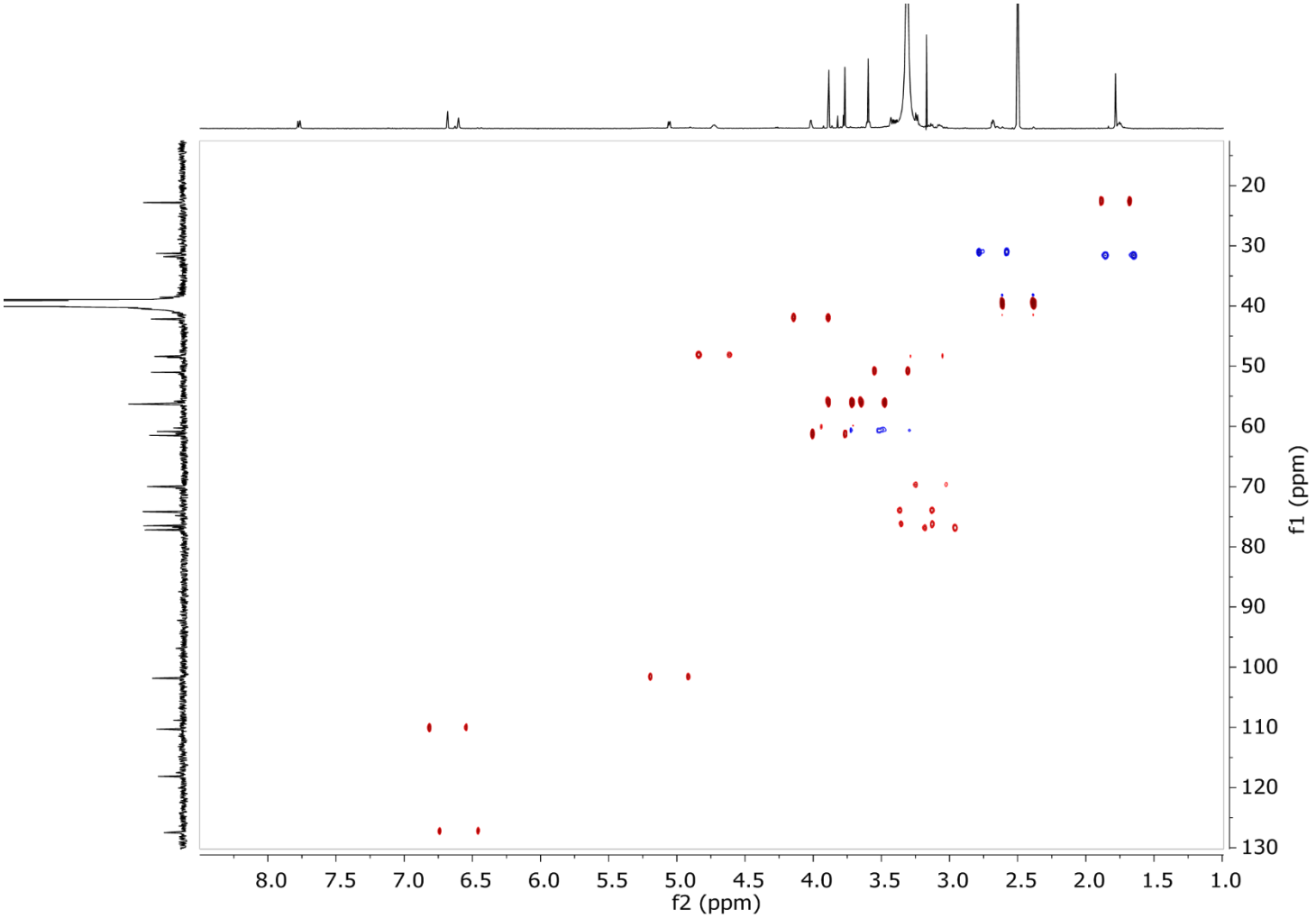

Figure S4. HSQC spectrum of compound **1** in DMSO-d_6

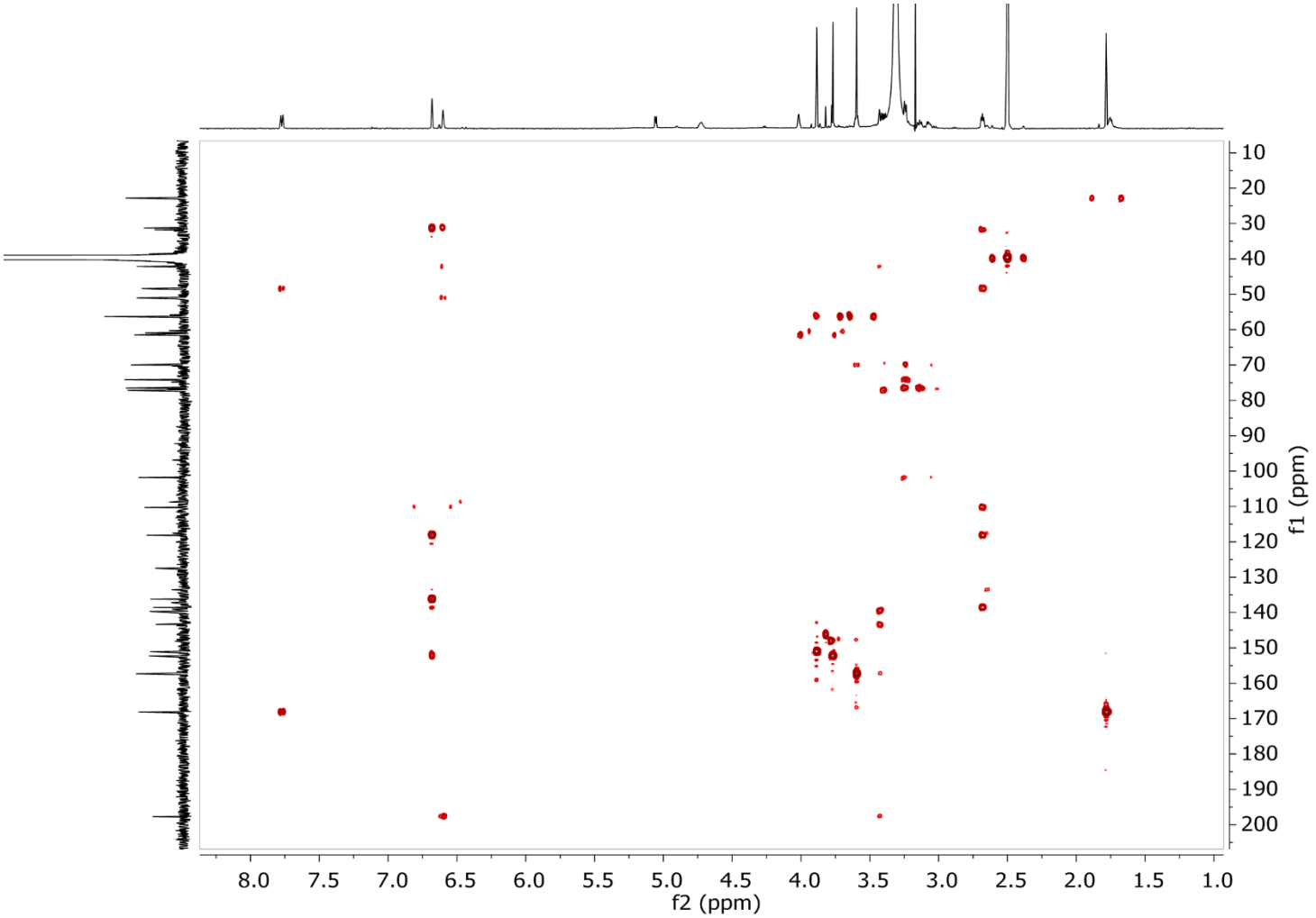

Figure S5. HMBC spectrum of compound **1** in DMSO-d_6

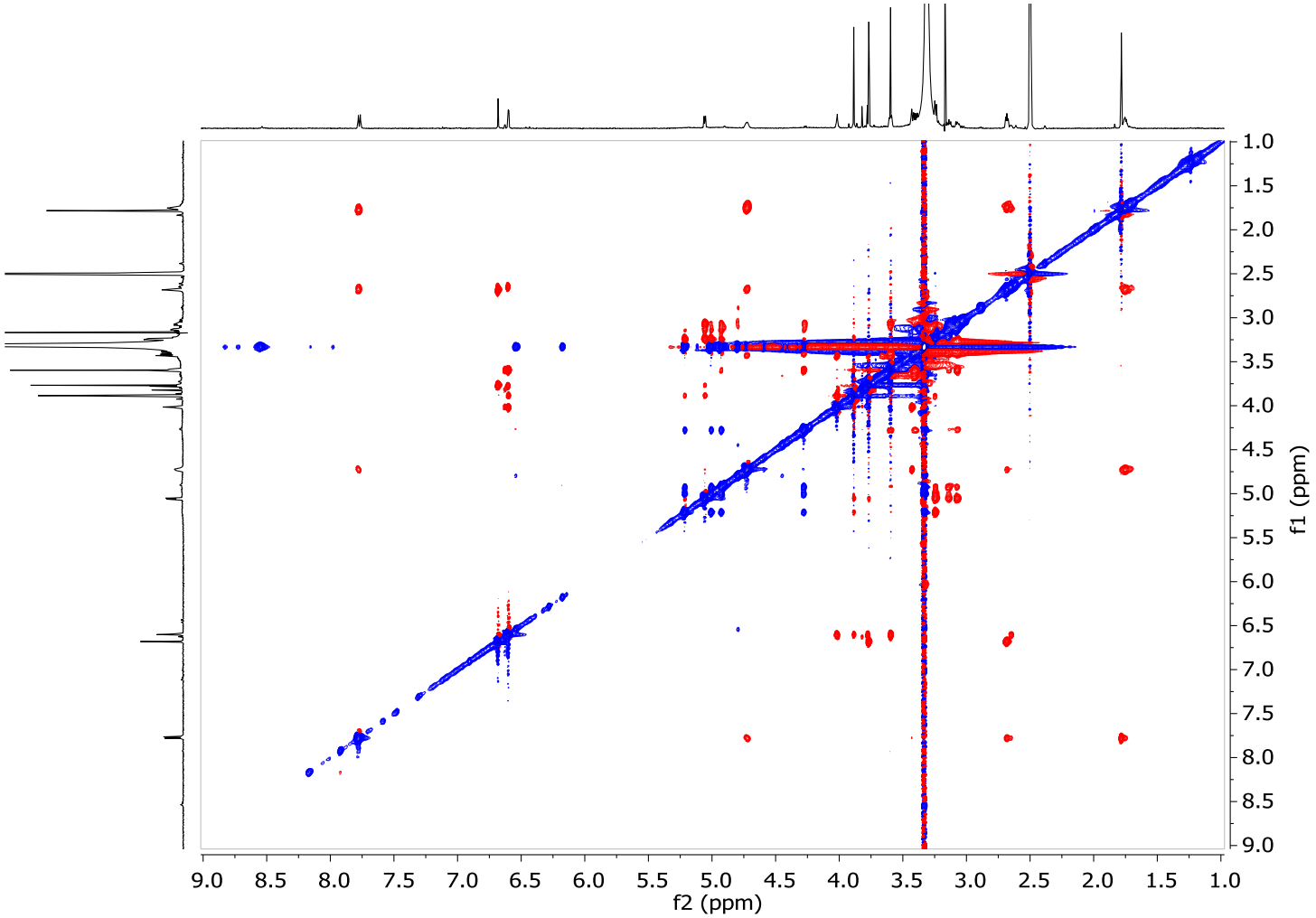

Figure S6. ROESYspectrum of compound **1** in DMSO-d_6

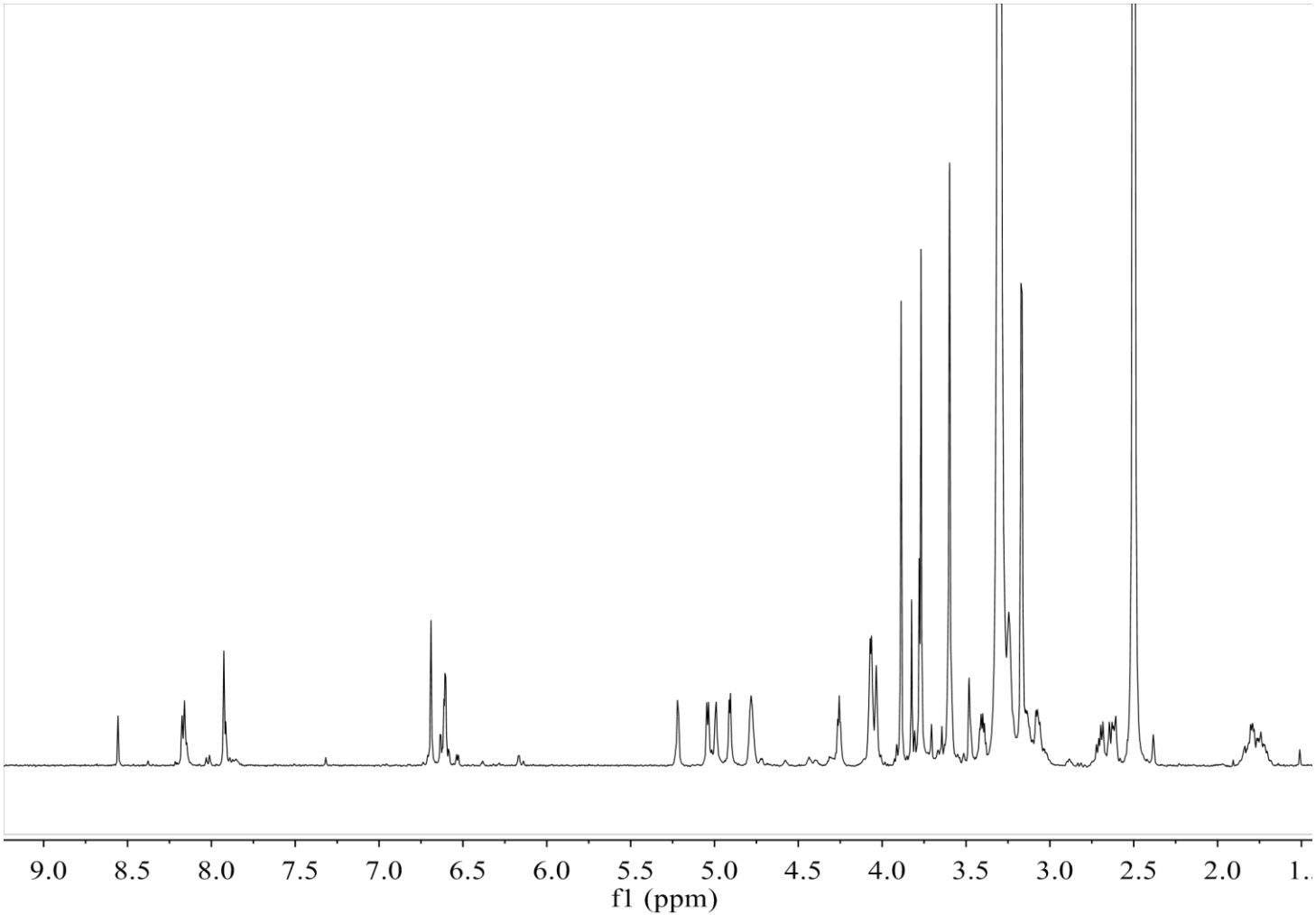

Figure S7. ^{1}H NMR spectrum of compound **2** in DMSO-d_6

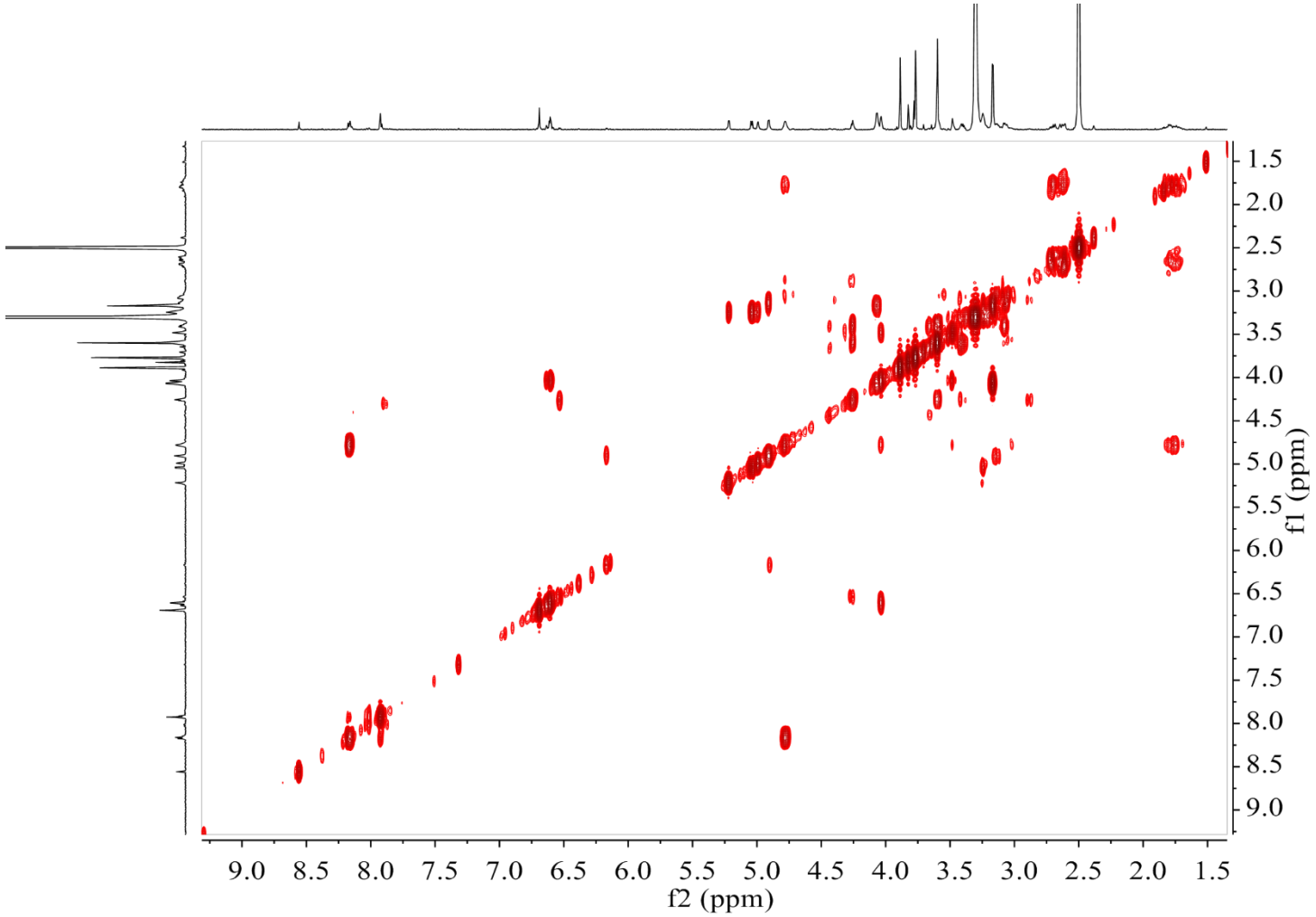

Figure S8. COSY spectrum of compound **2** in DMSO-d_6

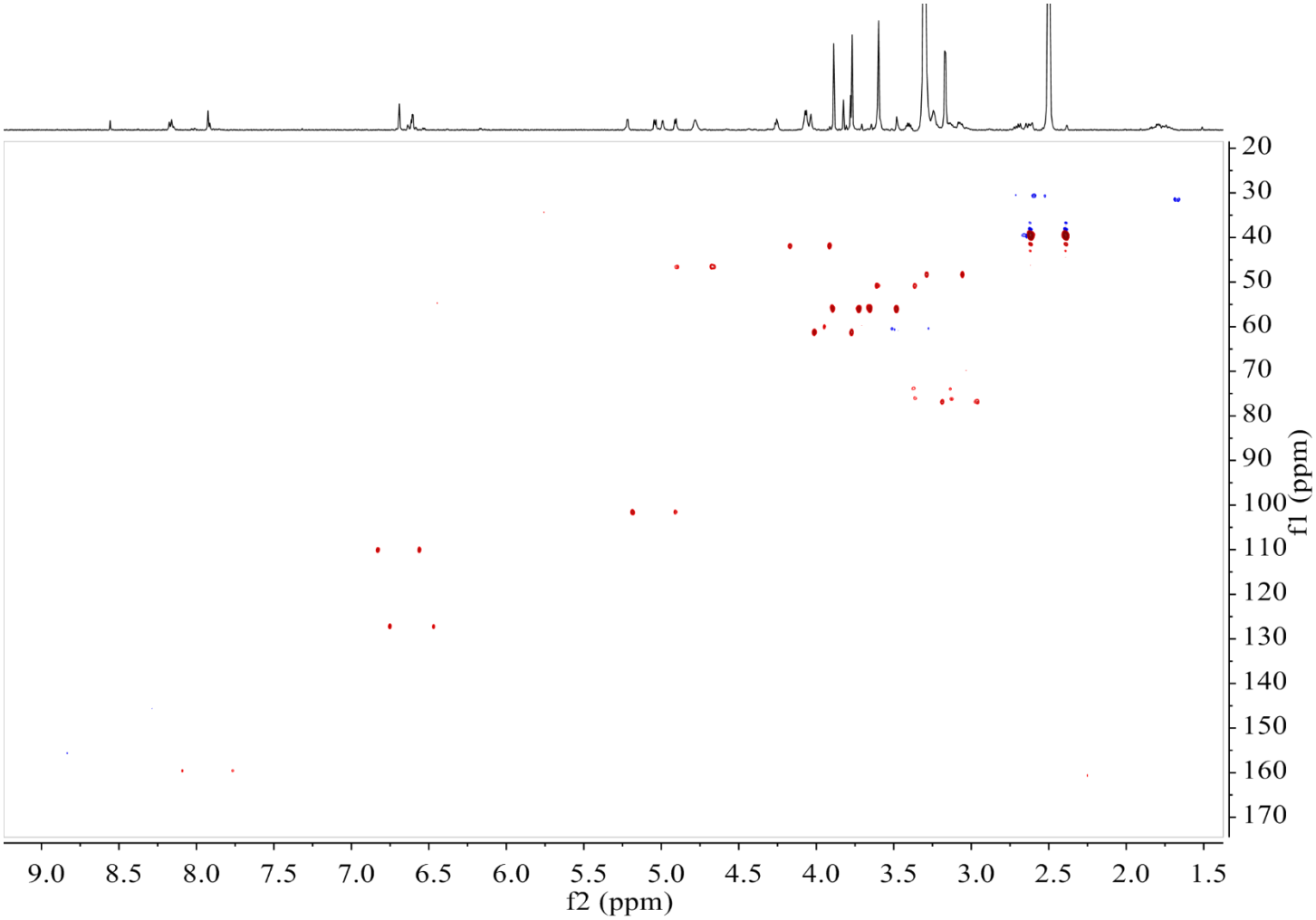

Figure S9. HSQC spectrum of compound **2** in DMSO-d_6

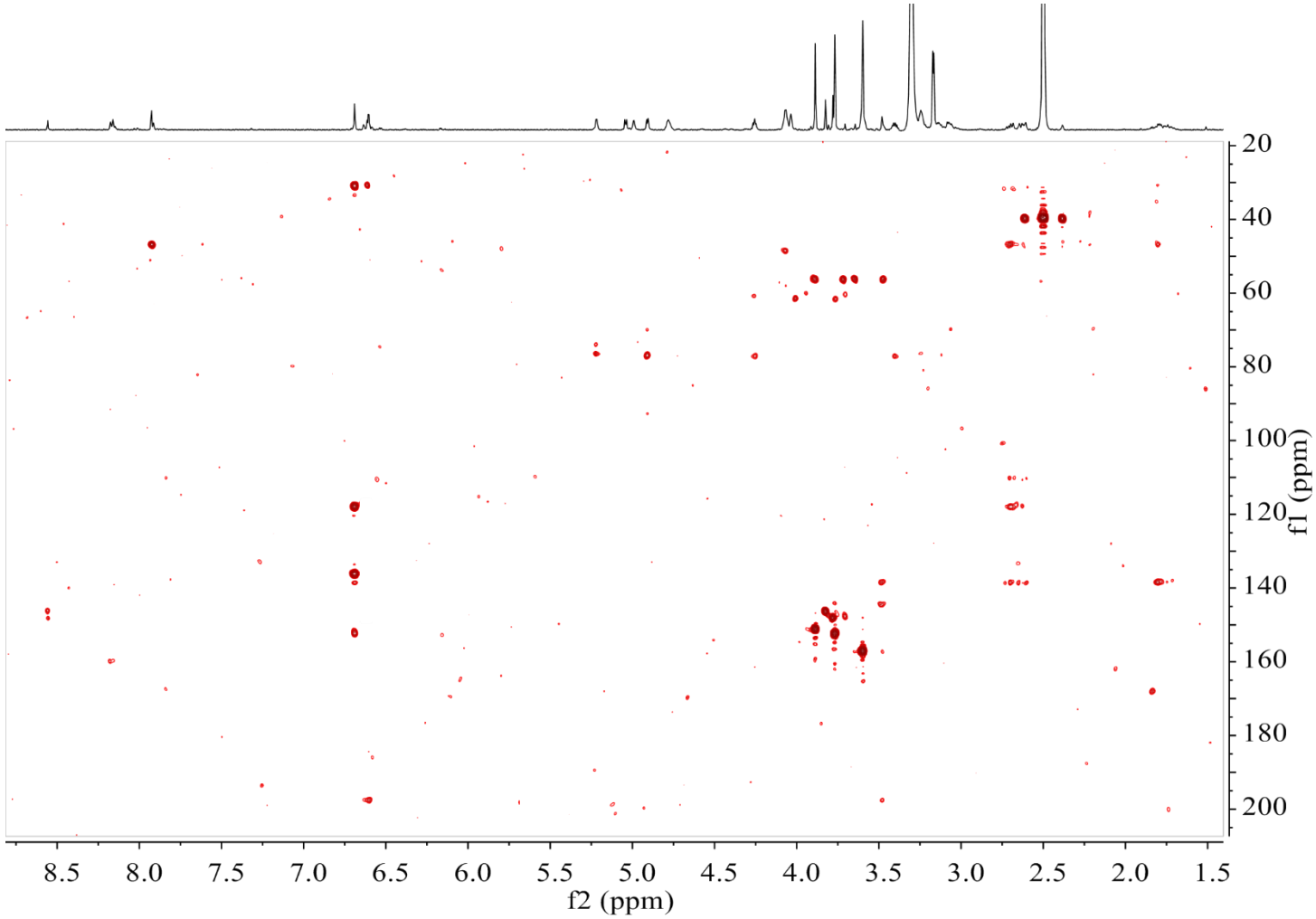

Figure S10. HMBC spectrum of compound **2** in DMSO-d_6

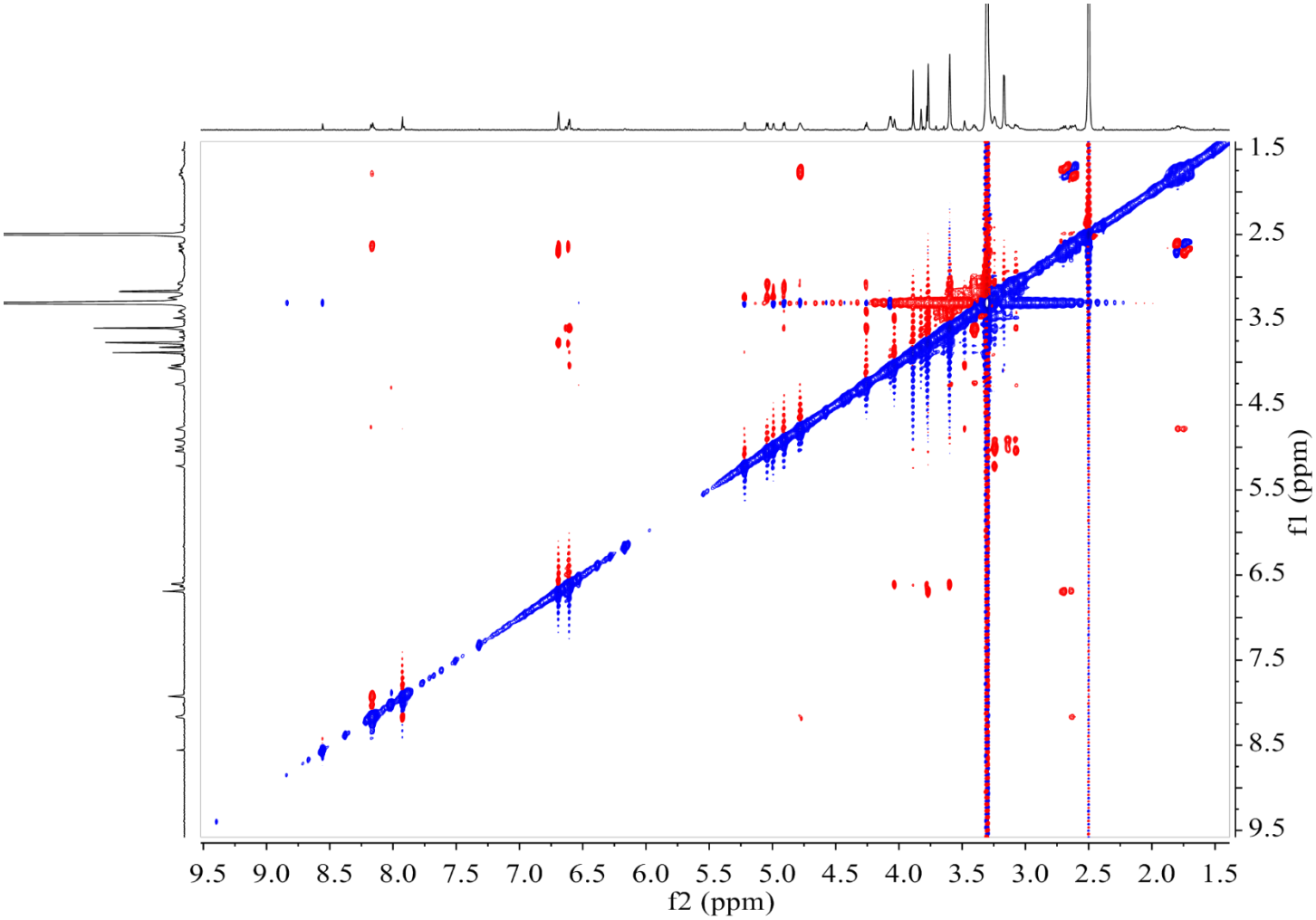

Figure S11. ROESYspectrum of compound **2** in DMSO-d_6

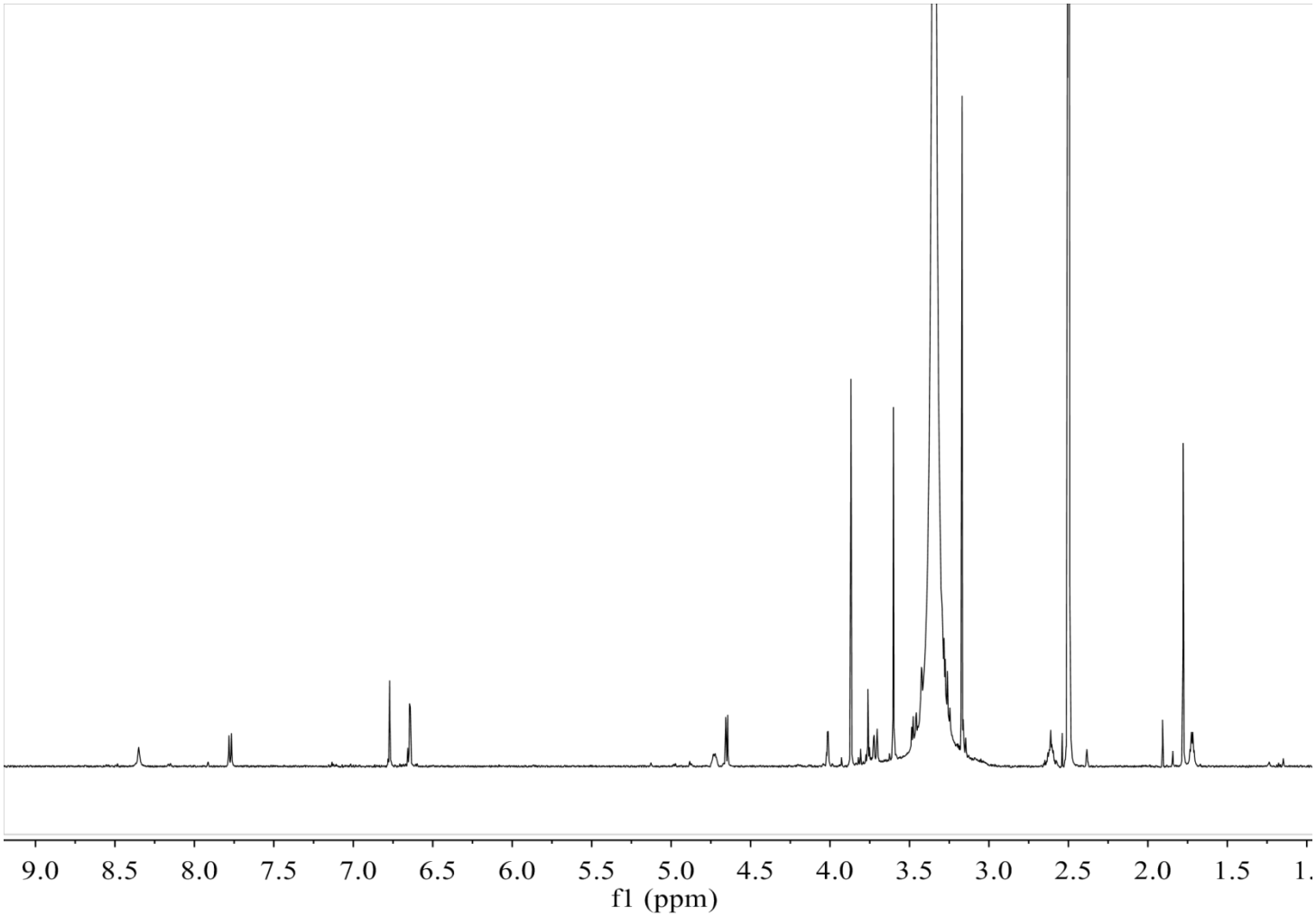

Figure S12. ^{1}H NMR spectrum of compound **3** in DMSO-d_6

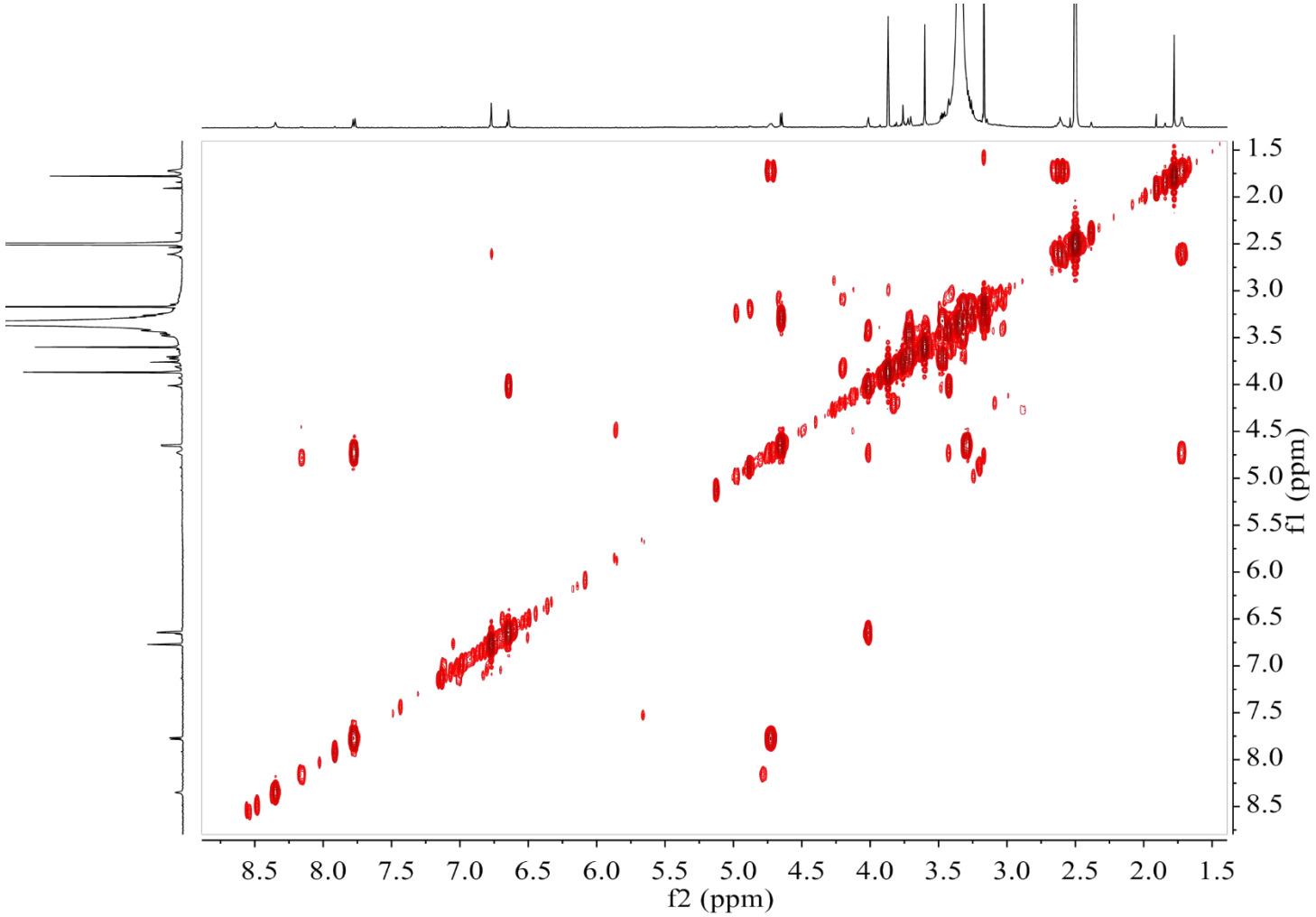

Figure S13. COSY spectrum of compound **3** in DMSO-d_6

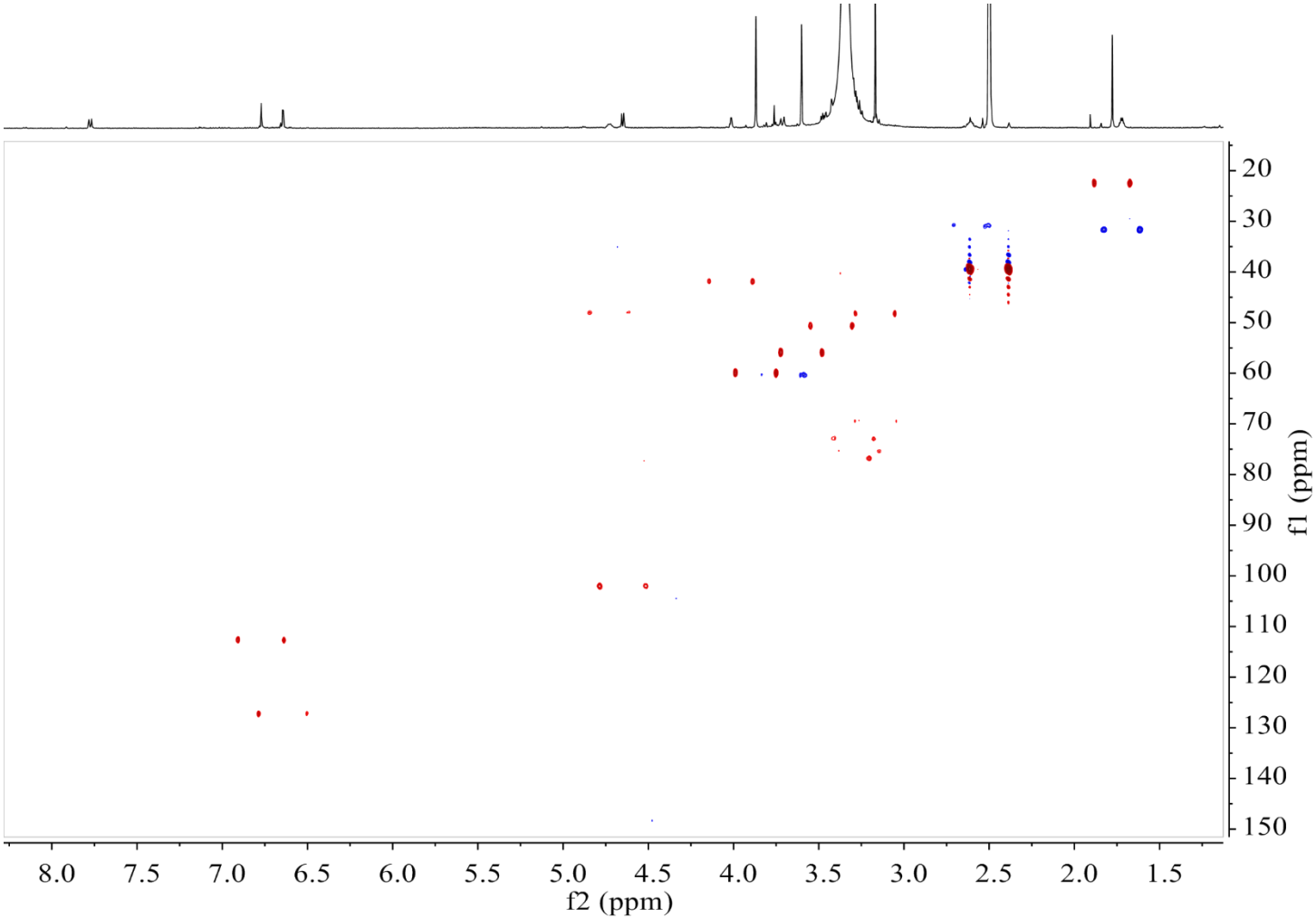

Figure S14. HSQC spectrum of compound **3** in DMSO-d_6

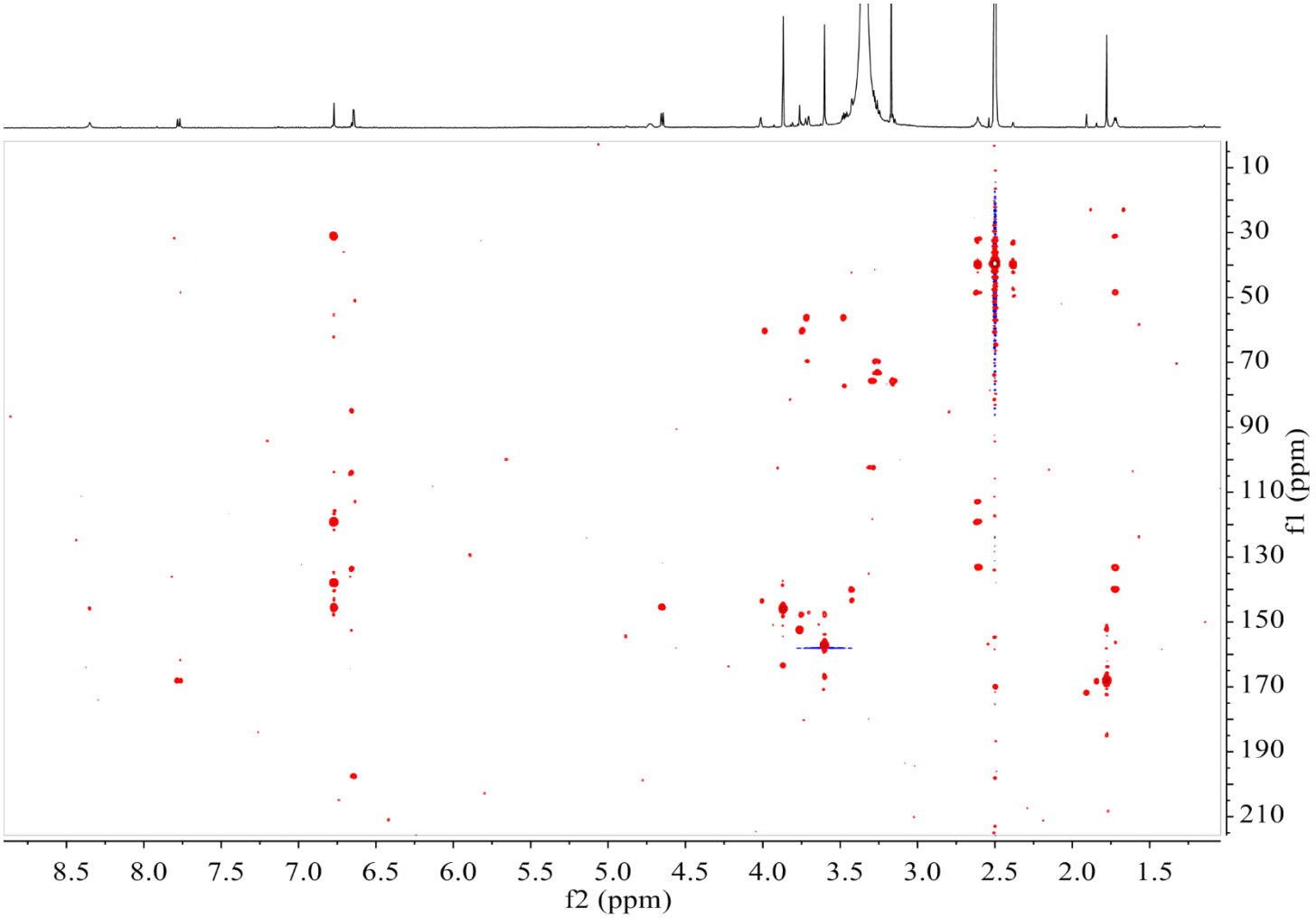

Figure S15. HMBC spectrum of compound **3** in DMSO-d_6

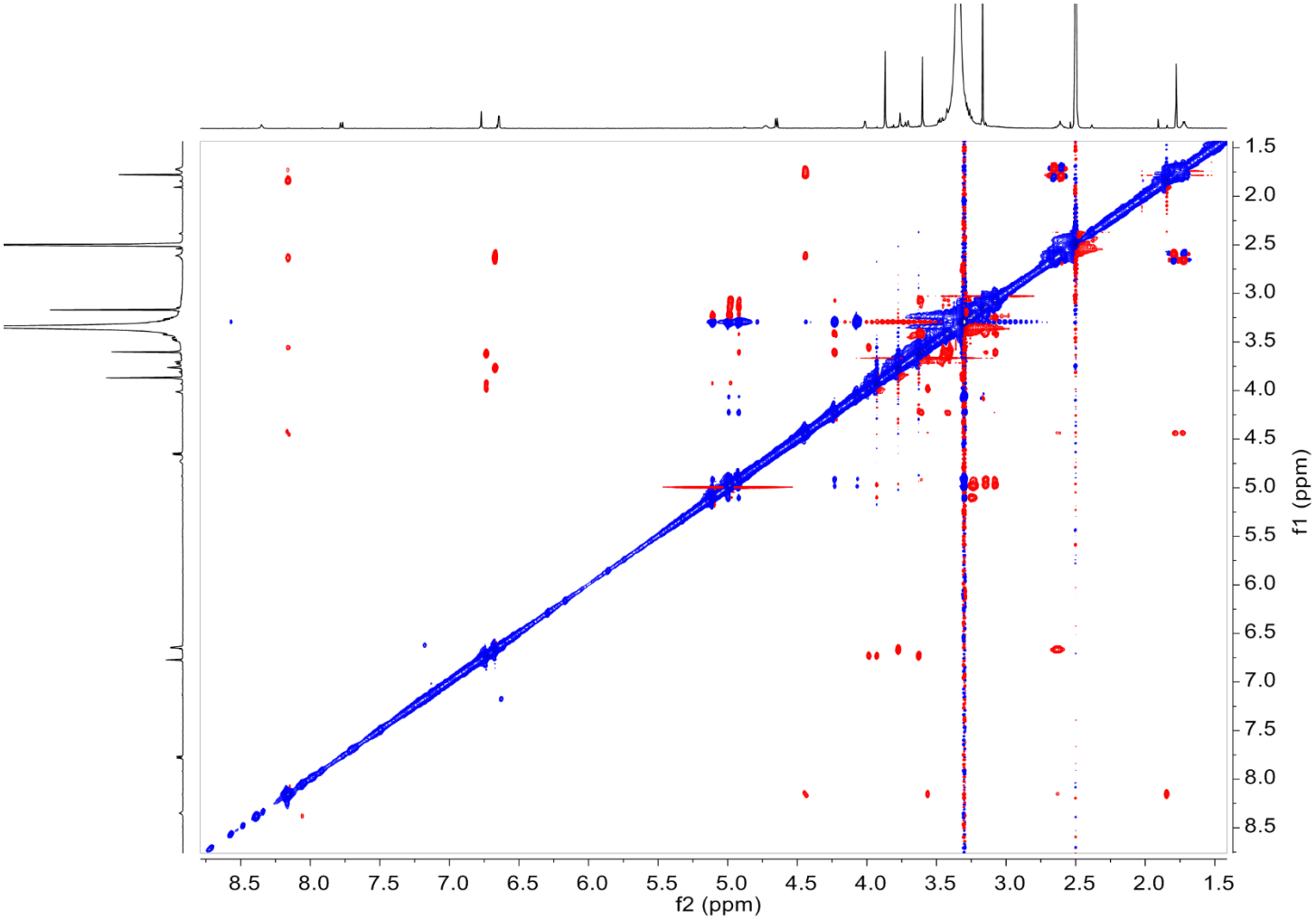

Figure S16. ROESYspectrum of compound **3** in DMSO-d_6

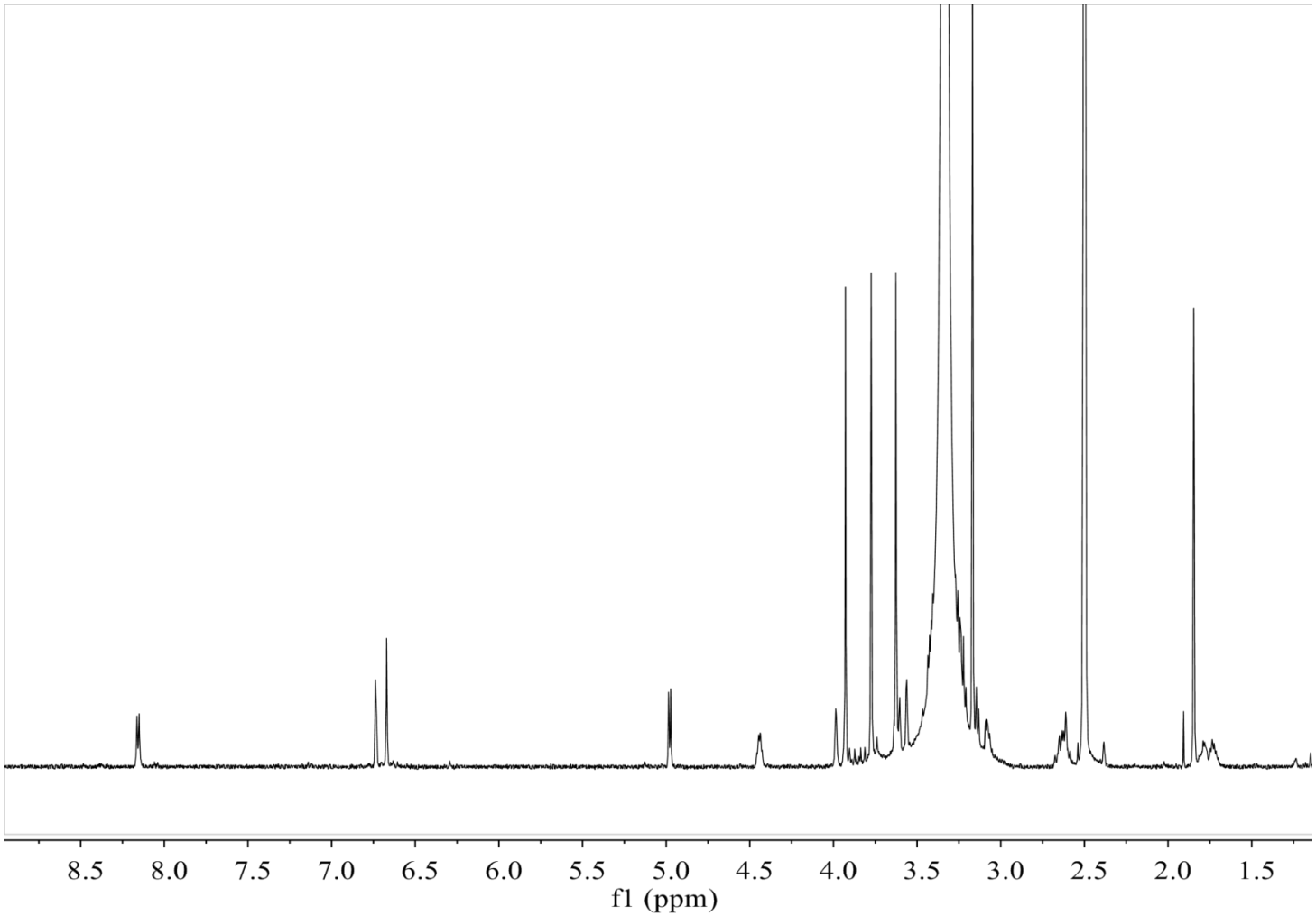

Figure S17. ^{1}H NMR spectrum of compound **4** in DMSO-d_6

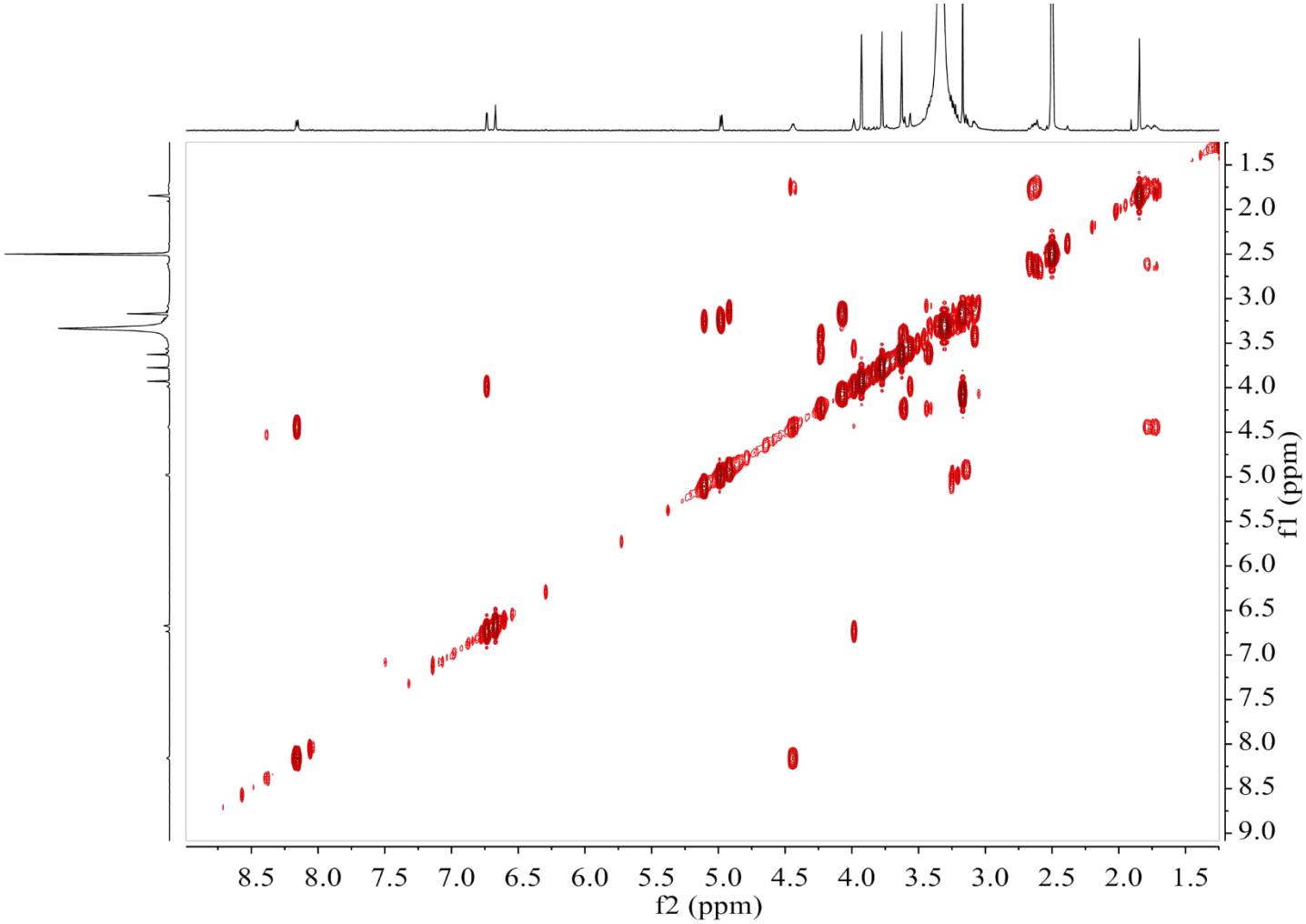

Figure S18. COSY spectrum of compound **4** in DMSO-d_6

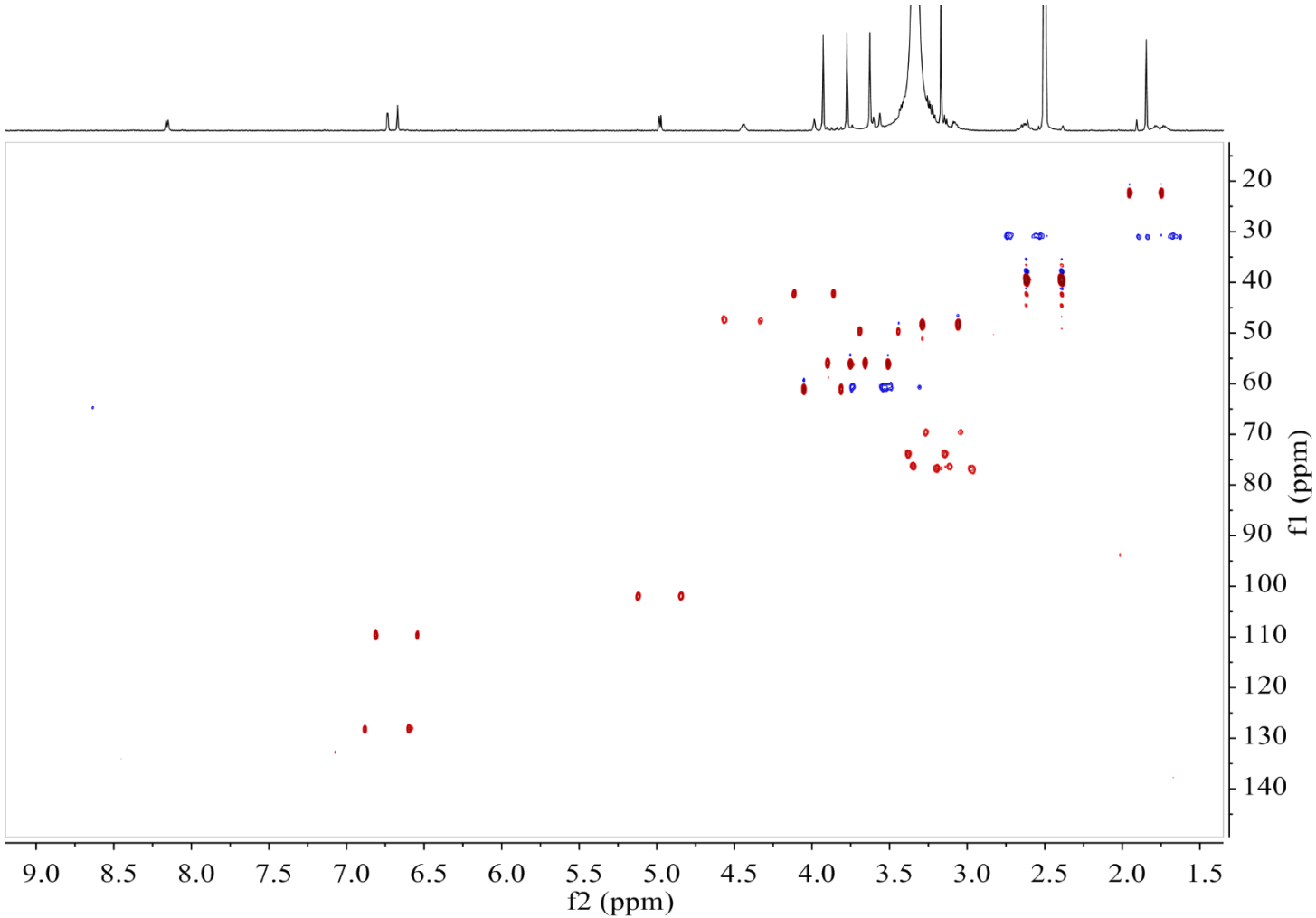

Figure S19. HSQC spectrum of compound **4** in DMSO-d_6

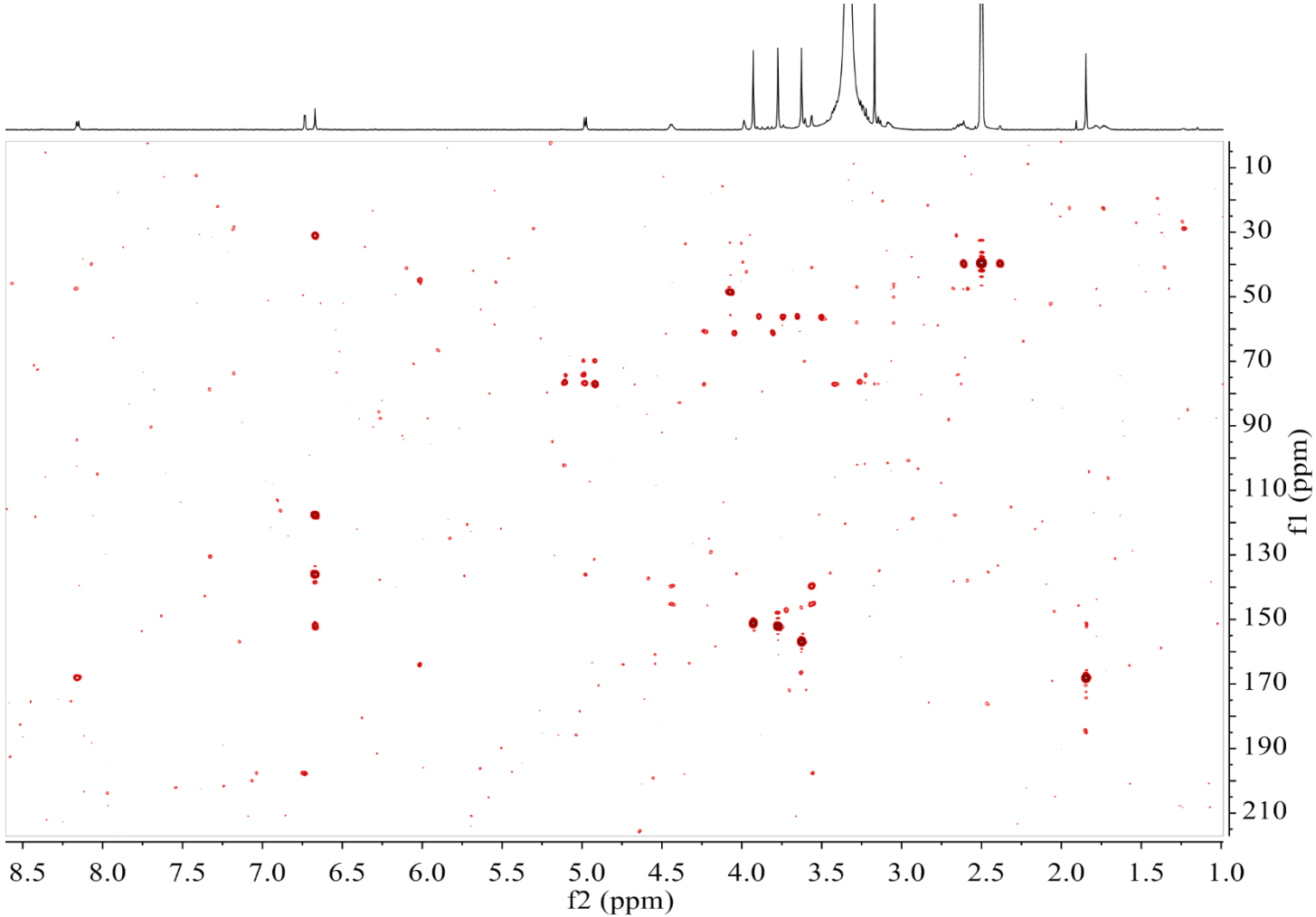

Figure S20. HMBC spectrum of compound **4** in DMSO-d_6

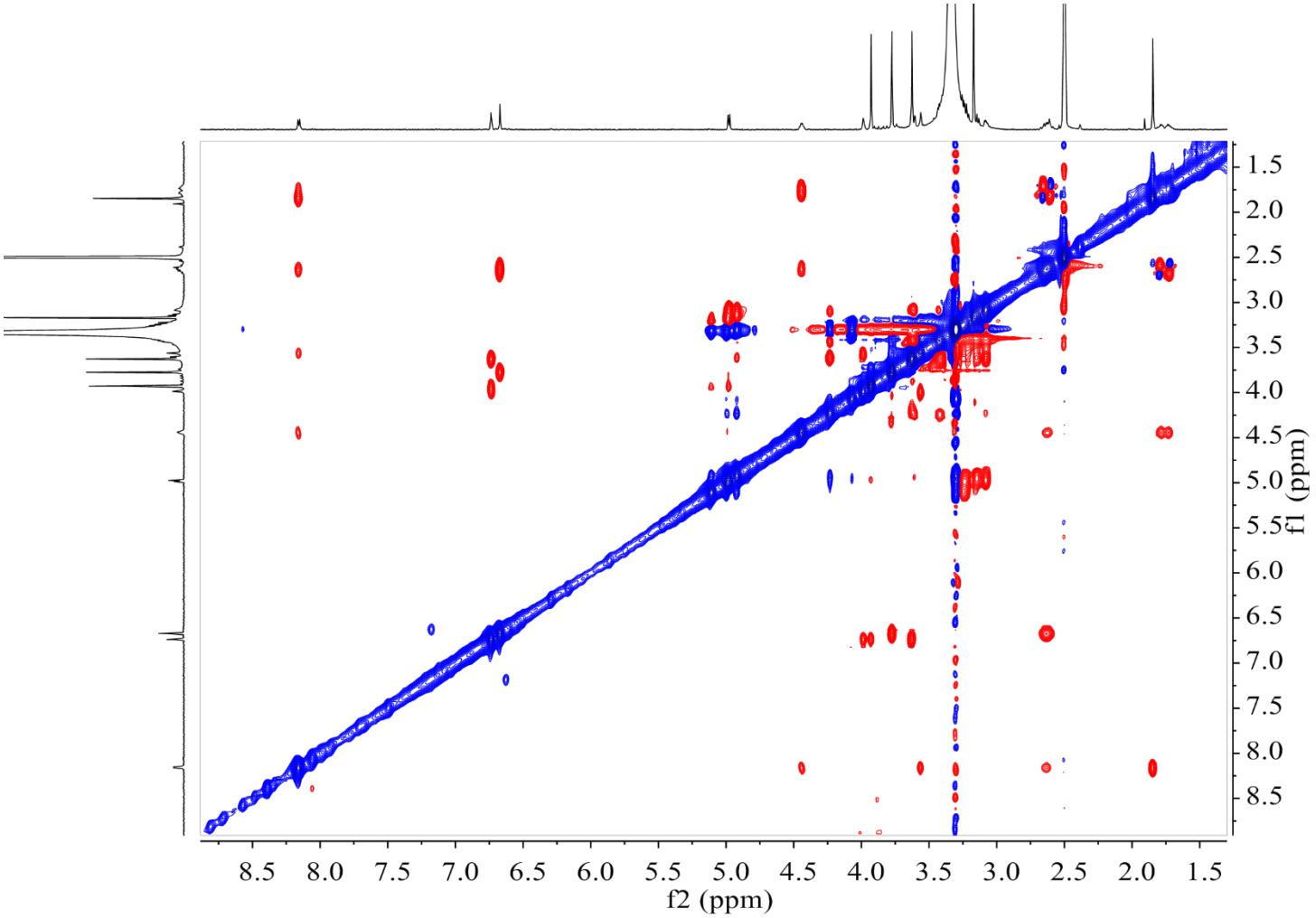

Figure S21. ROESYspectrum of compound **4** in DMSO-d_6

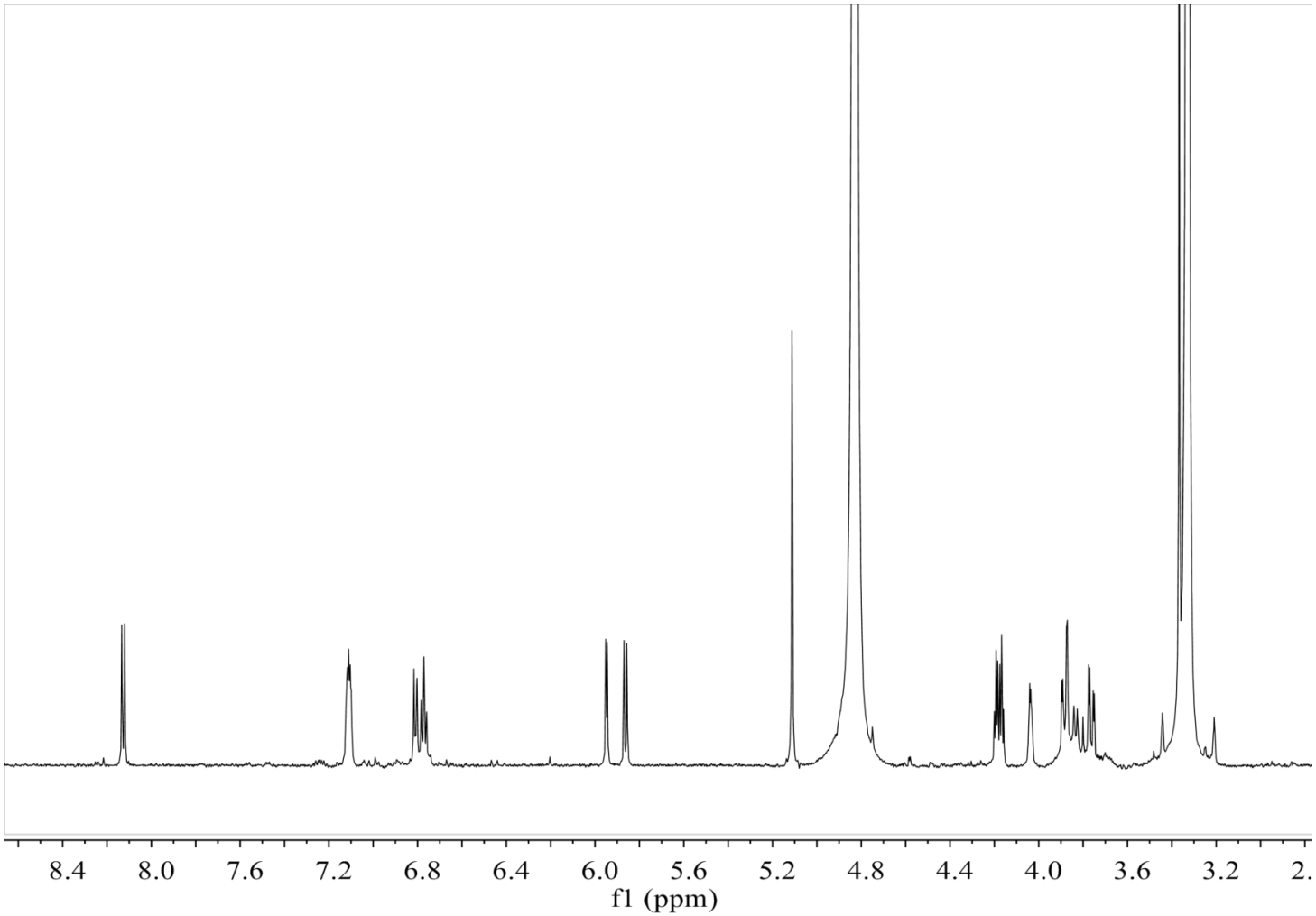

Figure S22. ^{1}H NMR spectrum of compound **15** in MeOH-d_4

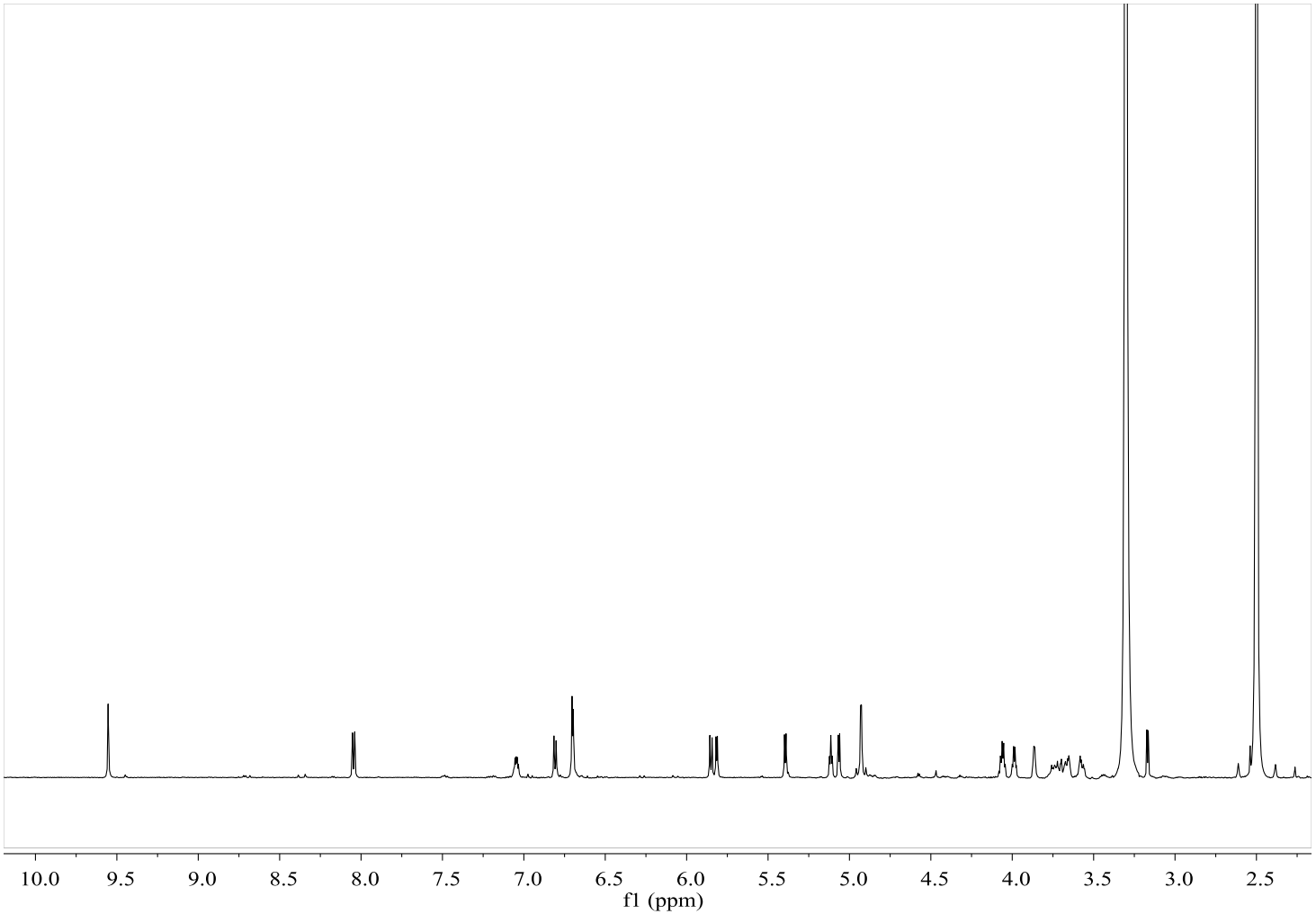

Figure S23. ^{1}H NMR spectrum of compound **15** in DMSO-d_6

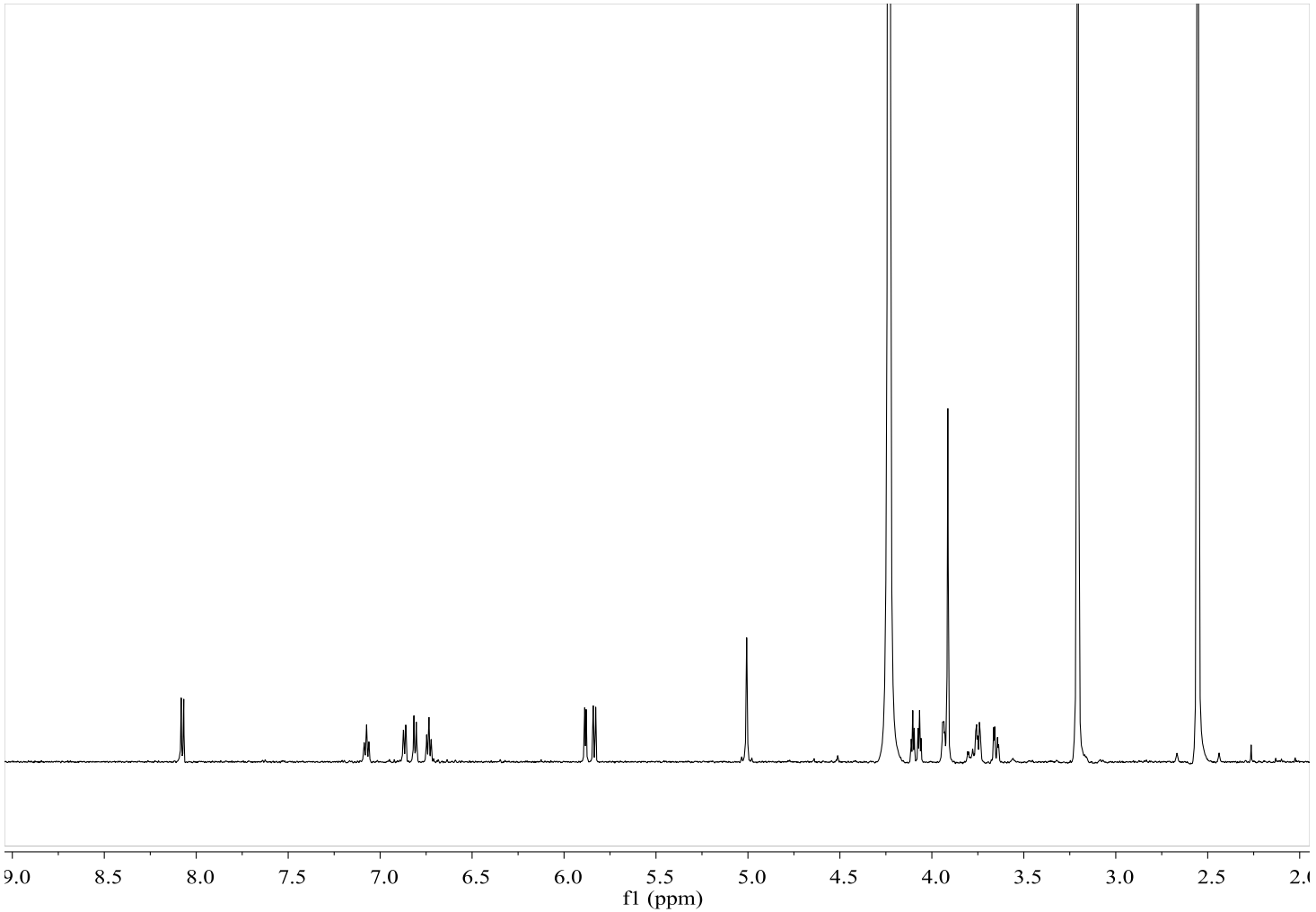

Figure S24. ^{1}H NMR spectrum of compound **15** in DMSO-d_6:MeOH-d_4 (1:1)

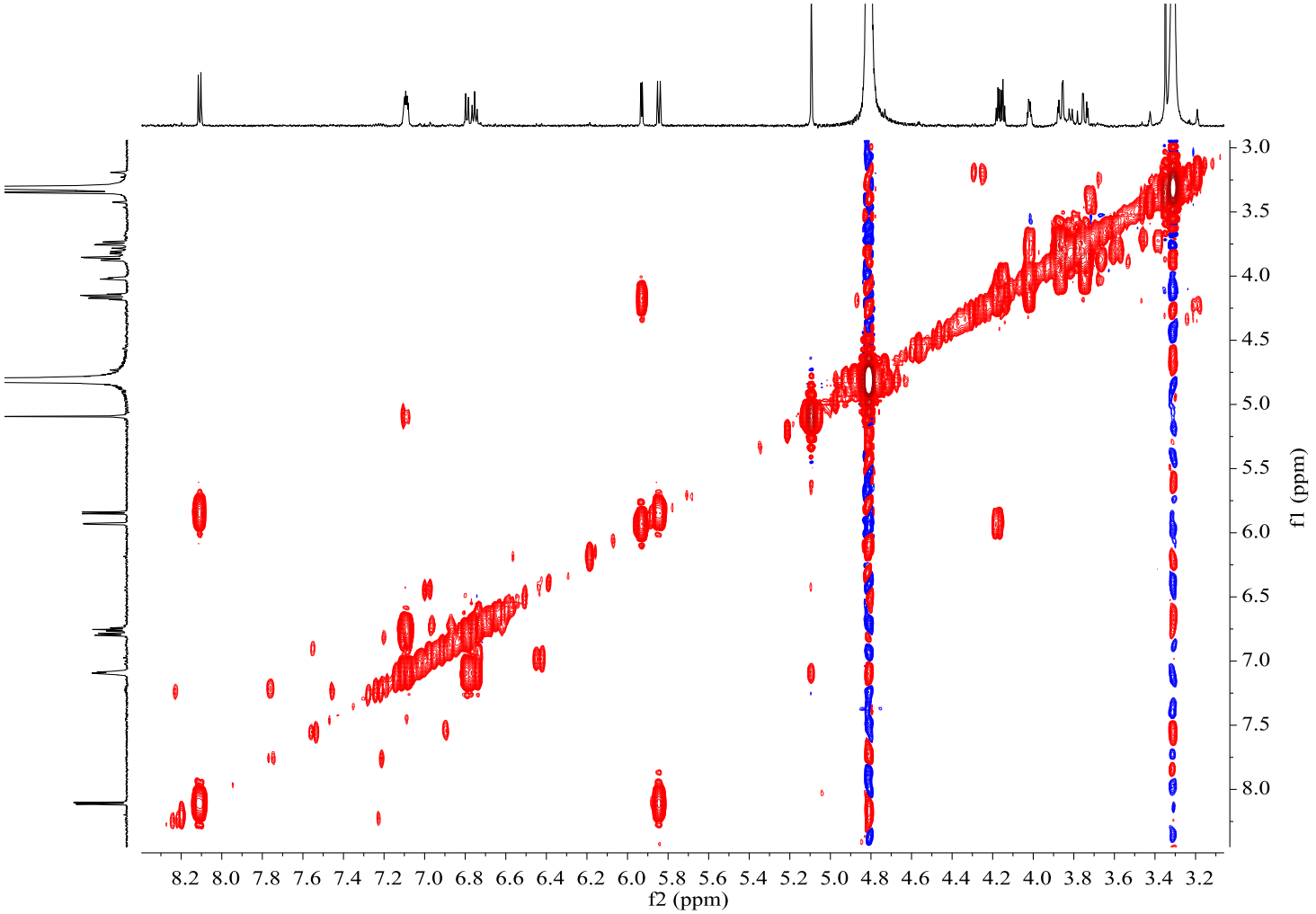

Figure S25. COSY spectrum of compound **15** in MeOH-d_4

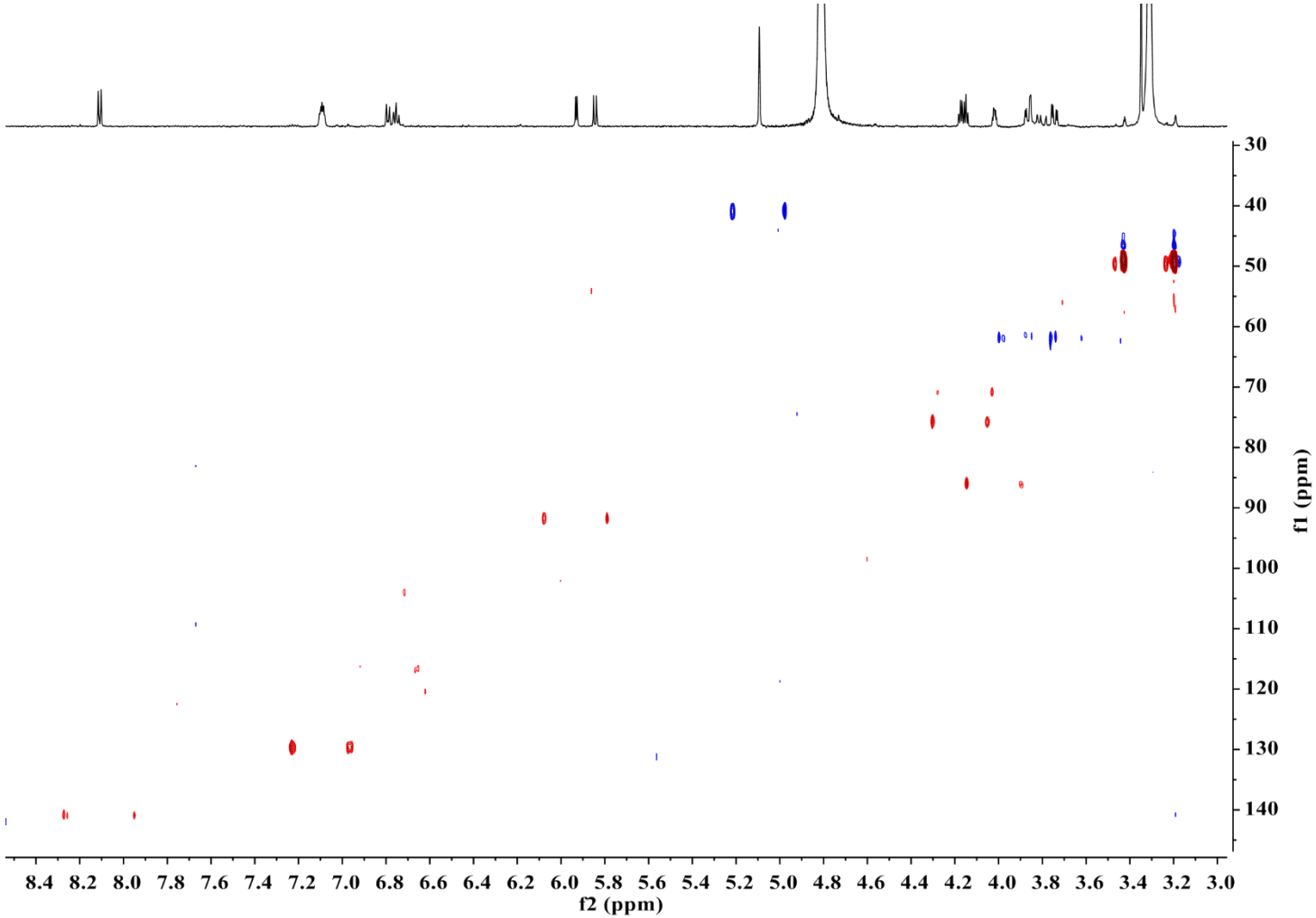

Figure S26. HSQC spectrum of compound **15** in MeOH-d_4

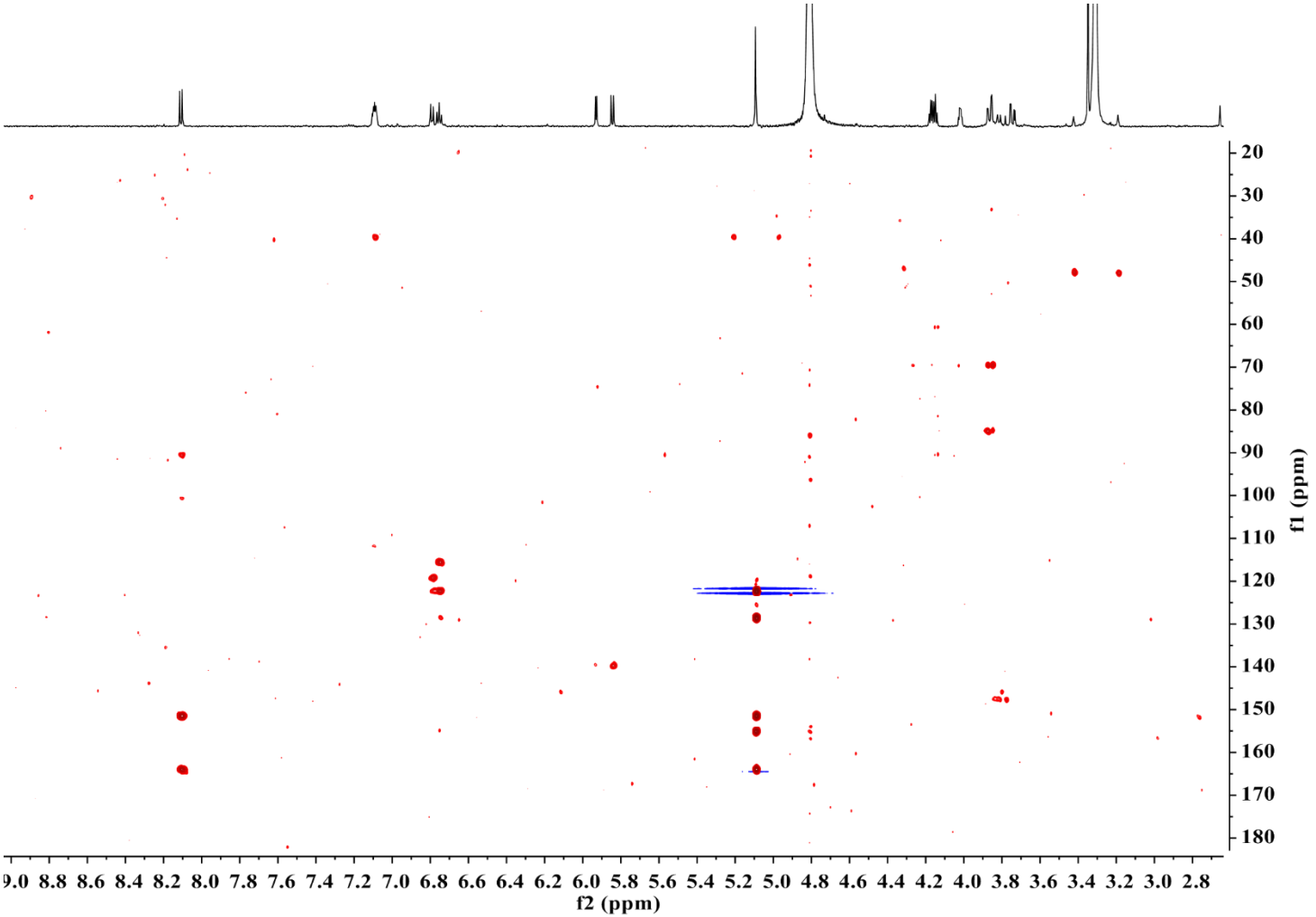

Figure S27. HMBC spectrum of compound **15** in MeOH-d_4

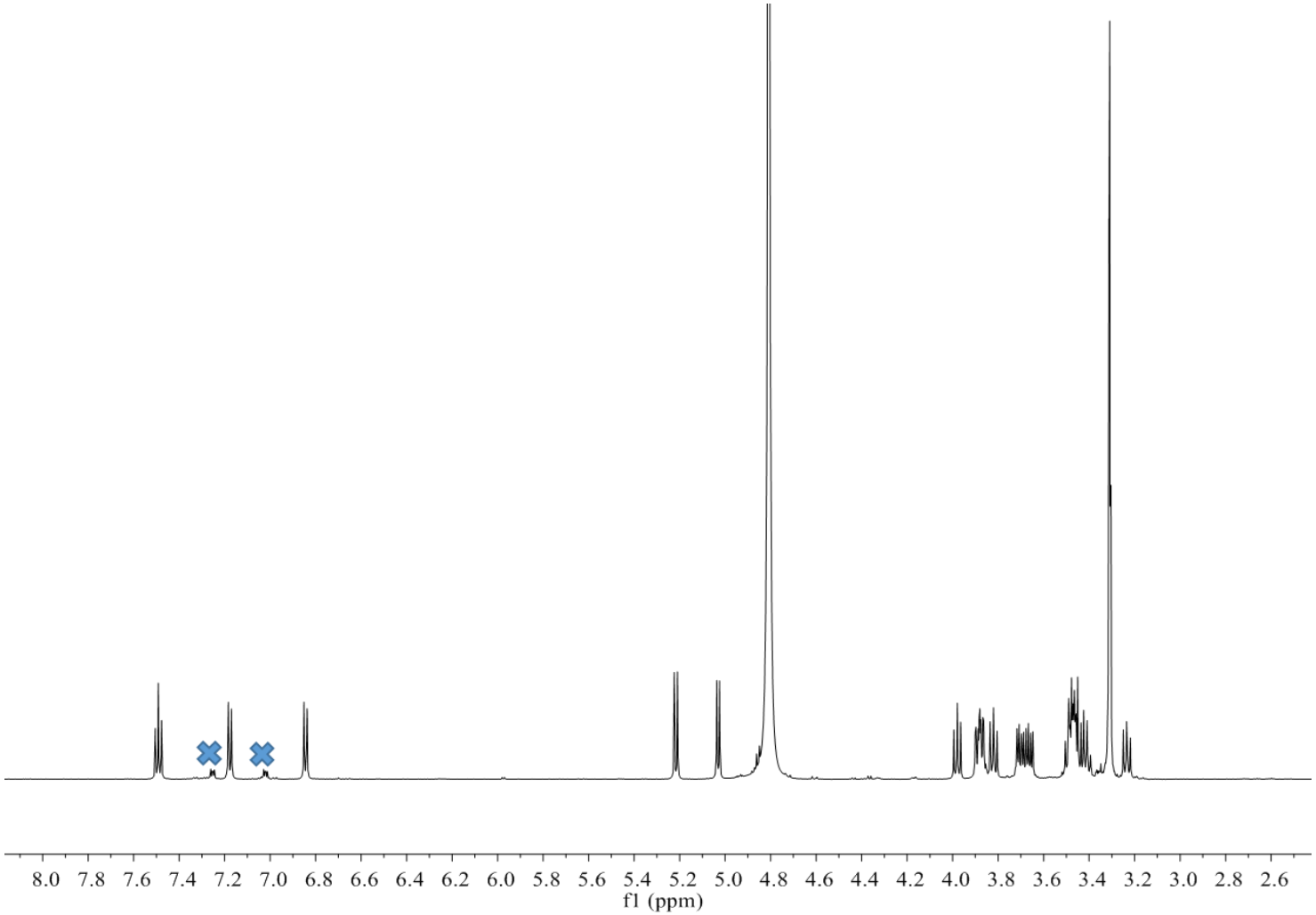

Figure S28. ^{1}H NMR spectrum of compound **19** in MeOH-d_4 (✖:The sample was contaminated with plasticizer)

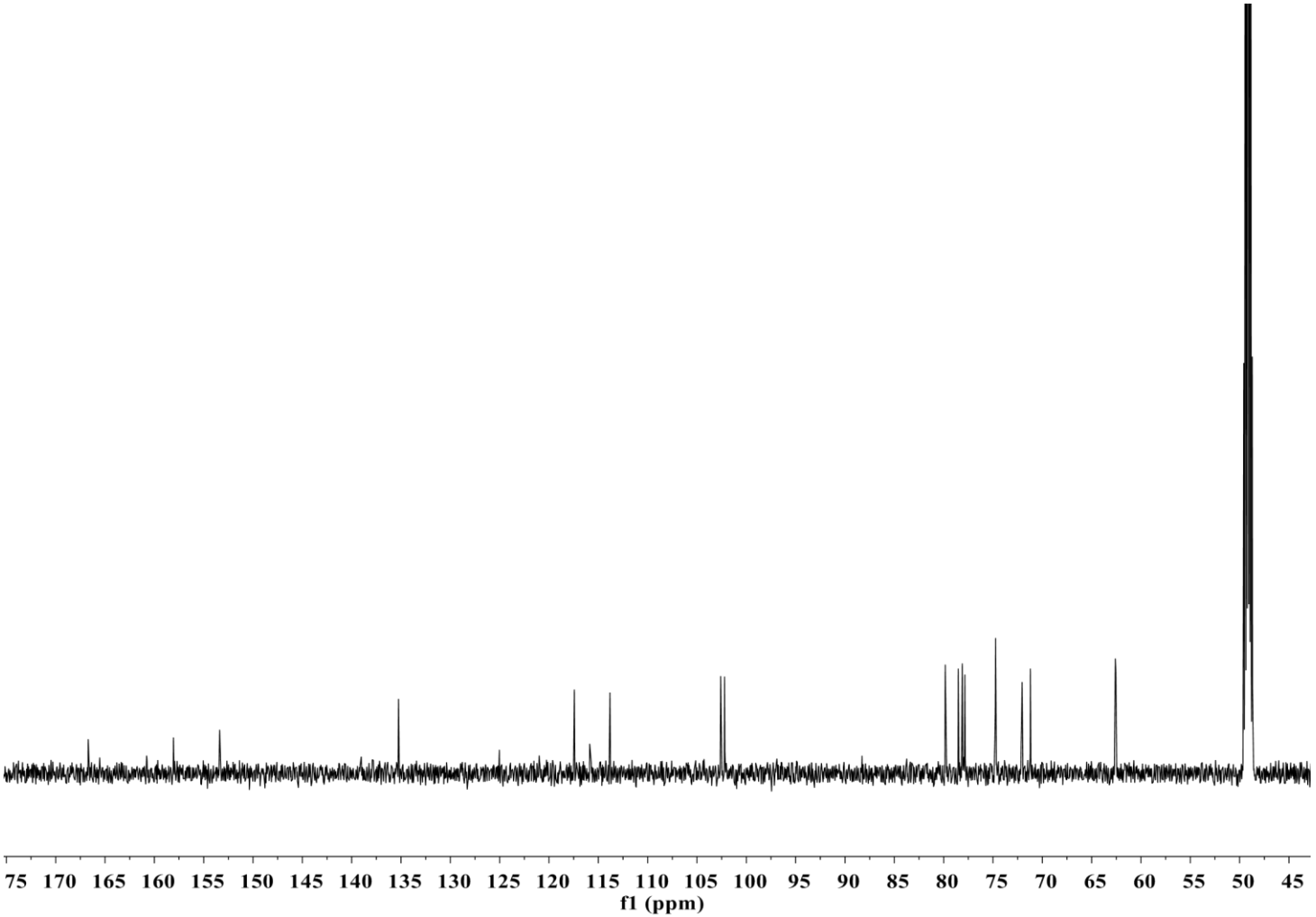

Figure S29. ^{13}C NMR spectrum of compound **19** in MeOH-d_4

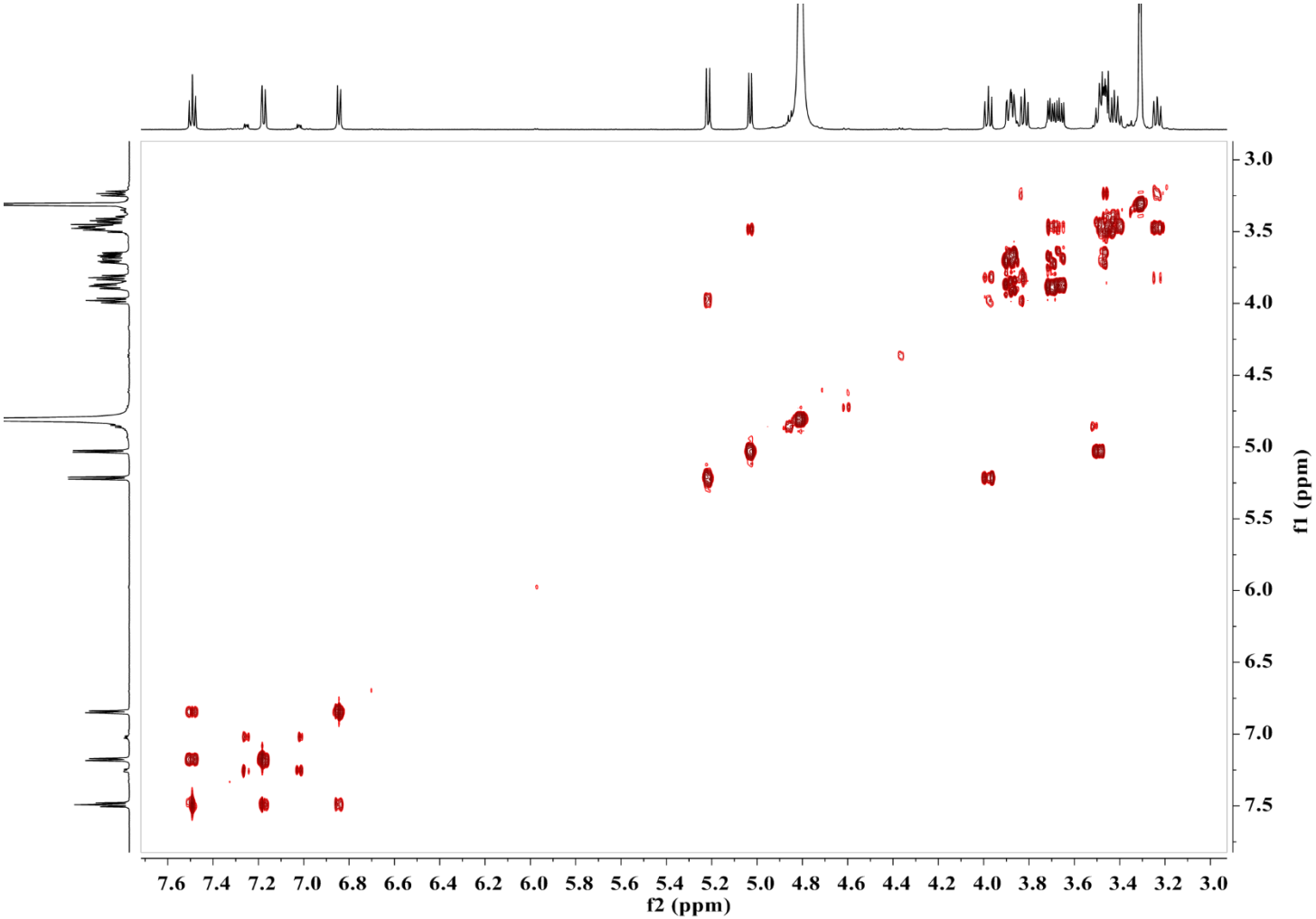

Figure S30. COSY spectrum of compound **19** in MeOH-d_4

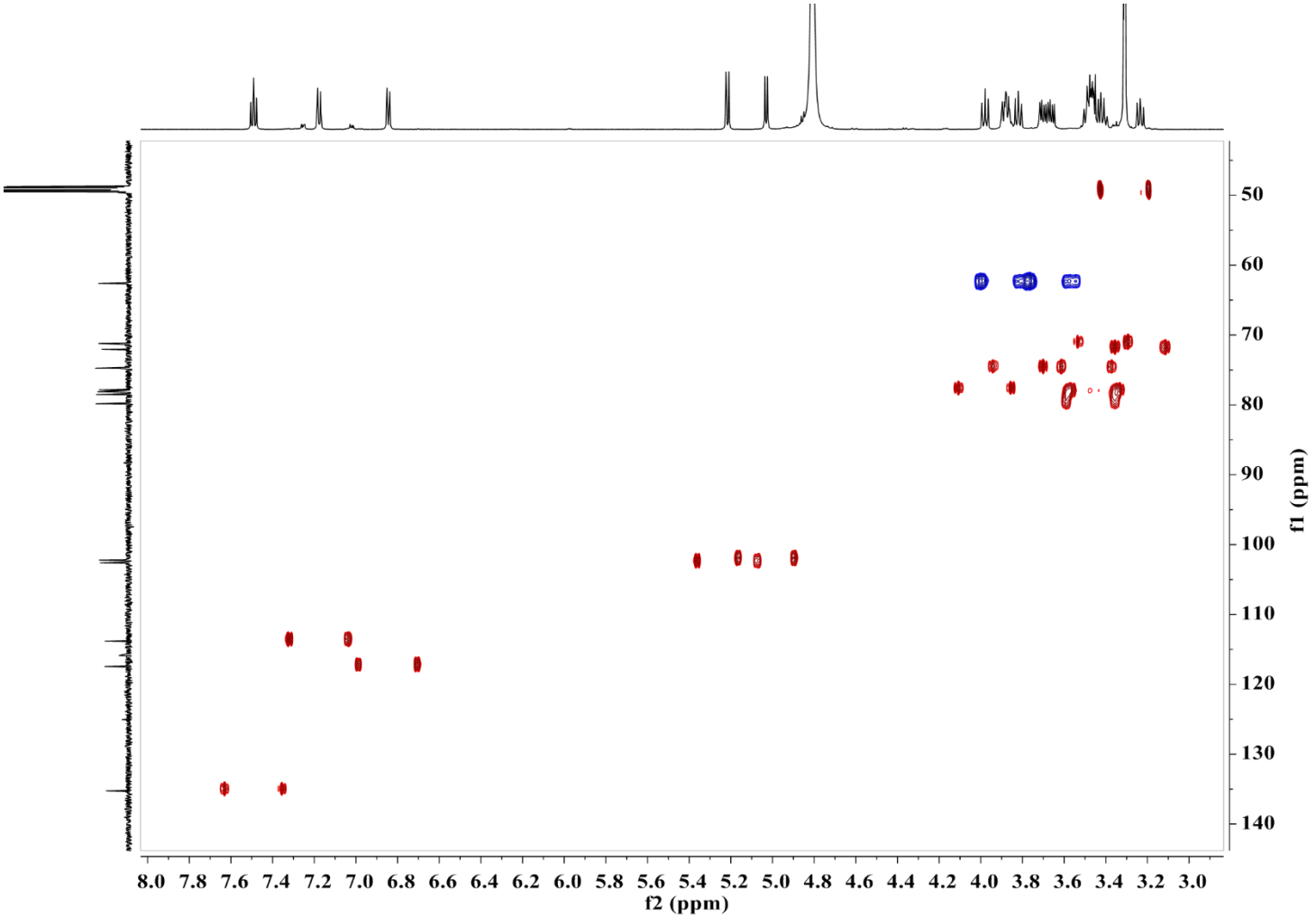

Figure S31. HSQC spectrum of compound **19** in MeOH-d_4

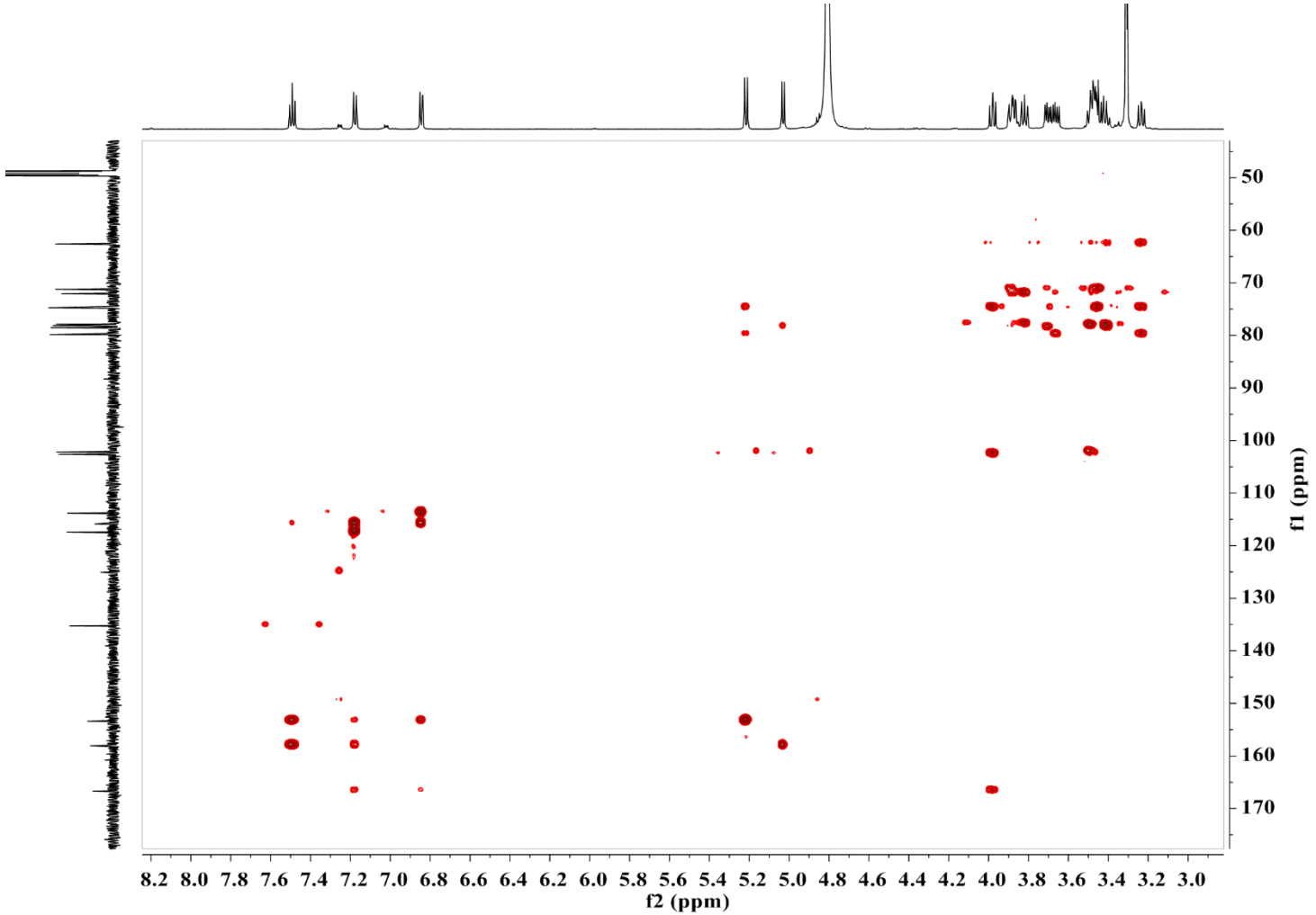

Figure S32. HMBC spectrum of compound **19** in MeOH-d_4

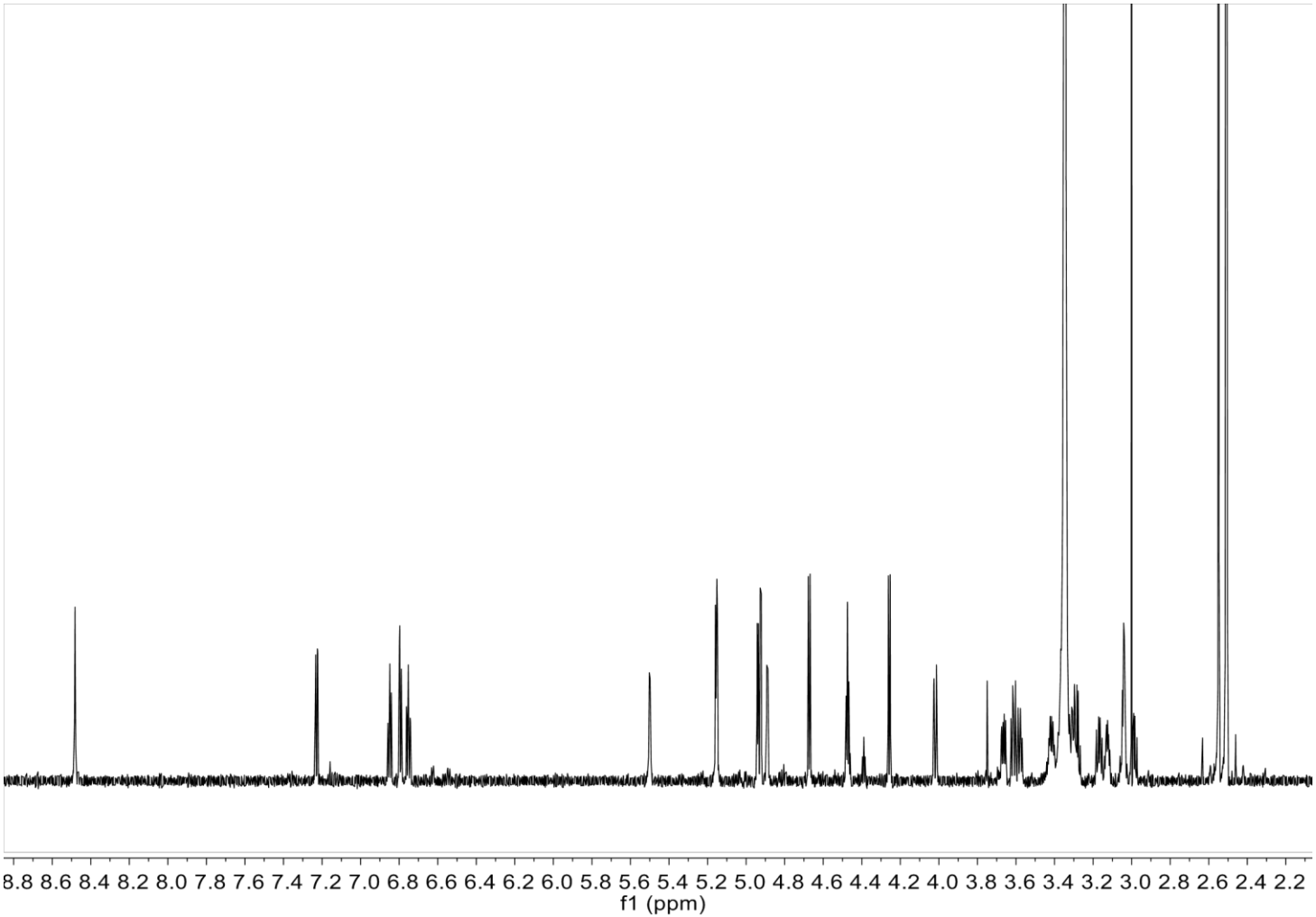

Figure S33. ^{1}H NMR spectrum of compound **22** in DMSO-d_6

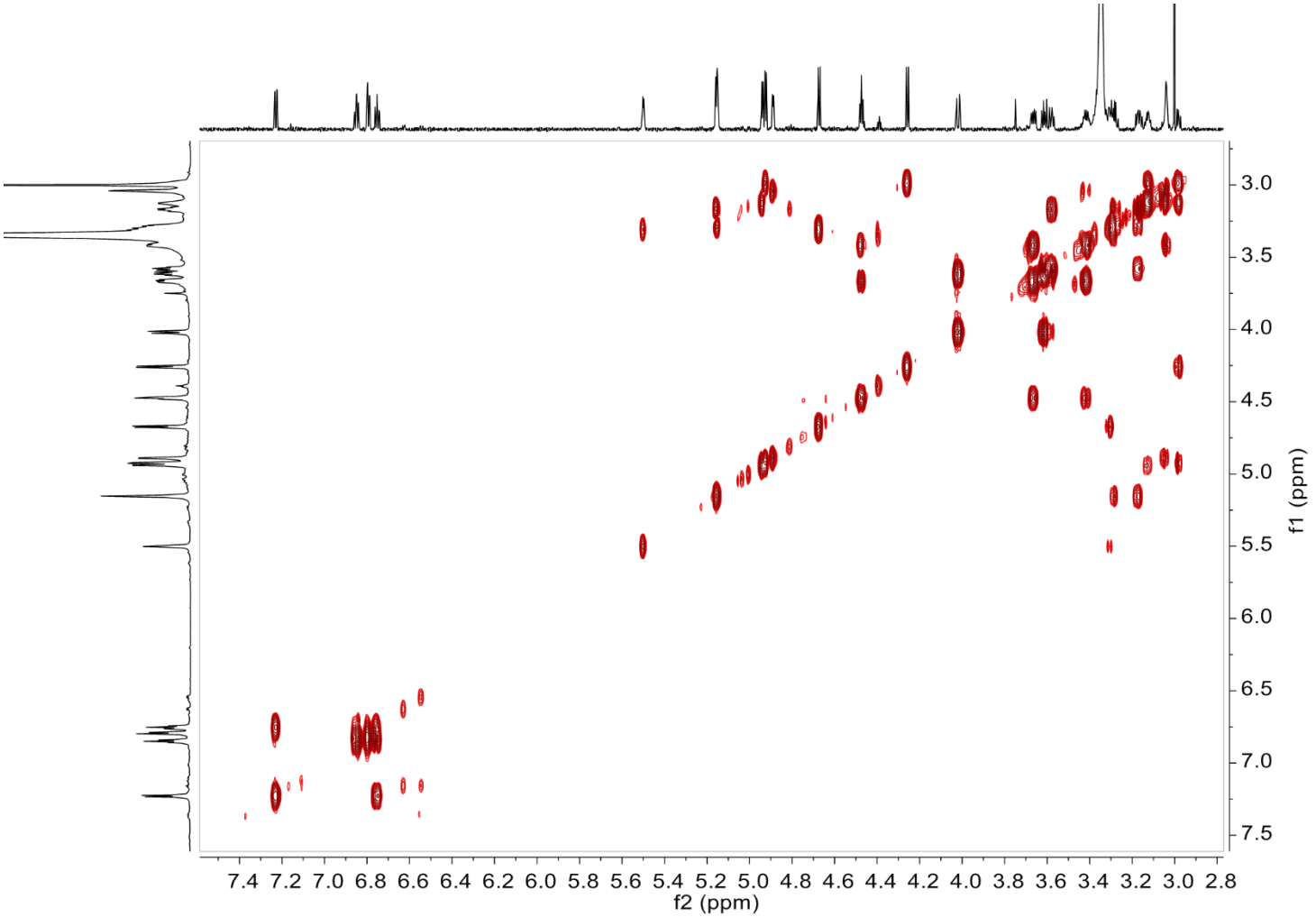

Figure S34. COSY spectrum of compound **22** in DMSO-d_6

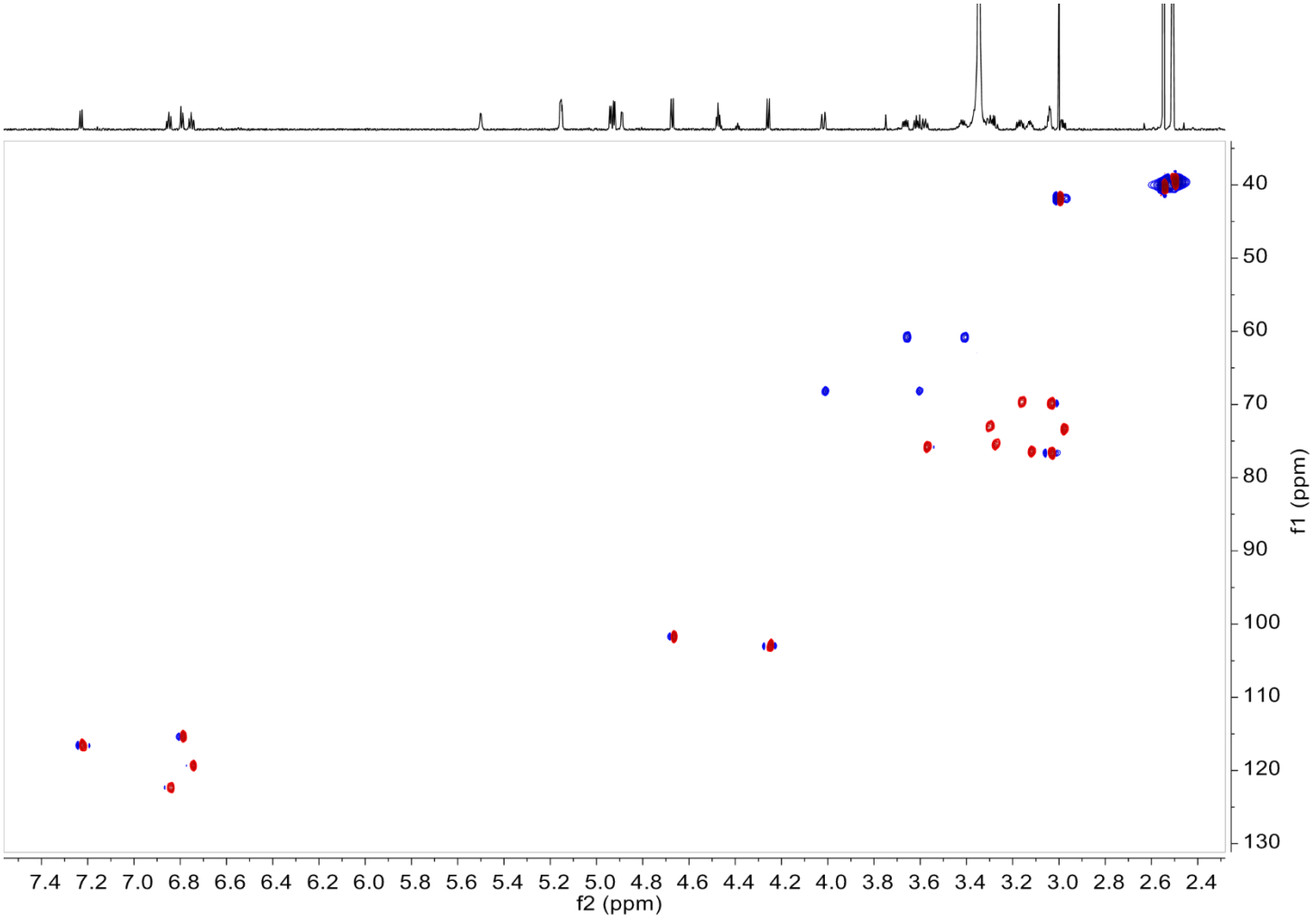

Figure S35. HSQC spectrum of compound **22** in DMSO-d_6

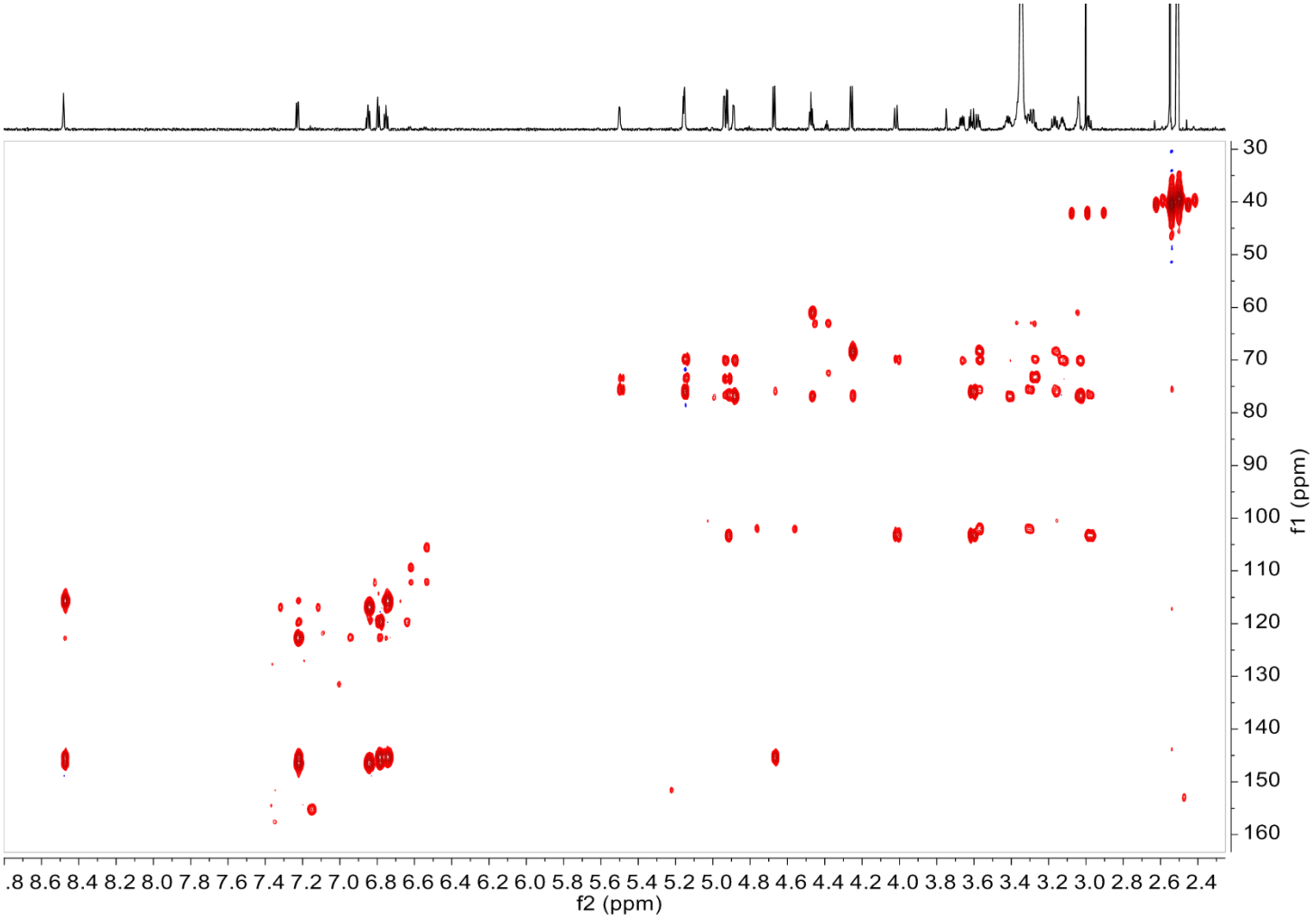

Figure S36. HMBC spectrum of compound **22** in DMSO-d_6

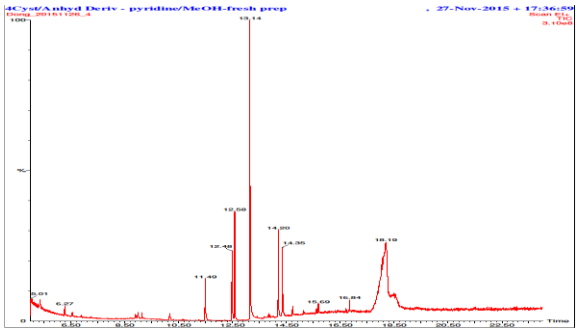

D-glucose

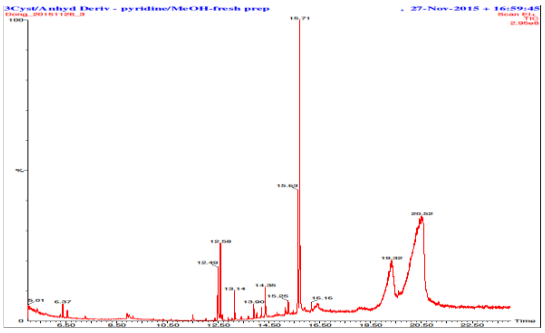

L-glucose

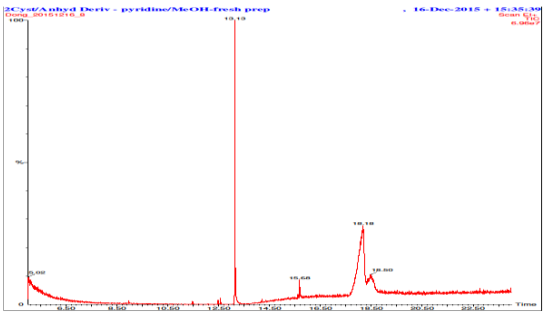

Sugar from hydrolysis of **1**

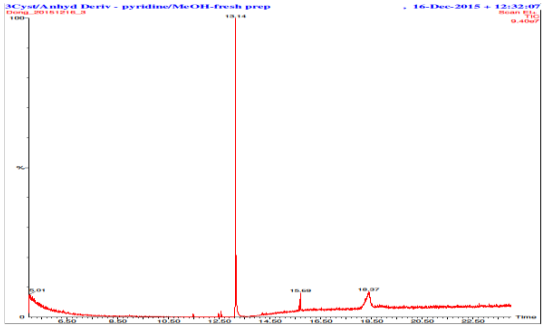

Sugar from hydrolysis of **2**

Sugar from hydrolysis of **3**

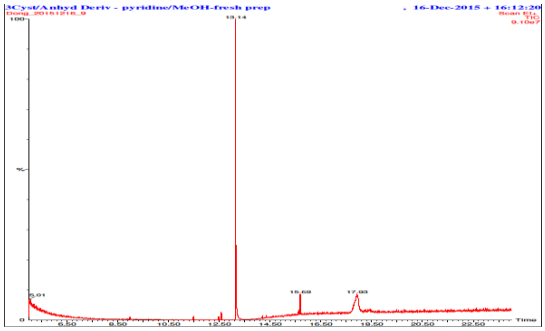

Sugar from hydrolysis of **4**

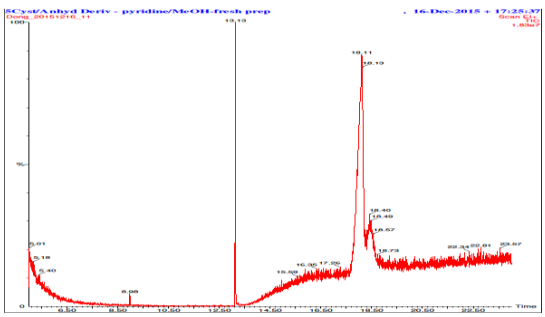

Sugar from hydrolysis of **19**

Sugar from hydrolysis of **22**

Figure S37. GC-MS analysis of acetylated thiazolidine derivatives

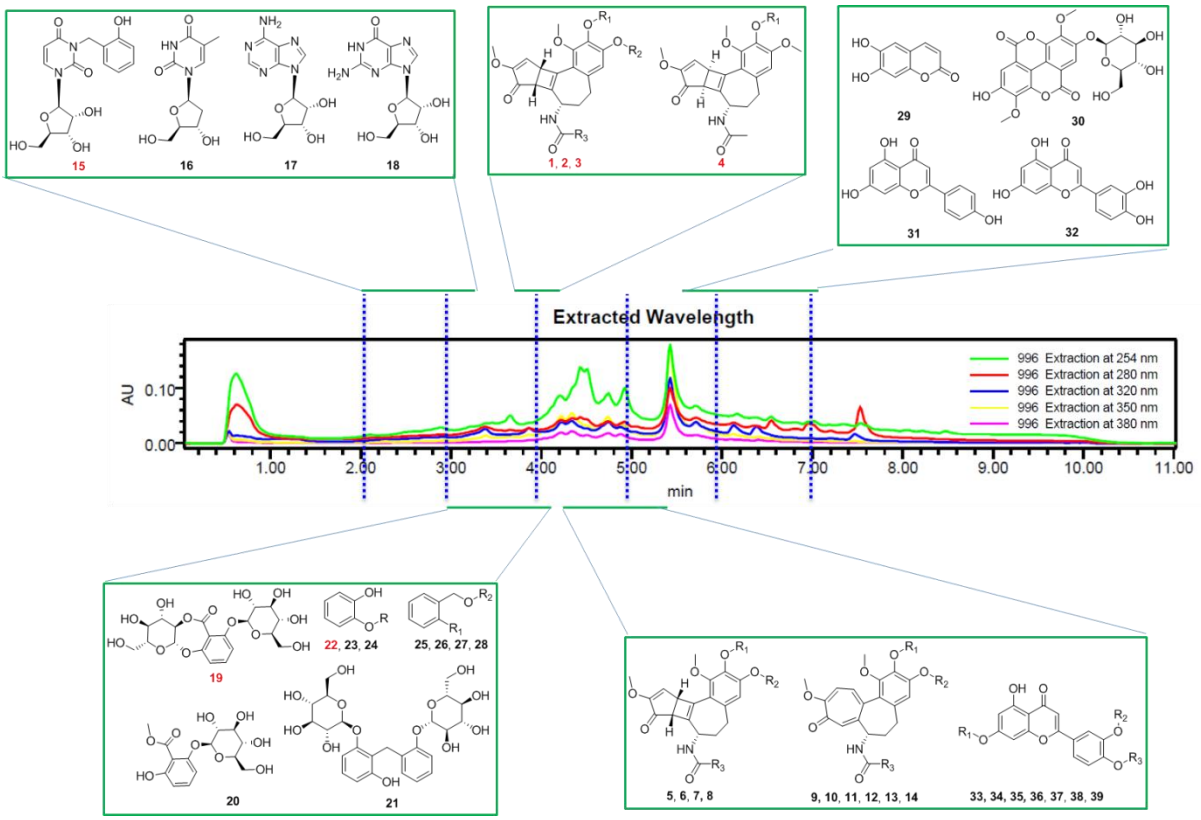

Figure S38. HPLC chromatogram of lead-like enhanced extract of the Australian plant *Gloriosa superba* L. and compounds isolated from different lead-like enhanced fractions

Table S1. The drug- and lead-like physicochemical properties

The drug- and lead-like physicochemical properties of these 39 natural products were calculated using Instant JChem (version 15.10.26.0). The parameters including molecular weight (MW), log *P*, number of hydrogen bond acceptors (HBA), and number of hydrogen bond donors (HBD) were analyzed against Lipinski's rule-of-five (Table **S1** and Figure **S39**).

Table **S1**. Physicochemical Profiling of Isolated Natural Products **1**-**39** from *Gloriosa superba* L.

Compound	Physicochemical parameters[a]				
	MW	log *P*	HBA	HBD	No. of Violations
1	547.56	-1.51	11	5	2
2	533.53	-1.56	11	5	2
3	533.53	-1.66	11	6	3
4	547.56	-1.51	11	5	2
5	385.42	0.76	6	2	0
6	371.39	0.71	6	2	0
7	385.42	0.85	6	1	0
8	399.44	0.90	6	1	0
9	399.44	1.46	6	1	0
10	385.42	1.32	6	2	0
11	385.42	1.32	6	2	0
12	385.42	1.41	6	1	0
13	371.39	1.27	6	2	0
14	383.40	1.40	6	1	0
15	460.39	-2.85	12	7	2
16	242.23	-1.12	5	3	0
17	267.25	-2.09	8	4	0
18	283.24	-2.71	8	5	0
19	350.33	-0.77	7	4	0
20	330.29	-0.25	8	5	0
21	554.55	-2.24	13	10	3
22	434.39	-2.67	12	8	2
23	434.39	-2.67	12	8	2
24	272.25	-0.90	7	5	0
25	286.28	-1.37	7	5	0
26	286.28	-0.87	7	5	0
27	448.42	-3.14	12	8	2
28	432.42	-2.34	11	7	2

29	178.14	1.18	3	2	0
30	492.39	-0.96	11	5	1
31	286.24	2.40	6	4	0
32	270.24	2.71	5	3	0
33	610.52	-2.13	16	10	3
34	610.52	-2.13	16	10	3
35	594.52	-0.59	15	9	3
36	608.55	-0.44	15	8	3
37	448.38	0.14	11	7	2
38	462.41	0.28	11	6	2
39	448.38	0.14	11	7	2

[a] All physicochemical properties, including molecular weight (MW), log *P*, hydrogen bond acceptors (HBA) and hydrogen bond donors (HBD), were calculated using Instant JChem (version 15.10.26.0).

The results (Table **S1** and Figure **S37**) suggested that the majority of isolated natural products obeyed Lipinski's rule-of-five in terms of log *P* < 5 (100%), MW < 500 Da (76.9%), HBA < 10 (53.8%) and HBD < 5 (64.1%).

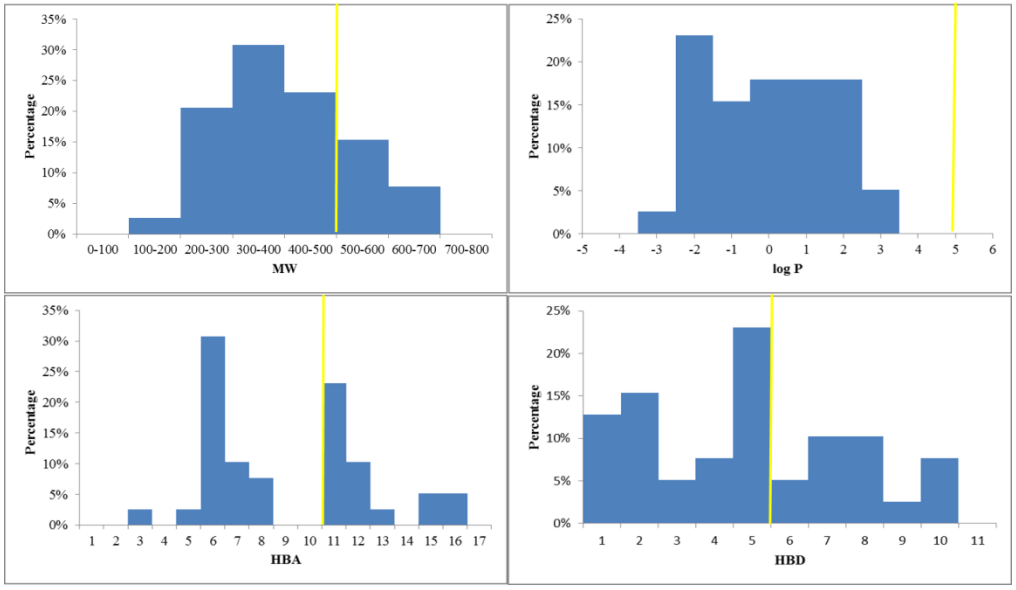

Figure S39. Physicochemical property histograms (MW, log *P*, HBD, and HBA) for compounds isolated from *Gloriosa superba* L. In each case the orange line indicates the maximum desirable value for oral bioavailability defined by Lipinski's rule-of-five: MW < 500 Da; log *P* < 5, HBA < 10 and HBD < 5.

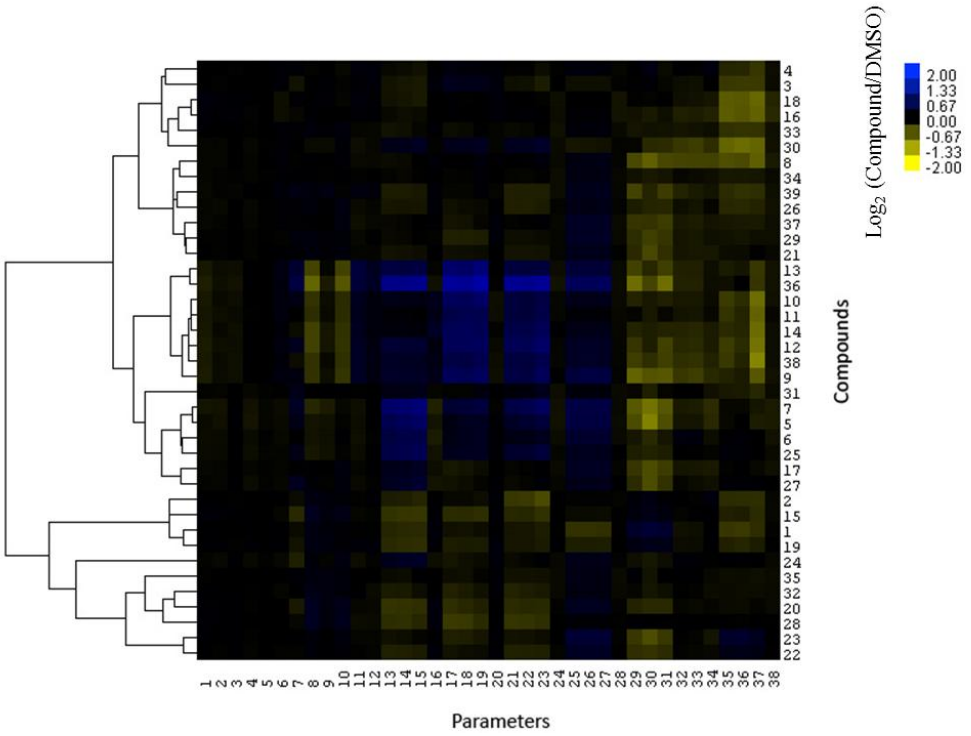

Figure S40. Heatmap depicting the cytological profile of metabolites from *Gloriosa superba* L. at 10 µM on 38 parameters based on the log_2 ratio of compound and vehicle (DMSO). The effects of compounds were plotted as log_2 ratio to the DMSO control. Yellow shows a decrease versus vehicle and blue shows an increase versus vehicle. Individual compounds are presented on the y-axis with individual features on the x-axis. 1. Nucleus area (µm²) 2. Nucleus morphology Width (µm) 3. Nucleus morphology Length (µm) 4. Nucleus morphology Ratio Width to Length 5. Nucleus morphology Roundness 6. Nucleus marker texture index 7. Nucleus marker intensity 8. Cell area (µm²) 9. Cell Width (µm) 10. Cell Length (µm) 11. Cell Ratio Width to Length 12. Cell Roundness 13. *α*-Tubulin marker intensity in the cytoplasm 14. *α*-Tubulin marker intensity in outer region of cytoplasm 15. *α*-Tubulin marker intensity in inner region of cytoplasm 16. *α*-Tubulin marker texture index 17. Mitochondria marker intensity in the cytoplasm 18. Mitochondria marker intensity in outer region of cytoplasm 19. Mitochondria marker intensity in inner region of the cytoplasm 20. Mitochondria marker texture index 21. LC3b marker intensity in the cytoplasm 22. LC3b marker intensity in the outer region of the cytoplasm 23. LC3b marker intensity in inner region of cytoplasm 24. LC3b marker texture index 25. Lysosome Marker Intensity Mean 26. Lysosome Marker Intensity Outer Region Mean 27 Lysosome Marker Intensity Inner Region Mean 28. Lysosomes Marker Texture index. 29. Number of EEA1 Marker Spots in cytoplasm 30. Number of EEA1 Marker Spots in inner region of cytoplasm 31. Number of EEA1 Marker Spots in Outer Region of cytoplasm 32. Number of EEA1 Marker Spots per Area of cytoplasm 33. EEA1 Marker Intensity in outer region of cytoplasm 34 EEA1 Marker Intensity in inner region of cytoplasm 35. EEA1 Marker Intensity in the cytoplasm 36. Number of EEA1 Marker Spots per Area of Outer Region 37 Number of EEA1 Marker Spots per Area of inner region of cytoplasm 38. EEA1 Marker Texture Index

Chapter Four. A Grand Challenge (Ⅲ): Unbiased Phenotypic Function of Metabolites from *Alangium villosum* against Parkinson's Disease

Dongdong Wang,[†] Yunjiang Feng,[†] Mariyam Murtaza,[†] Stephen A. Wood,[†] George D. Mellick,[†] Paul I. Forster[‡] and Ronald J. Quinn[†,*]

[†] Eskitis Institute for Drug Discovery, Griffith University, Brisbane, QLD 4111, Australia

[‡] Queensland Herbarium, Brisbane Botanic Gardens, Brisbane, QLD 4066, Australia

ABSTRACT

As part of a continuing research program aiming to identify chemical probes to interrogate Parkinson's disease (PD), an Australian plant *Alangium villosum* subsp. *tomentosum* (F. Muell.) Bloemb was chemically and biologically investigated. Chemical investigation resulted in the isolation of four new benzoquinolizidine *N*-oxides, namely, tubulosine N_{β}^{5}-oxide (**1**), isotubulosine N_{α}^{5}-oxide (**2**), 9-demethyltubulosine N_{β}^{5}-oxide (**3**) and 9-demethylisotubulosine N_{α}^{5}-oxide (**4**), four new benzoquinolizidine alkaloids, namely, 1',2'-dehydro-9-demethyltubulosine (**10**), 7',9-*O*-didemethylcephaeline (**13**), 7',9-*O*-didemethylisocephaeline (**14**) and 7',9-didemethylpsychotrine (**15**), together with the previously reported natural products, seven benzoquinolizidine alkaloids (**5**-**9**, **11** and **12**), eight tetrahydroisoquinoline monoterpene glycosides (**16**-**23**), six lignan glycosides (**24**-**29**), one iridoid glycoside (**30**), one secoiridoid glycoside (**31**), one monoterpene alkaloid (**32**), two sesquiterpenoids (**33** and **34**), one sesquiterpenoid naphthol (**35**) and its glycoside (**36**) and eight triterpenoids (**37**-**44**). Compounds **1**-**15** and **20**-**23** were purified as their trifluoroacetate salt. The chemical structures of the eight new compounds (**1**-**4**, **10** and **13**-**15**) were characterized by extensive analyses of NMR and mass spectroscopic data. The absolute configurations of the new compounds were determined by CD measurements. The phenotypic profiles of all metabolites were produced by an unbiased assay using a human olfactory neurosphere-derived (hONS) cell model of PD. Tubulosine and its congeners **1**-**11**, displayed phenotypic profiles with major effects on α-tubulin and EEA-1-related cytological markers in the PD patient derived hONS cells.

INTRODUCTION

As part of a research program aiming to identify chemical probes to interrogate Parkinson's disease using an unbiased phenotypic assay,[1] an Australian plant *Alangium villosum* subsp. *tomentosum* (F.Muell.) Bloemb. was selected from Nature Bank for chemical and biological investigation.[2-4] The cytological profiles of the 44 isolated natural products were examined using the human olfactory neurosphere-derived (hONS) cells from a Parkinson's disease patient.[5]

Plants belonging to the genus *Alangium* (family: Cornaceae) have around 40 species,[6] all of which are shrubs or small trees except *Alangium kwangsiense*. Most of the species are native to tropical and subtropical regions of east and southeast Asia.[7] The species *Alangium chinense* is considered one of the fifty commonly used herbs in traditional Chinese medicine. The root bark of *Alangium lamarckii* was extensively used in folk medicine as an anthelmintic, purgative, emetic, and febrifuge agent, as well as in the treatment of leprosy and other skin diseases.[8] The species *Alangium villosum* can be found in Southeast Asia, Australia and the western Pacific Islands. *Alangium villosum* subsp. *tomentosum* (F. Muell.) Bloemb. can grow 20 meters high and widely spread in Queensland, New South Wales and Malesia.[9]

The genus *Alangium* is the source of over 190 characterized natural products,[10] consisting of benzoquinolizidine and tetrahydroisoquinoline-monoterpene skeleton alkaloids, terpenoids and simple aromatic structural classes. They have been reported with diverse biological activities including antioxidant,[11,12] antimicrobial,[13] antifertility,[14] antiarthritic,[15] antidiabetic,[16,17] antibacterial,[18,19] anticancer,[20] antifungal,[21] DNA

damaging[22,23] and dihydrofolate reductase inhibitory activity.[24] The extract of *Alangium villosum* roots was reported to have anti-inflammatory activity.[25] Tetrahydroisoquinoline type alkaloids, such as alangiside, emetine, tubulosine and deacetylisoipecoside, have been frequently isolated from the genus *Alangium*, with well-established biosynthetic pathway.[8,26-28]

Chemical investigations of the Australian plant *A. villusom* subsp. *tomentosum* (F. Muell.) Bloemb resulted in the isolation of four new benzoquinolizidine *N*-oxides, namely, tubulosine N_{β}^{5}-oxide (**1**), isotubulosine N_{α}^{5}-oxide (**2**), 9-demethyltubulosine N_{β}^{5}-oxide (**3**) and 9-demethylisotubulosine N_{α}^{5}-oxide (**4**), four new benzoquinolizidine alkaloids, namely, 1',2'-dehydro-9-demethyltubulosine (**10**), 7',9-*O*-didemethylcephaeline (**13**), 7',9-*O*-didemethylisocephaeline (**14**) and 7',9-didemethylpsychotrine (**15**), together with 36 known natural products including tubulosine (**5**),[29,30] isotubulosine (**6**),[31,32] 9-demethyltubulosine (**7**),[33] 9-demethylisotubulosine (**8**),[32,34] deoxytubulosine (**9**),[35,36] 1',2'-didehydrotubulosine (**11**),[37] 9-demethylprotoemetinol (**12**),[38,39] demethyalangiside (**16**),[8,27] alangiside (**17**),[27,40] 3-*O*-demethyl-2-*O*-methylalangiside (**18**),[41] 2'-sinapoyldemethylalangiside (**19**),[42] 6-*O*-methyl-*N*-deacetylisoipecosidic acid (**20**),[43] 7-*O*-methyl-*N*-deacetylisoipecosidic acid (**21**),[43] *N*-deacetylisoipecoside (**22**),[28] 6-*O*-methyl-*N*-deacetylipecosidic acid (**23**),[44] (+)-isolarisiresinol 3α-*O*-β-D-glucopyranoside (**24**),[45] (−)-isolarisiresinol 3α-*O*-β-D-glucopyranoside (**25**),[46] (+)-5'-methoxyisolariciresinol 3α-*O*-β-D-glucopyranoside (**26**),[46] (-)-5'-methoxyisolariciresinol 3α-*O*-β-D-glucopyranoside (**27**),[46] (+)-lyoniresinol 3α-*O*-β-D-glucopyranoside (**28**),[47,48] (-)-lyoniresinol 3α-*O*-β-D-glucopyranoside (**29**),[46-48] loganic acid (**30**),[49] sweroside (**31**),[50] fragraeoside (**32**),[51] (1*S*)-lacinilene C (**33**),[52] (1ζ)-1-methoxylacinilene C (**34**),[53] 2,7-dihydroxycadalene (**35**),[54]

alangicadinoside C (**36**),[55] 27-*O*-trans-caffeoylcylicodiscic acid (**37**),[56] messagenic acid B (**38**),[57] cylicodiscic acid (**39**),[58] betulinic acid (**40**),[59] botulin (**41**),[59,60] 3-hydroxy-30-nor-20-oxo-28-lupanoic acid (**42**),[60,61] betulonic acid (**43**)[62,63] and betulone (**44**).[64] Because trifluoroacetic acid (TFA) was used in mobile phase in HPLC purification, compounds **1**-**15** and **20**-**23** were purified as their trifluoroacetate salt. The chemical structures of the compounds were elucidated using a series of spectrometric and spectroscopic techniques.

On the basis of previous work, we developed a theoretical framework that explains that all natural products interact with biologically relevant space.[65,66] All of the 44 isolated compounds were subjected to an unbiased phenotypic assay on hONS cells followed by analysis of cytological effects. Herein, we report the isolation and structure elucidation of the eight new compounds (**1**-**4**, **10** and **13**-**15**) as well as the cytological profiles of all of the isolated natural products from *A. villusom* subsp. *tomentosum* (F. Muell.) Bloemb using the human olfactory neurosphere-derived (hONS) cells from a Parkinson's disease patient, which models functional aspects of Parkinson's disease.

RESULTS AND DISCUSSION

The air-dried and ground plant of *A. villusom* subsp. *tomentosum* (F. Muell.) Bloemb. (20 g) was sequentially extracted with *n*-hexane, CH_2Cl_2 and MeOH. The CH_2Cl_2/MeOH extracts were combined and fractionated using a C_{18} bonded silica flash column. Subsequently four fractions were collected by eluting with stepwise MeOH/H_2O gradients (10% MeOH/90% H_2O, 50% MeOH/50% H_2O, 90% MeOH/10% H_2O and MeOH, respectively; each containing 0.1% TFA).

Previous chemical investigations on the genus *Alangium* and its related genera have revealed that they are a particularly rich source of benzoquinolizidine alkaloids.[40,67,68] The ^{1}H NMR spectrum in DMSO-d_6 of the 50% MeOH/50% H_2O fraction displayed numbers of methoxyl singlets between δ_H 3.50 and 3.80, ethyl groups at δ_H 0.85-0.93, 1.82-1.64 and 1.35-1.20, and aromatic signals between δ_H 6.70 and 7.20, together with exchangeable aminic protons between δ_H 8.50 and 11.20, indicating the presence of tubulosine and emetine alkaloids. HPLC purification of the fraction by C_{18} bonded silica HPLC (gradient MeOH/H_2O with 0.1% TFA) yielded four new benzoquinolizidine *N*-oxides, namely, tubulosine N_β^5-oxide (**1**), isotubulosine N_α^5-oxide (**2**), 9-demethyltubulosine N_β^5-oxide (**3**) and 9-demethylisotubulosine N_α^5-oxide (**4**), four new benzoquinolizidine alkaloids, namely, 1',2'-dehydro-9-demethyltubulosine (**10**), 7',9-*O*-didemethylcephaeline (**13**), 7',9-*O*-didemethylisocephaeline (**14**) and 7',9-didemethylpsychotrine (**15**), along with tubulosine and its analogues (**5**-**9**, **11** and **12**).

The ^{1}H NMR spectrum of the 90% MeOH/10% H_2O fraction contained some intriguing signals indicative of tetrahydroisoquinoline monoterpene, lignan and iridoid glycosidic type molecules. Further purification of the fraction led to the isolation of 17 known metabolites (**16**-**32**). Further purification of the MeOH fraction resulted in the isolation of 12 known metabolites (**33**-**44**). Compounds **1**-**15** and **20**-**23** were purified as their trifluoroacetate salt. In total, forty-four structurally diverse secondary metabolites were isolated from the prolific Australian plant *A. villusom* subsp. *tomentosum* (F. Muell.) Bloemb.

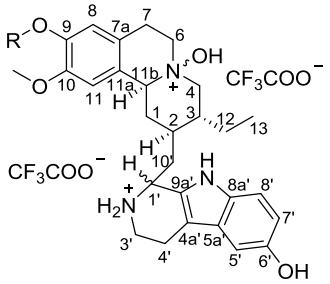

1 R=CH_3, N^5 β-OH, 1' β-H
2 R=CH_3, N^5 α-OH, 1' α-H
3 R=H, N^5 β-OH, 1' β-H
4 R=H, N^5 α-OH, 1' α-H

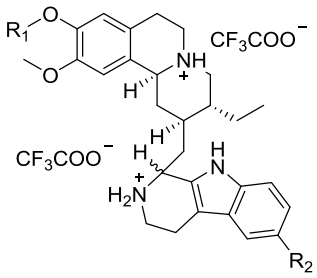

5 R_1=CH_3, R_2=OH, 1' β-H
6 R_1=CH_3, R_2=OH, 1' α-H
7 R_1=H, R_2=OH, 1' β-H
8 R_1=H, R_2=OH, 1' α-H
9 R_1=R_2=H, 1' β-H

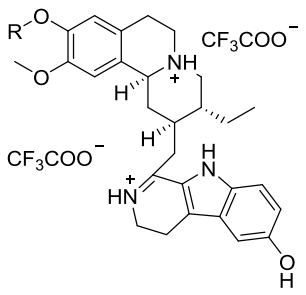

10 R=H
11 R=CH_3

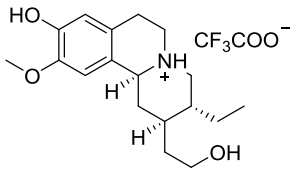

12

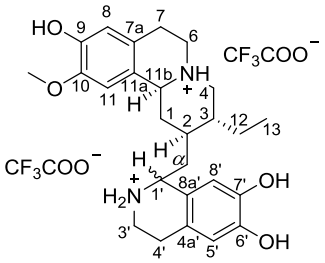

13 1' β-H
14 1' α-H

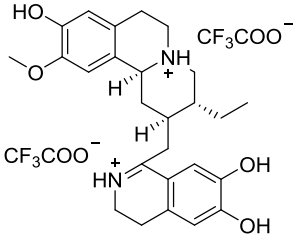

15

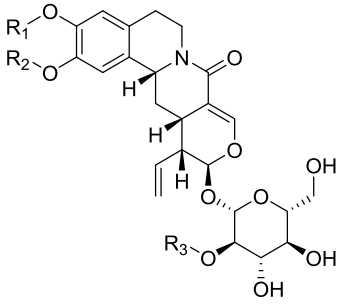

16 R_1=R_2=R_3=H
17 R_1=CH_3, R_2=R_3=H
18 R_1=R_3=H, R_2=CH_3
19 R_1=R_2=H, R_3=sinapinoyl

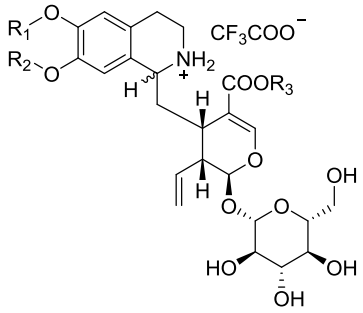

20 R_1=CH_3, R_2=R_3=H, 1 α-H
21 R_1=R_3=H, R_2=CH_3, 1 α-H
22 R_1=R_2=H, R_3=CH_3, 1 α-H
23 R_1=CH_3, R_2=R_3=H, 1 β-H

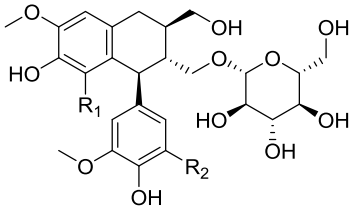

24 R_1=R_2=H, (+)
25 R_1=R_2=H, (-)
26 R_1=OCH_3, R_2=H, (+)
27 R_1=OCH_3, R_2=H, (-)
28 R_1=R_2=OCH_3, (+)
29 R_1=R_2=OCH_3, (-)

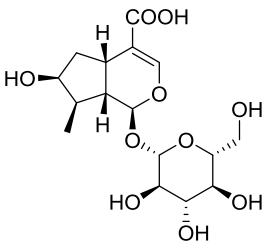

30

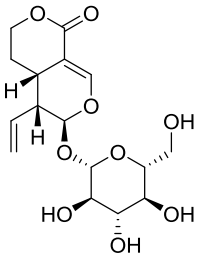

31

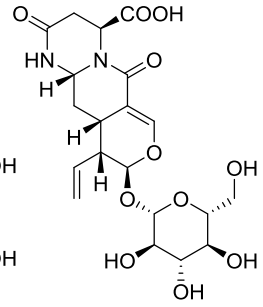

32

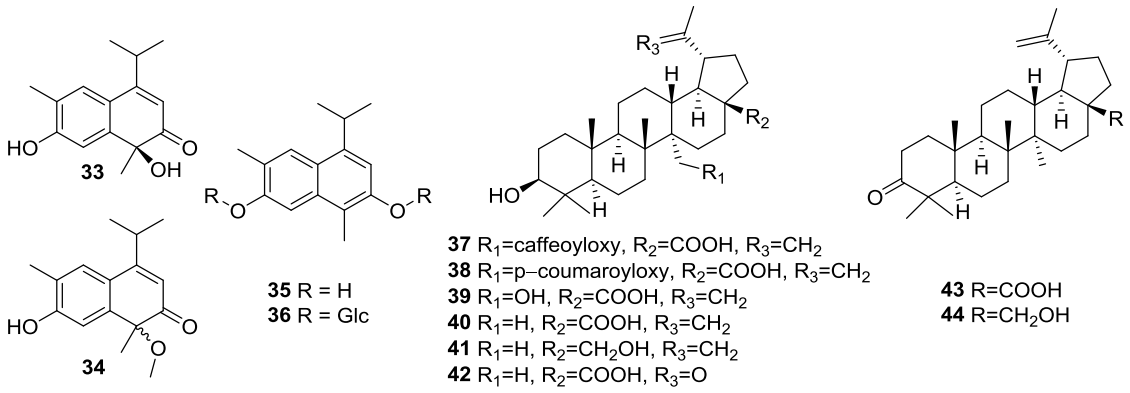

Tubulosine N_{β}^{5}-oxide (**1**), was isolated as an optically active odorless pale yellow powder with an $[\alpha]_D$ value at +11.0. The HRESIMS data gave an adduct $[M+H]^+$ ion at *m*/*z* 492.2856, which was consistent with a molecular formula of $C_{29}H_{37}N_3O_4$, and implied 13 degrees of unsaturation. It showed UV maxima at 205, 229, 258, 279, 314 and 370 nm, and IR bands at 3420, 2994, 1683, 1515, 1206, 1179 and 1033 cm^{-1}, indicative of benzoquinolizidine and tryptoline chromophores.[30,31,69] Its ^1H NMR spectrum, in combination with HSQC experimental data, suggested two aromatic singlets at δ_H 6.92 and 6.90, an AMX spin system for three aromatic protons at δ_H 7.15, 6.78 and 6.65, four methine signals (δ_H 5.13, 4.77, 1.97 and 1.92), eight methylene signals (δ_H 4.18/4.00, 3.92/3.72, 3.72/3.31, 3.31/3.05, 2.94/1.77, 2.93/2.90, 2.18/2.10 and 1.68/1.28), two singlets for methoxyl groups at δ_H 3.78 and 3.76, one methyl triplet at δ_H 0.90 (t, 7.5) and four exchangeable proton singlets (δ_H 12.64, 10.80, 9.67 and 9.03) (Table 1). The ^{13}C NMR data which was extracted from the HSQC and HMBC spectra contained fourteen aromatic carbons (δ_C 150.8, 147.7, 147.7, 130.2, 130.2, 126.2, 123.6, 121.8, 111.6, 111.4, 111.3, 109.7, 104.6 and 101.8), four sp^3 hybridized methines (δ_C 69.5, 49.1, 35.7 and 32.2), eight sp^3 hybridized methylenes (δ_C 67.3, 61.5, 41.1, 34.0, 27.7, 22.7, 21.0 and 17.6), two methoxyl carbons (δ_C 55.4 and 55.4) and a methyl carbon (δ_C 9.7) (Table 2). These spectral features were similar to those of tubulosine (**5**) TFA salt, except for the replacement of an

exchangeable signal at δ_H 10.25 by a sharp singlet at δ_H 12.64 (Table 1). There were also notable changes in chemical shifts of H-4, H-6 and H-11b in **1** at δ_H 3.92/3.72, 4.18/4.00 and 4.77 in comparison with those in **5** at δ_H 3.64/3.02, 3.68/3.47 and 4.23 ($\Delta\delta_{H\text{-}4}$ = 0.28 and 0.70 ppm, $\Delta\delta_{H\text{-}6}$ = 0.50 and 0.53 ppm, $\Delta\delta_{H\text{-}11b}$ = 0.54 ppm), which could be due to the influence of an oxygen atom attached to the N^5 position. Together with the 16 mass units excess in the mass spectroscopic data, compound **1** was deduced as an N^5-oxide derivative of **5**. This was supported by the presence of the exchangeable proton singlet at δ_H 12.64 resulting from the protonation of the *N*-oxide group by TFA. The proposed structure of **1** was also consistent with its carbon data extracted from the HSQC and HMBC spectra (Table 2). Remarkable changes of carbon chemical shifts of C-4, C-6 and C-11b in **1** were observed at δ_C 67.3, 61.5 and 69.5, instead of those in **5** at δ_C 57.4, 50.9 and 62.0 ($\Delta\delta_{C\text{-}4}$ = 9.9 ppm, $\Delta\delta_{C\text{-}6}$ = 10.6 ppm, $\Delta\delta_{C\text{-}11b}$ = 7.5 ppm). The cross-peaks between H-8 and 9-OMe, H-11 and 10-OMe in the ROESY spectrum established the placement of the two methoxyl groups, respectively. On the basis of the foregoing data, the planar structure of tubulosine N_β^5-oxide (**1**) was established as TFA salt (Figure 1).

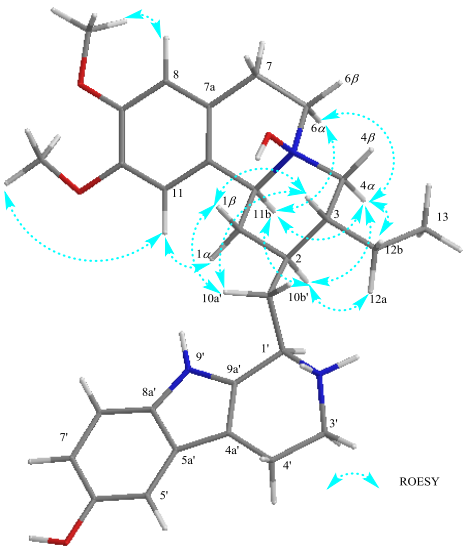

Figure 1. Key ROESY correlations for tubulosine N_β^5-oxide (**1**)

Table 1. ^{1}H NMR Spectroscopic Data (600 MHz for **1**-**9**, **11** and 800 MHz for **10**, DMSO-d_6) for compounds **1**-**11**

position	Compounds δ_H (J in Hz)										
	1	**2**	**3**	**4**	**5**	**6**	**7**	**8**	**9**	**10**	**11**
1α	2.94 m	2.57 m	2.92 m	2.59 m	3.04 m	2.76 m	2.99 m	2.74 m	3.04 m	2.32 m	2.36 m
1β	1.77 m	1.73 m	1.72 m	1.73 m	1.41 m	1.35 m	1.38 m	1.77 m	1.42 m	1.33 m	1.35 m
2	1.92 m	1.92 m	1.91 m	1.96 m	1.91 m	1.93 m	1.87 m	1.94 m	1.90 m	2.01 m	2.08 m
3	1.97 m	1.83 m	1.96 m	1.82 m	1.63 m	1.65 m	1.60 m	1.63 m	1.64 m	1.69 m	1.70 m
4α	3.72 m	3.70 m	3.66 m	3.68 m	3.02 m	2.98 m	2.97 m	2.96 m	3.04 m	2.98 m	3.00 m
4β	3.92 m	4.11 dd (12.6, 3.6)	3.91 m	4.07 dd (12.5, 3.5)	3.64 m	3.61 m	3.60 m	3.60 m	3.67 m	3.60 m	3.61 m
N-5	12.64 s	12.99 s	12.61 s	12.78 s	10.25 br s	9.95 br s	10.03 br s	9.80 br s	9.92 br s	9.61 br s	9.77 br s
6α	4.18 m	4.34 m	4.14 m	4.30 m	3.68 m	3.64 m	3.61 m	3.61 m	3.70 m	3.61 m	3.59 m
6β	4.00 m	3.82 m	3.96 m	3.79 m	3.47 m	3.40 m	3.41 m	3.39 m	3.49 m	3.30 m	3.32 m
7	3.31 m	3.26 m	3.24 m	3.26 m	3.19 m	3.16 m	3.11 m	3.11 m	3.22 m	3.00 m	3.12 m
7	3.05 m	3.03 m	2.97 m	2.96 m	2.97 m	2.92 m	2.85 m	2.87 m	2.98 m	2.85 m	2.87 m
8	6.90 s	6.86 s	6.69 s	6.66 s	6.84 s	6.80 s	6.62 s	6.61 s	6.86 s	6.58 s	6.78 s
9			9.27 s	9.21 s			9.22 s	9.21 s			
11	6.92 s	6.74 s	6.90 s	6.76 s	6.98 s	6.68 s	6.93 s	6.66 s	6.97 s	6.40 s	6.45 s
11b	4.77 br d (11.9)	4.65 br dd (12.4, 1.8)	4.72 br d (12.0)	4.62 br dd (12.5, 1.8)	4.23 br t (10.7)	4.23 br s	4.18 br t (10.3)	4.19 br s	4.24 br t (10.5)	4.18 br s	4.21 br s
12	1.68 m	1.68 m	1.68 m	1.67 m	1.68 m	1.69 m	1.64 m	1.68 m	1.68 m	1.81 m	1.81 m
12	1.28 m	1.31 m	1.26 m	1.30 m	1.23 m	1.28 m	1.20 m	1.23 m	1.23 m	1.35 m	1.33 m
13	0.90 t (7.5)	0.92 t (7.5)	0.90 t (7.5)	0.90 t (7.5)	0.89 t (7.4)	0.85 t (7.4)	0.86 t (7.4)	0.85 t (7.5)	0.89 t (7.5)	0.92 t (7.4)	0.93 t (7.4)
1'	5.13 br t (9.9)	4.80 br s	5.10 br t (9.9)	4.78 br s	5.09 br t (9.9)	4.90 br s	5.08 br t (9.9)	4.90 br s	5.15 br t (9.9)		
N-2'	9.67 br s	9.66 br s	9.70 br s	9.68 br s	10.02 br s	9.75 br s	9.93 br s	9.75 br s	9.76 br s		
N-2'	9.03 br s	9.07 br s	9.04 br s	9.04 br s	9.24 br s	9.22 br s	9.22 br s	9.21 br s	9.12 br s		
3'	3.72 m	3.68 m	3.72 m	3.68 m	3.73 m	3.68 m	3.67 m	3.68 m	3.77 m	3.97 m	3.96 m

3'	3.31 m	3.34 m	3.31 m	3.32 m	3.33 m	3.43 m	3.30 m	3.41 m	3.35 m	3.92 m	3.93 m
4'	2.93 m	2.89 m	2.93 m	2.93 m	2.95 m	2.97 m	2.90 m	2.97 m	3.02 m	3.22 m	3.19 m
4'	2.90 m	2.85 m	2.91 m	2.88 m	2.90 m	2.88 m	2.80 m	2.86 m	3.00 m		
5'	6.78 d (2.4)	6.76 d (2.4)	6.77 d (2.4)	6.75 d (2.3)	6.78 d (2.3)	6.77 d (2.5)	6.75 d (2.4)	6.77 d (2.4)	7.51 dd (8.0, 1.2)	6.96 d (2.4)	6.97 d (2.4)
6'	8.73 s	8.72 s	8.72 s	8.73 s	8.73 s	8.72 s	8.75 s	8.75 s	7.03 ddd (8.0, 8.0, 1.2)	8.72 s	8.73 s
7'	6.65 dd (8.6, 2.4)	6.64 dd (8.6, 2.4)	6.65 dd (8.6, 2.4)	6.62 dd (8.6, 2.3)	6.64 dd (8.6, 2.3)	6.64 dd (8.5, 2.5)	6.62 dd (8.6, 2.4)	6.65 dd (8.6, 2.4)	7.12 ddd (8.0, 8.0, 1.2)	7.04 dd (8.9, 2.4)	7.04 dd (9.0, 2.4)
8'	7.15 d (8.6)	7.13 d (8.6)	7.17 d (8.6)	7.14 d (8.6)	7.16 d (8.6)	7.17 d (8.5)	7.14 d (8.6)	7.17 d (8.6)	7.39 dd (8.0, 1.2)	7.40 d (8.9)	7.39 d (9.0)
N-9'	10.80 s	10.70 s	10.80 s	10.69 s	10.87 s	10.85 s	10.87 s	10.86 s	11.18 s	12.22 s	12.22 s
10'	2.18 m	2.12 m	2.18 m	2.09 m	2.16 m	2.42 m	2.14 m	2.42 m	2.18 m	3.36 m	3.32 m
10'	2.10 m	1.92 m	2.10 m	1.91 m	2.00 m	1.75 m	1.96 m	1.76 m	2.04 m	2.86 m	2.86 m
9-OMe	3.78 s	3.75 s			3.76 s	3.75 s			3.77 s		3.70 s
10-OMe	3.76 s	3.73 s	3.76 s	3.74 s	3.75 s	3.58 s	3.75 s	3.57 s	3.76 s	3.39 s	3.39 s

Table 2. ^{13}C NMR Spectroscopic Data (150 MHz for **1**-**9**, **11** and 200 MHz for **10**, DMSO-d_6) for compounds **1**-**11**

position	Compounds										
	1	**2**	**3**	**4**	**5**	**6**	**7**	**8**	**9**	**10**	**11**
1	27.7	37.8	27.9	38.1	33.4	33.9	33.4	34.0	33.3	32.9	33.0
2	32.2	32.7	32.1	32.7	33.5	34.1	33.8	34.0	33.7	37.2	37.6
3	35.7	38.0	35.8	37.9	39.7	39.4	40.0	39.3	39.8	39.8	38.8
4	67.3	70.6	67.2	70.2	57.4	57.1	17.6	57.1	57.5	56.7	56.8
6	61.5	53.0	61.4	53.1	50.9	50.4	50.9	50.3	50.5	50.4	50.2
7	22.7	22.9	22.8	22.8	25.5	25.0	25.6	24.7	25.6	24.6	24.8
7a	123.6	123.3	123.6	121.2	124.4	124.3	124.8	124.4	124.3	124.0	124.6
8	111.3	110.9	115.1	114.4	111.9	111.4	115.8	115.0	112.3	114.1	114.3
9	147.7	148.2	146.7	146.2	149.1	149.1	147.3	146.7	148.7	146.6	148.3
10	147.7	147.7	146.7	146.8	148.2	148.0	147.4	146.8	147.7	146.6	147.6
11	109.7	109.8	110.4	110.3	109.5	108.6	110.4	108.8	110.1	107.9	107.8
11a	121.8	120.7	120.2	121.8	124.0	123.7	122.8	122.2	123.5	121.7	121.6
11b	69.5	70.6	69.8	70.5	62.0	61.7	62.5	61.6	62.3	61.6	61.8
12	21.0	21.1	21.1	21.3	22.0	21.4	22.2	21.3	22.1	22.0	23.0
13	9.7	9.9	9.9	9.9	10.6	9.6	10.7	9.9	10.3	10.1	10.3
1'	49.1	49.0	49.0	49.3	49.7	50.8	49.9	50.7	50.0	167.2	167.9
3'	41.1	40.5	41.1	40.2	41.5	40.0	41.8	40.0	41.8	41.6	41.6
4'	17.6	17.7	17.7	17.8	18.3	17.8	18.6	17.8	18.5	18.6	18.5
4a'	104.6	104.9	104.8	104.8	105.6	105.3	105.8	105.1	105.8	121.7	122.6
5a'	126.2	126.3	126.6	126.3	127.0	127.0	127.7	127.0	125.7	124.7	125.4
5'	101.8	101.4	101.9	101.7	102.3	101.8	102.6	101.9	118.5	102.7	102.6
6'	150.8	150.8	150.5	150.7	151.1	151.2	151.3	150.9	119.5	152.6	153.0
7'	111.6	111.8	111.7	111.6	112.0	111.6	112.4	111.6	122.3	121.0	121.7
8'	111.4	111.2	111.3	111.3	111.9	111.3	112.2	111.3	111.8	113.7	113.7
8a'	130.2	130.0	130.3	130.3	130.8	131.1	130.9	130.6	136.2	135.9	135.7
9a'	130.2	130.0	130.3	130.3	130.8	131.1	130.9	130.6	130.1	127.6	127.7
10'	34.0	33.0	34.1	33.0	34.3	34.2	34.8	34.2	34.5	34.5	34.2
9-OMe	55.4	55.4			56.0	55.3			56.2		55.0
10-OMe	55.4	55.4	56.3	55.2	56.0	55.3	56.9	55.4	56.2	55.5	55.4

Isotubulosine N_α^5-oxide (**2**) was recognized as a stereoisomer of **1** from its HRESIMS with an adduct $[M+H]^+$ ion at *m*/*z* 492.2855, which in conjunction with NMR data enabled the establishment of a molecular formula of $C_{29}H_{37}N_3O_4$. The ^1H NMR

spectrum of **2** was reminiscent of that of **1** (Table 1). However, a careful comparison of the two spectra revealed significant differences in chemical shifts of H-1, H-3, H-4, H-6 and H-11b in **2** at δ_H 2.57/1.73, 1.83, 4.11/3.70, 4.34/3.82 and 4.65 in comparison with those in **1** at δ_H 2.94/1.77, 1.97, 3.92/3.72, 4.18/4.00 and 4.77. It was consistent with its ^{13}C NMR data derived from the HSQC and HMBC spectra (Table 2). Notable changes in carbon chemical shifts of C-1, C-3, C-4, C-6 and C-11b in **2** were also observed at δ_C 37.8, 38.0, 70.6, 53.0, and 70.6, instead of those in **1** at δ_C 27.7, 35.7, 67.3, 61.5 and 69.5. A careful comparison of the two spectra also showed the significant differences in proton chemical shifts of H-1' and H-10' in **2** at δ_H 4.80 and 2.12/1.92, instead of those in **1** at δ_H 5.13 and 2.18/2.10. ROESY correlations between H-8 and 9-OMe, H-11 and 10-OMe established the placement of the two methoxyl groups, respectively. On the basis of comparison of the physical and spectral data, compound **2** was assigned as a stereoisomer of **1**.

The HRESIMS data ($[M+H]^+$ *m/z* 478.2715) for 9-demethyltubulosine N_β^5-oxide (**3**) supported a molecular formula of $C_{28}H_{34}N_3O_4$, for 13 degrees of unsaturation. Inspection of the 1D and 2D NMR spectra of **3** suggested that it was structurally related to **1** (Table 1 and 2). However, the ^1H NMR spectrum of **3** indicated the presence of only one methoxyl singlet at δ_H 3.76. The ROESY correlation between the methoxyl singlet at δ_H 3.76 and H-11 at δ_H 6.90 confirmed the methoxyl was attached to C-10. The planar structure of 9-demethyltubulosine N_β^5-oxide was therefore deduced as **3**.

The fourth compound, 9-demethylisotubulosine N_α^5-oxide (**4**) was recognized as an stereoisomer of **3** from its HRESIMS of an adduct $[M+H]^+$ ion at *m/z* 478.2698, which in conjunction with NMR data enabled the establishment of a molecular formula of $C_{28}H_{34}N_3O_4$. The ^1H NMR spectrum of **4** was very similar to that of **2**, except for the

absence of a methoxyl singlet at δ_H 3.75 (Table 1). The ROESY correlation between the methoxyl singlet at δ_H 3.74 and H-11 at δ_H 6.76 confirmed the methoxyl was attached to the C-10 position. The planar structure of 9-demethylisotubulosine N_α^5-oxide was therefore deduced as **4**.

The relative configurations of the benzoquinolizidine moiety in **1** were determined by the ROESY experiment (Figure 1). The ROESY correlations between H-2 (δ_H 1.92) and H-4α (δ_H 3.72), H-2 (δ_H 1.92) and H-11b (δ_H 4.77), H-4α (δ_H 3.72) and H-11b (δ_H 4.77), H-6α (δ_H 4.18) and H-11b (δ_H 4.77) were observed, indicating their cis disposition and N^5-OH was at the β side of the benzoquinolizidine ring. On the other hand, ROESY cross-peaks were observed between H-1β (δ_H 1.77) and H-3 (δ_H 1.97), H-1β (δ_H 1.77) and H-10a' (δ_H 2.18), thereby confirming the β-orientation of H-3. As a result, the C-10' methylene group could be placed on the β-face of the molecule (Figure 1). Given the free rotation of the methylene linkage between the benzoquinolizidine and tryptoline moieties, the relative configuration of H-1' cannot be determined by the ROESY experiment.

The relative configurations of the benzoquinolizidine moiety in **2** were determined by the ROESY experiment. The ROESY correlations between H-2 (δ_H 1.92) and H-4α (δ_H 3.70), H-2 (δ_H 1.92) and H-11b (δ_H 4.65), H-11b (δ_H 4.65) and H-4α (δ_H 3.70), H-4α (δ_H 3.70) and H-12a (δ_H 1.68), H-11b (δ_H 4.65) and H-12a (δ_H 1.68), indicating their cis disposition. The N^5-OH group was deduced at the α side of the benzoquinolizidine ring on the basis of ROESY correlations between H-11b (δ_H 4.65) and N^5-OH (δ_H 12.99), H-4α (δ_H 3.70) and N^5-OH (δ_H 12.99). On the other hand, ROESY cross-peaks were observed between H-1β (δ_H 2.57) and H-3 (δ_H 1.83), H-1β (δ_H 2.57) and H-10b' (δ_H 1.92), thereby confirming the β-orientation of H-3. As a result, the C-10' methylene group could be placed

on the β-face of the molecule. Given the free rotation of the methylene linkage between the benzoquinolizidine and tryptoline moieties, the relative configuration of H-1' cannot be determined by the ROESY experiment.

The relative configurations of the benzoquinolizidine moiety in **3** were determined by the ROESY experiment (Figure 1). The ROESY correlations between H-2 (δ_H 1.91) and H-4α (δ_H 3.66), H-2 (δ_H 1.91) and H-11b (δ_H 4.72), H-4α (δ_H 3.66) and H-11b (δ_H 4.72), H-6α (δ_H 4.14) and H-11b (δ_H 4.72) were observed, indicating their cis disposition and N^5-OH was at the β side of the benzoquinolizidine ring. On the other hand, ROESY cross-peaks were observed between H-1β (δ_H 1.72) and H-3 (δ_H 1.96), H-1β (δ_H 1.72) and H-10a' (δ_H 2.18), thereby confirming the β-orientation of H-3. As a result, the C-10' methylene group could be placed on the β-face of the molecule. Given the free rotation of the methylene linkage between the benzoquinolizidine and tryptoline moieties, the relative configuration of H-1' cannot be determined by the ROESY experiment.

The relative configurations of the benzoquinolizidine moiety in **4** were determined by the ROESY experiment. The ROESY correlations between H-2 (δ_H 1.96) and H-4α (δ_H 3.68), H-2 (δ_H 1.96) and H-11b (δ_H 4.62), H-11b (δ_H 4.62) and H-4α (δ_H 3.68), H-4α (δ_H 3.68) and H-12a (δ_H 1.67), H-11b (δ_H 4.62) and H-12a (δ_H 1.67), indicating their cis disposition. The N^5-OH group was deduced at the α side of the benzoquinolizidine ring on the basis of ROESY correlations between H-11b (δ_H 4.62) and N^5-OH (δ_H 12.78), H-4α (δ_H 3.68) and N^5-OH (δ_H 12.78). On the other hand, ROESY cross-peaks were observed between H-1β (δ_H 2.57) and H-3 (δ_H 1.82), H-1β (δ_H 2.57) and H-10b' (δ_H 1.91), thereby confirming the β-orientation of H-3. As a result, the C-10' methylene group could be placed on the β-face of the molecule. Given the free rotation of the methylene linkage between the

benzoquinolizidine and tryptoline moieties, the relative configuration of H-1' cannot be determined by the ROESY experiment.

The effects of the substituents and the basic skeleton on the chirality of tubulosine and isotubulosine type alkaloids have been discussed in the literature.[37,69-71] Two partial chromophores, a tetrahydroisoquinoline and a tetrahydrocarboline (tryptoline) moiety, contributed to the major Cotton effects (CEs) at 280, 240 and 225 nm in tubulosine alkaloids and, four major CEs at 310, 278, 238 and 218 nm in isotubulosine alkaloids. In general, for tubulosine alkaloids, where the absolute configuration defined as (2*S*,3*R*,11b*S*,1'*R*), have a strong negative CE at around 225 nm, a medium positive CE at around 240 nm and a weak negative CE at 280 nm. In comparison, for isotubulosine type alkaloids, where the absolute configuration defined as (2*S*,3*R*,11b*S*,1'*S*), with only one chiral center different at C-1', have a strong negative CE at around 218 nm, a medium positive CE at 240 nm and, a strong positive CE at 278 nm and an extra negative CE at 310 nm. The CD spectra of compounds **5**, **7** and **9** were in agreement with the published data,[37] indicating the absolute configurations of **5**, **7** and **9** as (2*S*,3*R*,11b*S*,1'*R*) (Figure 2a). The CD spectra of compounds **6** and **8** were in agreement with the published data (Figure 2b),[37,69] indicating the absolute configurations of **6** and **8** as (2*S*,3*R*,11b*S*,1'*S*). The major differences of the CEs at around 280 nm were ascribed to be the effects of the absolute confirmation at the C-1' position.

The absolute configurations at the C-1' position of compound **1**-**4** were determined using the circular dichroism experiments. The observed negative CEs at around 278 nm in compound **1** and **3** indicated a *R*-configuration at C-1' (Figure 2a). In contrast, the observed positive CE at 278 nm in compound **2** and **4** suggested a *S*-configuration at C-1' (Figure

2b). The similar coupling constant of H-1' and H-10', along with the chemical shifts of H-1' as in **1**, **3**, **5**, **7** and **9** were consistent with the assignment, as to those in **2**, **4**, **6** and **8** (Table 1).

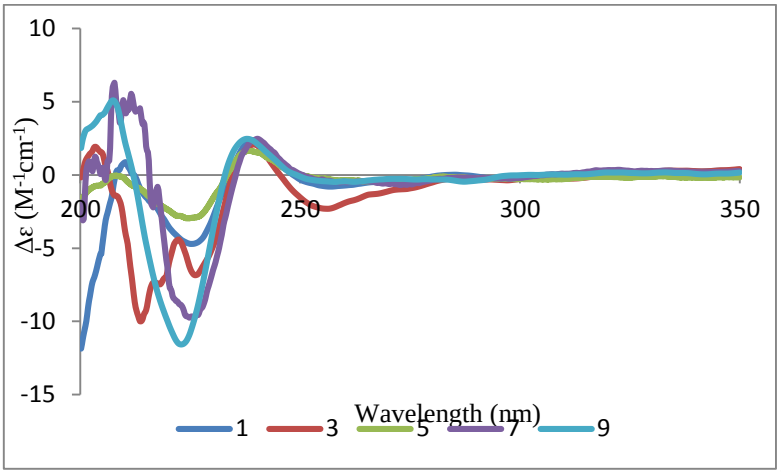

2a

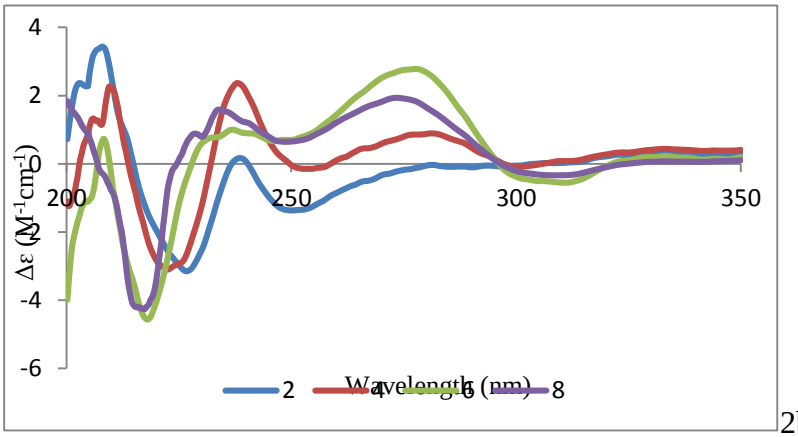

2b

Figure 2. CD spectra of compounds **1-9** in MeOH.

The absolute configurations at C-2, C-3 and C-11b in **1-4** were deduced to be (2*S*,3*R*,11b*S*) by the similarity of the CD spectral data with those of **5-9**, respectively. Furthermore, on the basis of the ROESY correlations, the *S*-absolute configuration at the N^5 positions in **1** and **3** and the *R*-absolute configuration at the N^5 positions in **2** and **4** were

deduced. Herein, the absolute configurations of (2*S*,3*R*,5*S*,11b*S*,1'*R*) were determined for **1** and **3** and, absolute configurations of (2*S*,3*R*,5*R*,11b*S*,1'*S*) were determined for **2** and **4**.

1',2'-Dehydro-9-demethyltubulosine (**10**) was obtained as an optically active amorphous powder with an $[\alpha]_D$ value at +50.0. Its molecular formula of $C_{28}H_{34}N_3O_3$ was assigned based on the HRESIMS data for $[M+H]^+$ at *m*/*z* 460.2595, which was consistent with 14 degrees of unsaturation. It showed UV maxima at 230, 283 and 375 nm, and IR bands at 3440, 2981, 1686, 1522, 1441, 1202, 1181, 1023 and 1000 cm^{-1}, indicative of benzoquinolizidine and dihydrocarboline chromophores. Its ^1H NMR spectrum exhibited signals for an ethyl group at δ_H 0.92, 1.35, and 1.81, singlets for two aromatic protons at δ_H 6.58 and 6.40, three aromatic protons at δ_H 7.40, 7.04 and 6.96 for an AMX spin system for three aromatic protons at δ_H 7.40, 7.04 and 6.96, one methoxyl singlet at δ_H 3.39 and exchangeable signal at δ_H 12.22 (Table 1). These spectral features were similar to those of 9-demethyltubulosine (**7**) and 9-demethylisotubulosine (**8**), except for the absence of H-1' methine signal, which appeared at δ_H 5.08 in **7** and δ_H 4.90 in **8**, suggesting that **10** was the 1',2'-dehydrogenated analogue of **7** and **8**. The assignment was supported by the observation of the carbon chemical shift of C-1' at δ_C 167.2, in comparison with $\delta_{C\text{-}1'}$ 49.9 in **7** and $\delta_{C\text{-}1'}$ 50.7 in **8**. The planar structure of **10** was therefore deduced.

The relative configuration of **10** was deduced by the ROESY experiment. The ROESY correlations between H-2 (δ_H 2.01) and H-4α (δ_H 2.98), H-2 (δ_H 2.01) and H-11b (δ_H 4.18), H-4α (δ_H 2.98) and H-11b (δ_H 4.18), H-6α (δ_H 3.61) and H-11b (δ_H 4.18) were observed, indicating their cis disposition. On the other hand, ROESY cross-peaks were observed between H-1β (δ_H 1.33) and H-3 (δ_H 1.69), H-1β (δ_H 1.33) and H-10a' (δ_H 3.36), thereby confirming the β-orientation of H-3. As a result, the C-10' methylene group could

be placed on the β-face of the molecule. The CD spectrum of 10 showed a negative Cotton effect at 23 nm and a positive CE at 210 nm in MeOH, similar to that observed for **11** and also explicable in terms of the aromatic quadrant rule as well as in literature,[37] suggesting (2*S*,3*R*,11b*S*) absolute configuration for **10**.

7',9-*O*-Didemethylcephaeline (**13**), was isolated as an optically active amorphous powder with an $[\alpha]_D$ value at +12.2. The HRESIMS data gave a $[M+H]^+$ ion at *m*/*z* 439.2610, which was consistent with a molecular formula of $C_{26}H_{34}N_2O_4$, and implied 11 degrees of unsaturation. It showed UV maxima at 203, 230sh and 285 nm, IR bands at 3446, 3000, 1685, 1533, 1468, 1204, 1179, 1028 and 1000 cm^{-1}, indicative of tetrahydroisoquinoline chromophores. The ^1H NMR spectrum contained four aromatic singlets (δ_H 6.91, 6.67, 6.64 and 6.59), four methines (δ_H 4.73, 4.18, 1.76 and 1.60), eight methylene moieties (δ_H 3.62/3.41, 3.62/2.95, 3.49/3.22, 3.13/2.92, 2.92/2.80, 2.89/1.36, 2.14/1.68 and 1.60/1.26), one methoxyl singlet (δ_H 3.78), one methyl triplet (δ_H 0.88, t, 9.2 Hz) and three broad exchangeable protons (δ_H 9.62, 9.32 and 8.74) (Table 3). Analysis of the HSQC and HMBC spectra indicated that the molecule contained twelve aromatic carbons (δ_C 147.4, 146.9, 144.5, 144.5, 124.3, 123.2, 122.3, 121.9, 114.9, 114.9, 112.9 and 109.7), four sp^3 hybridized methines (δ_C 61.8, 50.7, 38.5 and 33.7), eight sp^3 hybridized methylenes (δ_C 56.3, 50.7, 37.8, 35.4, 32.8, 24.4, 24.3, 21.1), one methoxyl carbon (δ_C 56.3) and a methyl carbon (δ_C 9.6) (Table 3). These spectral features were similar to those of benzoquinolizidine alkaloids such as emetine and cephaeline.[72,73] In comparison with emetine, compound **13** had only one methoxyl singlet instead of four in emetine. ROESY correlations between H-11 and the methoxyl singlet at δ_H 3.78, H-11 and H-1 indicated that the methoxyl group was attached at the C-10 position, therefore, three hydroxyl groups

were present at C-9, C-6' and C-7', respectively. On the basis of the foregoing data, the planar structure of 7',9-*O*-didemethylcephaeline was established as **13**. Because TFA was used throughout the purification process, the counterion for 7',9-*O*-didemethylcephaeline (**13**) was trifluroacetate.

Table 3. NMR spectroscopic data (600 or 800 MHz, DMSO-d_6) for compounds **13**-**15**

position	**13**		**14**		**15**	
	δ_C, type	δ_H (*J* in Hz)	δ_C, type	δ_H (*J* in Hz)	δ_C, type	δ_H (*J* in Hz)
1	32.8, CH_2	2.91, m 1.36, m	33.8, CH_2	2.92, m 1.30, m	32.8, CH_2	2.40, m 1.36, m
2	33.7, CH	1.78, m	34.6, CH	1.74, m	37.2, CH	1.94, m
3	38.5, CH	1.60, m	39.2, CH	1.60, m	39.0, CH	1.70, m
4	56.3, CH_2	3.64, m 2.95, m	56.8, CH_2	3.57, m 2.98, m	56.1, CH_2	3.62, m 2.96, m
N-5		9.67, br s		9.66, br s		9.72, br s
6	50.7, CH_2	3.63, m 3.43, m	50.7, CH_2	3.63. m 3.35, m	50.6, CH_2	3.61, m 3.30, m
7	24.4, CH_2	3.12, m 2.87, m	24.4, CH_2	3.10, m 2.88, m	23.9, CH_2	3.09, m 2.86, m
7a	124.3, C		124.3, C		123.3, C	
8	114.9, CH	6.63, s	114.9, CH	6.63, s	114.9, CH	6.61, s
9	146.9, C		146.4, C		145.8, C	
10	147.4, C		146.5, C		146.2, C	
11	109.7, CH	6.90, s	109.3, CH	6.89, s	108.5, CH	6.65, s
11a	121.9, C		122.0, C		122.1, C	
11b	61.8, CH	4.18, m	61.7, CH	4.26, m	61.0, CH	4.19, m
12	21.1, CH_2	1.68, m 1.21, m	21.6, CH_2	1.60, m 1.23, m	21.4, CH_2	1.85, m 1.37, m
13	9.6, CH_3	0.88, t (7.5)	9.9, CH_3	0.79, t (7.5)	9.9, CH_3	0.95, t (7.5)
α	35.4, CH_2	2.15, m 1.68, m	36.1, CH_2	2.22, m 1.60, m	35.3, CH_2	3.45, m 2.62, m
1'	50.7, CH	4.73, m	51.1, CH	4.58, m	174.5, C	
N-2'		9.32, br s 8.74, br s		9.29, br s 8.88, br s		
3'	39.6, CH_2	3.49, m 3.22, m	37.8, CH_2	3.47, m 3.33, m	40.2, CH_2	3.86, m 3.71, m
4'	24.3, CH_2	2.95, m 2.81, m	24.4, CH_2	2.92, m 2.85, m	24.0, CH_2	3.03, m 2.85, m
4a'	122.3, C		121.8, C		132.6, C	
5'	114.9, CH	6.59, s	115.1, CH	6.60, s	114.9, CH	6.89, s
6'	144.5, C		145.0, C		154.7, C	
7'	144.5, C		144.3, C		145.3, C	

8'	112.9, CH	6.67, s		113.2, CH	6.74, s	116.5, CH	7.36, s
8a'	123.2, C			123.6, C		122.6, C	
10-OMe	56.3, CH_3	3.78, s		55.7, CH_3	3.78, s	55.3, CH_3	3.67, s

7',9-*O*-Didemethylisocephaeline (**14**), was recognized as an isomer of **13** from its HRESIMS $[M+H]^+$ at *m*/*z* 439.2610, which in conjunction with NMR data enabled the establishment of a molecular formula of $C_{26}H_{34}N_2O_4$. The ^1H NMR spectum had similar feature to **13** (Table 3). The only notable difference was the shielding effect in the chemical shift of H-1' at δ_H 4.58 in **14** instead of at δ_H 4.73 in **13** ($\Delta\delta_H$ = 0.15 ppm). The reasonable assumption was that the stereochemistry at C-1' in **14** was opposite to that in **13**. This will be futher discussed later on. The position of the methoxyl group was determined to be attached to C-10 due to the cross-peaks between H-11 and 10-OMe, H-11 and H-1 in the ROESY spectrum of **14**. Compound **14** was assigned the isomer of **13** based on comparison of the physical and spectral data.

7',9-Didemethylpsychotrine (**15**), was obtained as an optically active amorphous powder. Its molecular formula of $C_{26}H_{32}N_2O_4$ was assigned based on the HRESIMS data for $[M+H]^+$ at *m*/*z* 437.2436, which was consistent with 12 degrees of unsaturation. It showed UV maxima at 203, 230, 282 and 369 nm, and IR bands at 3376, 2941, 1680, 1445, 1318, 1203 and 1175 cm^{-1}, indicative of benzoquinolizidine and dihydroisoquinoline chromophores. Its ^1H NMR spectrum exhibited signals for an ethyl group at δ_H 0.95, 1.37, and 1.85, singlets for four aromatic protons at δ_H 7.36, 6.89, 6.65 and 6.61, and singlet for methoxyl group at δ_H 3.77 and exchangeable signals at δ_H 9.72. These spectral features were similar to those of **13** and **14**, except for the absence of the H-1' signal, which appeared at δ_H 4.73 in **13** and δ_H 4.60 in **14**, in combination with the 2 mass units less than **13** and **14** suggested that **15** was a 1',2'-dehydrogenated analogue of **13** and **14**. The proposed

structure of **15** was consistent with its 2D spectrum, where C-1' was observed at δ_C 174.5, instead of at δ_C 50.7 in **13** and δ_C 51.1 in **14**. Thus, the planar structure of alkaloid **15** was determined to be 7',9-didemethylpsychotrine.

Compound **13** exhibited a positive CE at 237 nm and a negative CE at 290 nm, respectively, in its CD spectrum (Figure 4). The relevance of these CEs to the issue of absolute configuration at the C-11b and C-1' benzylic stereocenters is explicable in terms of the aromatic quadrant rule.[70,74] When viewed along the C-9-C-11a-C-11b axis, N-5 and the C-4 methylene are in the positive lower right quadrant, and the C-1 methylene and C-2 methine are in the negative left lower quadrant for the *S* absolute configuration at C-11b shown in structure **13**. The contribution of these substituents to the observed CEs will thus largely cancel each other out. However, when viewed along the C-6'-C-8'a-C-1' axis, the C-3 methylene group is located in the positive left upper quadrant and the C-14 methylene group and all of its substituent tricyclic ring system are in the positive right lower quadrant. Collectively these quadrant projections then explain the high-amplitude positive Cotton effect for the $A_{1g}\rightarrow B_{1u}$ aromatic transition at 237 nm, and hence the *S* absolute configuration of compound 1 at C-1'. Since the signs of the quadrants are reversed when considering the ca. 290 nm ($A_{1g}\rightarrow B_{1u}$) transition because of the antipodal natures of "normal" aromatic ellipticities,[70] the negative CE at 290 nm in the CD spectrum of **13** was also readily explicable. Cephaeline and emetine with their C-1' R absolute configuration showed similar CEs in the corresponding regions of their CD spectra.[67] Compound **13** thus possesses the same spatial arrangement of substituents at C-1' as cephaeline and emetine,[67] with a *R* absolute configuration at this stereocenter. Collectively, the CD and ROESY data

then permitted assignment of (2*R*,3*R*,11b*S*,1'R) absolute configuration to compound **13** and (2*R*,3*R*,11b*S*,1'*S*) absolute configuration to compound **14**.

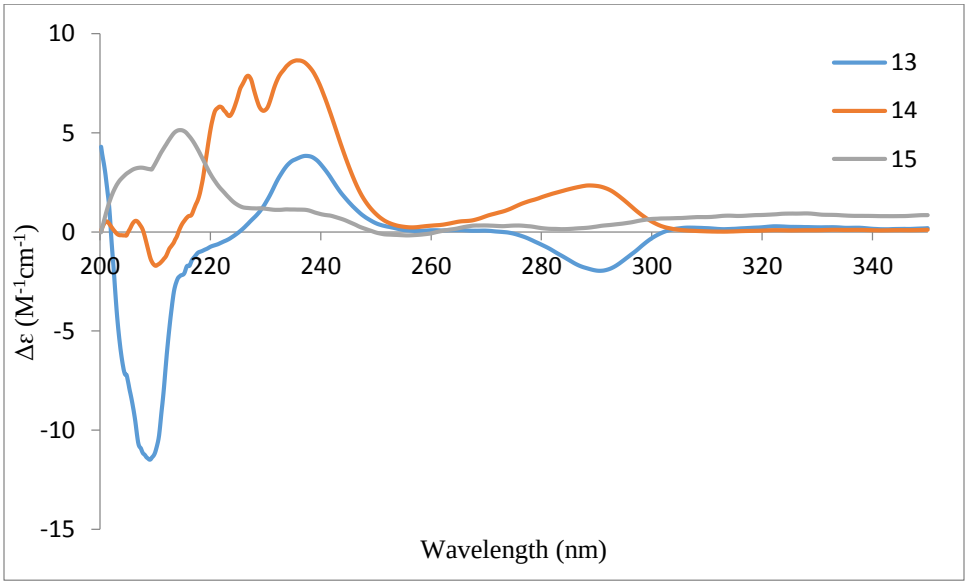

Figure 4. CD spectra of compound **13**-**15** in MeOH.

(1*S*)-Lacinilene C (**33**) was isolated as an optically active white amorphous powder with an $[\alpha]_D$ value at -33.3. It was recognized as the enantiomer of lacinilene C, (1*R*)-form with an positive $[\alpha]_D$ value (+37.7).[54] (1ζ)-1-Methoxylacinilene C (**34**), was isolated as racemic in comparison with reported optically active (1S)-1-methoxylacinilene C.[53]

Consistent with the extraction and fractionation protocol developed in-house to prepare a Nature Bank fraction library targeting drug-like molecules, the isolated compounds were distributed within this lead-like space (Five Fractions in Figure 6).[3,75] The data suggested that 55% of the isolated metabolites obeyed Linpinski's Rule of five in terms of log *P* < 5 (81.8%), MW < 500 Da (63.6%), HBA < 10 (72.7%) and HBD < 5 (65.9%). The physicochemical property of all isolated compounds were calculated using Instant JChem (version 15.10.26.0) and were provided in the Supporting Information.[76]

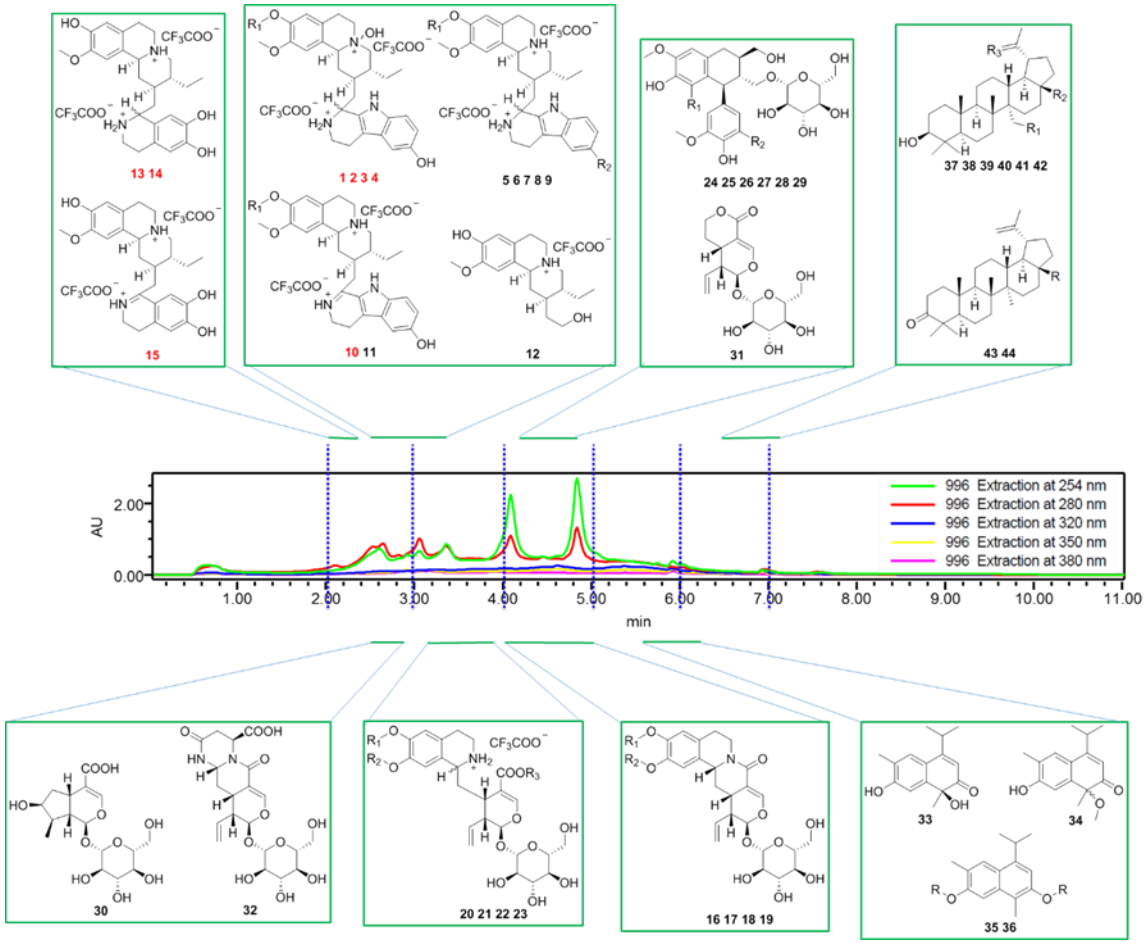

Figure 6. HPLC chromatogram of lead-like enhanced extract of the Australian plant *Alangium villosum* subsp. *tomentosum* (F.Muell.) *Bloemb* and chemical structures isolated from different lead-like enhanced fractions.

The cytological profiles of the 44 secondary metabolites from the Australian plant *Alangium villosum* subsp. *tomentosum* (F. Muell.) Bloemb were examined to identify congeneric chemical series by coupling an unbiased multidimensional phenotype assay using nontransformed and nonimmortalized hONS cells, which were primary cells derived from a Parkinson's disease patient. hONS cells were treated with 10 μM of each compound for 24 h. Cytological parameters were assessed by staining with fluorescent probes targeting various cellular pathways and organelles implicated in Parkinson's disease. These included mitochondria, early endosomes, lysosomes, microtubule-based cytoskeleton, and

autophagosomes. In total, 38 phenotypic features across the individual cell line were generated. The identified compounds were subsequently analyzed to depict the cytological profile of the metabolites using bar chart as shown in Figure 6.

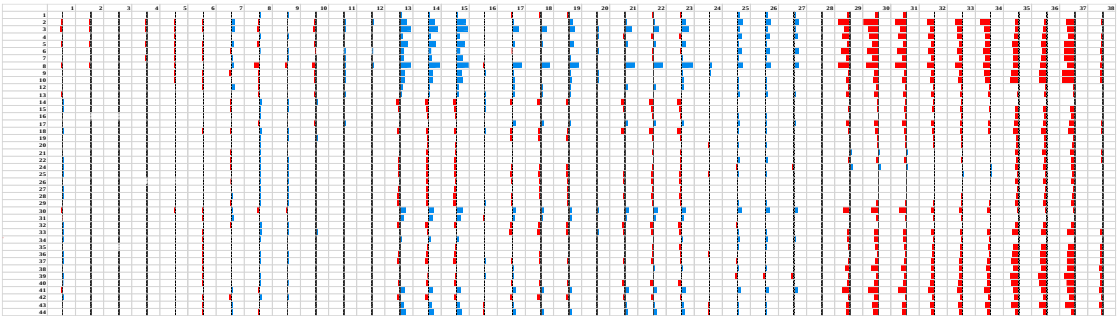

Figure 7. Bar chart depicting the cytological profile of metabolites from *Alangium villosum* subsp. *tomentosum* (F. Muell.) Bloemb at 10 µM on 38 parameters based on the $\log_2$ ratio of compound and vehicle (DMSO). Red shows a decrease versus vehicle and blue shows an increase versus vehicle. Individual compounds are presented on the y-axis with individual features on the x-axis. 1. Nucleus area (µm²) 2. Nucleus morphology width (µm) 3. Nucleus morphology length (µm) 4. Nucleus morphology ratio width to length 5. Nucleus morphology roundness 6. Nucleus marker texture index 7. Nucleus marker intensity 8. Cell area (µm²) 9. Cell width (µm) 10. Cell length (µm) 11. Cell ratio width to length 12. Cell roundness 13. α-Tubulin marker intensity in the cytoplasm 14. α-Tubulin marker intensity in outer region of cytoplasm 15. α-Tubulin marker intensity in inner region of cytoplasm 16. α-Tubulin marker texture index 17. Mitochondria marker intensity in the cytoplasm 18. Mitochondria marker intensity in outer region of cytoplasm 19. Mitochondria marker intensity in inner region of the cytoplasm 20. Mitochondria marker texture index 21. LC3b marker intensity in the cytoplasm 22. LC3b marker intensity in the outer region of the cytoplasm 23. LC3b marker intensity in inner region of cytoplasm 24. LC3b marker texture index 25. Lysosome marker intensity mean 26. Lysosome marker intensity outer region mean 27 Lysosome marker intensity inner region mean 28. Lysosome marker texture index. 29. Number of EEA1 marker spots in cytoplasm 30. Number of EEA1 marker spots in inner region of cytoplasm 31. Number of EEA1 marker spots in outer region of cytoplasm 32. Number of EEA1 marker spots per Area of cytoplasm 33. EEA1 marker intensity in outer region of cytoplasm 34 EEA1 marker intensity in inner region of cytoplasm 35. EEA1 marker intensity in the cytoplasm 36. Number of EEA1 marker spots per area of outer region 37 Number of EEA1 marker spots per Area of inner region of cytoplasm 38. EEA1 marker texture index.

Most of the metabolites from *Alangium villosum* subsp. *tomentosum* (F.Muell.) Bloemb did not exhibit alterations to nuclear and cellular parameters at 10 μM suggesting that those natural products are not very cytotoxic to the hONS cell model of Parkinson's disease. In our assay, the tubulosine congeners **1-11** displayed moderate phenotypic perturbation on the α-tubulin and EEA-1 related parameters while only had slight effects on the lysosome related parameters (Figure 7). None of the three emetine alkaloids **13-15**, and eight tetrahydroisoquinoline monoterpene glycosides **16-23**, another two types of tetrahydroisoquinoline skeleton alkaloids, showed similar phenotypic profile to tubulosine congeners, indicating the changing of the indole moiety in the molecules abolished the phenotypic effects. The triterpenoid type metabolites **37-44** showed moderate effects on EEA-1 related parameters and much weaker perturbation on the α-tubulin related cytological parameters compared to the tubulosine congeners **1-11**.

A number of bioactive compounds and drugs were tetrahydroisoquinoline skeleton alkaloids.[77,78] Endogenous neurotoxic tetrahydroisoquinoline derivatives such as norsalsolinol continue to be investigated as possible causes for some conditions such as Parkinson's disease.[79-84] As tetrahydroisoquinoline alkaloids, tubulosine congeners **1-11** have moderate effects on α-tubulin in cells from Parkinson's disease patients, while emetine and alangiside analogues **13-23** showed slight effects, suggesting that these compounds may be used as important tools to probe the mechanism and to identify molecular targets for Parkinson's disease.

EXPERIMENTAL SECTION

General Experimental Procedures. Optical rotations were recorded on a JASCO P-1020 polarimeter (10 cm cell). IR, UV and circular dichroism spectra were required on a Bruker Tensor 27 spectrophotometer, a CAMSPEC M501 UV/vis spectrophotometer and a JASCO J-720 spectropolarimeter, respectively. A free and open source software SDAR was used for the analysis and processing of UV and CD data.[85] NMR spectra were recorded in DMSO-d_6 (δ_H 2.50 and δ_C 39.5) or CD_3OD (δ_H 3.31 and δ_C 49.2) at 30 ℃ on a Varian Unity INOVA 600 MHz spectrometer equipped with a triple-resonance cryoprobe or at 25 ℃ on a Bruker Avance HDX 800 MHz spectrometer equipped with a TCI cryoprobe. The low-resolution mass spectrum (LRESIMS) was recorded on a Mariner time of flight (TOF) bio-spectrometer equipped with a Gilson 215 eight probe injector and a Waters LCMS system equipped with a Luna C_{18} column (3 μm, 100 Å, 50 × 4.6 mm), a PDA detector, and a ZQ ESI mass spectrometer. The high-resolution mass spectrum (HRESIMS) was recorded on a Bruker Daltonics SolariX 12 T Fourier transform mass spectrometer. An Edwards Instrument Company Bioline orbital shaker was used for extraction. The HPLC system included a Waters 600 pump fitted with a 996 photodiode array detector and Gilson FC204 fraction collector. A ThermoElectron Betasil C_{18} column (5 μm, 21.2 × 150 mm) and a Phenomenex Luna C_{18} column (5 μm, 10 × 250 mm) were used for semipreparative HPLC. All solvents used for extraction, chromatography, $[\alpha]_D$, IR, UV, CD and MS were Lab-Scan HPLC grade, and the H_2O was Millipore Milli-Q PF filtered.

Plant Material. The plant material of *Alangium villosum* subsp. *tomentosum* (F. Muell.) Bloemb was collected from Kilkivan, Queensland, Australia. Collection and taxonomic identification were undertaken by P. I. Forster from the Queensland Herbarium.

A voucher specimen (AQ606931) has been deposited at the Queensland Herbarium, Brisbane, Australia.

Extraction and Isolation. The air-dried and ground plant of *A. villosum* (20 g) was sequentially extracted with *n*-hexane (250 mL) for 2 h at room temperature. The hexane extract was filtered under gravity and discarded. Then 250 mL of CH_2Cl_2 was added to the biota and extracted for 2 h. The CH_2Cl_2 extract was filtered, and the biota was further extracted with two lots of 250 mL of methanol for 2 h and overnight, successively. All CH_2Cl_2 and MeOH extracts were combined and dried to afford the crude extract. The crude extract was fractionated using C_{18} bonded silica flash column. Four fractions were collected by eluting with stepwise gradients with 0.1% TFA (10% MeOH/90% H_2O, 50% MeOH /50% H_2O, 90% MeOH/10% H_2O and MeOH, respectively). A portion of 50% MeOH/50% H_2O fraction was pre-adsorbed onto cotton and packed dry into a stainless steel cartridge (10 × 30 mm). This cartridge was subsequently chromatographed by HPLC (gradient MeOH/H_2O with 0.1% TFA) using a semipreparative reversed phase Betasil C_{18} column (21.2 mm × 150 mm). Initial isocratic conditions of 20% MeOH were used for 10 min then a linear gradient from 20 to 70% MeOH was performed over 40 min and continued isocratic for 10 min at a flow rate of 9 mL/min. Sixty fractions were collected by 1 min increments over 60 min to afford tubulosine N_{β}^5-oxide (**1**, 1.6 mg, 0.008% dry wt), isotubulosine $N\alpha^5$-oxide (**2**, 0.4 mg, 0.002% dry wt), 9-demethyltubulosine N_{β}^5-oxide (**3**, 0.8 mg, 0.004% dry wt), 9-demethylisotubulosine $N\alpha^5$-oxide (**4**, 0.4 mg, 0.002% dry wt), 1',2'-dehydro-9-demethyltubulosine (**10**, 0.4 mg, 0.002% dry wt), 7',9-*O*-didemethylcephaeline (**13**, 0.8 mg, 0.004% dry wt), 7',9-*O*-didemethylisocephaeline (**14**, 1.2 mg, 0.006% dry wt), 7',9-didemethylpsychotrine (**15**, 0.4 mg, 0.002% dry wt), along with tubulosine and its

analogues (**5**-**9**, **11** and **12**). The 90% MeOH/10% H_2O fraction was chromatographed by HPLC (gradient MeOH/H_2O with 0.1% TFA) using the same semipreparative C_{18} column eluting with 20% MeOH/80% H_2O to 70% MeOH/30% H_2O, which led to the isolation of eight tetrahydroisoquinoline monoterpene glycosides (**16**-**23**), six lignan glycosides (**24**-**29**), one iridoid glycoside (**30**), one secoiridoid glycoside (**31**) and one monoterpene alkaloid (**32**). Purification of the MeOH fraction using the same semipreparative C_{18} column eluting with 60% MeOH/40% H_2O to 100% MeOH resulted in the isolation of two sesquiterpenoids (**33** and **34**), one sesquiterpenoid naphthol (**35**) and its glycoside (**36**), and eight triterpenoids (**37**-**44**).

*Tubulosine N_{β}^{5}-oxide (**1**):* yellowish powder; $[\alpha]_D^{25}$ +11.0 (c 0.100, CH_3OH); UV/Vis λ_{max}^{MeOH} nm (log ε): 205 (4.31), 229 (3.89), 258 (3.51), 279 (3.53), 314 (3.24), 370 (3.06) nm; IR (null): 3420, 2994, 1683, 1515, 1206, 1179, 1033 cm^{-1}; ^{1}H and ^{13}C NMR data (DMSO-d_6), Tables 1 and 2; (+)-LRESIMS *m/z* 492 (100) $[M+H]^+$; (+)-HRESIMS *m/z* 492.2856 ($C_{29}H_{38}N_3O_4$ $[M+H]^+$ requires 492.2857).

*Isotubulosine N_{α}^{5}-oxide (**2**):* yellowish powder; $[\alpha]_D^{25}$ +12.0 (c 0.050, CH_3OH); UV/Vis λ_{max}^{MeOH} nm (log ε): 204 (4.32), 226 (3.88), 258 (3.47), 279 (3.47), 312 (3.15), 366 (2.89); IR (null): 3436, 3000, 1690, 1525, 1442, 1203, 1190, 1025, 1000 cm^{-1}; ^{1}H and ^{13}C NMR data (DMSO-d_6), Tables 1 and 2; (+)-LRESIMS *m/z* 492 (100) $[M+H]^+$; (+)-HRESIMS *m/z* 492.2855 ($C_{29}H_{38}N_3O_4$ $[M+H]^+$ requires 492.2857).

*9-Demethyltubulosine N_{β}^{5}-oxide (**3**):* yellowish powder; $[\alpha]_D^{25}$ +14.0 (c 0.099, CH_3OH); UV/Vis λ_{max}^{MeOH} nm (log ε): 203 (4.27), 221 (3.88), 258 (3.43), 278 (3.43), 311 (3.13), 369 (2.97); IR (null): 3376, 2979, 1684, 1526, 1471, 1203, 1175, 1026, 1000 cm^{-1};

^{1}H and ^{13}C NMR data (DMSO-d_6), Tables 1 and 2; (+)-LRESIMS *m/z* 478 (100) $[M+H]^+$; (+)-HRESIMS *m/z* 478.2715 ($C_{29}H_{38}N_3O_4$ $[M+H]^+$ requires 478.2700).

*9-Demethylisotubulosine N_α^5-oxide (**4**):* yellowish powder; $[\alpha]_D^{25}$ +14.0 (c 0.074, CH_3OH); UV/Vis λ_{max}^{MeOH} nm (log ε): 203 (4.27), 221 (3.88), 258 (3.43), 278 (3.43), 311 (3.13), 369 (2.97); IR (null): 3376, 2979, 1684, 1526, 1471, 1203, 1175, 1026, 1000 cm^{-1}; ^{1}H and ^{13}C NMR data (DMSO-d_6), Tables **1** and **2**; (+)-LR-ESI-MS *m/z* 478 (100) $[M+H]^+$; (+)-HRESIMS *m/z* 478.2698 ($C_{29}H_{38}N_3O_4$ $[M+H]^+$ requires 478.2700).

*1',2'-Dehydro-9-demethyltubulosine (**10**):* yellowish powder; $[\alpha]_D^{25}$ +13.7 (c 0.044, CH_3OH); UV/Vis λ_{max}^{MeOH} nm (log ε): 230 (3.80), 283 (3.39), 375 (3.44); IR (null): 3440, 2981, 1686, 1522, 1441, 1202, 1181, 1023, 1000 cm^{-1}; ^{1}H and ^{13}C NMR data (DMSO-d_6), Tables 1 and 2; (+)-LRESIMS *m/z* 478 (100) $[M+H]^+$; (+)-HRESIMS *m/z* 460.2596 ($C_{28}H_{34}N_3O_3$ $[M+H]^+$ requires 460.2595).

*7',9-O-didemethylcephaeline (**13**):* yellowish powder; $[\alpha]_D^{25}$ +11.7 (c 0.085, CH_3OH); UV/Vis λ_{max}^{MeOH} nm (log ε): 206 (4.37), 230 (3.66), 288 (3.39); IR (null): 3237, 3000, 1677, 1533, 1468, 1204, 1179 cm^{-1}; ^{1}H and ^{13}C NMR data (DMSO-d_6), Table 3; (+)-LRESIMS *m/z* 439 (100) $[M+H]^+$; (+)-HRESIMS *m/z* 439.2597 ($C_{26}H_{35}N_2O_4$ $[M+H]^+$ requires 439.2591).

*7',9-O-didemethylisocephaeline (**14**):* yellowish powder; $[\alpha]_D^{25}$ +12.2 (c 0.180, CH_3OH); UV/Vis λ_{max}^{MeOH} nm (log ε): 203 (4.34), 230 (3.99), 285 (3.64); IR (null): 3446, 3000, 1685, 1533, 1468, 1204, 1179, 1028, 1000 cm^{-1}; ^{1}H and ^{13}C NMR data (DMSO-d_6),

Tables 3; (+)-LRESIMS *m/z* 439 (100) $[M+H]^+$; (+)-HRESIMS *m/z* 439.2610 ($C_{26}H_{35}N_2O_4$ $[M+H]^+$ requires 439.2591).

*7',9-Didemethylpsychotrine (**15**):* yellowish powder; $[\alpha]_D^{25}$ +11.5 (c 0.085, CH_3OH); UV/Vis λ_{max}^{MeOH} nm (log ε): 203 (4.34), 230 (3.82), 282 (3.36), 369 (3.55); IR (null): 3376, 2941, 1680, 1445, 1318, 1203, 1175 cm^{-1}; ^1H and ^{13}C NMR data (DMSO-d_6), Tables 3; (+)-LRESIMS *m/z* 437 (100) $[M+H]^+$; (+)-HRESIMS *m/z* 437.2436 ($C_{26}H_{35}N_2O_4$ $[M+H]^+$ requires 437.2435).

Biological Assay. Compounds were transferred into two optically clear bottom CellCarrier 384-well plates (PerkinElmer). hONS cells from the Parkinson's disease cell line C1 200 08 0013 were added to each well at a density of 1,350 cells per well in 50 µL of growth medium (DMEM/F12, 10% FBS) leading to a final concentration of 10 µM (0.6% DMSO) for each compound. 0.6% DMSO was used as negative control. The cells were incubated for 24 h at 37 ^oC under 5% CO_2.

Cell Staining. After 24 h of incubation, the medium was aspirated and one 384-well plate was treated with MitoTracker Orange CMTMRos (Invitrogen) (400 nM) for 30 min at 37 ^oC under 5% CO_2. The second 384-well plate was treated with LysoTracker Red DND-99 (Invitrogen) (100 nM) for 1 h at 37 ^oC under 5% CO_2. Cells were fixed in 4% paraformaldehyde for 5 min at room temperature (rt). Cells were washed twice with phosphate-buffered saline (PBS, Sigma-Aldrich) and treated with 3% goat serum (Sigma-Aldrich) and 0.2% Triton X-100 (Sigma-Aldrich) in PBS for 45 min at rt. Plates were incubated with primary antibodies. Mouse anti-α-tubulin 1/4000 (Sigma-Aldrich) and rabbit anti-LC3b 1/335 (Sigma-Aldrich) were added to the plate already treated with

MitoTracker and mouse anti-EEA1 1/200 (Sigma-Aldrich) was added to the plate previously treated with LysoTracker. Plates were incubated at rt for 1 h then washed twice with PBS. Secondary antibodies goat anti-mouse Alexa-647 1/500 (Invitrogen) and goat anti-rabbit Alexa-488 1/500 (Invitrogen) were added to the first plate and goat anti-mouse Alexa-488 1/500 (Invitrogen) was added to the second plate for 30 min at rt. Cells were washed twice with PBS and stained with 4',6'-diamidino-2-phenylindole 1/5000 (Dapi, Invitrogen) and with CellMask Deep Red 1/5000 (Invitrogen) for the plate treated with LysoTracker and incubated for 10 min at rt. Cells were washed twice with PBS and plates were stored in the dark at 4 ^{o}C with 25 μL of PBS/well.

Imaging and Image Analysis Plates were imaged automatically using Operetta (PerkinElmer), a high content imaging system using a 20× high numerical aperture objective lens. Six images per well for each wavelength were collected. Individual cell segmentation was done using the Harmony software and measurements for each cell were performed generating 38 parameters from six dyes: Dapi, *α*-tubulin staining, MitoTracker Orange CMTMRos, LC3b staining, LysoTracker Red DND-99 and EEA1 staining. The normality of the data was checked for each parameter and a $\log_2$ transform was made when required in order to perform a *t*-test to identify significant changes when compared to DMSO. The log2 compound/DMSO ratio was clustered using Cluster 3.0 software (uncentered correlation and centroid linkage) and analyzed using Java TreeView.

ASSOCIATED CONTENT

Supporting Information.

The Supporting Information is available free of charge on the ACS Publications website at

DOI:

1D and 2D NMR spectra for compounds **1-4**, **10**, and **13-15**.

AUTHOR INFORMATION

Corresponding Author

*Tel: +64 7 3735 6009. E-mail: r.quinn@griffith.edu.au.

Notes

The authors declare no competing financial interest.

ACKNOWLEDGEMENTS

This research was supported by Australian Research Council *Discovery Projects* funding (project number DP130102400). D. W. thanks Griffith University for a GUIPRS scholarship.

REFERENCES

(1) Wang, D.; Feng, Y.; Murtaza, M.; Wood, S.; Mellick, G.; Hooper, J. N. A.; Quinn, R. J. *J. Nat. Prod.* **2016**.

(2) Harvey, A. L.; Edrada-Ebel, R.; Quinn, R. J. *Nat. Rev. Drug Discov.* **2015**, *14*, 111-129.

(3) Camp, D.; Davis, R. A.; Campitelli, M.; Ebdon, J.; Quinn, R. J. *J. Nat. Prod.* **2012**, *75*, 72-81.

(4) Feng, Y.; Campitelli, M.; Davis, R. A.; Quinn, R. J. *Mar. Drugs* **2014**, *12*, 1169-1184.

(5) Matigian, N.; Abrahamsen, G.; Sutharsan, R.; Cook, A. L.; Vitale, A. M.; Nouwens, A.; Bellette, B.; An, J.; Anderson, M.; Beckhouse, A. G. *Dis. Model. Mech.* **2010**, *3*, 785-798.

(6) Xiang, Q.-Y. J.; Thomas, D. T.; Xiang, Q. P. *Mol. Phylogenet. Evol.* **2011**, *59*, 123-138.

(7) Feng, C.-M.; Manchester, S. R.; Xiang, Q.-Y. *Mol. Phylogenet. Evol.* **2009**, *51*, 201-214.

(8) Itoh, A.; Tanahashi, T.; Nagakura, N. *J. Nat. Prod.* **1995**, *58*, 1228-1239.

(9) Govindarajalu, E. In *Proceedings of the Indian Academy of Sciences-Section B*; Springer: 1972; Vol. 75, p 221-230.

(10) Dictionary of Natural Products; Chapman and Hall/CRC Press: London, UK, 2005 (http://www.crcpress.com).

(11) Kumar, R.; Hemalatha, S. *J. Chem. Pharm. Res.* **2011**, *3*, 259-267.

(12) Jain, V. C.; Patel, N.; Shah, D. P.; Patel, P. K.; Joshi, B. H. *Global J. Pharmacol.* **2010**, *4*, 13-18.

(13) Pandian, M.; Banu, G.; Kumar, G. *Indian J. Pharmacol.* **2006**, *38*, 203.

(14) Murugan, V.; Shareef, H.; Ramasarma, G.; Ramanathan, M.; Suresh, B. *Indian J. Pharmacol.* **2000**, *32*, 388.

(15) Jubie, S.; Jawahar, N.; Koshy, R.; Gowramma, B.; Murugan, V.; Suresh, B. *Rasayan J. Chem* **2008**, *1*, 433-436.

(16) Kumar, R.; Pate, D. K.; Prasad, S. K.; Sairam, K.; Hemalatha, S. *Asian Pac. J. Trop. Med.* **2011**, *4*, 904-909.

(17) Kalarani, D.; Dinakar, A.; Senthilkumar, N. *Asian J. Pharm. Clin. Res.* **2011**, *4*, 131-133.

(18) Mosaddik, M. A.; Kabir, K. E.; Hassan, P. *Fitoterapia* **2000**, *71*, 447-449.

(19) Natarajan, E.; Kumar, S. S.; Xavier, T. F.; Selvi, V. K. **2004**.

(20) Haque, I. E. *Int. J. Cancer Res.* **2011**, *7*, 254-262.

(21) Wuthi-udomlert, M.; Prathanturarug, S.; Wongkrajang, Y. *Southeast Asian J. Trop.*

Med. Public Health **2002**, *33*, 152-154.

(22) Ma, J.; Hecht, S. M. *Chem. Commun.* **2004**, 1190-1191.

(23) Xu, Y.-m.; Deng, J.-Z.; Ma, J.; Chen, S.-N.; Marshall, R.; Jones, S. H.; Johnson, R. K.; Hecht, S. M. *Biorg. Med. Chem.* **2003**, *11*, 1593-1596.

(24) Rao, K. N.; Venkatachalam, S. R. *Biorg. Med. Chem.* **1999**, *7*, 1105-1110.

(25) Ahad, H. A.; Sreeramulu, J.; Budideti, K. K. R.; Pulaganti, M.; Battula, S. P.; More, S. *TBAP* **2012**, *2*, 99-103.

(26) Nagakura, N.; Höfle, G.; Zenk, M. H. *J. Chem. Soc., Chem. Commun.* **1978**, 896-898.

(27) Itoh, A.; Tanahashi, T.; Nagakura, N. *Phytochemistry* **1991**, *30*, 3117-3123.

(28) De-Eknamkul, W.; Ounaroon, A.; Tanahashi, T.; Kutchan, T. M.; Zenk, M. H. *Phytochemistry* **1997**, *45*, 477-484.

(29) Brauchli, P.; Deulofeu, V.; Budzikiewicz, H.; Djerassi, C. *J. Am. Chem. Soc.* **1964**, *86*, 1895-1896.

(30) Ma, W.-W.; Anderson, J.; McKenzie, A.; Byrn, S.; McLaughlin, J.; Hudson, M. *J. Nat. Prod.* **1990**, *53*, 1009-1014.

(31) Ohba, M.; Hayashi, M.; Fujii, T. *Chem. Pharm. Bull.* **1985**, *33*, 3724-3730.

(32) Ohba, M.; Hayashi, M.; Fujii, T. *Heterocycles* **1980**, *14*, 299-302.

(33) Popelak, A.; Haack, E.; Spingler, H. *Tetrahedron Lett.* **1966**, *7*, 1081-1085.

(34) Fujii, T.; Ohba, M. *Chem. Pharm. Bull.* **1985**, *33*, 4314-4319.

(35) Battersby, A. R.; Merchant, J. R.; Ruveda, E. A.; Salgar, S. S. *Chem. Commun. (London)* **1965**, 315-317.

(36) Kametani, T.; Suzuki, Y.; Ihara, M. *Can. J. Chem.* **1979**, *57*, 1679-1681.

(37) Itoh, A.; Ikuta, Y.; Tanahashi, T.; Nagakura, N. *J. Nat. Prod.* **2000**, *63*, 723-725.

(38) Ali, E.; Sinha, R.; Achari, B.; Pakrashi, S. *Heterocycles* **1982**, *19*, 2301-2304.

(39) FURL, T.; Ohba, M.; Ali, E.; Suzuki, H.; Sakaguchi, J. *Chem. Pharm. Bull.* **1987**, *35*, 2755-2760.

(40) Shoeb, A.; Raj, K.; Kapil, R. S.; Popli, S. P. *J. Chem. Soc., Perkin Trans. 1* **1975**, 1245-1248.

(41) Itoh, A.; Tanahashi, T.; Nagakura, N.; Nayeshiro, H. *Phytochemistry* **1994**, *36*, 383-387.

(42) Itoh, A.; Tanahashi, T.; Nagakura, N. *Phytochemistry* **1996**, *41*, 651-656.

(43) Itoh, A.; Tanahashi, T.; Tabata, M.; Shikata, M.; Kakite, M.; Nagai, M.; Nagakura, N. *Phytochemistry* **2001**, *56*, 623-630.

(44) Tanahashi, T.; Kobayashi, C.; Itoh, A.; Nagakura, N.; Inoue, K.; Kuwajima, H.; Wu, H.-X. *Chem. Pharm. Bull.* **2000**, *48*, 415-419.

(45) Otsuka, H.; Hirata, E.; Shinzato, T.; Takeda, Y. *Chem. Pharm. Bull.* **2000**, *48*, 1084-1086.

(46) Achenbach, H.; Löwel, M.; Waibel, R.; Gupta, M.; Solis, P. *Planta Med.* **1992**, *58*, 270-272.

(47) Ono, M.; Mishima, K.; Yamasaki, T.; Masuoka, C.; Okawa, M.; Kinjo, J.; Ikeda, T.; Nohara, T. *J. Nat. Med.* **2009**, *63*, 86-90.

(48) Ohashi, K.; Watanabe, H.; Okumura, Y.; Uji, T.; Kitagawa, I. *Chem. Pharm. Bull.* **1994**, *42*, 1924-1926.

(49) Boros, C. A.; Stermitz, F. R. *J. Nat. Prod.* **1991**, *54*, 1173-1246.

(50) Zhou, Y.; Di, Y. T.; Gesang, S.; Peng, S. L.; Ding, L. S. *Helv. Chim. Acta* **2006**, *89*, 94-102.

(51) Lambert, L. K.; Ross, B. P.; Deseo, M. A.; Garson, M. J. *Aust. J. Chem.* **2011**, *64*, 489-494.

(52) Pailee, P.; Prachyawarakorn, V.; Ruchirawat, S.; Mahidol, C. *Chem. Asian J.* **2015**, *10*, 910-914.

(53) Zhang, Y.; Liu, Y.-B.; Li, Y.; Ma, S.-G.; Li, L.; Qu, J.; Zhang, D.; Chen, X.-G.; Jiang, J.-D.; Yu, S.-S. *J. Nat. Prod.* **2013**, *76*, 1058-1063.

(54) Stipanovic, R. D.; Greenblatt, G. A.; Beier, R. C.; Bell, A. A. *Phytochemistry* **1981**, *20*, 729-730.

(55) Otsuka, H.; Yao, M.; Hirata, E.; Takushi, A.; Takeda, Y. *Phytochemistry* **1996**, *41*, 1351-1355.

(56) Pailee, P.; Prachyawarakorn, V.; Mahidol, C.; Ruchirawat, S.; Kittakoop, P. *Eur. J. Org. Chem.* **2011**, *2011*, 3809-3814.

(57) Macías, F. A.; Simonet, A. M.; Galindo, J. C. *J. Chem. Ecol.* **1997**, *23*, 1781-1803.

(58) Zhu, W.; Shen, Y.; Hong, X.; Zuo, G.; Yang, X.; Hao, X. *Acta Botanica Sinica* **2001**, *44*, 354-358.

(59) Uddin, G.; Waliullah, B. S. S.; Alam, M.; Sadat, A.; Ahmad, A.; Uddin, A. *Middle East J. Sci. Res.* **2011**, *8*, 85-91.

(60) Fujioka, T.; Kashiwada, Y.; Kilkuskie, R. E.; Cosentino, L. M.; Ballas, L. M.; Jiang, J. B.; Janzen, W. P.; Chen, I.-S.; Lee, K.-H. *J. Nat. Prod.* **1994**, *57*, 243-247.

(61) Denisenko, M.; Samoshina, N.; Denisenko, V.; Dmitrenok, P. *Chem. Nat. Compd.* **2011**, *47*, 741-748.

(62) Bastos, D. Z.; Pimentel, I. C.; de Jesus, D. A.; de Oliveira, B. H. *Phytochemistry* **2007**, *68*, 834-839.

(63) González, A. G.; Amaro, J.; Fraga, B. M.; Luis, J. G. *Phytochemistry* **1983**, *22*, 1828-1830.

(64) Boryczka, S.; Michalik, E.; Kusz, J.; Nowak, M.; Chrobak, E. *Acta Crystallogr. Sect. Sect. E: Struct. Rep. Online* **2013**, *69*, o795-o796.

(65) McArdle, B. M.; Campitelli, M. R.; Quinn, R. J. *J. Nat. Prod.* **2006**, *69*, 14-17.

(66) Kellenberger, E.; Hofmann, A.; Quinn, R. J. *Nat. Prod. Rep.* **2011**, *28*, 1483-1492.

(67) Fujii, T.; Kogen, H.; Ohba, M. *Tetrahedron Lett.* **1978**, *19*, 3111-3114.

(68) Atsuko, I.; Tanahash, T.; Nagakura, N. *Chem. Pharm. Bull.* **1994**.

(69) Fujii, T.; Ohba, M.; Hatakeyama, H. *Chem. Pharm. Bull.* **1987**, *35*, 2355-2359.

(70) DeAngelis, G.; Wildman, W. *Tetrahedron* **1969**, *25*, 5099-5112.

(71) Snatzke, G.; Wollenberg, G.; Hrbek, J.; Šantavý, F.; Blaha, K.; Klyne, W.; Swan, R. *Tetrahedron* **1969**, *25*, 5059-5086.

(72) Muhammad, I.; Dunbar, D. C.; Khan, S. I.; Tekwani, B. L.; Bedir, E.; Takamatsu, S.; Ferreira, D.; Walker, L. A. *J. Nat. Prod.* **2003**, *66*, 962-967.

(73) Wiegrebe, W.; Kramer, W. J.; Shamma, M. *J. Nat. Prod.* **1984**, *47*, 397-408.

(74) Snatzke, G. *Angewandte Chemie International Edition in English* **1968**, *7*, 14-25.

(75) Quinn, R. J.; Carroll, A. R.; Pham, N. B.; Baron, P.; Palframan, M. E.; Suraweera, L.; Pierens, G. K.; Muresan, S. *J. Nat. Prod.* **2008**, *71*, 464-468.

(76) Instant JChem, version 15.10.26.10; ChemAxon Kft: Budapest, Hungary, 2015.

(77) Mitchinson, A.; Nadin, A. *J. Chem. Soc., Perkin Trans. 1* **2000**, 2862-2892.

(78) Scott, J. D.; Williams, R. M. *Chem. Rev.* **2002**, *102*, 1669-1730.

(79) Kotake, Y.; Tasaki, Y.; Makino, Y.; Ohta, S.; Hirobe, M. *J. Neurochem.* **1995**, *65*, 2633-2638.

(80) McNaught, K. S. P.; Carrupt, P.-A.; Altomare, C.; Cellamare, S.; Carotti, A.; Testa, B.; Jenner, P.; Marsden, C. D. *Biochem. Pharmacol.* **1998**, *56*, 921-933.

(81) Lorenc-Koci, E.; ŚmiaŁowska, M.; Antkiewicz-Michaluk, L.; GoŁembiowska, K.; Bajkowska, M.; Wolfarth, S. *Neuroscience* **1999**, *95*, 1049-1059.

(82) Storch, A.; Ott, S.; Hwang, Y.-I.; Ortmann, R.; Hein, A.; Frenzel, S.; Matsubara, K.; Ohta, S.; Wolf, H.-U.; Schwarz, J. *Biochem. Pharmacol.* **2002**, *63*, 909-920.

(83) Lorenc-Koci, E.; Antkiewicz-Michaluk, L.; Kamińska, A.; Lenda, T.; Zięba, B.; Wierońska, J.; Śmiałowska, M.; Schulze, G.; Rommelspacher, H. *Neuroscience* **2008**, *156*, 973-986.

(84) Kobayashi, H.; Fukuhara, K.; Tada-Oikawa, S.; Yada, Y.; Hiraku, Y.; Murata, M.; Oikawa, S. *J. Neurochem.* **2009**, *108*, 397-407.

(85) Weeratunga, S.; Hu, N.-J.; Simon, A.; Hofmann, A. *BMC Bioinformatics* **2012**, *13*, 201.

Supporting Information for Chapter Four

Supporting information for

A Grand Challenge (Ⅲ): Unbiased Phenotypic Function of Metabolites from *Alangium villosum* against Parkinson's Disease

Dongdong Wang,[†] Yunjiang Feng,[†] Mariyam Murtaza,[†] Stephen A. Wood,[†] George D. Mellick,[†] Paul I. Froster[‡] and Ronald J. Quinn[†,*]

[†]Eskitis Institute for Drug Discovery, Griffith University, Brisbane, QLD 4111, Australia.

[‡]Queensland Herbarium, Brisbane Botanic Gardens, Brisbane, QLD 4066, Australia

Corresponding author contact details: Tel: +61-7-37356006. Fax: +61-7-37356001. E-mail: r.quinn@griffith.edu.au

List of supporting information

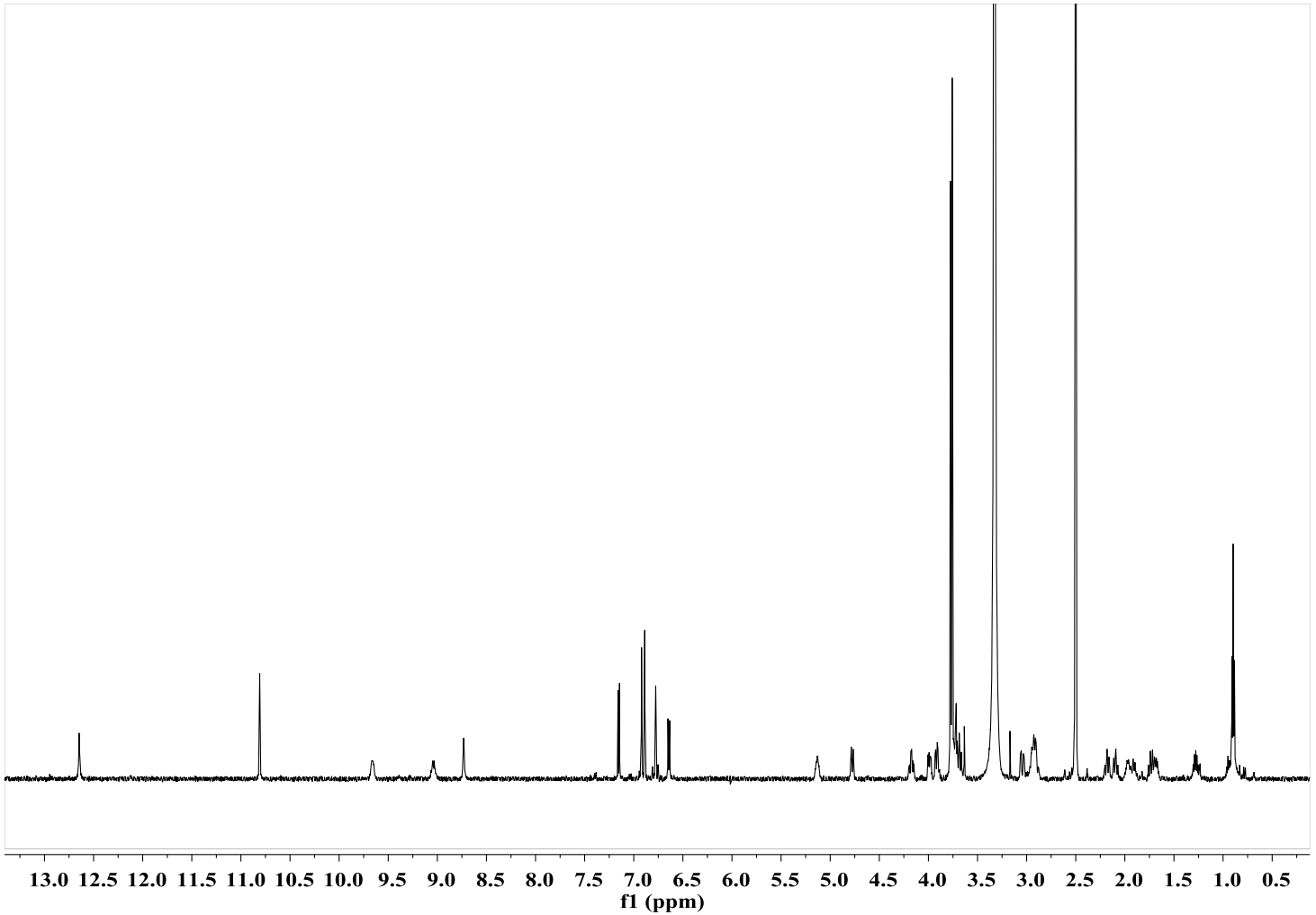

Figure S1. ^{1}H NMR spectrum of compound **1** in DMSO-d_6

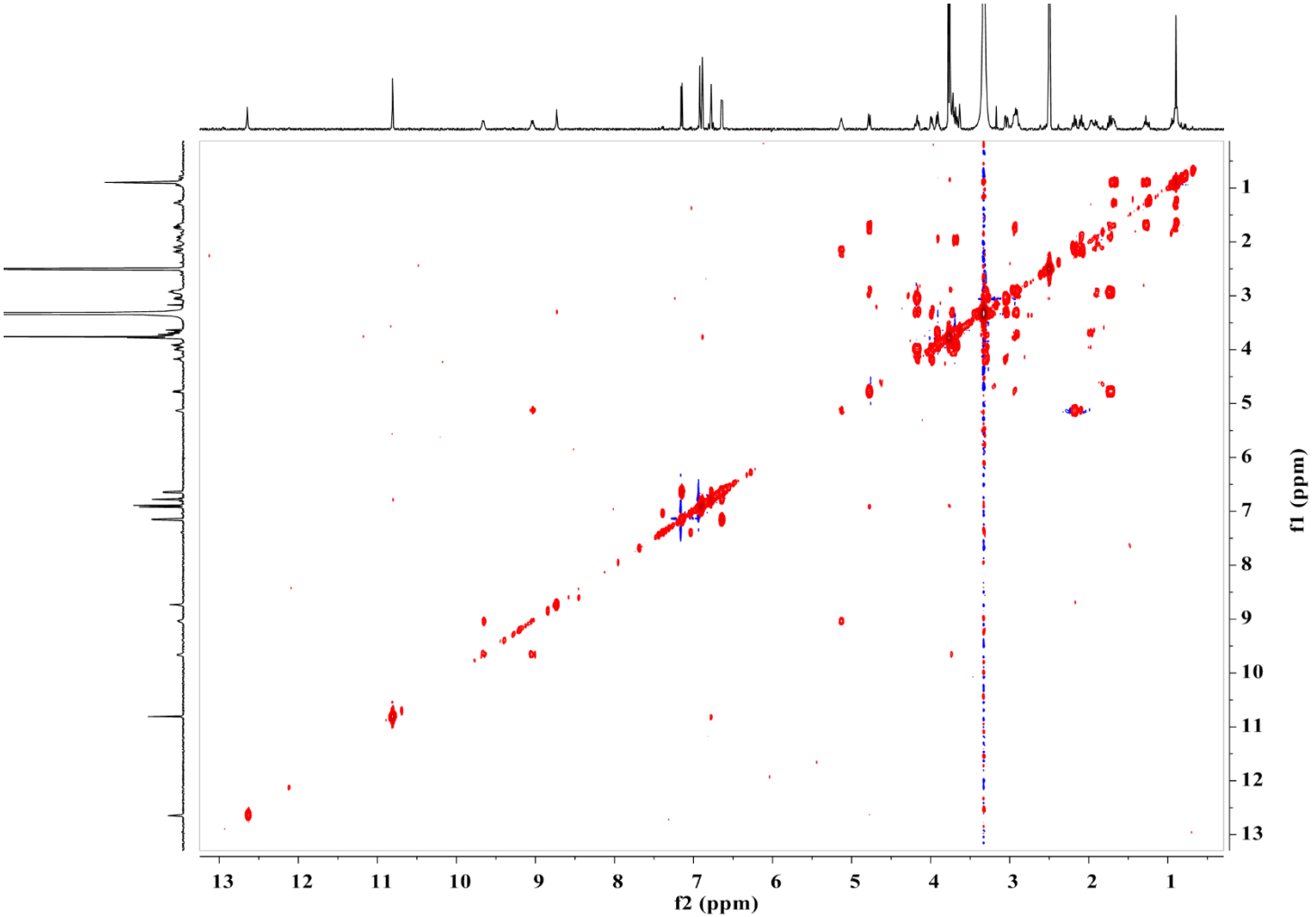

Figure S2. COSY spectrum of compound **1** in DMSO-d_6

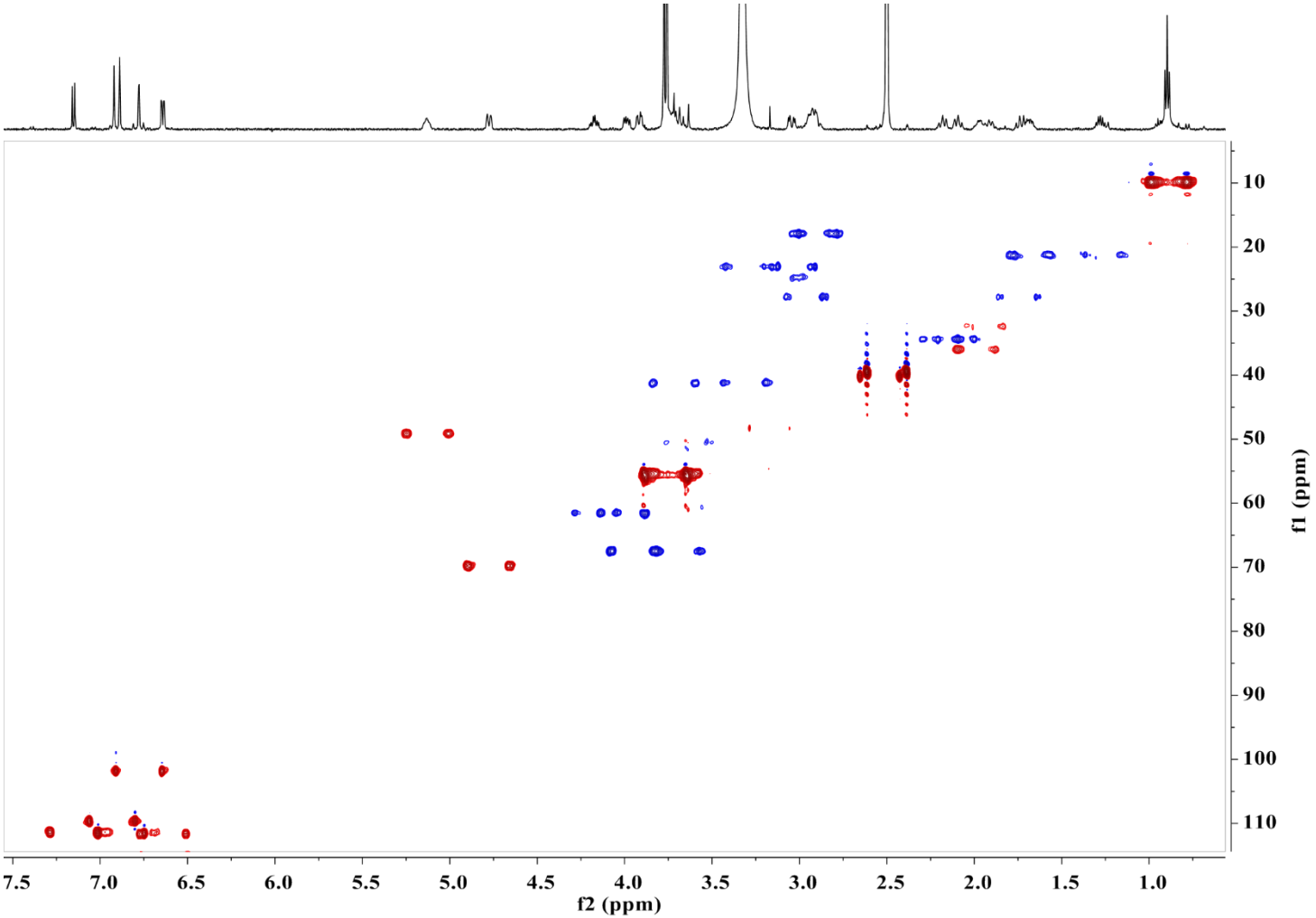

Figure S3. HSQC spectrum of compound **1** in DMSO-d_6

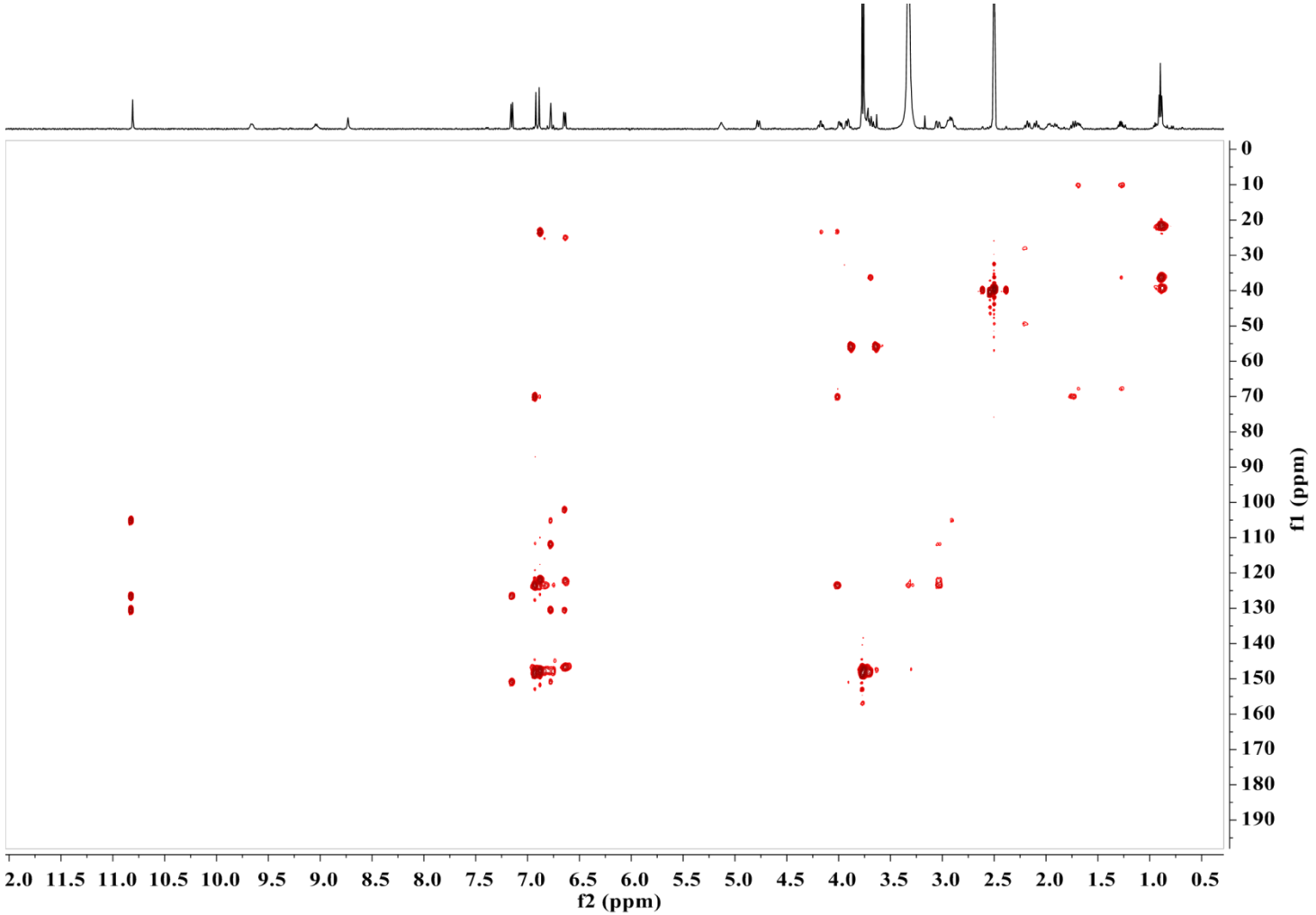

Figure S4. HMBC spectrum of compound **1** in DMSO-d_6

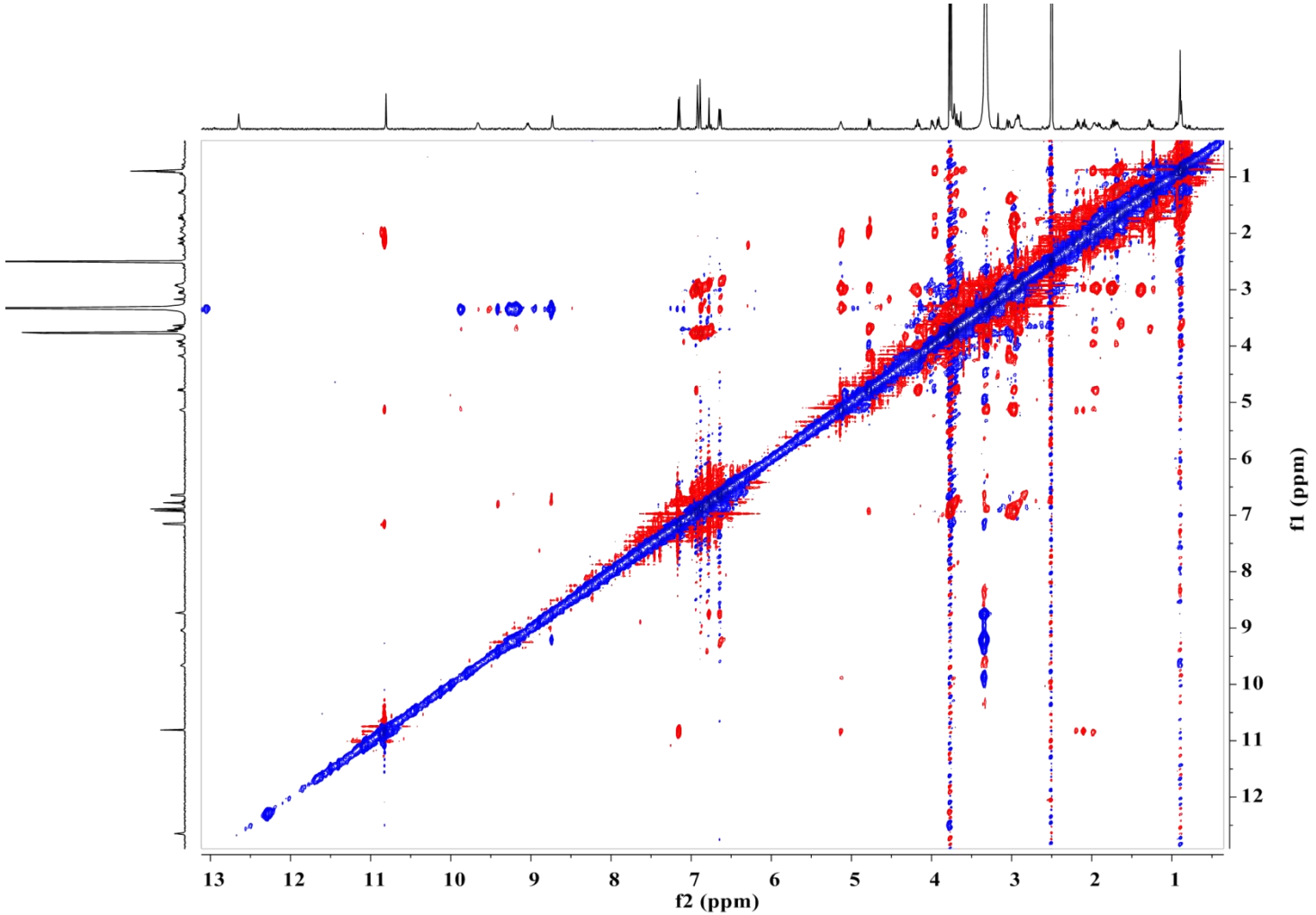

Figure S5. ROESYspectrum of compound **1** in DMSO-d_6

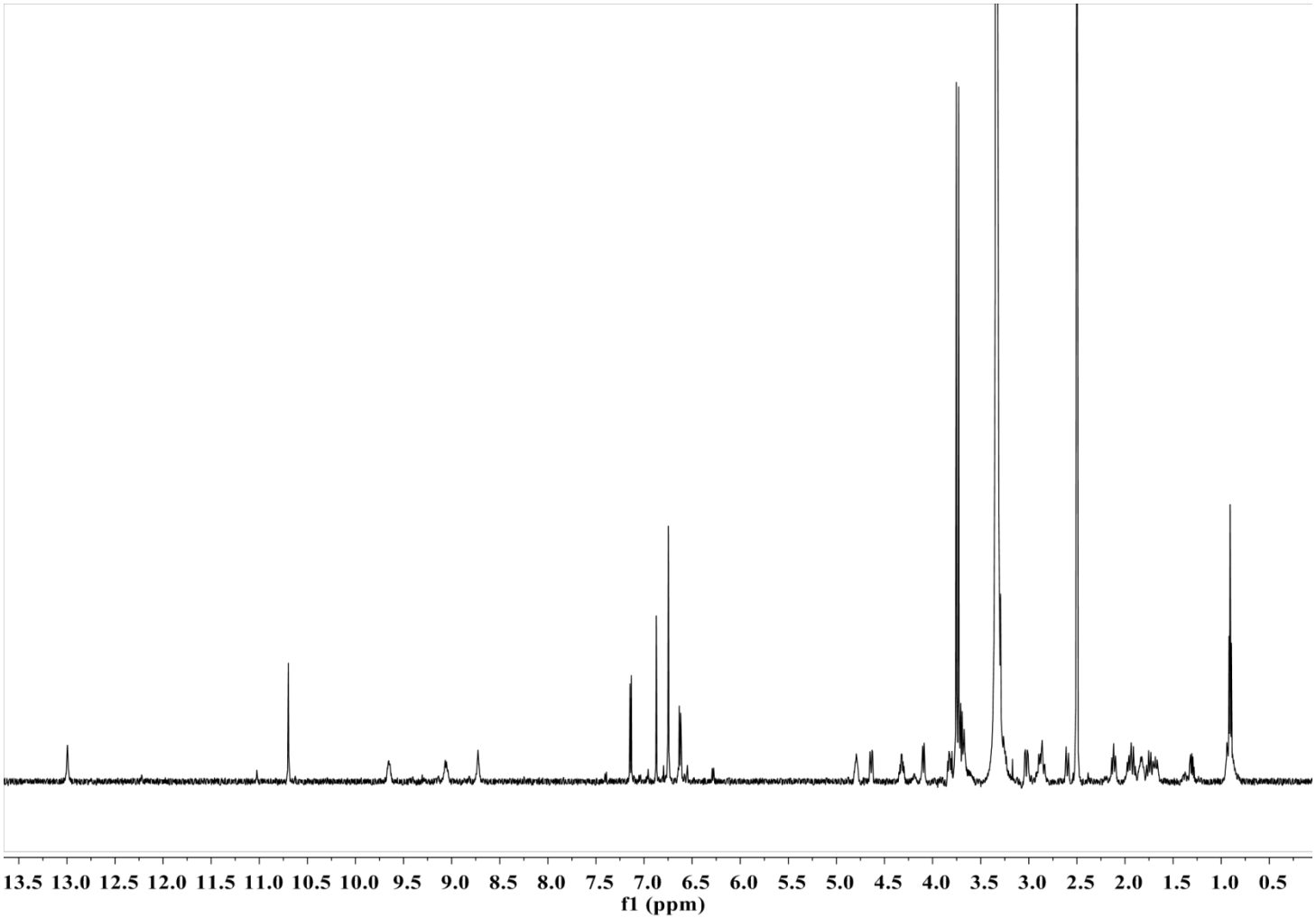

Figure S6. ^{1}H NMR spectrum of compound **2** in DMSO-d_6

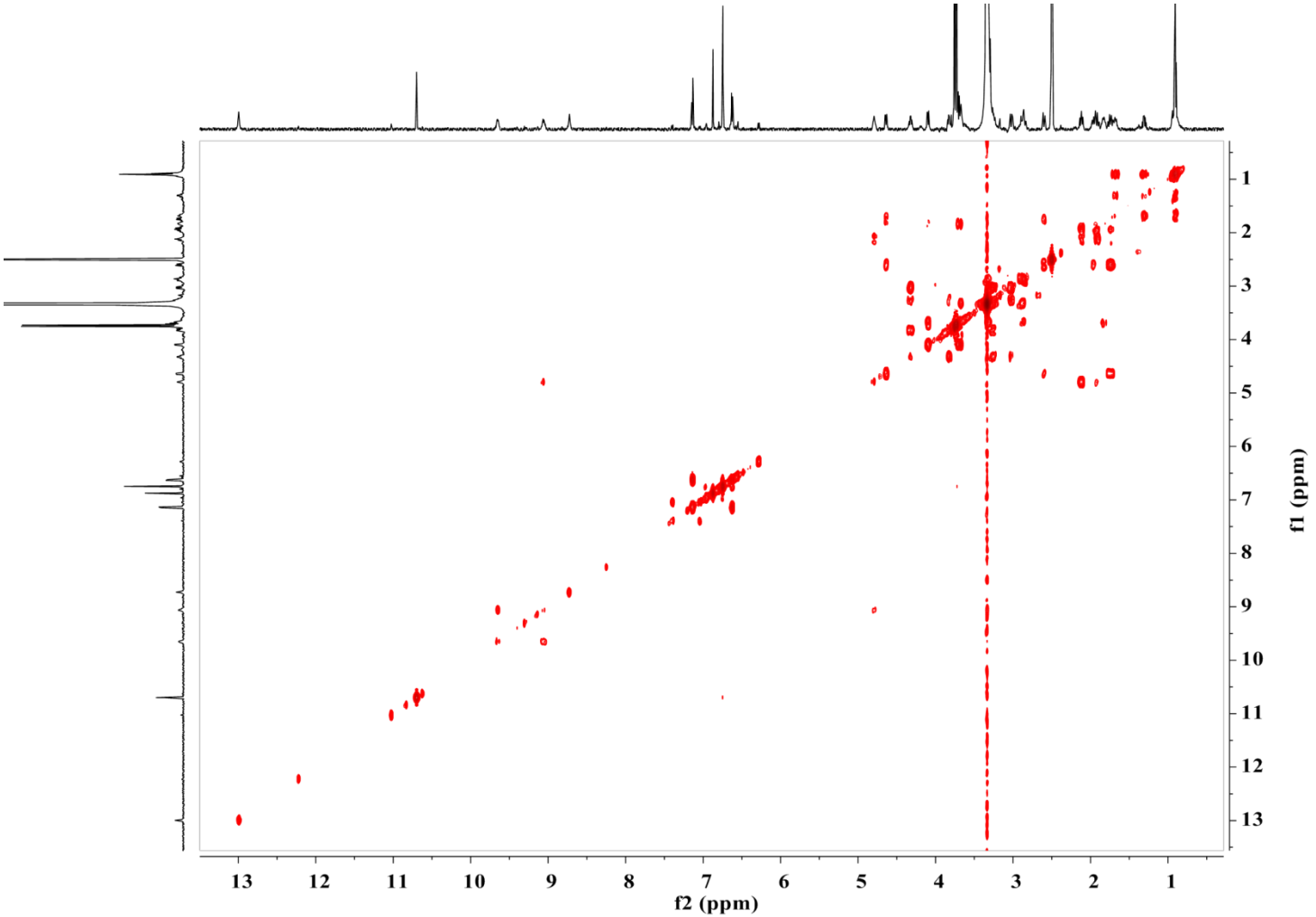

Figure S7. COSY spectrum of compound **2** in DMSO-d_6

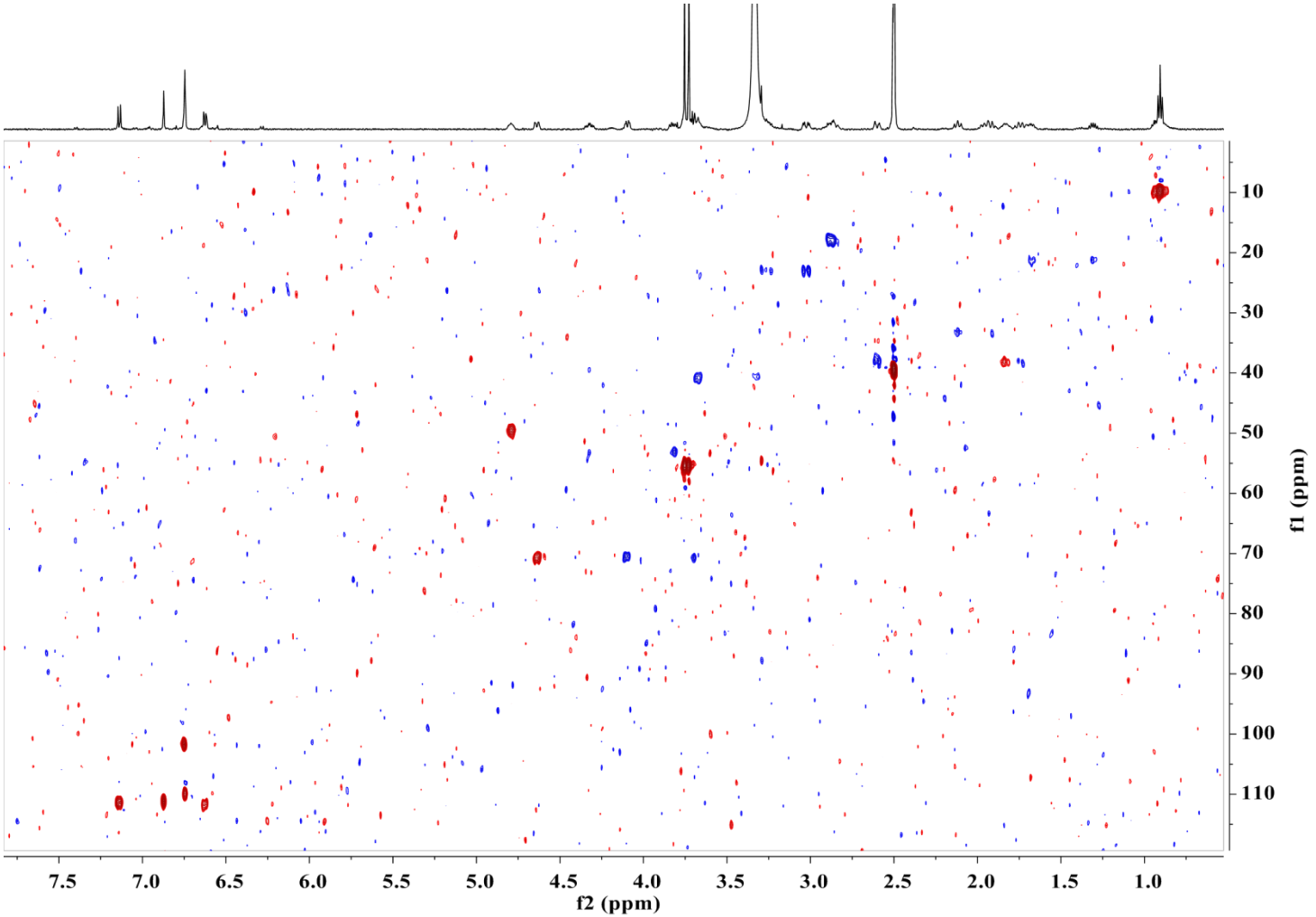

Figure S8. HSQC spectrum of compound **2** in DMSO-d_6

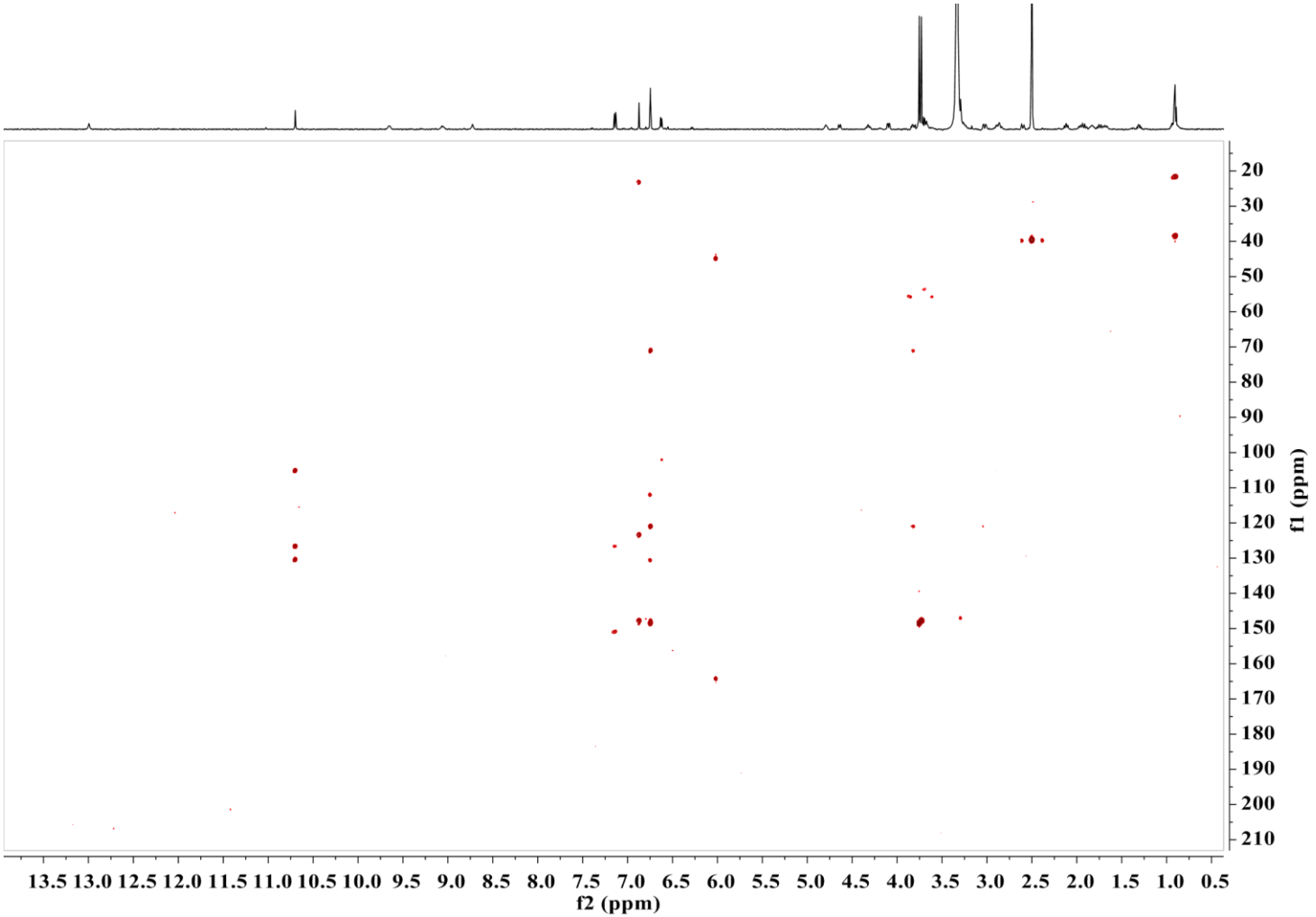

Figure S9. HMBC spectrum of compound **2** in DMSO-d_6

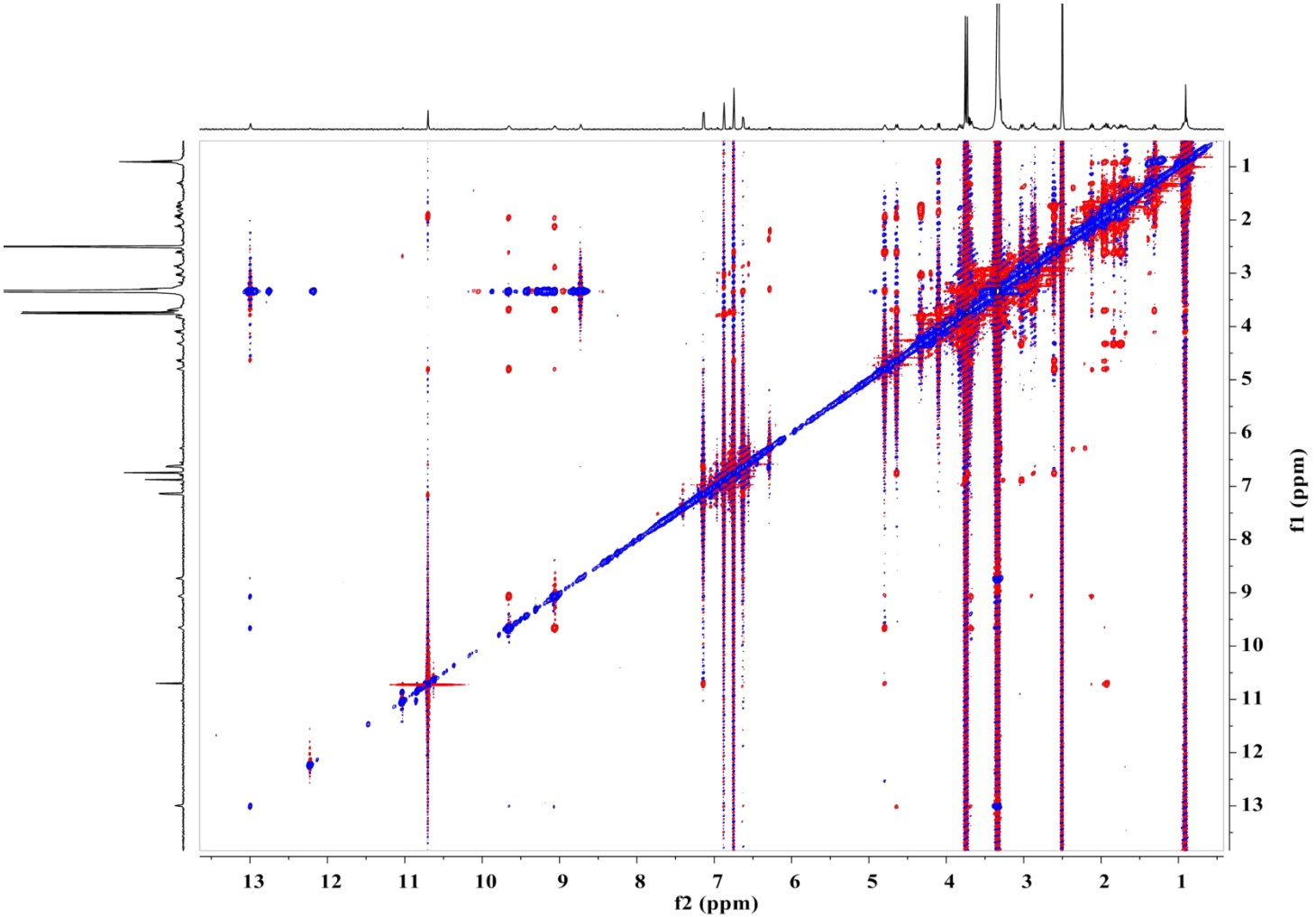

Figure S10. ROESYspectrum of compound **2** in DMSO-d_6

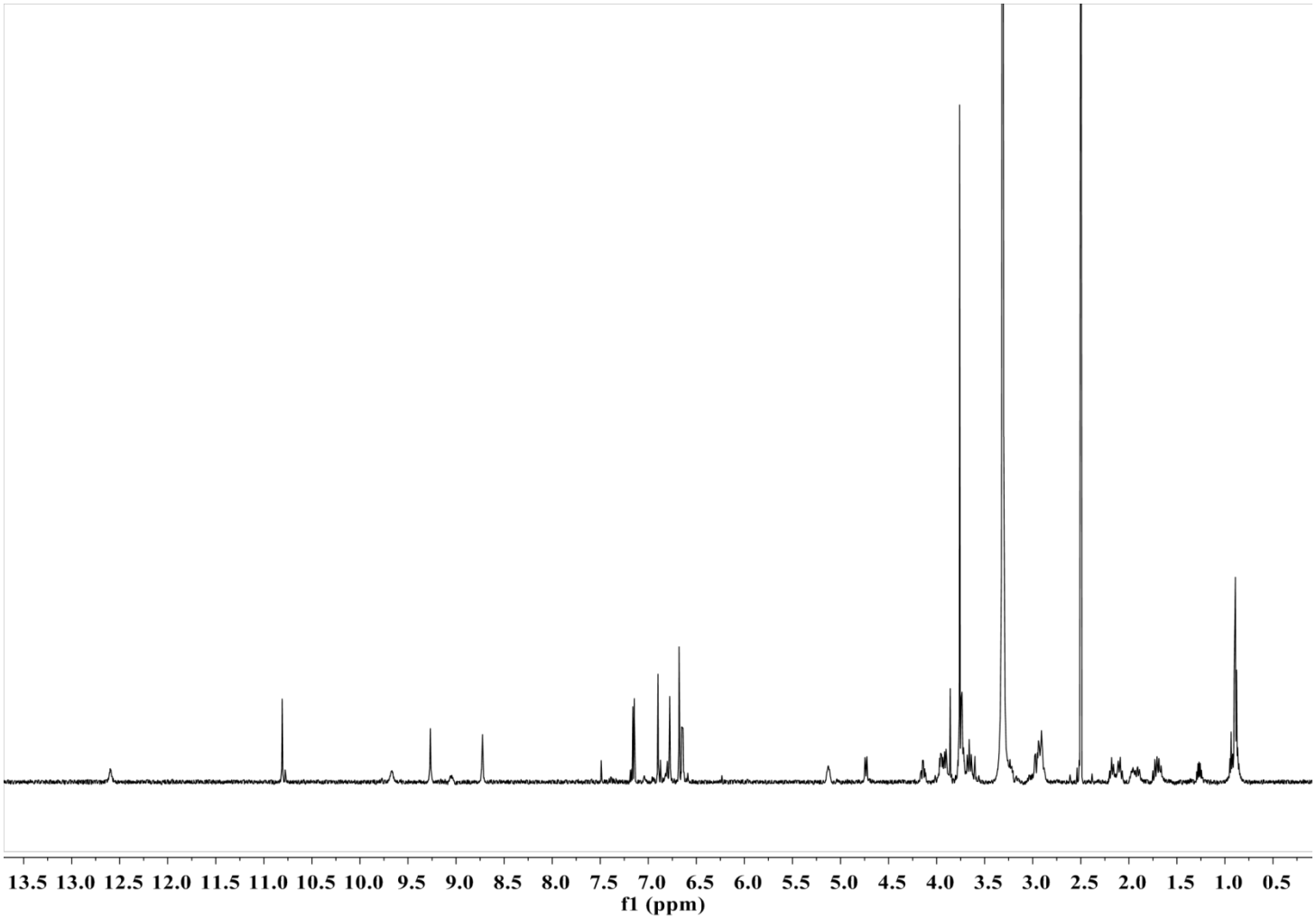

Figure S11. ^{1}H NMR spectrum of compound **3** in DMSO-d_6

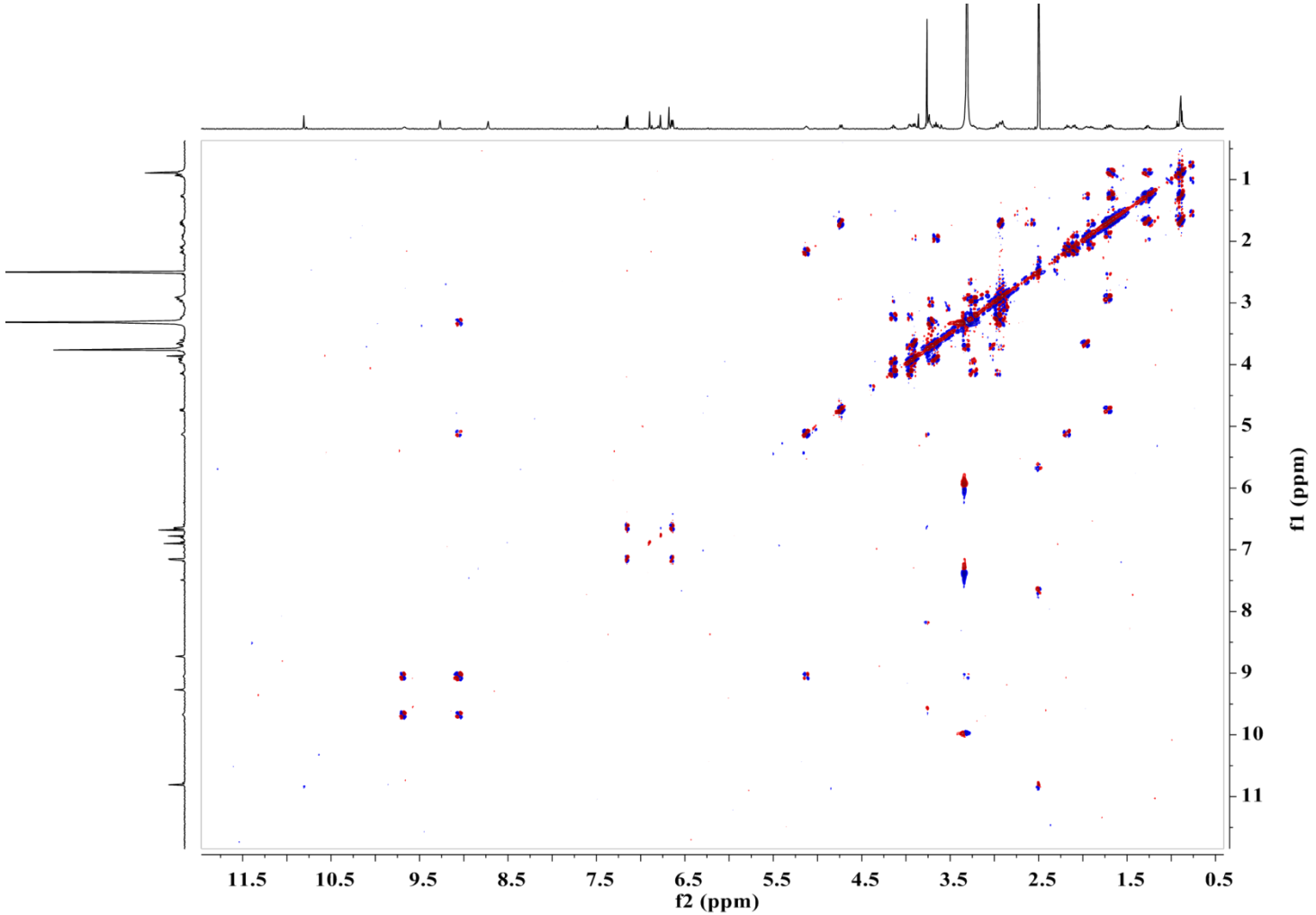

Figure S12. COSY spectrum of compound **3** in DMSO-d_6

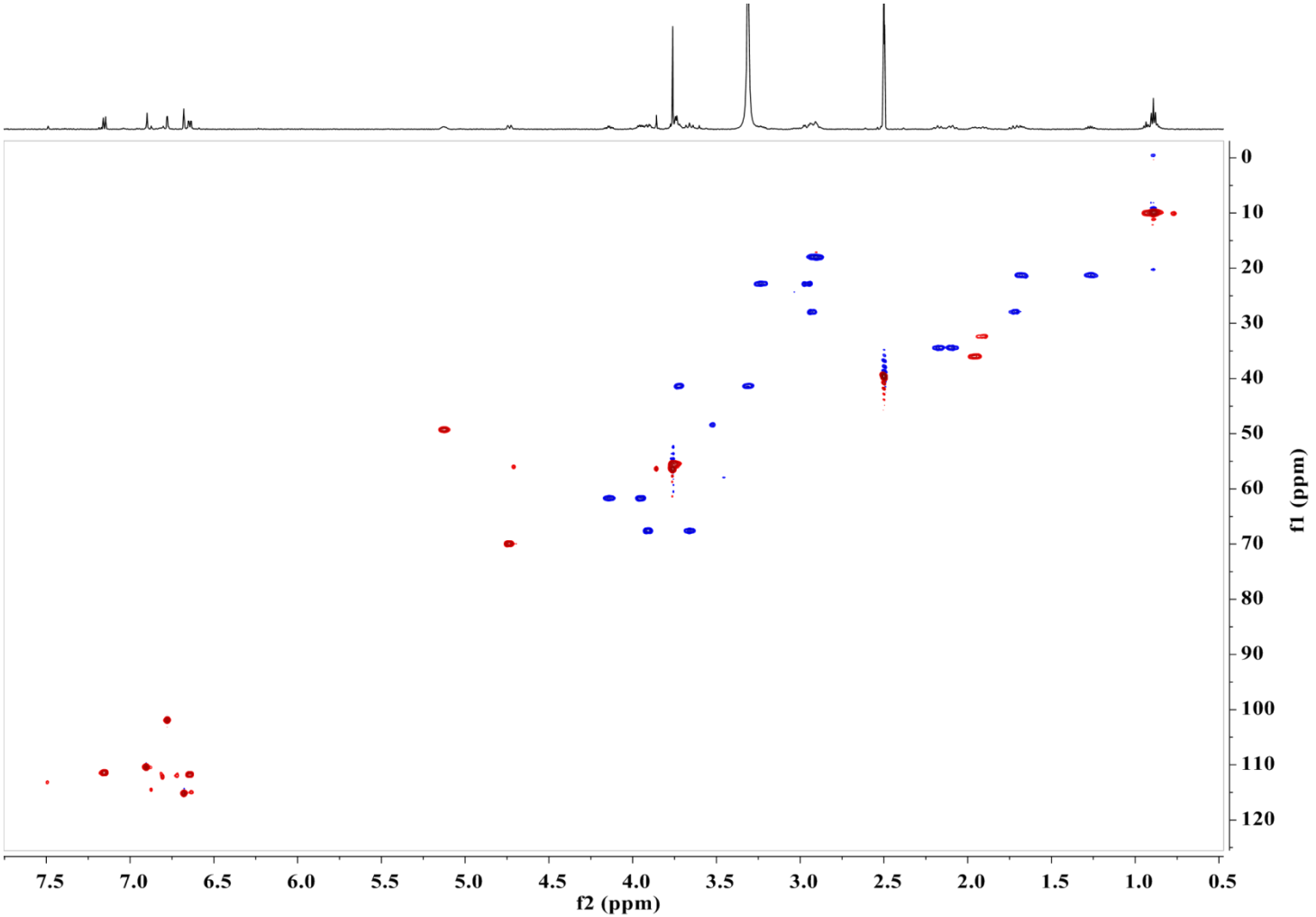

Figure S13. HSQC spectrum of compound **3** in DMSO-d_6

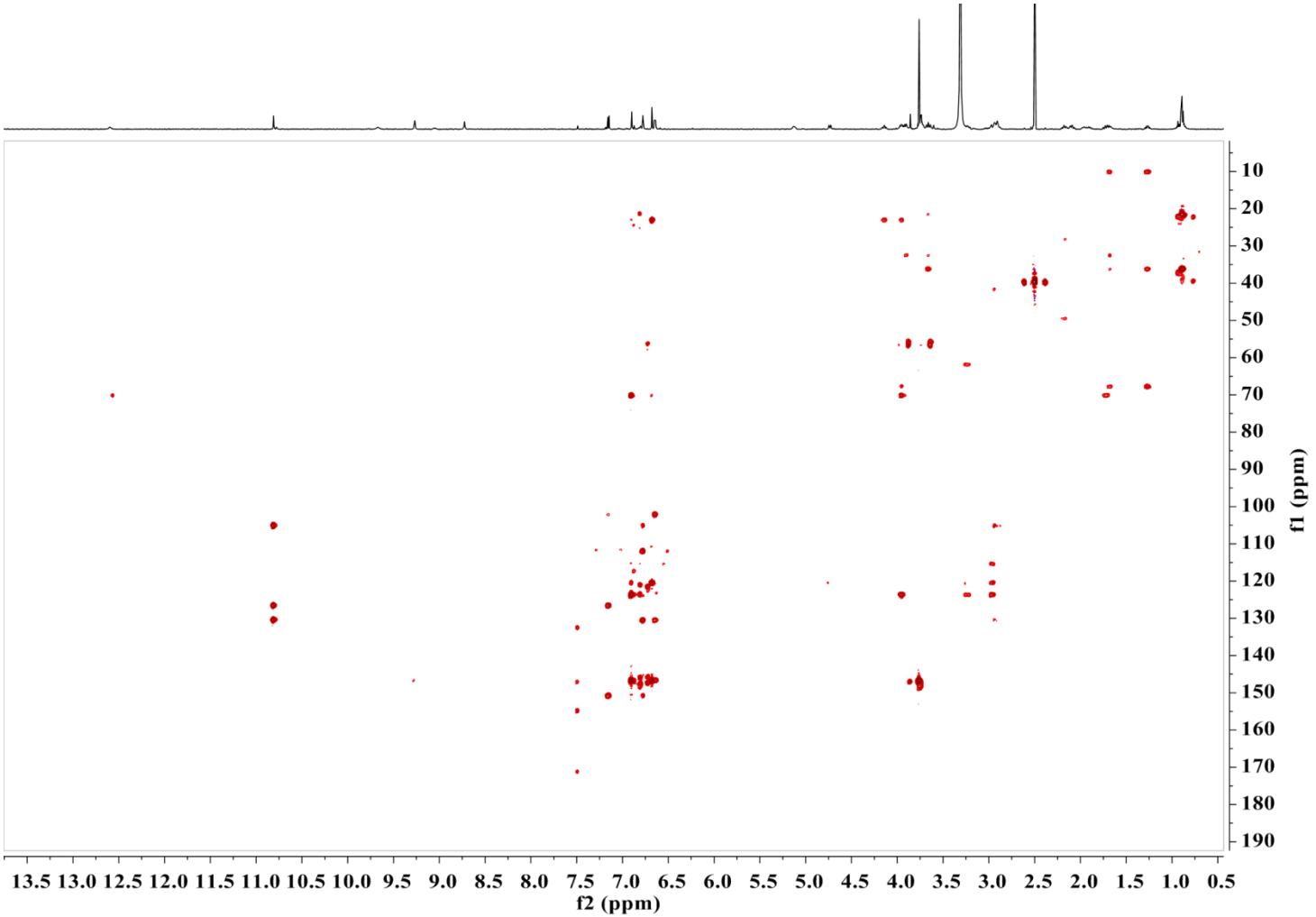

Figure S14. HMBC spectrum of compound **3** in DMSO-d_6

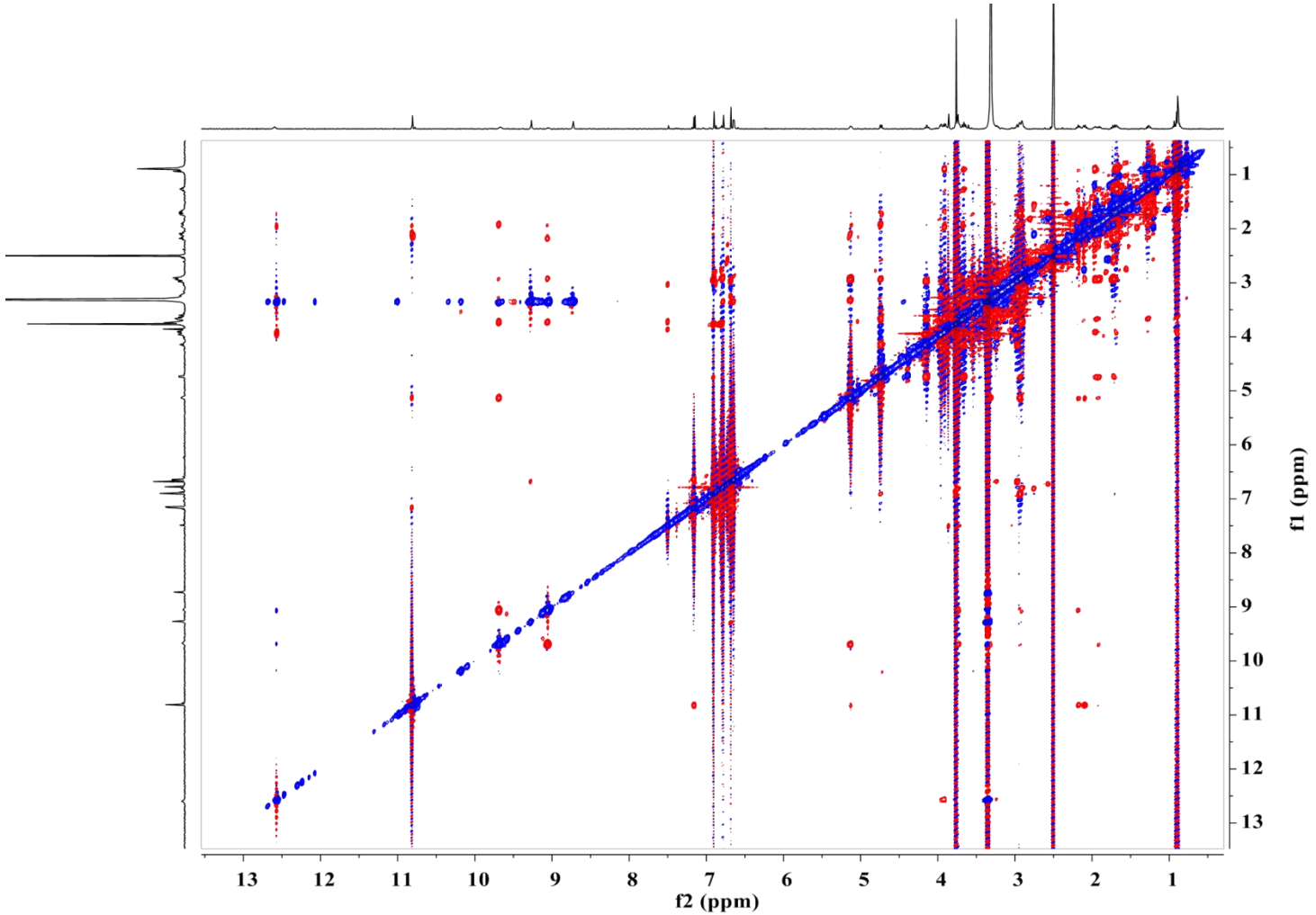

Figure S15. ROESYspectrum of compound **3** in DMSO-d_6

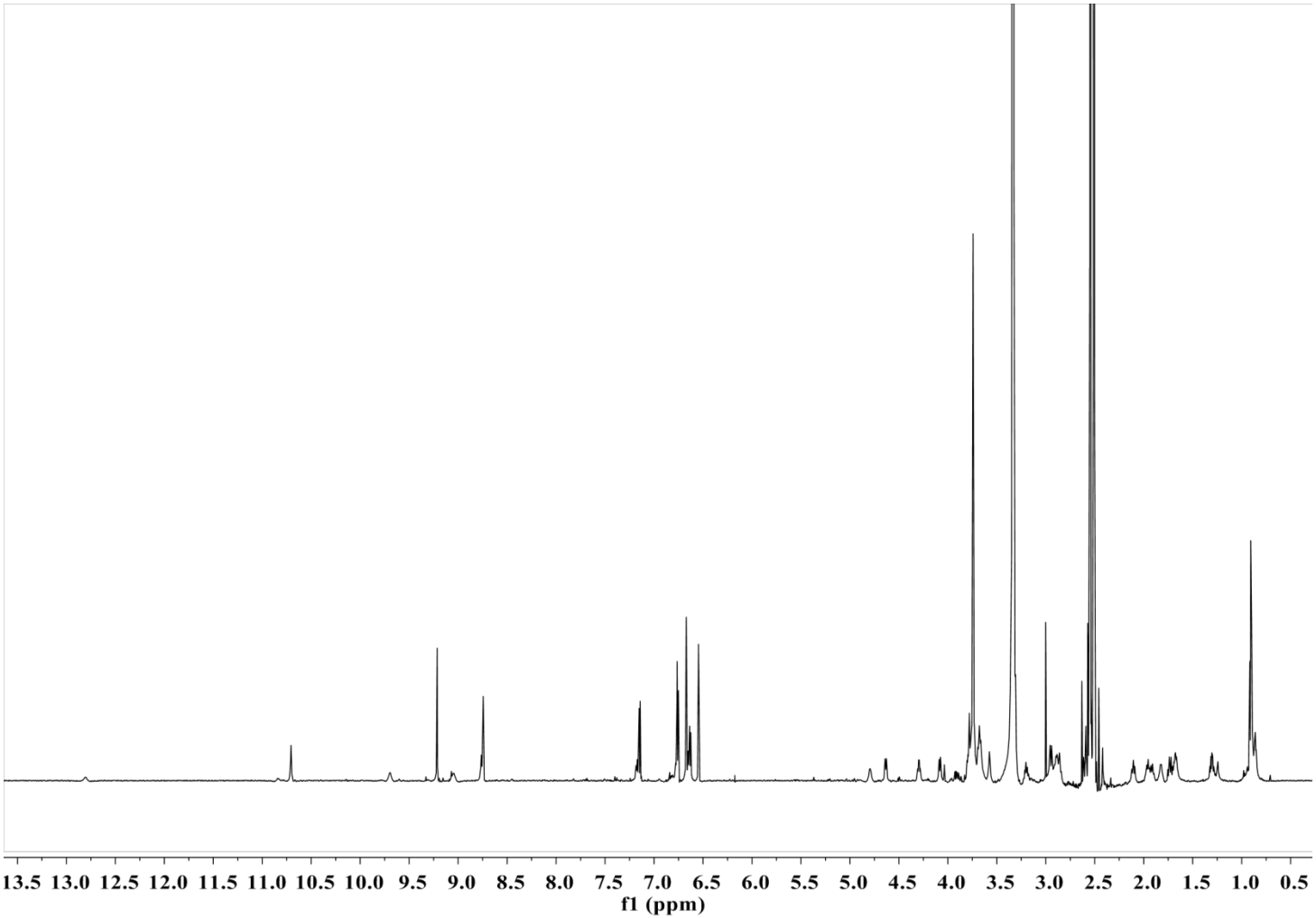

Figure S16. ^{1}H NMR spectrum of compound **4** in DMSO-d_6

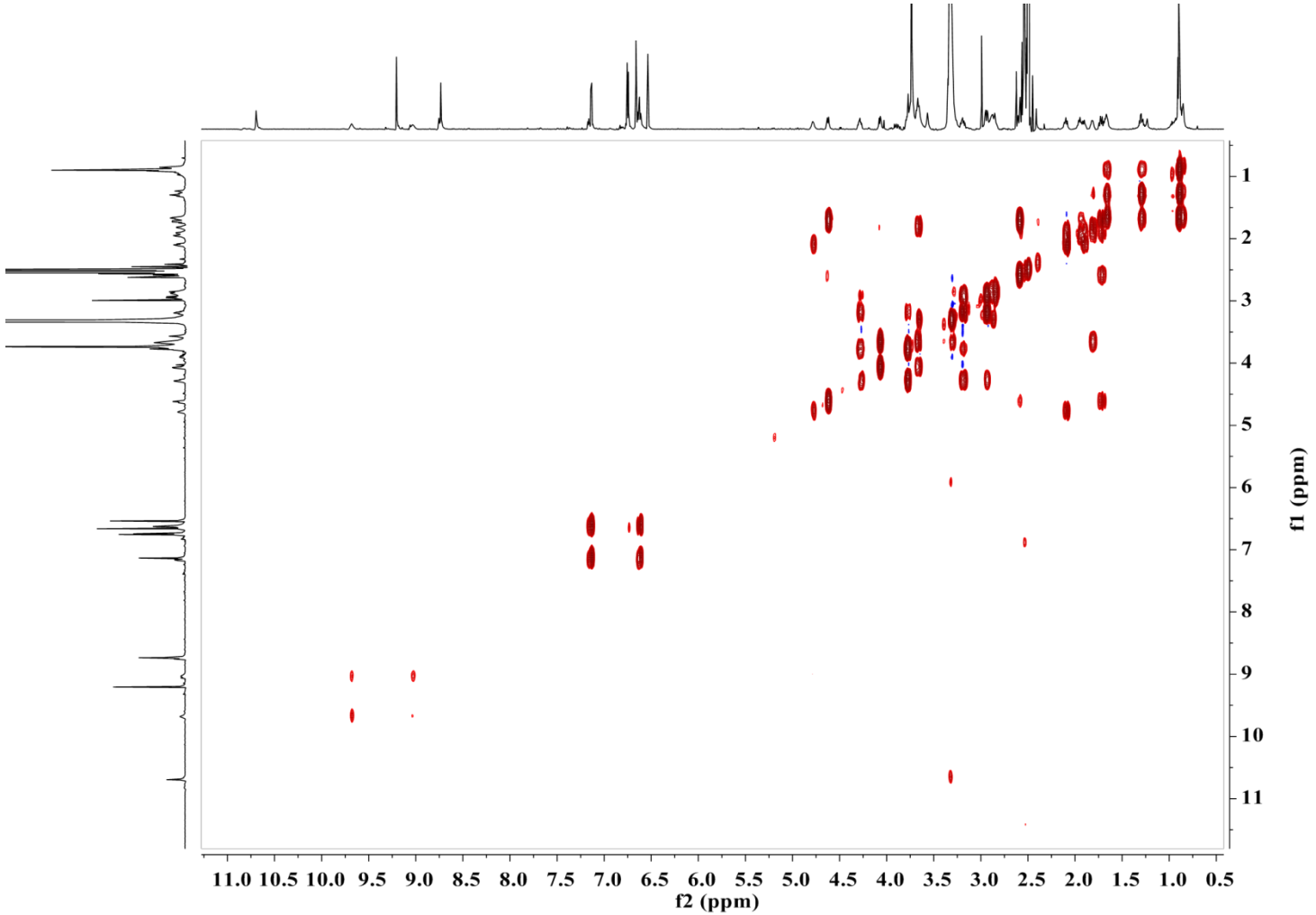

Figure S17. COSY spectrum of compound **4** in DMSO-d_6

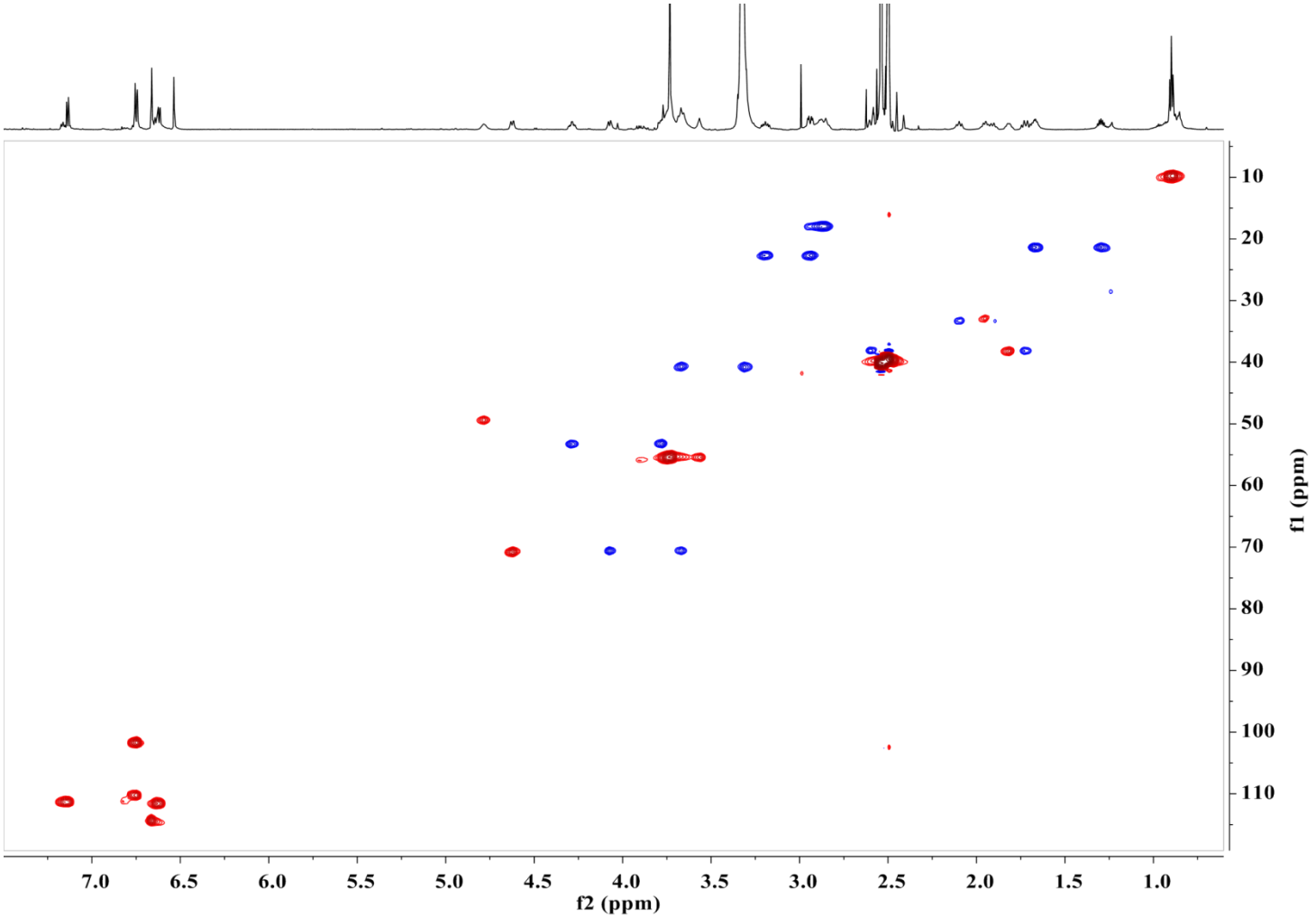

Figure S18. HSQC spectrum of compound **4** in DMSO-d_6

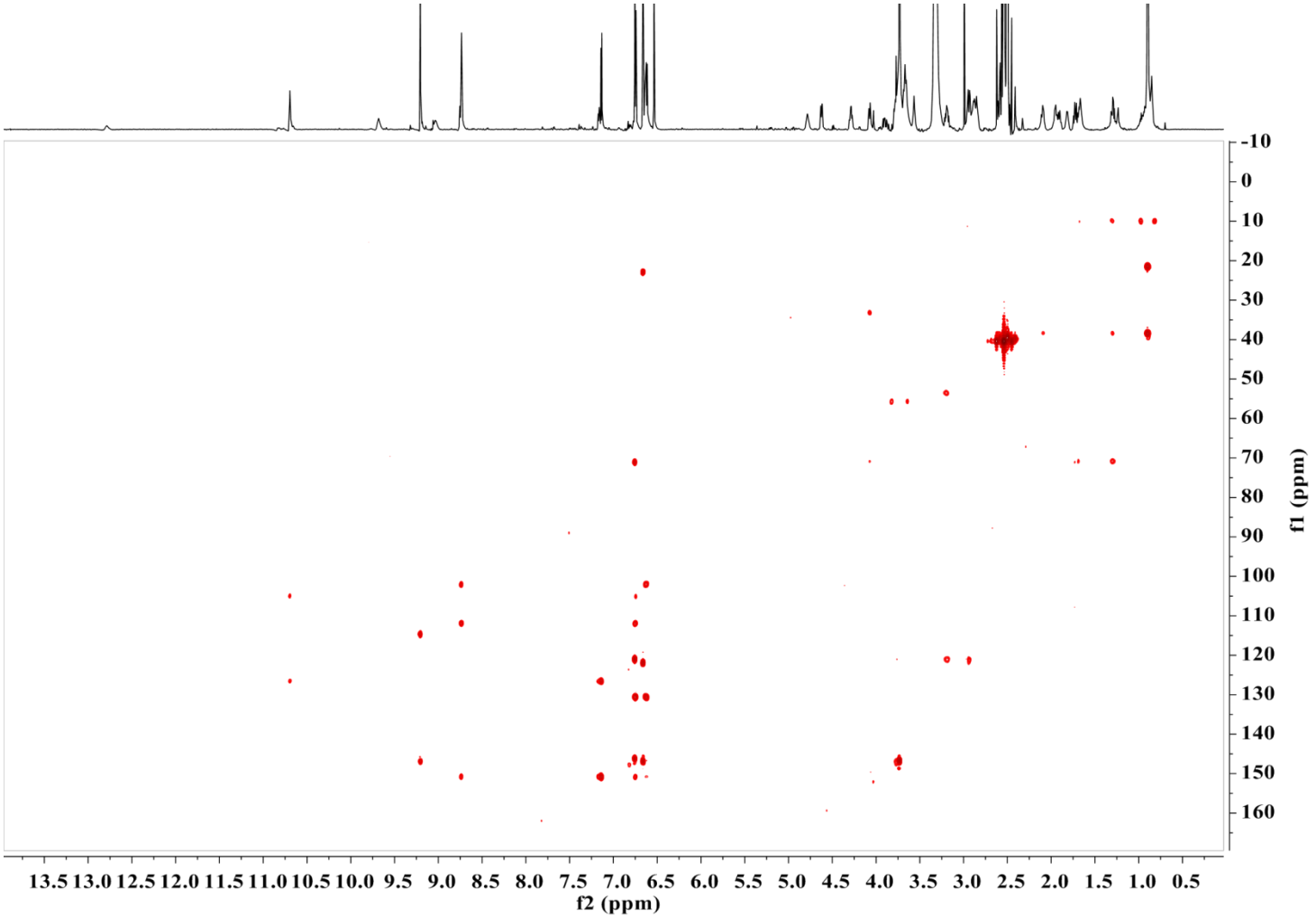

Figure S19. HMBC spectrum of compound **4** in DMSO-d_6

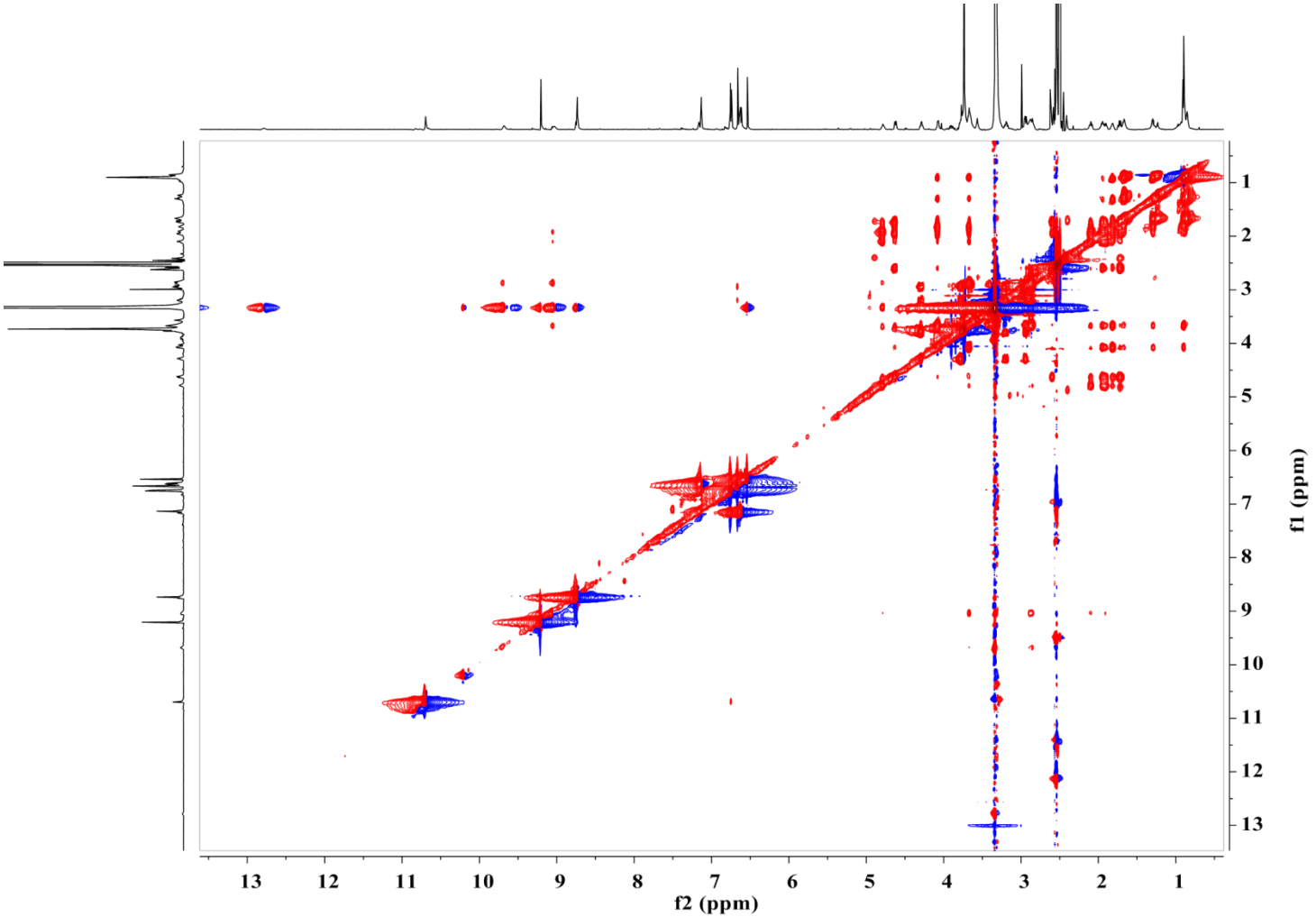

Figure S20. ROESYspectrum of compound **4** in DMSO-d_6

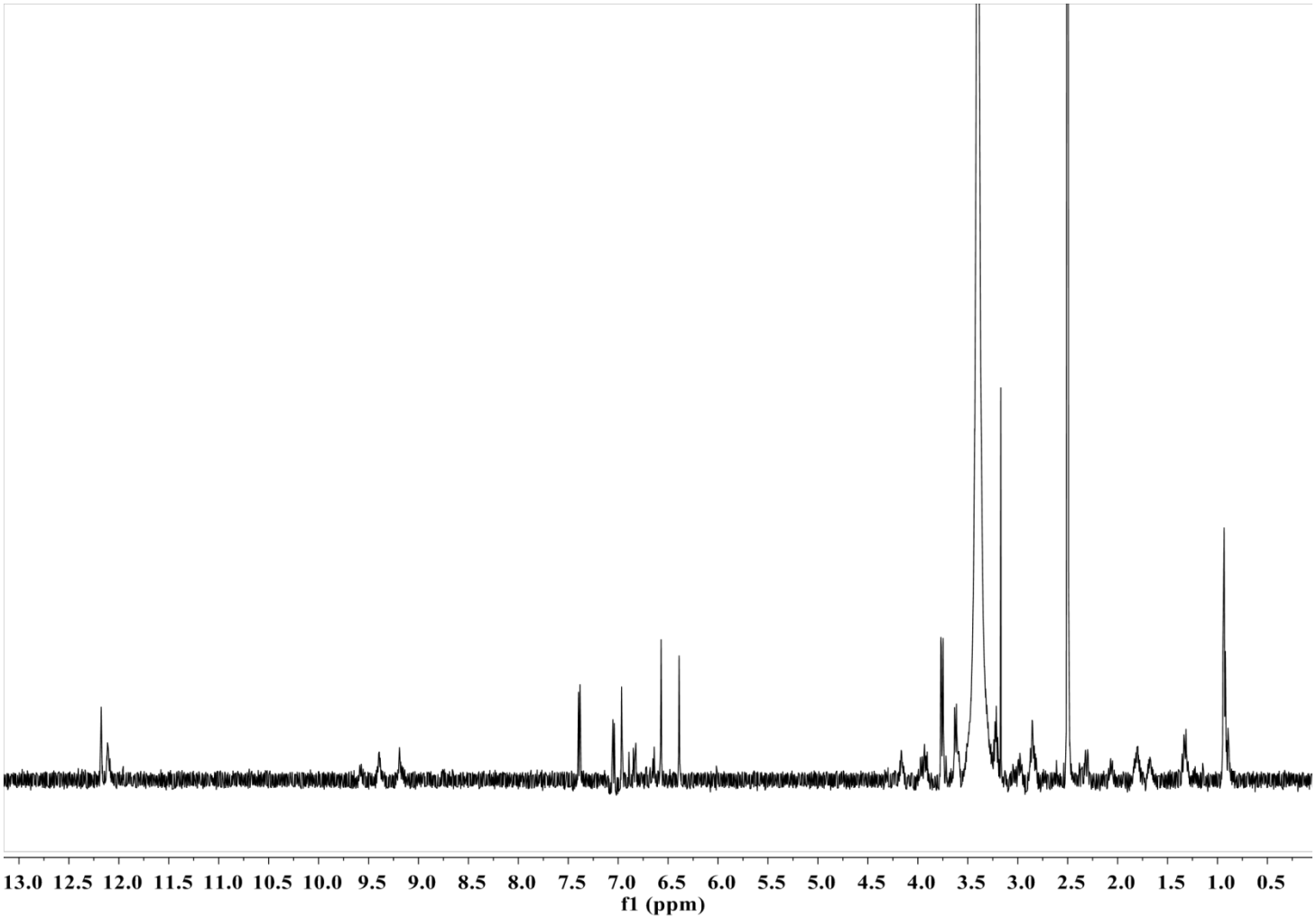

Figure S21. ^{1}H NMR spectrum of compound **10** in DMSO-d_6

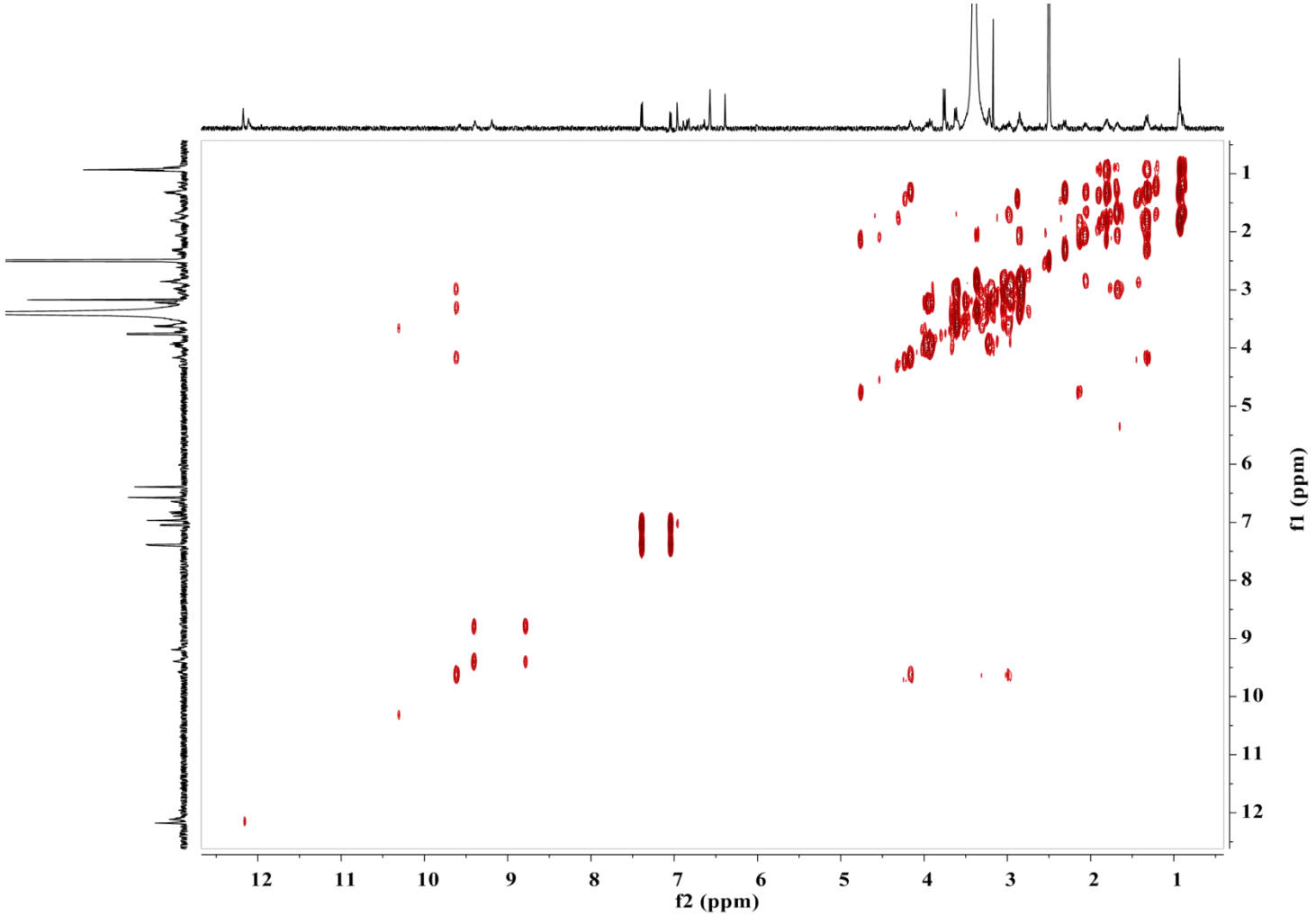

Figure S22. COSY spectrum of compound **10** in DMSO-d_6

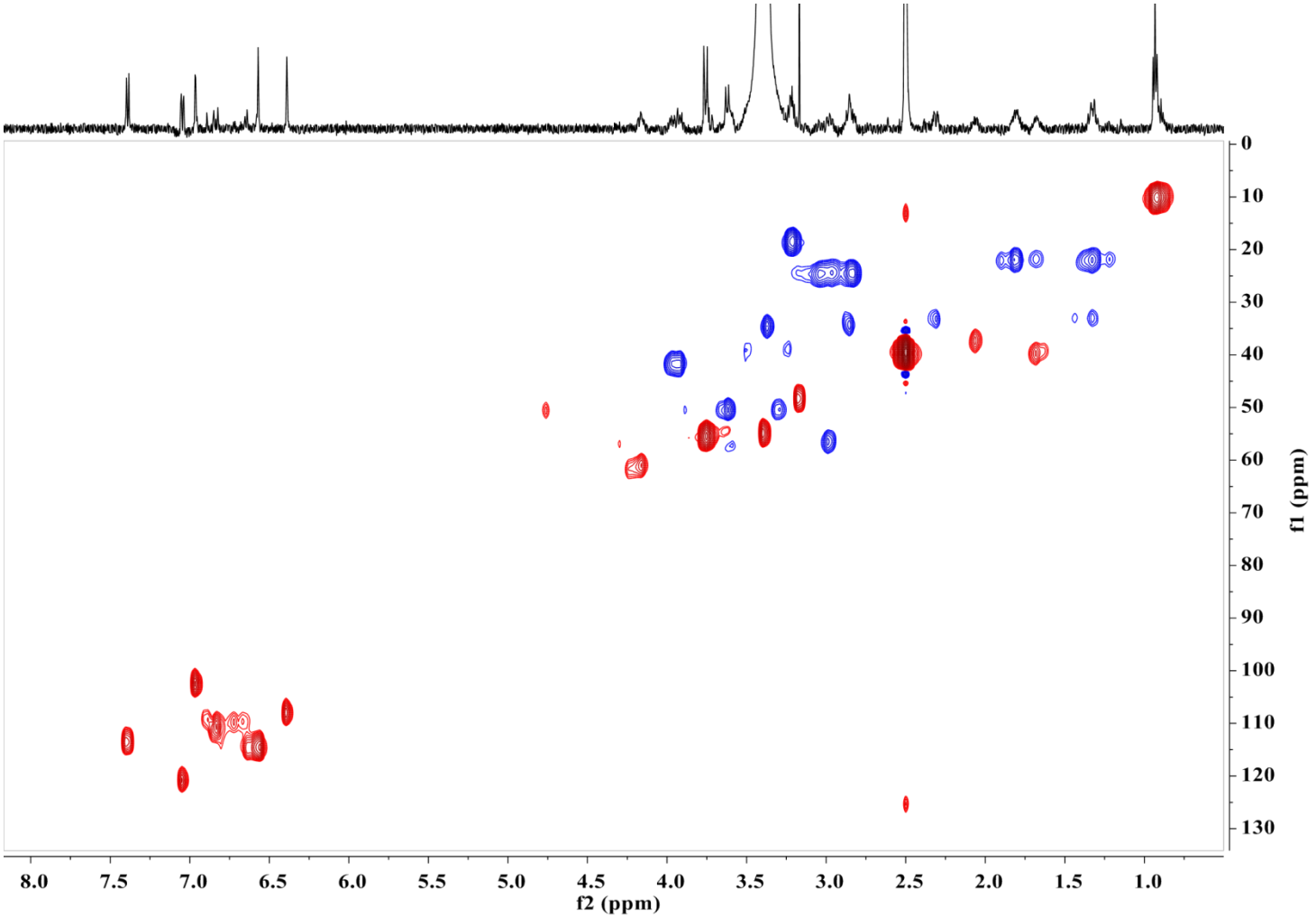

Figure S23. HSQC spectrum of compound **10** in DMSO-d_6

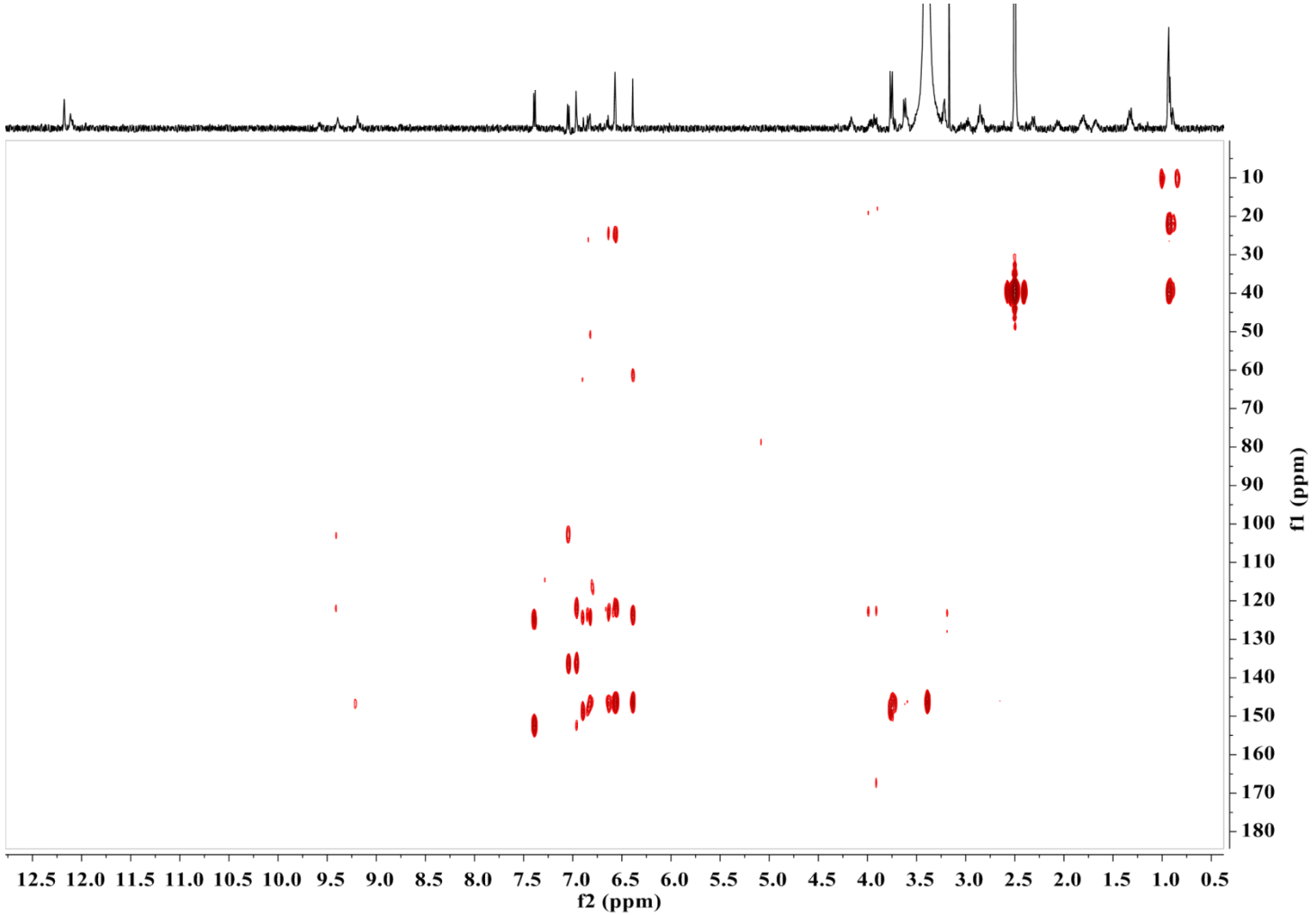

Figure S24. HMBC spectrum of compound **10** in DMSO-d_6

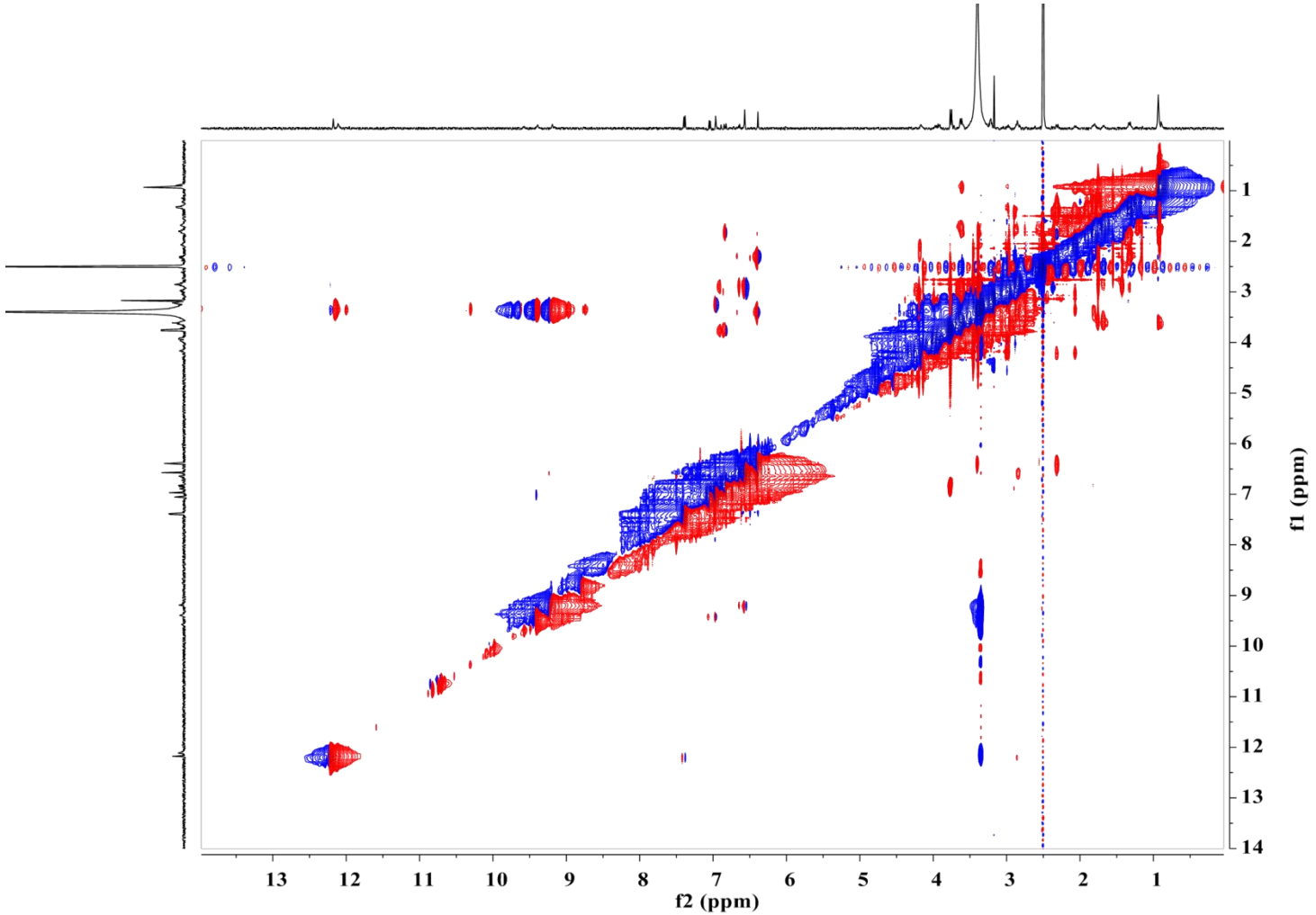

Figure S25. ROESYspectrum of compound **10** in DMSO-d_6

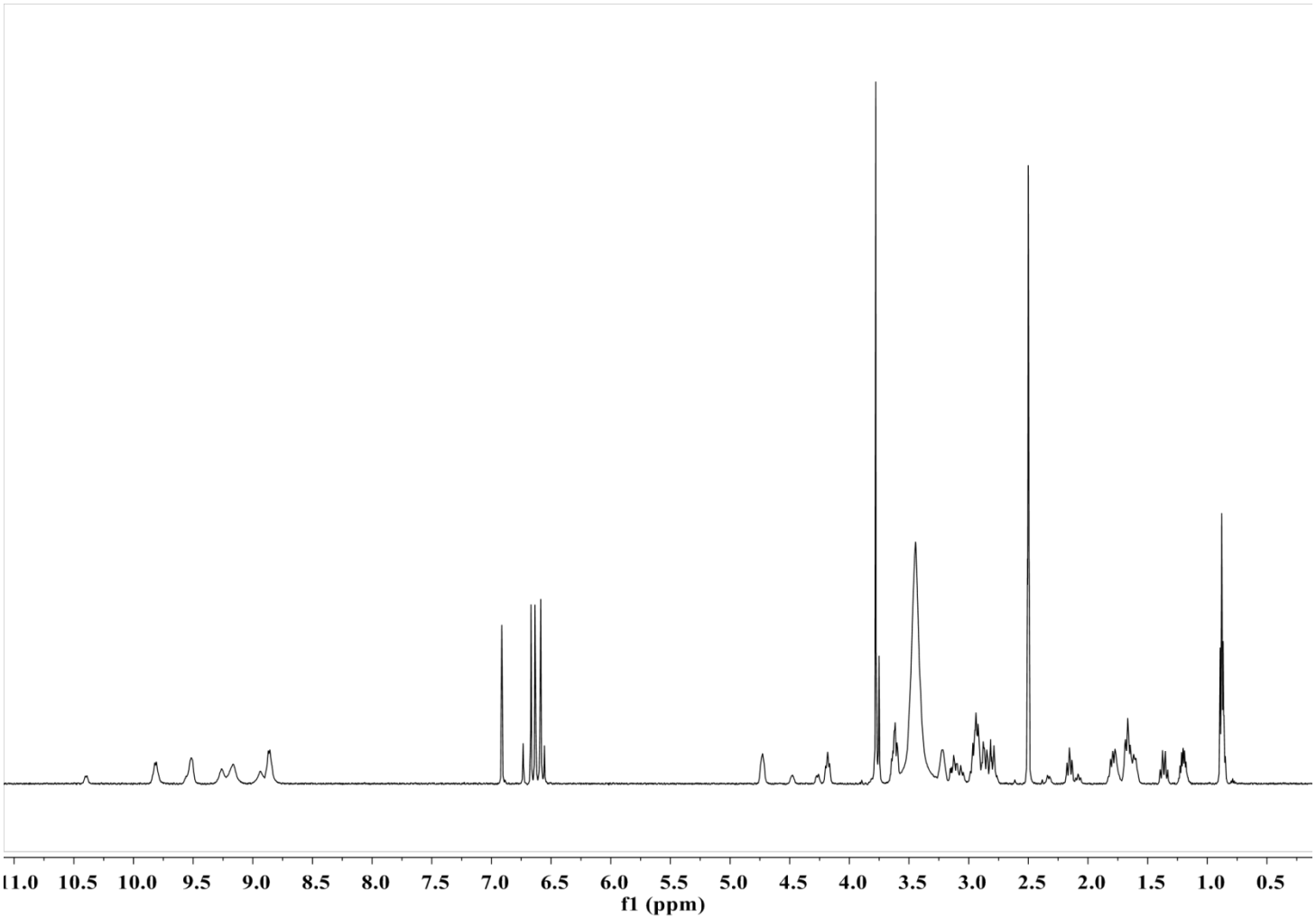

Figure S26. ^{1}H NMR spectrum of compound **13** in DMSO-d_6

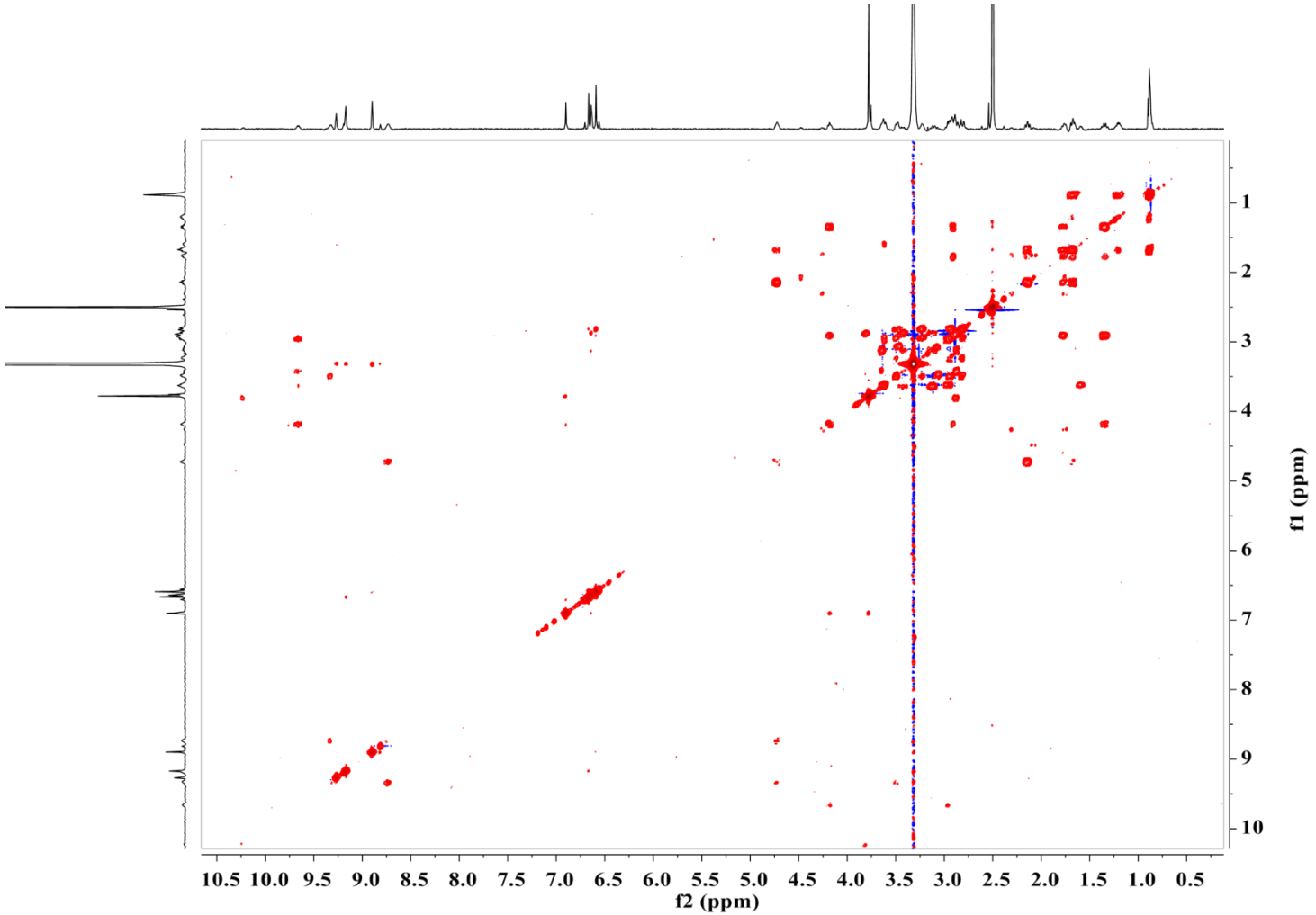

Figure S27. COSY spectrum of compound **13** in DMSO-d_6

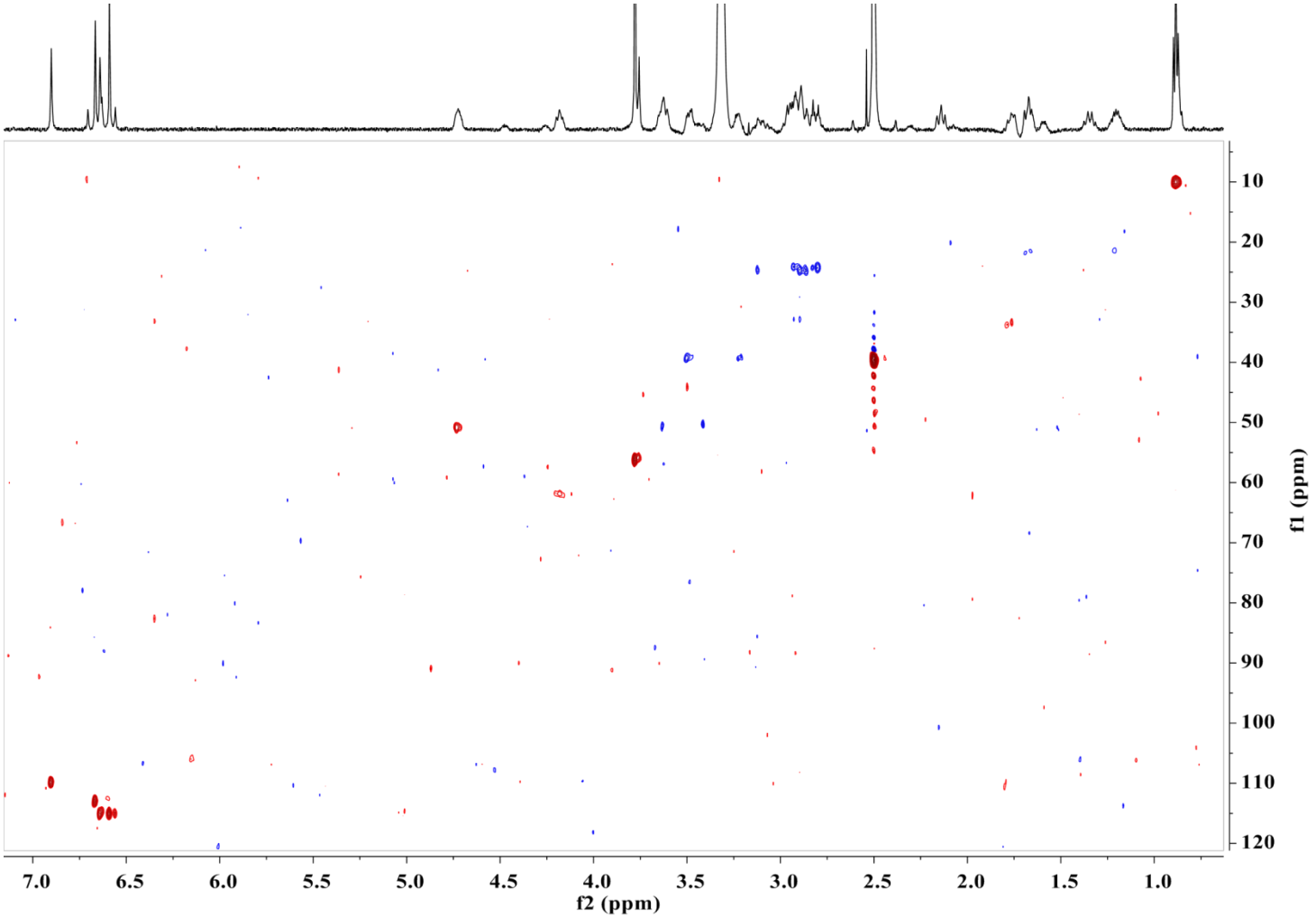

Figure S28. HSQC spectrum of compound **13** in DMSO-d_6

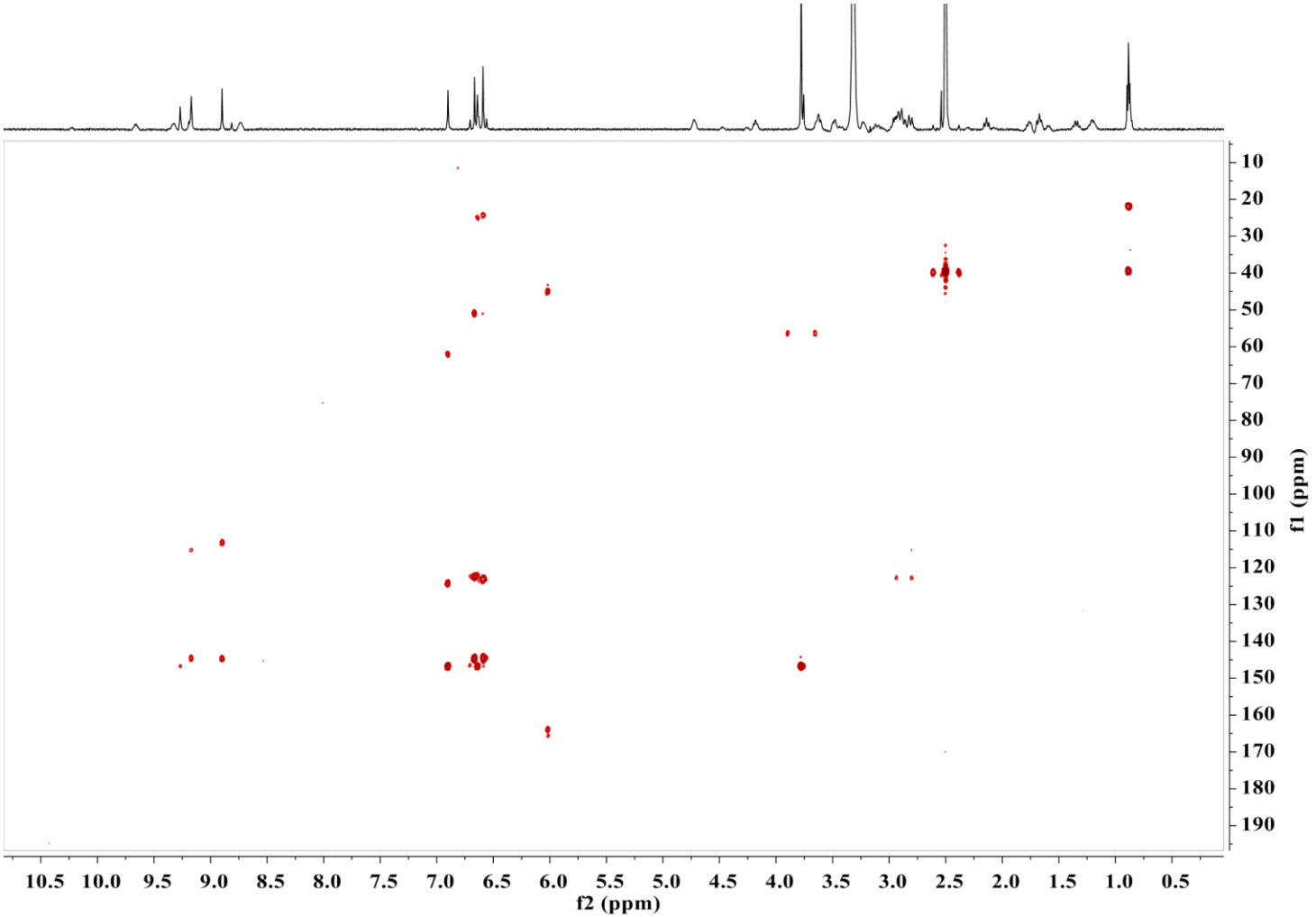

Figure S29. HMBC spectrum of compound **13** in DMSO-d_6

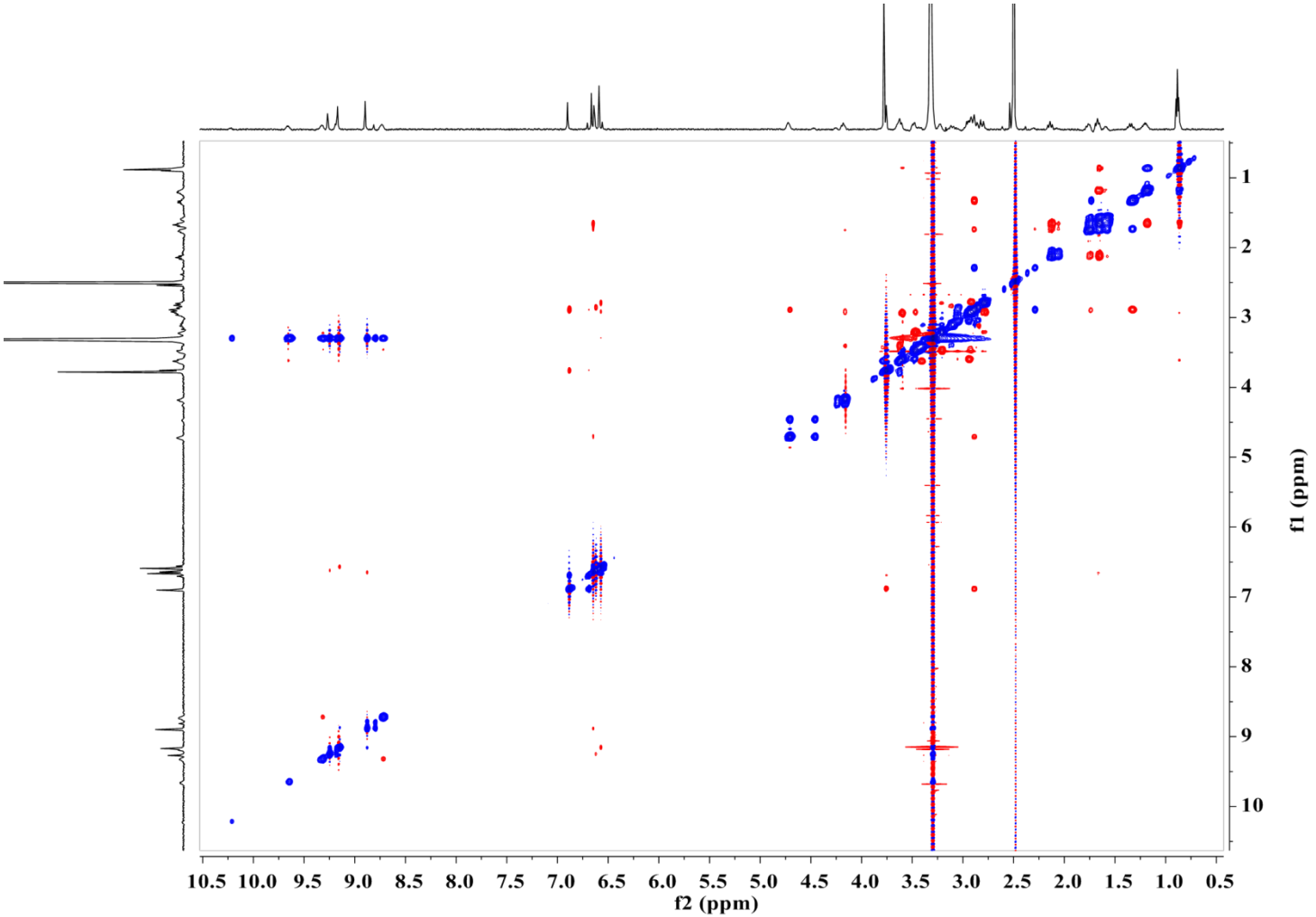

Figure S30. ROESYspectrum of compound **13** in DMSO-d_6

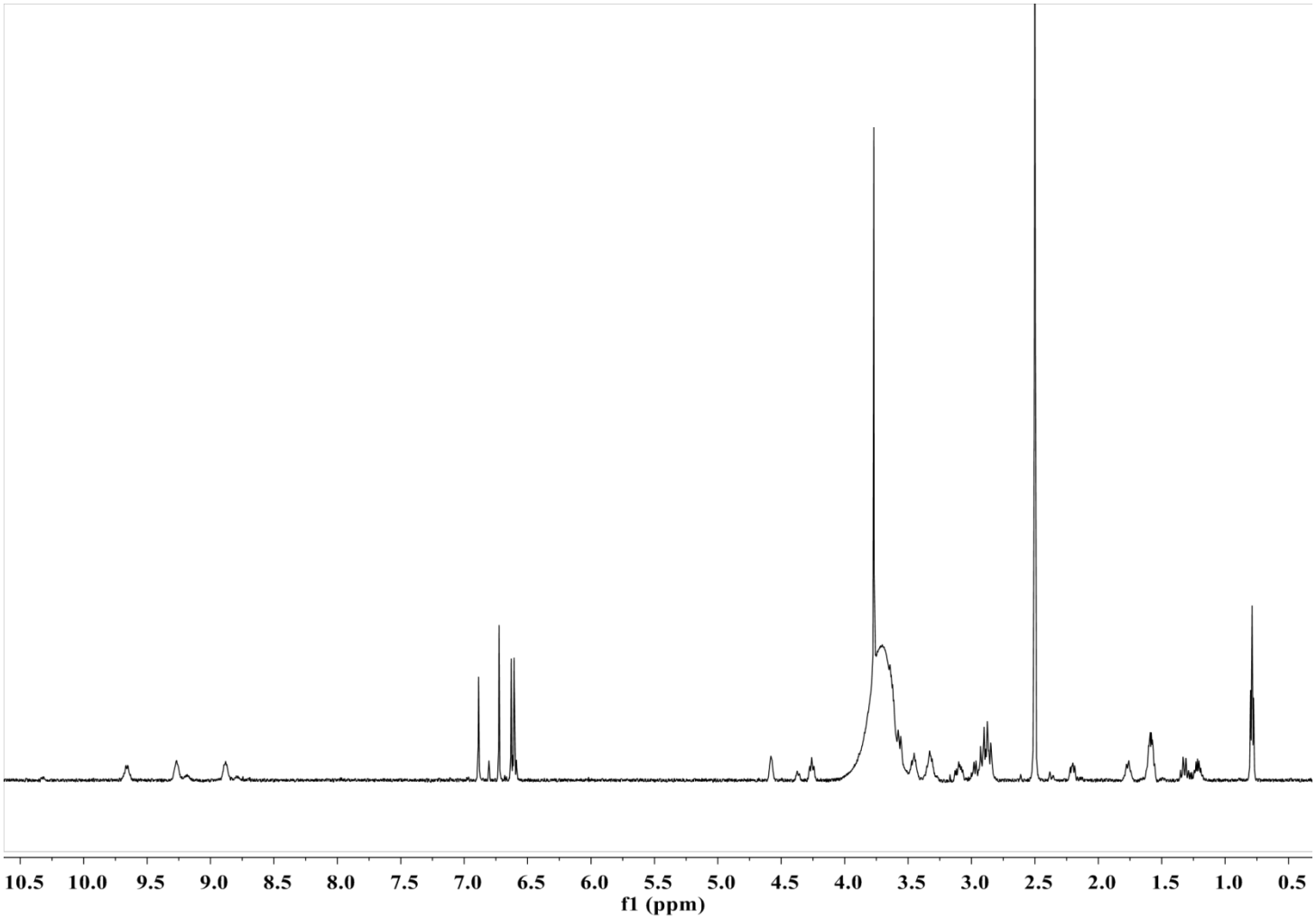

Figure S31. ^{1}H NMR spectrum of compound **14** in DMSO-d_6

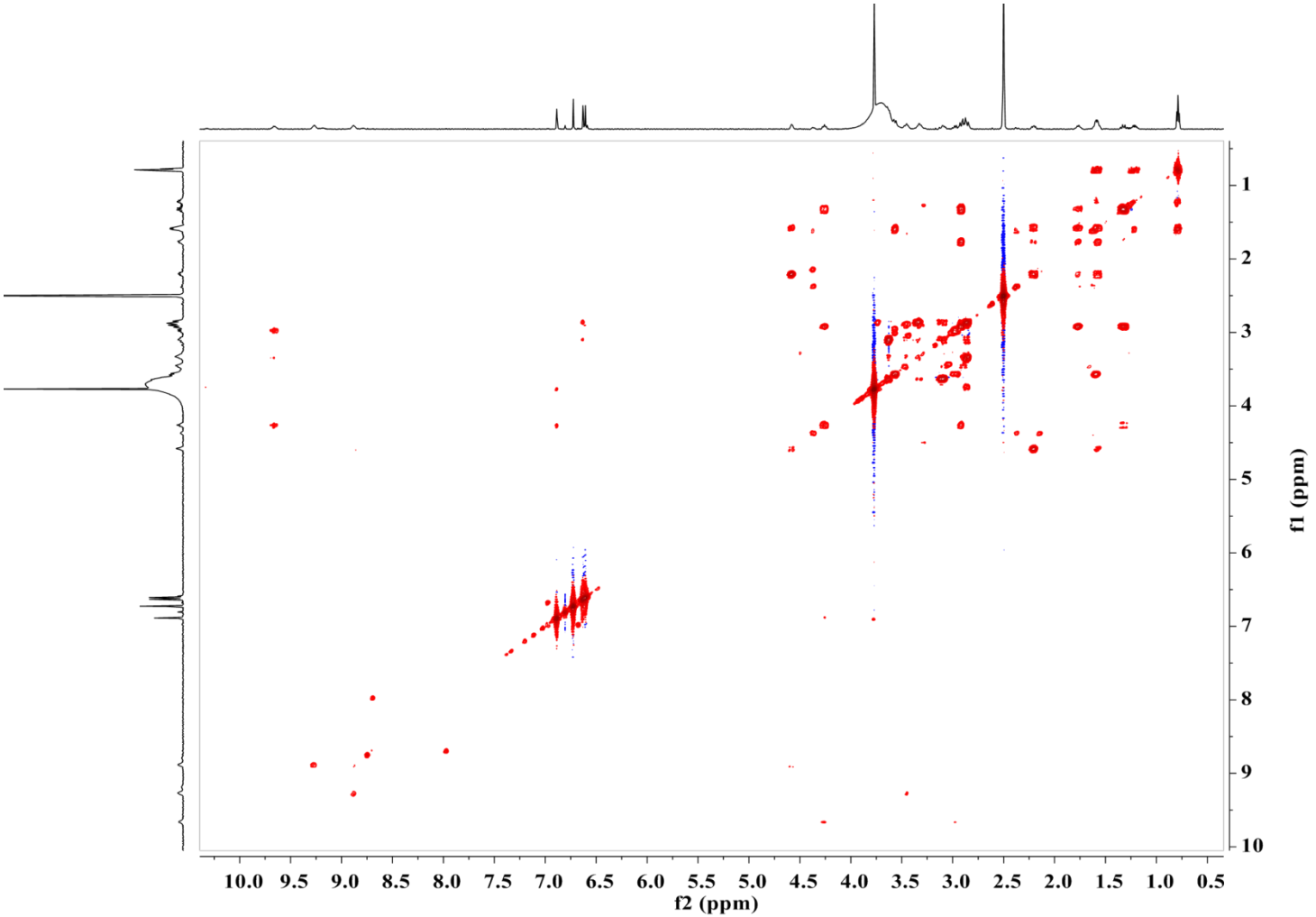

Figure S32. COSY spectrum of compound **14** in DMSO-d_6

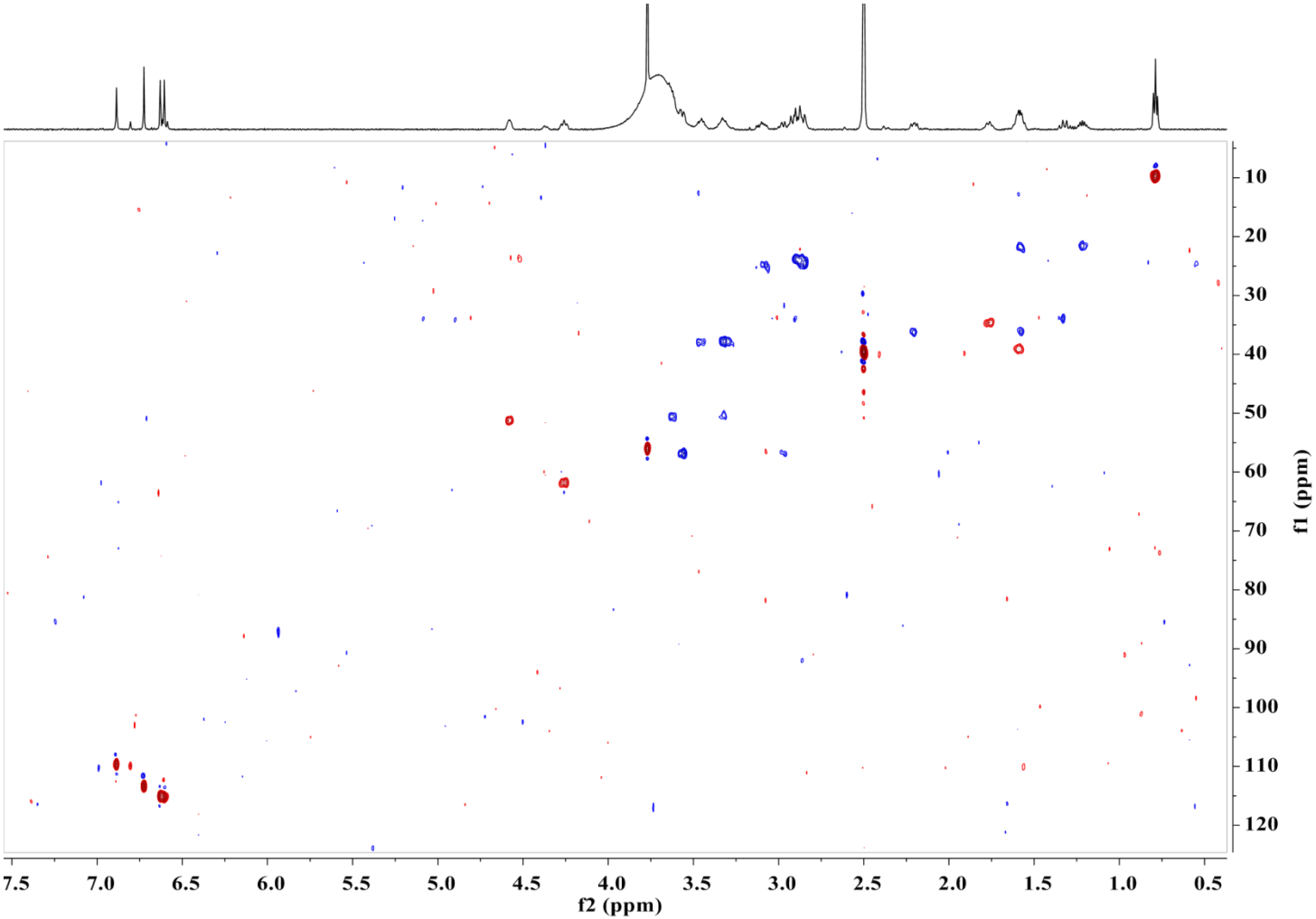

Figure S33. HSQC spectrum of compound **14** in DMSO-d_6

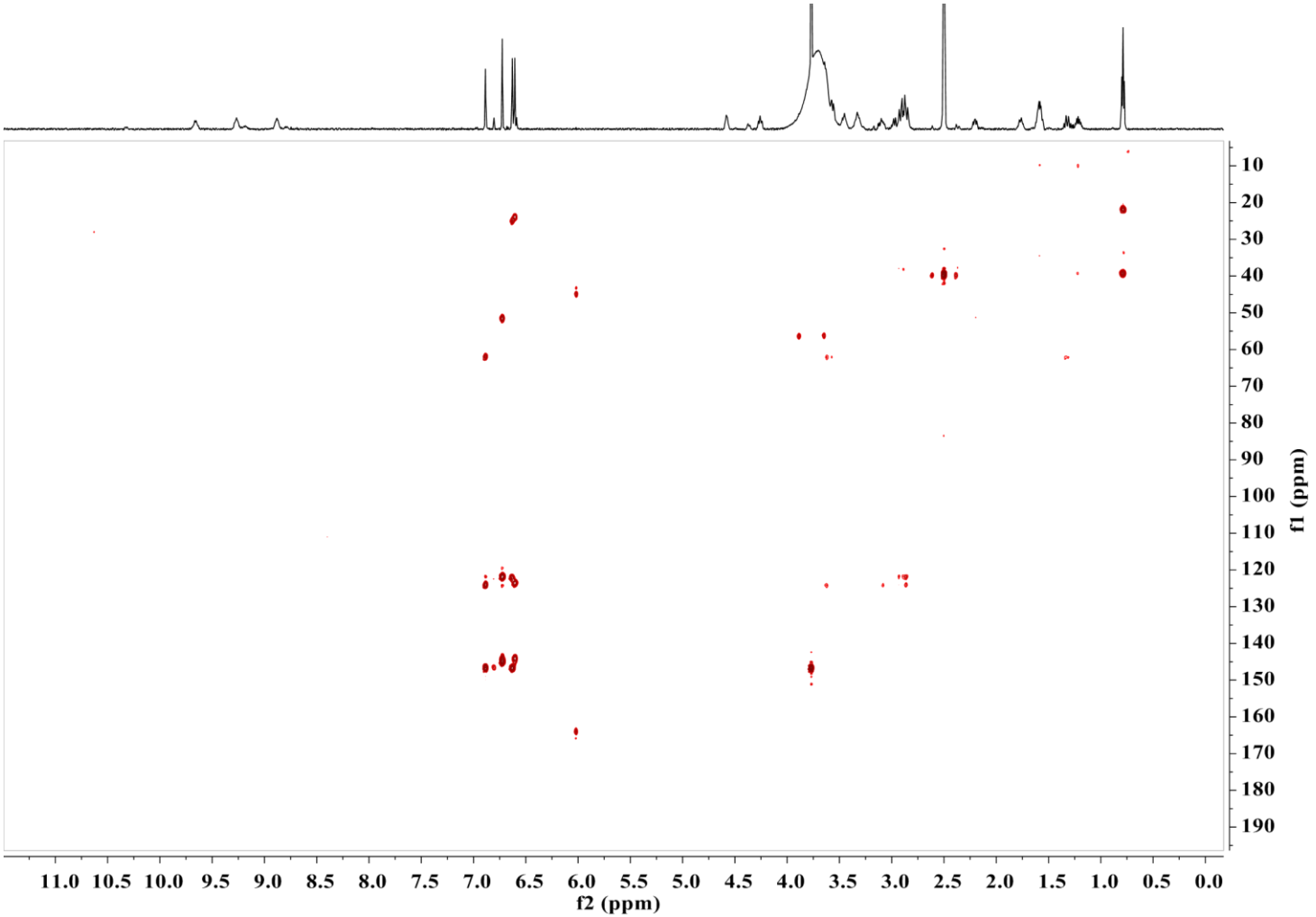

Figure S34. HMBC spectrum of compound **14** in DMSO-d_6

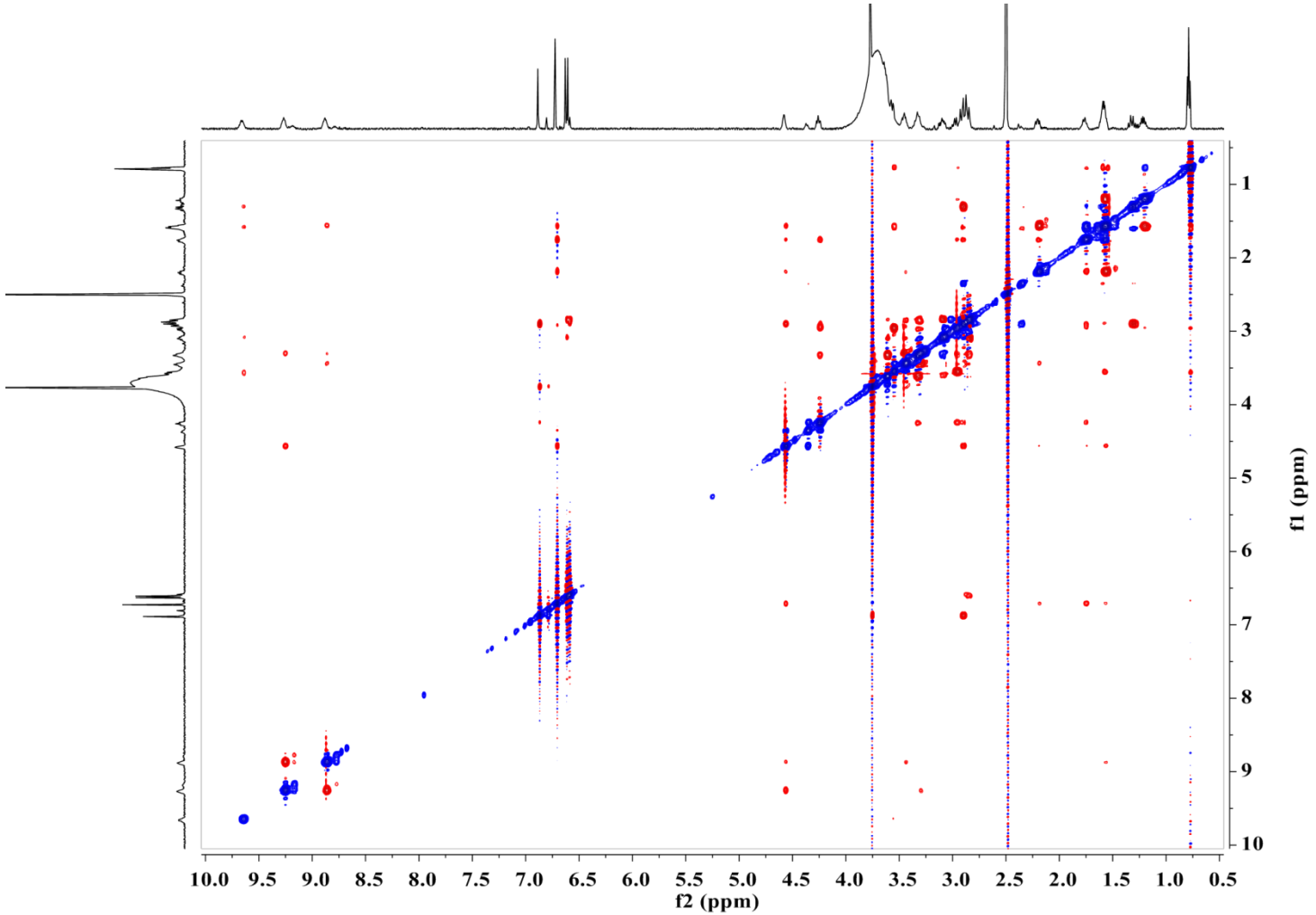

Figure S35. ROESYspectrum of compound **14** in DMSO-d_6

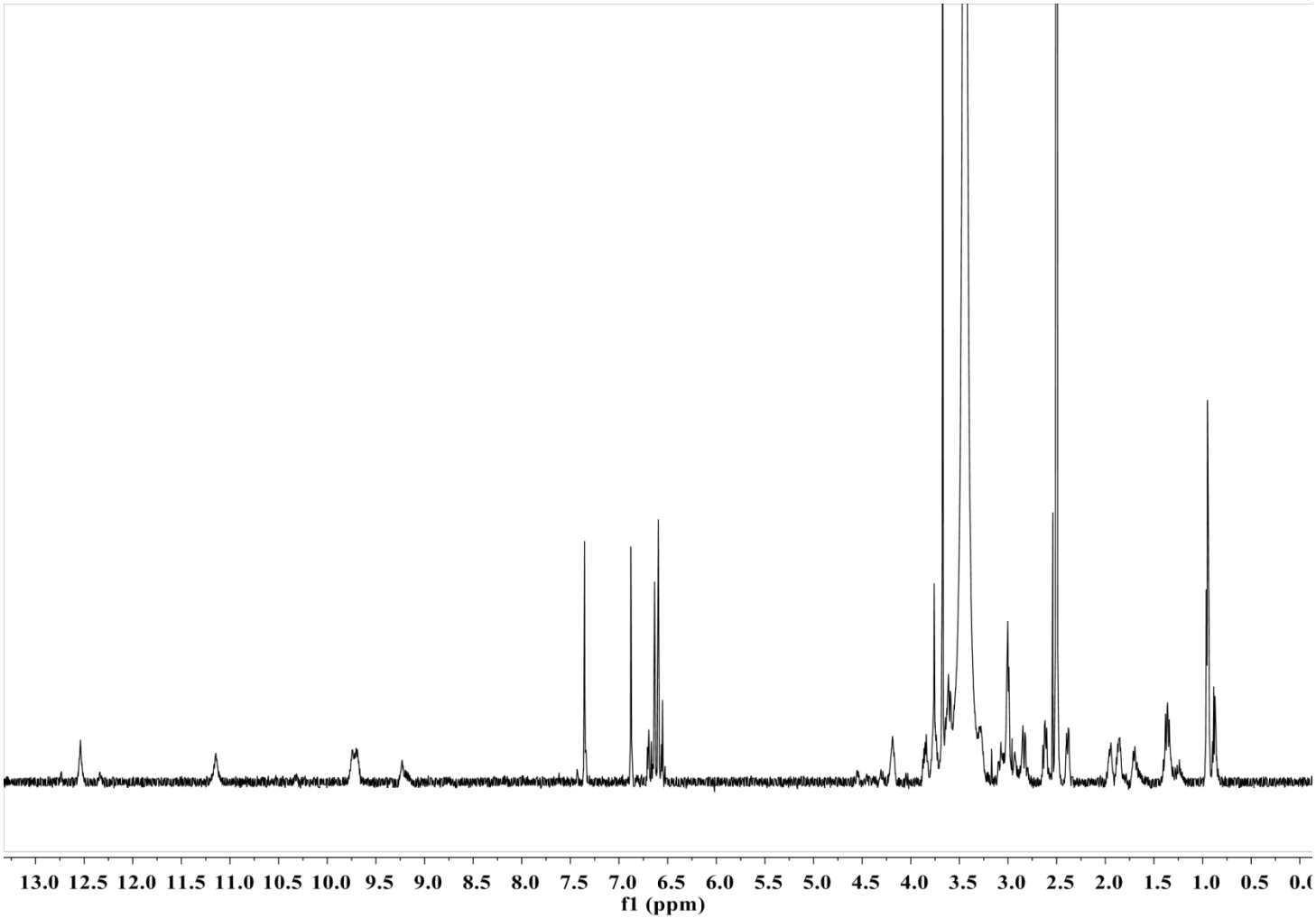

Figure S36. ^{1}H NMR spectrum of compound **15** in DMSO-d_6

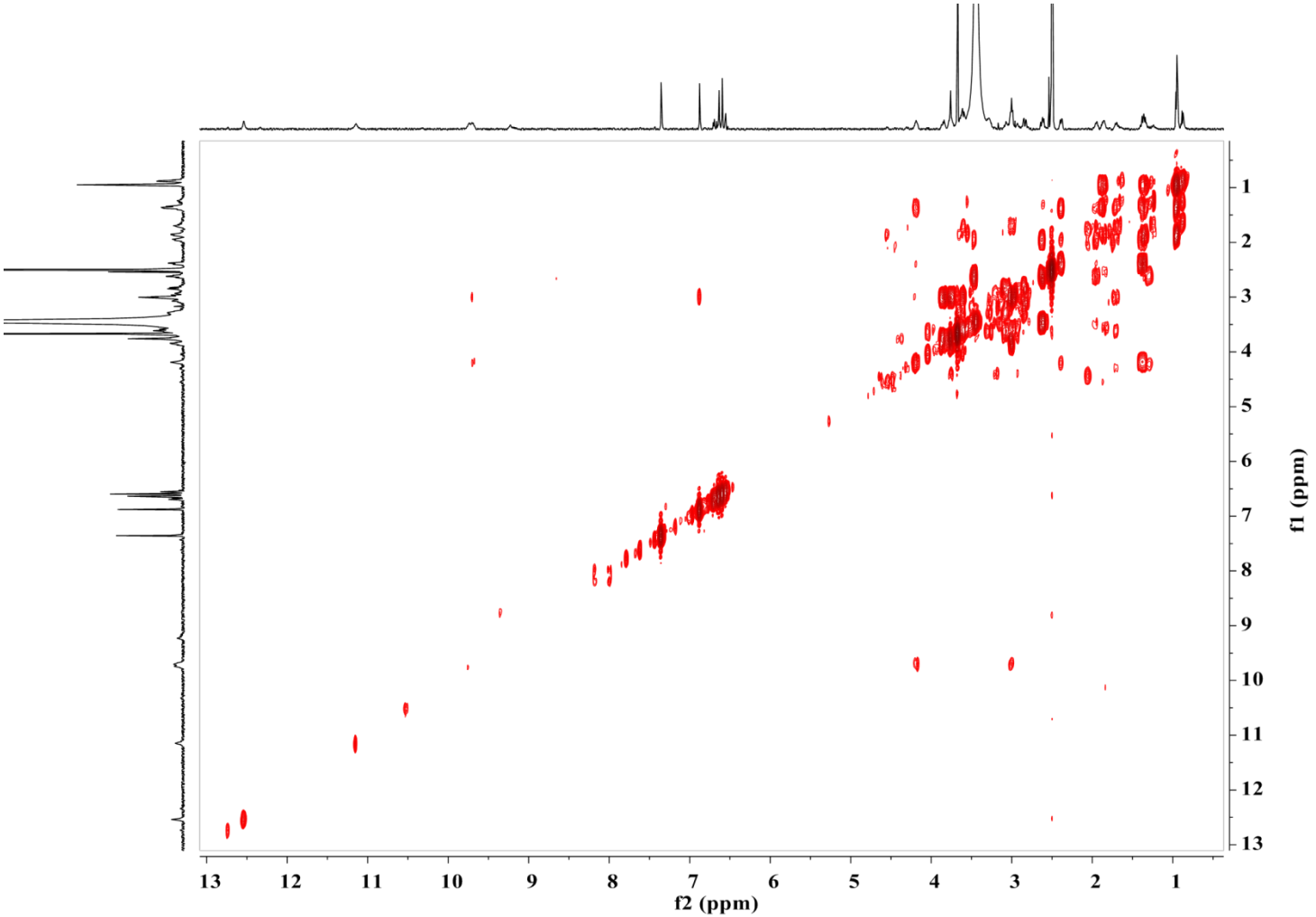

Figure S37. COSY spectrum of compound **15** in DMSO-d_6

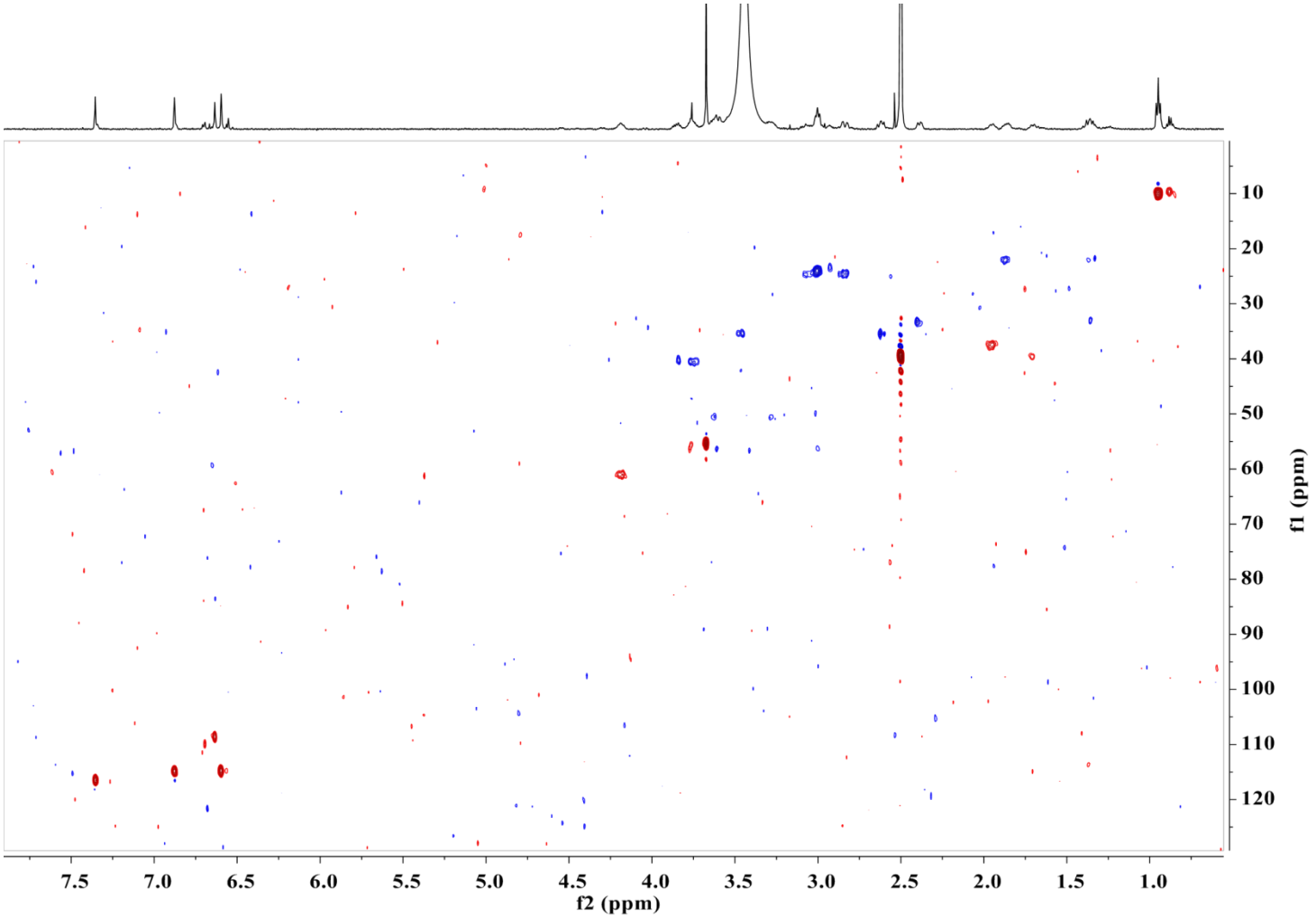

Figure S38. HSQC spectrum of compound **15** in DMSO-d_6

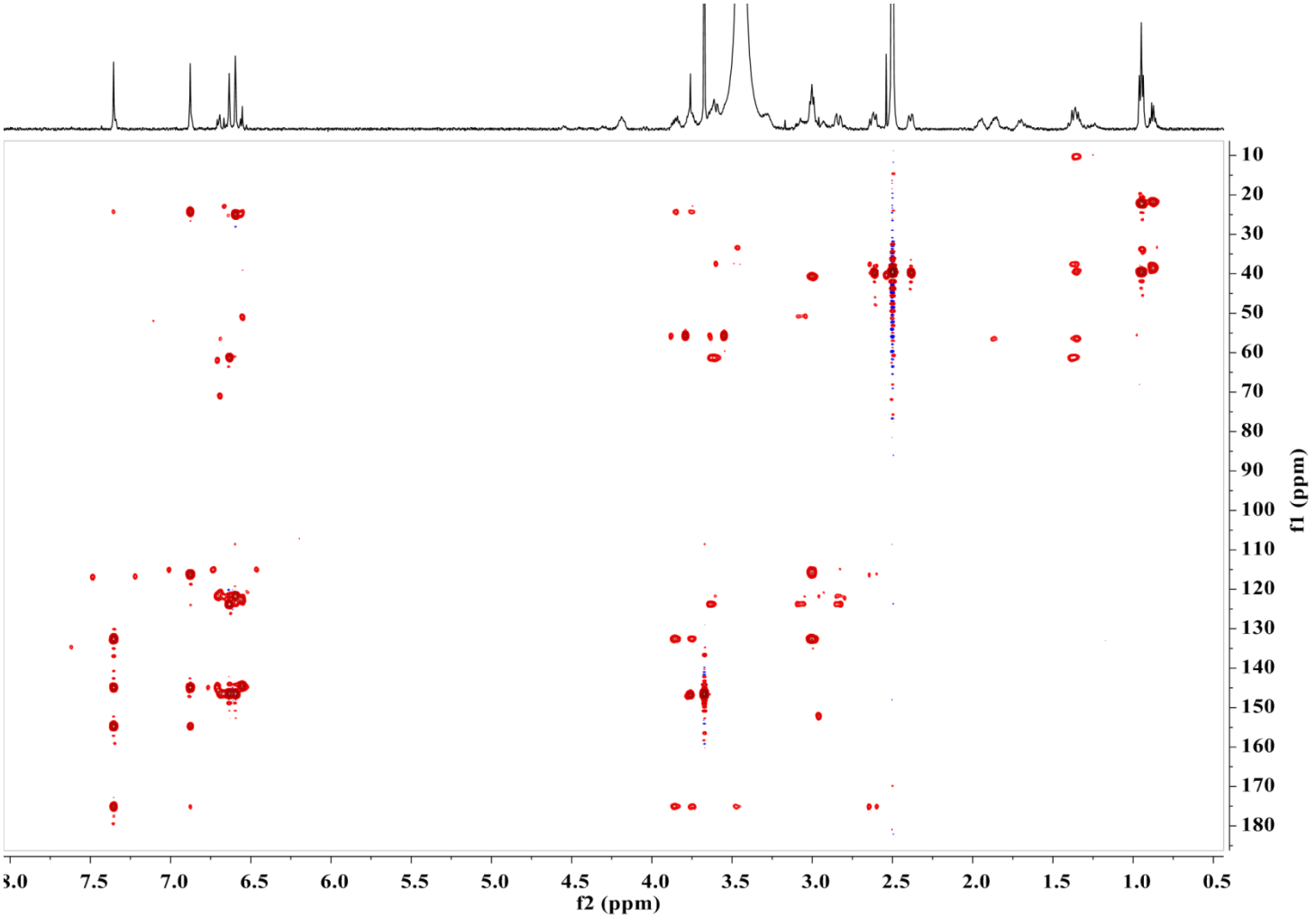

Figure S39. HMBC spectrum of compound **15** in DMSO-d_6

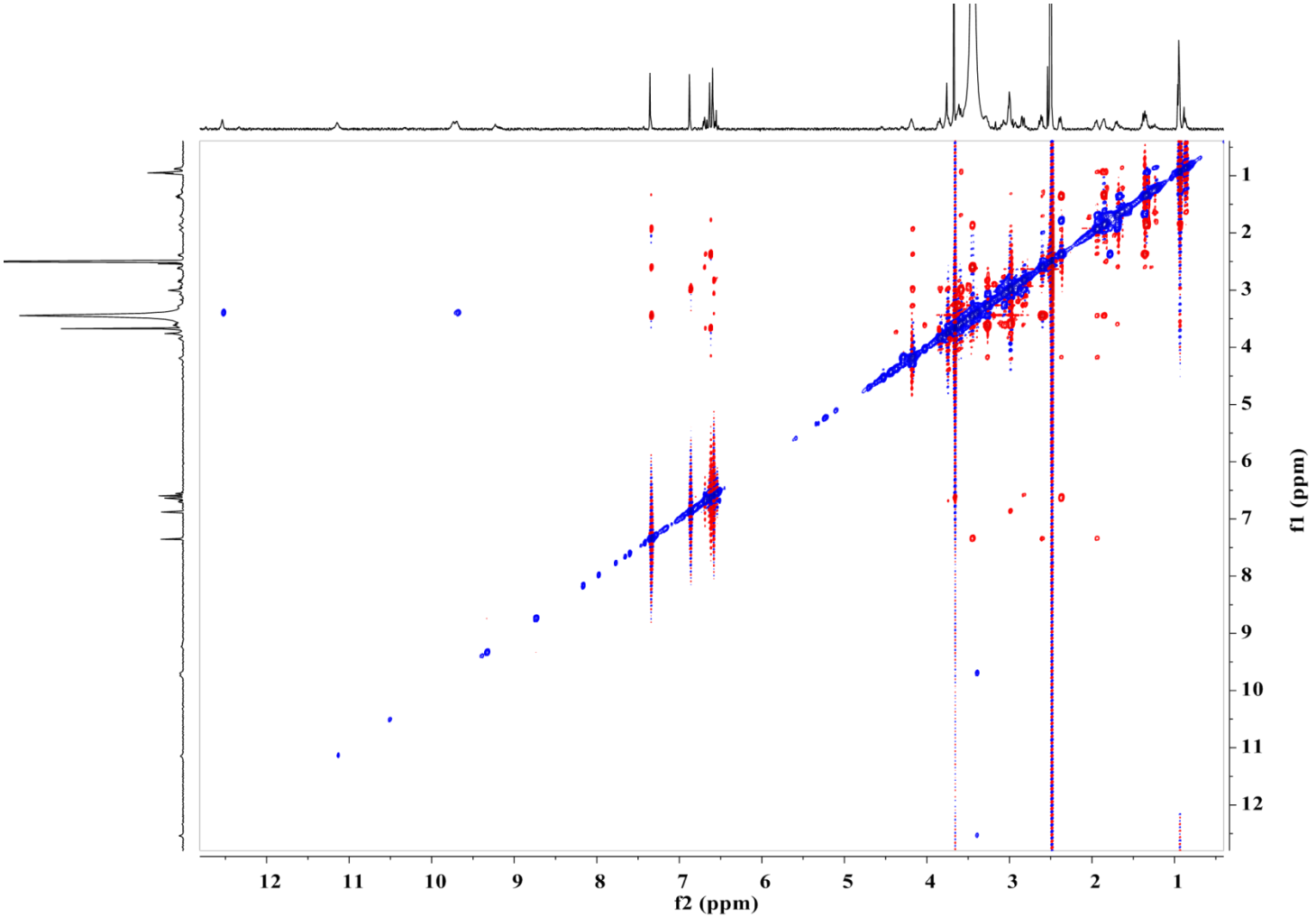

Figure S40. ROESYspectrum of compound **15** in DMSO-d_6

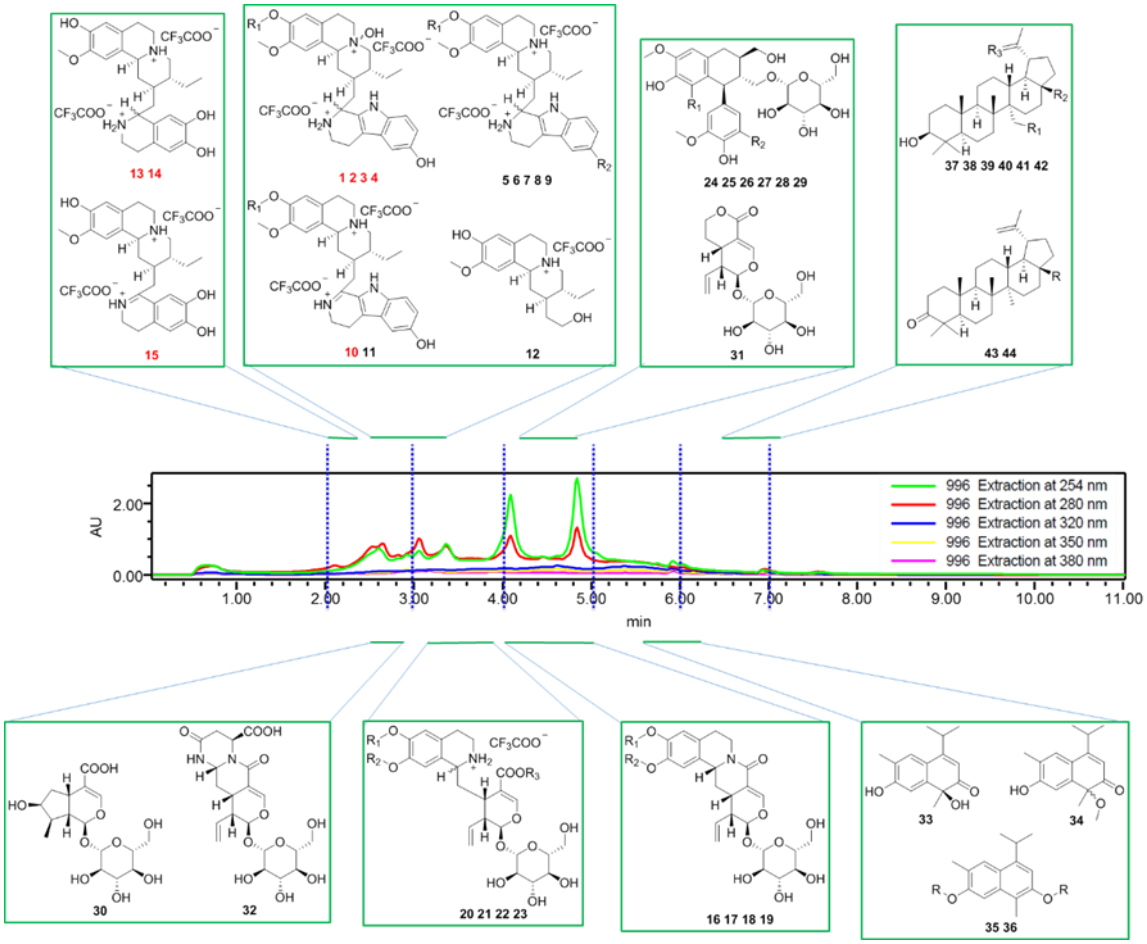

Figure S41. HPLC chromatogram of lead-like enhanced extract of the Australian plant *Alangium villosum* and compounds isolated from different lead-like enhanced fractions

Table S1. The drug- and lead-like physicochemical properties

The drug- and lead-like physicochemical properties of these 44 natural products were calculated using Instant JChem (version 15.10.26.0). The parameters including molecular weight (MW), log *P*, number of hydrogen bond acceptors (HBA), and number of hydrogen bond donors (HBD) were analyzed against Lipinski's rule-of-five (Table **S1** and Figure **S42**).

Table **S1**. Physicochemical Profiling of Isolated Natural Products **1**-**44** from *Alangium villosum.*

Compound	Physicochemical parameters[a]				
	MW	log P	HBA	HBD	No. of Violations
1	493.65	2.81	4	4	0
2	493.65	2.81	4	4	0
3	479.62	2.61	4	5	0
4	479.62	2.61	4	5	0
5	477.65	3.86	3	4	0
6	477.65	3.86	3	4	0
7	463.62	3.55	3	5	0
8	463.62	3.55	3	5	0
9	461.65	4.82	2	3	0
10	461.61	4.02	3	5	0
11	475.63	4.22	3	4	0
12	306.43	2.30	3	3	0
13	440.58	3.46	4	5	0
14	440.58	3.46	4	5	0
15	438.57	3.62	4	5	0
16	491.49	-0.65	10	6	1
17	505.52	-0.51	10	5	1
18	505.52	-0.51	10	5	1
19	697.69	1.76	13	6	3
20	524.54	-2.81	11	7	3
21	524.54	-2.81	11	7	3
22	524.54	-0.50	10	7	3
23	524.54	-2.81	11	7	3
24	522.55	0.01	11	7	3
25	522.55	0.01	11	7	3
26	552.57	-0.15	12	7	3
27	552.57	-0.15	12	7	3
28	582.60	-0.31	13	7	3
29	582.60	-0.31	13	7	3
30	376.36	-2.22	10	6	1
31	358.34	-1.13	8	4	0
32	470.43	-3.12	11	6	2

33	246.31	3.29	3	2	0
34	260.33	3.93	3	1	0
35	230.31	4.63	2	2	0
36	554.59	0.09	12	8	3
37	634.85	7.79	6	4	2
38	618.86	8.09	5	3	2
39	472.71	5.36	4	3	1
40	456.71	6.64	3	2	1
41	442.73	6.17	2	2	1
42	458.68	5.52	4	2	1
43	454.70	7.20	3	1	1
44	440.71	6.73	2	1	1

The results (Table **S1** and Figure **S42**) suggested that the majority of isolated natural products obeyed Lipinski's rule-of-five in terms of log P < 5 (81.8%), MW < 500 Da (63.6%), HBA < 10 (72.7%) and HBD < 5 (65.9%).

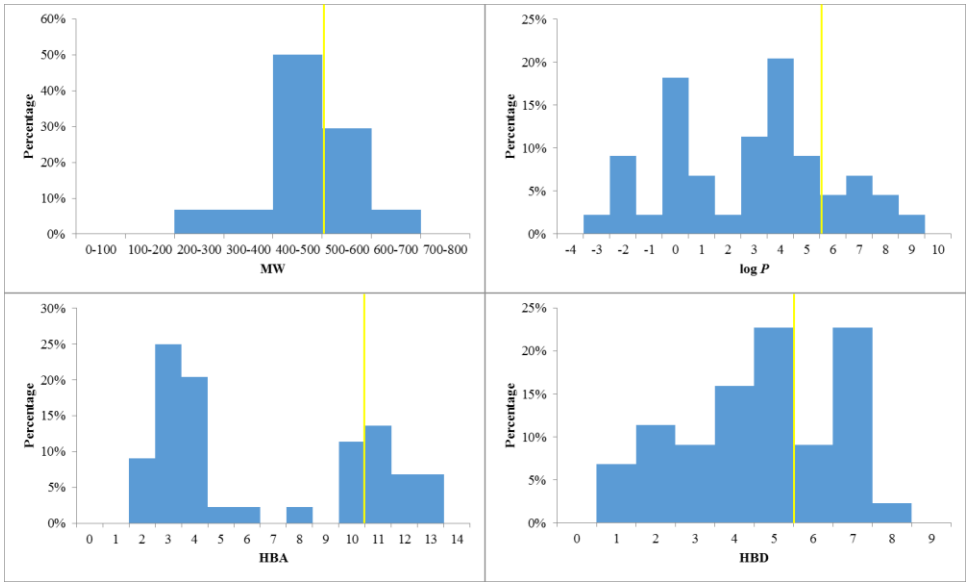

Figure **S42**. Physicochemical property histograms (MW, log P, HBD, and HBA) for compounds isolated from *Alangium villosum*. In each case the orange line indicates the maximum desirable value for oral bioavailability defined by Lipinski's rule-of-five: MW < 500 Da; log P < 5, HBA < 10 and HBD < 5.

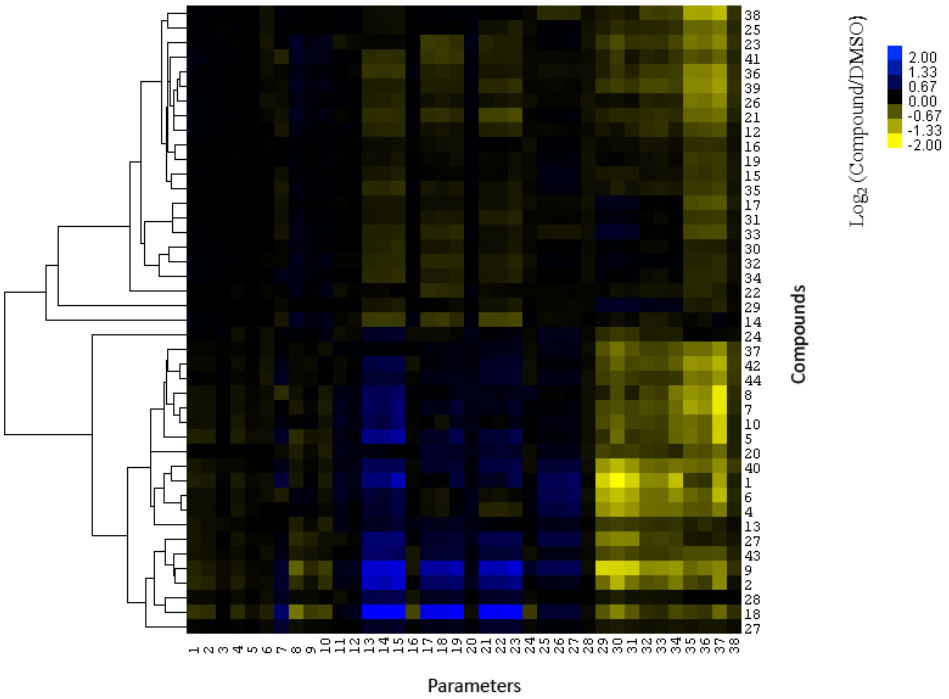

Figure S43. Heat map depicting the cytological profile of metabolites from *Alangium villosum* (AQ606931) at 10 µM on 38 parameters on the basis of the log_2 ratio of compound and vehicle (DMSO). The effects of compounds were plotted as log_2 ratio to the DMSO control. Yellow shows a decrease versus vehicle and blue shows an increase versus vehicle. Individual compounds are presented on the y-axis with individual features on the x-axis. 1. Nucleus area (µm²) 2. Nucleus morphology width (µm) 3. Nucleus morphology length (µm) 4. Nucleus morphology ratio width to length 5. Nucleus morphology roundness 6. Nucleus marker texture index 7. Nucleus marker intensity 8. Cell area (µm²) 9. Cell width (µm) 10. Cell length (µm) 11. Cell ratio width to length 12. Cell roundness 13. α-Tubulin marker intensity in the cytoplasm 14. α-Tubulin marker intensity in outer region of cytoplasm 15. α-Tubulin marker intensity in inner region of cytoplasm 16. α-Tubulin marker texture index 17. Mitochondria marker intensity in the cytoplasm 18. Mitochondria marker intensity in outer region of cytoplasm 19. Mitochondria marker intensity in inner region of the cytoplasm 20. Mitochondria marker texture index 21. LC3b marker intensity in the cytoplasm 22. LC3b marker intensity in the outer region of the cytoplasm 23. LC3b marker intensity in inner region of cytoplasm 24. LC3b marker texture index 25. Lysosome marker intensity mean 26. Lysosome marker intensity outer region mean 27 Lysosome marker intensity inner region mean 28. Lysosome marker texture index. 29. Number of EEA1 marker spots in cytoplasm 30. Number of EEA1 marker spots in inner region of cytoplasm 31. Number of EEA1 marker spots in outer region of cytoplasm 32. Number of EEA1 marker spots per Area of cytoplasm 33. EEA1 marker intensity in outer region of cytoplasm 34 EEA1 marker intensity in inner region of cytoplasm 35. EEA1 marker intensity in the cytoplasm 36. Number of EEA1 marker spots per area of outer region 37 Number of EEA1 marker spots per Area of inner region of cytoplasm 38. EEA1 marker texture index.

Chapter Five. Conclusion: physicochemical properties and ChemGPS analysis of natural product chemical probes

In many cases, natural product research stops when new structures and their associated biological activities are published. We have developed a strategy to prioritize these molecules for further evaluation. Chemical investigation of three selected biota samples following a HTS assay resulted in the isolation of 103 natural products (13 series) which perturbed Parkinson's disease patient derived hONS cells. We conducted further analysis to evaluate the drug-like properties and chemical space as well as the cytological profiling of these secondary metabolites. By a combined strategy using cytological profiling, Ro5 and ChemGPS analysis, three series of natural products were identified as ideal chemical probes to further investigate Parkinson's disease. They also can be used as lead compounds for future PD-drug development. (Figure 5.1).

5.1 Isolation of the natural products

A preliminary chemical analysis was conducted on the seven selected fractions using LC-MS and ^{1}H NMR spectroscopy. On the basis of the HPLC retention time, UV chromophore, MS and ^{1}H NMR spectroscopic data, *Jaspis splendens* (subject 1) showed three series of secondary metabolites including peptides, nucleosides and indole alkaloids. *Gloriosa superba* (subject 2) showed the presence of colchicine and lumicolchicine alkaloids, flavone glycosides, nucleosides and phenolic glycosides. There were evidence to suggest the presence of benzoquinolizidine alkaloids, tetrahydroisoquinoline-monoterpene alkaloids, terpenoids and simple aromatic structural classes in *Alangium villosum* (subject 3).

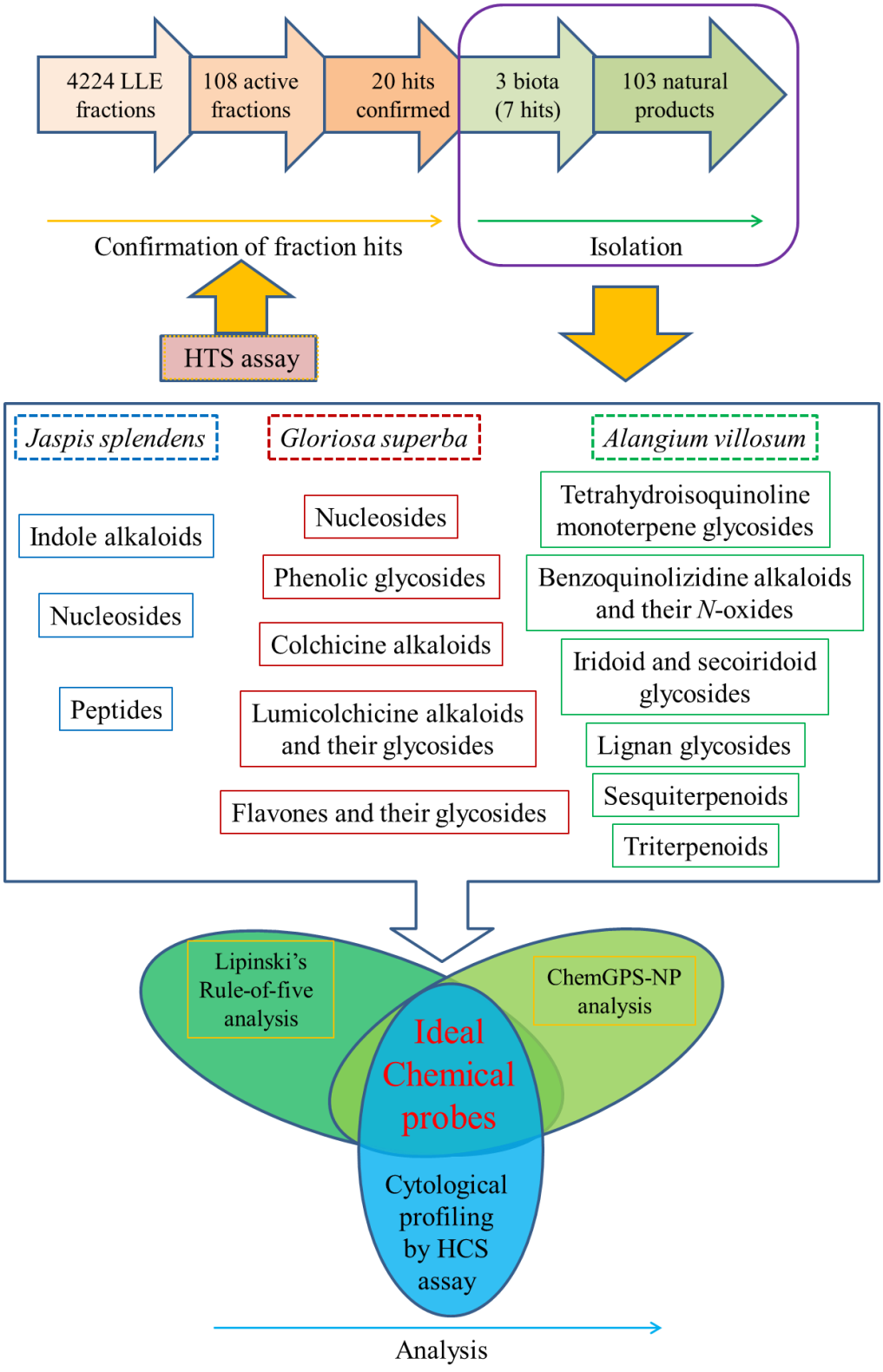

Figure 5.1 An overview of the project including the subject selection of hit fractions from the constructed Nature Bank LLE fraction library following a HTS assay, natural products isolated from three selected biota samples, the structure classes from each biota samples, the structure classes from each biota, Lipinski's rule of five and ChemGPS-NP principle component analysis and cytological profiling of the isolated compounds by a HCS assay.

The large scale isolation and purification was subsequently carried out on the three selected biota samples. Chemical investigation of the marine sponge *Jaspis splendens* (50 g) resulted in the isolation of 22 natural products (1-**1** to 1-**22**) as well as 39 secondary metabolites (2-**1** to 2-**39**) from *Gloriosa superba* L. (20 g) and 44 compounds (3-**1** to 3-**44**) from *Alangium villosum* (20 g), respectively. As an example, the 39 natural products isolated from *Gloriosa superba* L. were distributed in each lead-like enhanced fraction of the HPLC chromatogram (Figure 5.2).

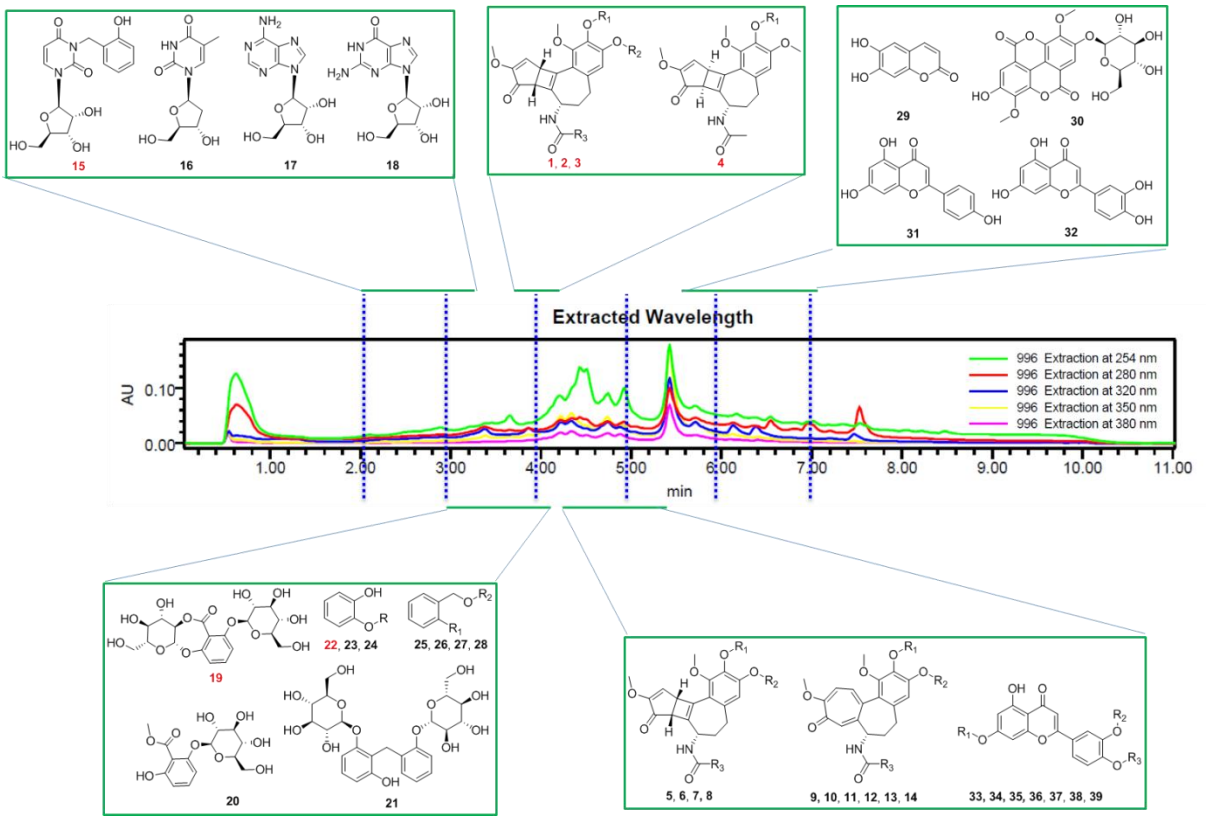

Figure 5.2 Chemical structures of the 39 natural products isolated from *Gloriosa superba* L. as well as their distributions in different LLE fractions as shown in the HPLC chromatogram.

Further analysis showed that the isolated compounds were distributed across all five lead-like enhanced fractions, with more than 75% originating from the relatively polar fractions 1 to 3 (Figure 5.3).

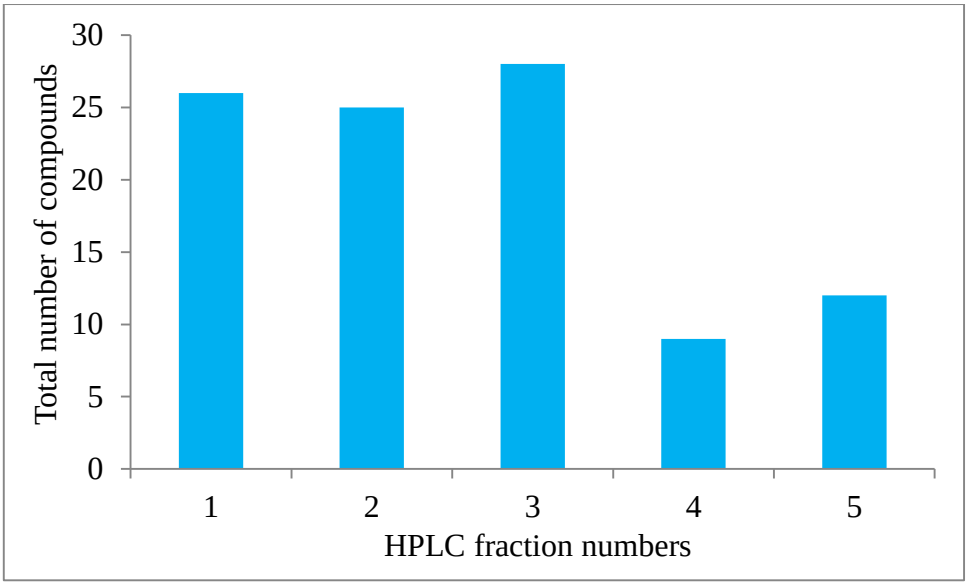

Figure 5.3 Bar chart depicting number of natural products in five LLE fractions

5.2 Physicochemical properties of isolated natural products

Neurodegenerative diseases such as PD, AD, HD, and others share common features at cellular and subcellular levels. The diseases also share common molecular signaling pathways that may lead to apoptosis, necroptosis, and inflammation.[1] Compounds with neuroprotective properties must possess certain physicochemical properties to allow brain penetration and exposure. Herein, we analyzed the four Lipinski's properties including MW, log *P*, HBA and HBD of the isolated 103 secondary metabolites (Table 1 and Figure 4). We then compared the set of data with that of the anti-PD compounds (drugs and candidates in clinical or preclinical trials) to evaluate the likelihood of the isolated natural products being useful anti-PD chemical probes and drug candidates. The drug- and lead-like physical and chemical properties of these isolated natural products were calculated using Instant JChem (version 15.10.26.0).[2]

Table 5.1 Physicochemical profiling of the 103 isolated natural products

Compounds	MW	Log *P*	HBA	HBD	Number of violations	In Figure 7
1-**1**	191.19	-0.46	5	1	0	
1-**2**	461.11	4.40	2	3	0	
1-**3**	201.26	-3.19	2	1	0	
1-**4**, 2-**18**	283.24	-2.71	8	5	0	
1-**5**	267.25	-2.01	8	4	0	
1-**6**, 2-**16**	242.23	-1.12	5	3	0	
1-**7**	291.27	-1.42	8	4	0	
1-**8**	292.25	-1.81	7	4	0	
1-**9**	324.29	-1.27	8	4	0	
1-**10**	309.28	-2.43	8	5	0	
1-**11**	192.18	0.28	4	2	0	
1-**12**	159.15	0.14	4	2	0	
1-**13**	177.17	-0.87	4	3	0	
1-**14**	239.12	2.26	1	2	0	
1-**15**	239.07	1.69	1	2	0	
1-**16**	238.09	1.76	2	3	0	
1-**17**	254.08	2.84	1	1	0	
1-**18**	709.68	5.04	5	4	2	√
1-**19**	723.67	4.69	6	4	1	√
1-**20**	727.70	4.38	7	6	2	√
1-**21**	695.66	4.80	5	4	1	√
1-**22**	788.58	5.81	5	4	2	√
2-**1**	547.56	-1.51	11	5	2	√
2-**2**	533.53	-1.56	11	5	2	√
2-**3**	533.53	-1.66	11	6	3	√
2-**4**	547.56	-1.51	11	5	2	√
2-**5**	385.42	0.76	6	2	0	
2-**6**	371.39	0.71	6	2	0	
2-**7**	385.42	0.85	6	1	0	
2-**8**	399.44	0.90	6	1	0	
2-**9**	399.44	1.46	6	1	0	
2-**10**	385.42	1.32	6	2	0	
2-**11**	385.42	1.32	6	2	0	
2-**12**	385.42	1.41	6	1	0	
2-**13**	371.39	1.27	6	2	0	
2-**14**	383.4	1.40	6	1	0	
2-**15**	350.33	-0.77	7	4	0	
2-**17**	267.25	-2.09	8	4	0	
2-**19**	460.39	-2.85	12	7	2	√
2-**20**	330.29	-0.25	8	5	0	
2-**21**	554.55	-2.24	13	10	3	√
2-**22**	434.39	-2.67	12	8	2	√
2-**23**	434.39	-2.67	12	8	2	√
2-**24**	272.25	-0.90	7	5	0	
2-**25**	286.28	-1.37	7	5	0	
2-**26**	286.28	-0.87	7	5	0	
2-**27**	448.42	-3.14	12	8	2	√
2-**28**	432.42	-2.34	11	7	2	√
2-**29**	178.14	1.18	3	2	0	
2-**30**	492.39	-0.96	11	5	1	√
2-**31**	286.24	2.40	6	4	0	
2-**32**	270.24	2.71	5	3	0	
2-**33**	610.52	-2.13	16	10	3	√
2-**34**	610.52	-2.13	16	10	3	√

2-**35**	594.52	-0.59	15	9	3	√
2-**36**	608.55	-0.44	15	8	3	√
2-**37**	448.38	0.14	11	7	2	√
2-**38**	462.41	0.28	11	6	2	√
2-**39**	448.38	0.14	11	7	2	√
3-**1**	493.65	2.81	4	4	0	
3-**2**	493.65	2.81	4	4	0	
3-**3**	479.62	2.61	4	5	0	
3-**4**	479.62	2.61	4	5	0	
3-**5**	477.65	3.86	3	4	0	
3-**6**	477.65	3.86	3	4	0	
3-**7**	463.62	3.55	3	5	0	
3-**8**	463.62	3.55	3	5	0	
3-**9**	461.65	4.82	2	3	0	
3-**10**	461.61	4.02	3	5	0	
3-**11**	475.63	4.22	3	4	0	
3-**12**	306.43	2.30	3	3	0	
3-**13**	440.58	3.46	4	5	0	
3-**14**	440.58	3.46	4	5	0	
3-**15**	438.57	3.62	4	5	0	
3-**16**	491.49	-0.65	10	6	1	√
3-**17**	505.52	-0.51	10	5	1	√
3-**18**	505.52	-0.51	10	5	1	√
3-**19**	697.69	1.76	13	6	3	√
3-**20**	524.54	-2.81	11	7	3	√
3-**21**	524.54	-2.81	11	7	3	√
3-**22**	524.54	-0.50	10	7	3	√
3-**23**	524.54	-2.81	11	7	3	√
3-**24**	522.55	0.01	11	7	3	√
3-**25**	522.55	0.01	11	7	3	√
3-**26**	552.57	-0.15	12	7	3	√
3-**27**	552.57	-0.15	12	7	3	√
3-**28**	582.60	-0.31	13	7	3	√
3-**29**	582.60	-0.31	13	7	3	√
3-**30**	376.36	-2.22	10	6	1	√
3-**31**	358.34	-1.13	8	4	0	
3-**32**	470.43	-3.12	11	6	2	√
3-**33**	246.31	3.29	3	2	0	
3-**34**	260.33	3.93	3	1	0	
3-**35**	230.31	4.63	2	2	0	
3-**36**	554.59	0.09	12	8	3	√
3-**37**	634.85	7.79	6	4	2	√
3-**38**	618.86	8.09	5	3	2	√
3-**39**	472.71	5.36	4	3	1	√
3-**40**	456.71	6.64	3	2	1	√
3-**41**	442.73	6.17	2	2	1	√
3-**42**	458.68	5.52	4	2	1	√
3-**43**	454.70	7.20	3	1	1	√
3-**44**	440.71	6.73	2	1	1	√

All physicochemical properties, including molecular weight (MW), log *P*, hydrogen bond acceptors (HBA) and hydrogen bond donors (HBD), were calculated using Instant JChem (version 15.10.26.0). The right column indicates if this compound falls into the orange rectangle (orange tick), blue rectangle (blue tick) or green ellipse (green tick) in Figure 7.

The results (Table 5.1 and Figure 5.4) suggested that the majority of isolated natural products obeyed Lipinski's rule-of-five in terms of MW < 500 Da (71%), log *P* < 5 (90%), HBA < 10 (71%) and HBD < 5 (71%).

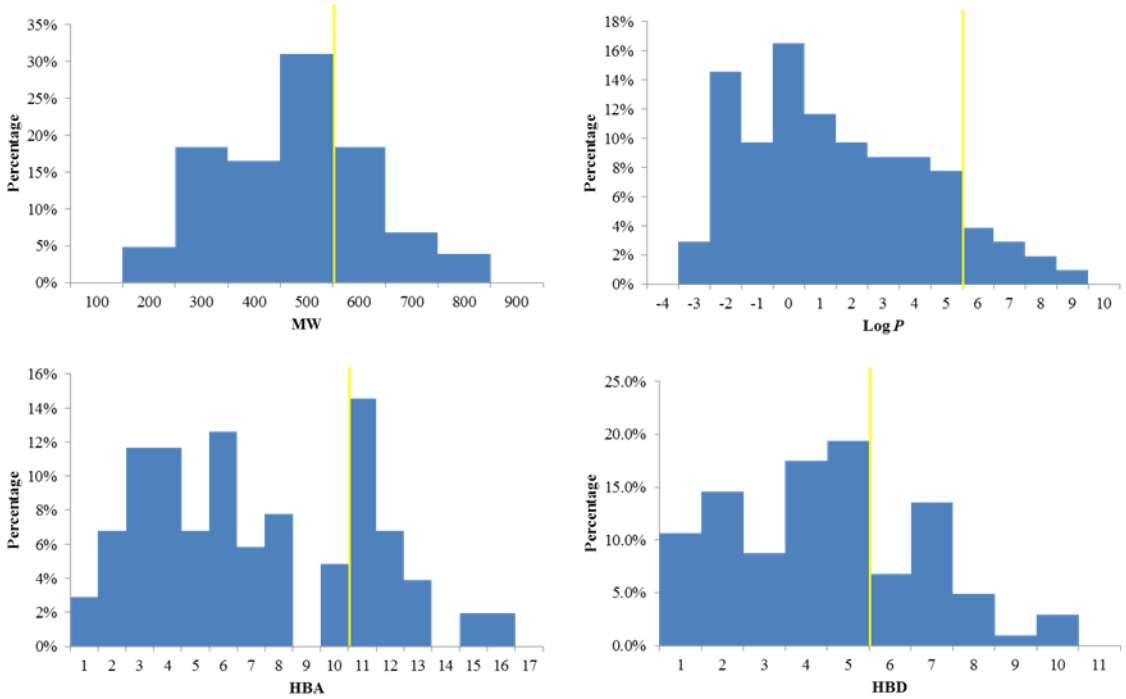

Figure 5.4 Analysis of physicochemical properties (MW, log P, HBA and HBD) of the 103 isolated natural products. In each case the yellow line indicates the maximum desirable value for oral bioavailability defined by Lipinski's rule of five: MW < 500 Da; log P < 5.

The existence of sugar moiety in the molecules provides more *O*-containing functionalities and hydroxyl groups, which might account for the violations of HBA and HBD values, as well as molecular weights. With respect to the isolated compounds set, 35 out of 103 compounds had two or more violations of the Lipinski's parameters. The structural survey of these 35 compounds further revealed that 30 of them contained at least one sugar moiety, such as *β*-lumicolchicosides A–C and *γ*-lumicolchicoside A (2-**1** to 2-**4**), gloriosides A and B (2-**19** and 2-**22**), 6-*O*-methyl-*N*-deacetylisoipecosidic acid (3-**20**), 7-*O*-methyl-*N*-deacetylisoipecosidic acid (3-**21**) and *N*-deacetylisoipecoside (3-**22**). All of the 30 compounds had the violation with HBA > 10, as well as 23 compounds had the violation with MW > 500. There were also 27 compounds contained one or two sugar moieties with the violation of HBD >

5. The eight triterpenoids (3-**37** to 3-**44**), which were isolated from the relatively nonpolar fractions of *Alangium villosum*, contributed to the violation with log *P* > 5. The other molecules with log *P* > 5 were two peptides isolated from the nonpolar part of *Jaspis splendens* (1-**18** and 1-**22**). The peptides (1-**18** to 1-**22**) were also the second group of compounds having the violation with MW > 500.

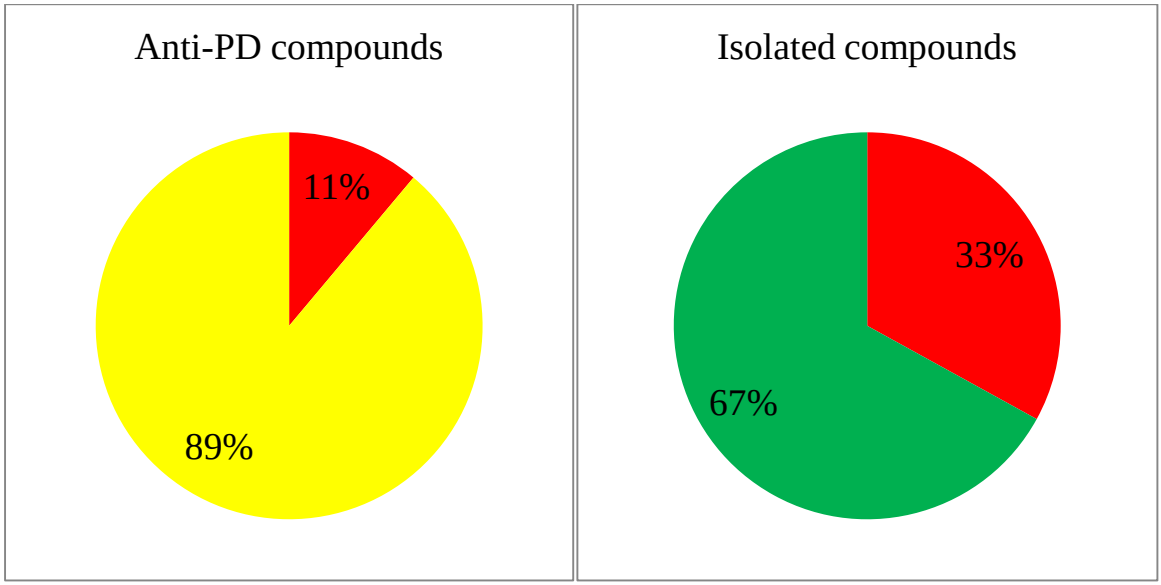

Figure 5.5 Pie chart presentation of the percentage of anti-PD compounds (left) and isolated compounds (right) obeying or violating Lipinski's rule of five. Non-compliant (more than one violation) is shown in red and compliant (less than two violations) in yellow and green, respectively.

In Chapter One, literature research on anti-PD natural products and derivatives identified a total of 36 small molecules. The structures of the 36 natural origin anti-PD compounds were converted into SMILES format and imported into Instant JChem to calculate the physicochemical parameters of each molecule. This has been discussed in details in Chapter One. The percentages of anti-PD compounds and the isolated compounds compliant with Lipinski's rule of five were depicted in Figure 5.5. The histograms for molecular weight (MW), calculated log *P*, hydrogen bond acceptors (HBA) and hydrogen bond donors (HBD) for two sets of compounds were shown in Figure 5.6.

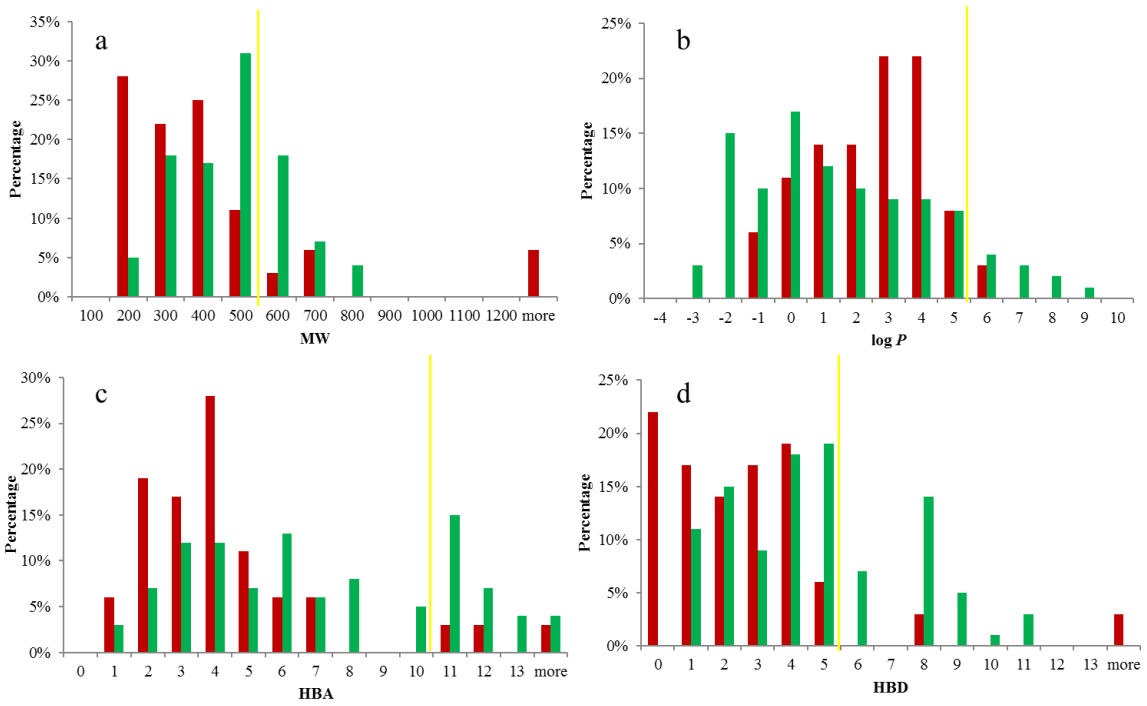

Figure 5.6 Physicochemical property histograms of anti-PD compounds (dark red) and isolated natural products (green): (a) molecular weight (MW), (b) calculated log *P*, (c) hydrogen bond acceptors (HBA), (d) hydrogen bond donors (HBD). In each case the yellow line indicates the maximum desirable value for oral bioavailability defined by Lipinski's Ro5: MW < 500 Da; log *P* < 5, HBA < 10 and HBD < 5.

It was found that 89% of anti-PD compounds had less than two violations of the Lipinski's parameters, with 83% having no violations. These values were decreased in the isolated compounds data set, with 67% less than 2 violations and 53% no violation, respectively.

The histogram of molecular weight (Figure 5.6a) showed that about 86% of the anti-PD compounds and 71% of the isolated compounds were distributed between molecular weights of 100–500 Da, with 75% of anti-PD compounds distributed at 200–400 Da while 31% of the isolated compounds peaked at 400–500 Da. About 14% of the anti-PD compounds had molecular weights over 500 Da while 29% of isolated compounds had molecular weights over 500. The calculated log *P* (Figure 5.6b) of the majority of both sets (97% for anti-PD compounds, 90% for isolated compounds) fell into the same region from -2 to 5 but the distribution maximum was between 2–4 for the anti-PD compounds (44%) and -3–0 for the

isolated compounds (42%). The overall percentage of compounds satisfying the log *P* criteria was decreased for the isolated compounds (90%) as compared to the anti-PD compounds (97%).

The histogram of hydrogen bond acceptors (HBA) (Figure 5.6c) showed that the majority of anti-PD compounds had HBA between 1–7 compared with the wide spread of HBA for isolated compounds. About 92% of the anti-PD compounds concentrated in a range of 1–7 while only 58% of the isolated compounds fall into the same range. The HBA values of the isolated compounds fluctuated from 1 to more than 13. The percentage of the isolated compounds with acceptable HBA (no more than 10) was 71% as compared to 92% for anti-PD compounds. The HBD histogram distribution (Figure 5.6d) showed that the majority of anti-PD compounds had HBD between 0–4, in contrast to 4–5 donors for the isolated compounds. About 94% of the anti-PD compounds had no more than 5 hydrogen bond donors while the number of the isolated compounds compliant with Ro5 was 71%.

The histograms of the four Lipinski's parameters showed more similarities between these two datasets on the properties of MW and the calculated log *P* than the hydrogen bond acceptors and donors. This is probably due to the fact that natural products, generally speaking, have more *O*-containing functionalities and hydroxyl groups. The percentages of the isolated compounds were lower than those of the anti-PD compounds in all Ro5 parameters except for the calculated log *P*.

5.3 ChemGPS-NP Analysis –comparison of physicochemical space of anti-PD compounds and isolated compounds

In contrast to Lipinski's parameters focusing on a restricted set of drug-like properties generated directly from the molecular structures, ChemGPS-NP is a tool tuned for identifying volumes of chemical space. In this analysis, individual coordinates are *t*-scored from principal component analysis (PCA) using 35 descriptors calculated from 1779 chemical structures, to

allow correlation to biological activities.[3] ChemGPS-NP has been designed to handle the chemical diversity of natural products. It can discover physiochemical properties not directly discernible from structural data, and can chart biologically relevant chemical space and provide an efficient mapping device for prediction of properties and activities of groups of compounds.[4] Therefore, ChemGPS-NP was used for principle component analysis of anti-PD compounds and isolated compounds to compare their distribution in physicochemical space.[5] While ChemGPS-NP is comprised of eight coordinate dimensions (principal components, PCs), the first three principle components explained 71% of the variance in the training data and can be interpreted as representing broad physical properties. For example, properties relating to size, shape, and polarizability were plotted in PC1; aromatic and conjugation related properties of the compounds were explained in PC2; lipophilicity, polarity, and H-bond capacity were expressed in PC3.

The analysis (Figure 5.7a) demonstrated the score plot of 36 anti-PD compounds (blue dots) and 103 isolated natural products (red dots). The graph shows that the majority of the anti-PD compounds concentrated in a relatively narrow area of physicochemical space, which means that these compounds shares similarities in the described parameters. Around 60% of the 103 isolated natural products are positioned within similar drug-like chemical space as the anti-PD compounds and when visualized using the most significant ChemGPS-NP coordinates in three dimensions. The peptides (1-**18** to 1-**22**), triterpenoids (2-**37** to 2-**44**) and most of sugar containing compounds, which are located well outside the cloud of points representing the anti-PD compounds, are circled by orange rectangle, blue rectangle and green ellipse in (5.7b – 5.7d), respectively. All these compounds possess higher molecular weights than 500, and/or have log *P* values > 5, and/or the HBA and HBD values exceed the Lipinski's rule of five.

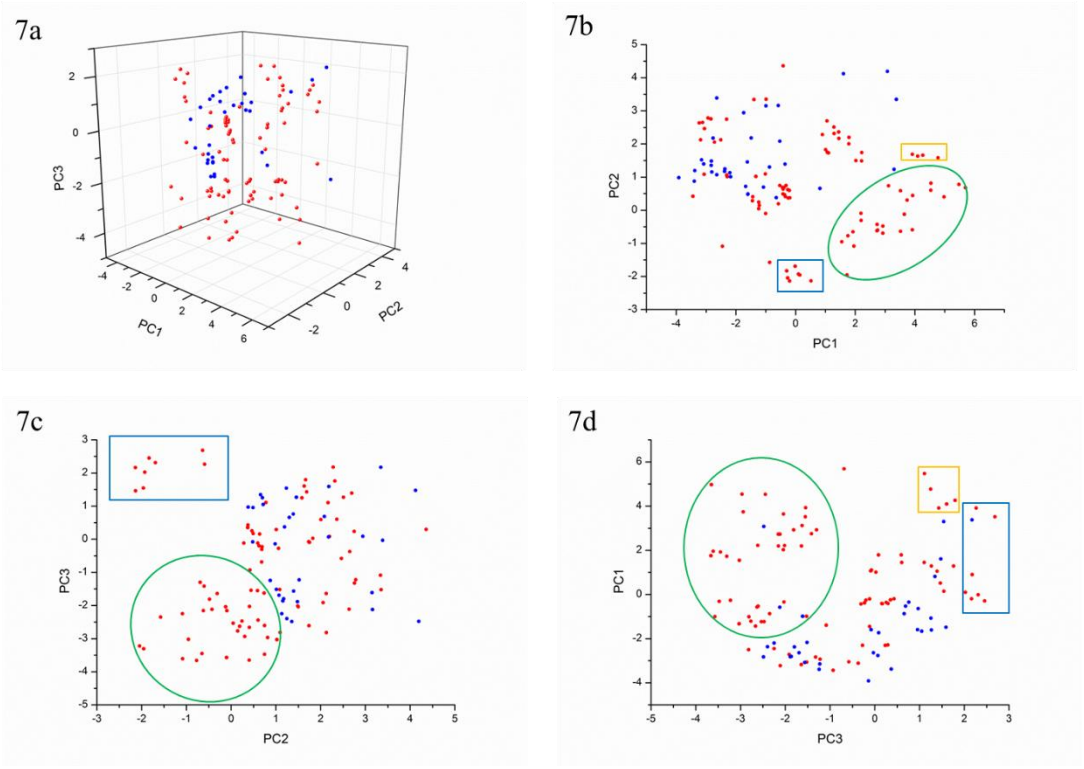

Figure 5.7 Distribution of 36 anti-PD compounds (blue dots) and isolated natural products (red dots) in ChemGPS-NP chemical space defined by the first three principle components: PC1 representing broad physical properties such as size, shape, and polarizability; PC2 representing aromatic and conjugation related properties; PC3 representing lipophilicity, polarity, and H-bond capacity. (a-d) 3D and 2D plots comparison of the physicochemical space of anti-PD compounds and the isolated compounds. The peptides, triterpenoids and some sugar containing compounds, which were located well outside the cloud of points representing the anti-PD compounds, were circled by orange rectangle, blue rectangle and green ellipse in (b - d), respectively.

In summary, the majority of the anti-PD compounds are compliant with the Lipinski's rules and concentrated in a narrow area of physicochemical space. The 2D plots identify a narrow area of physicochemical space for the anti-PD compounds (Figure 5.7b-5.7d) that also contains around 60% isolated natural compounds. The clusters of isolated compounds enclosed within the orange rectangle, blue rectangle and green ellipse are the exceptions and may constitute other special classes. Details of these compounds are indicated in Table 5.1.

5.4 Cytological profiling of the isolated compounds

On the basis of previous work, we had developed a theoretical framework that explains that all natural products interact with biologically relevant space. All compounds were subjected to an unbiased phenotypic assay on hONS cells followed by cluster analysis of cytological effects. The cytological profiles of all isolated secondary metabolites from the Australian marine sponge *Jaspis splendens* and two Australian plants *Gloriosa superba* and *Alangium villosum* were examined to identify congeneric chemical series by coupling an unbiased multidimensional phenotype assay using nontransformed and nonimmortalized hONS cells, which are primary cells derived from a Parkinson's disease patient (Figure 5.8).

As shown in Figure 8, a number of structural classes in the three green rectangles were identified which had significant phenotypic perturbation on hONS cells. Jaspamycin (1-**8**) had significant or moderate effects on most markers (Figure 5.9). β-Lumicolchicine analogues (2-**5** to 2-**8**) showed moderate effects on α-tubulin related parameters while colchicine (2-**9**) and its congeners (2-**10** to 2-**14**) displayed major effects on mitochondria and autophagy related parameters. Tubulosine congeners (3-**1** to 3-**11**) also had moderate effects on α-tubulin markers.

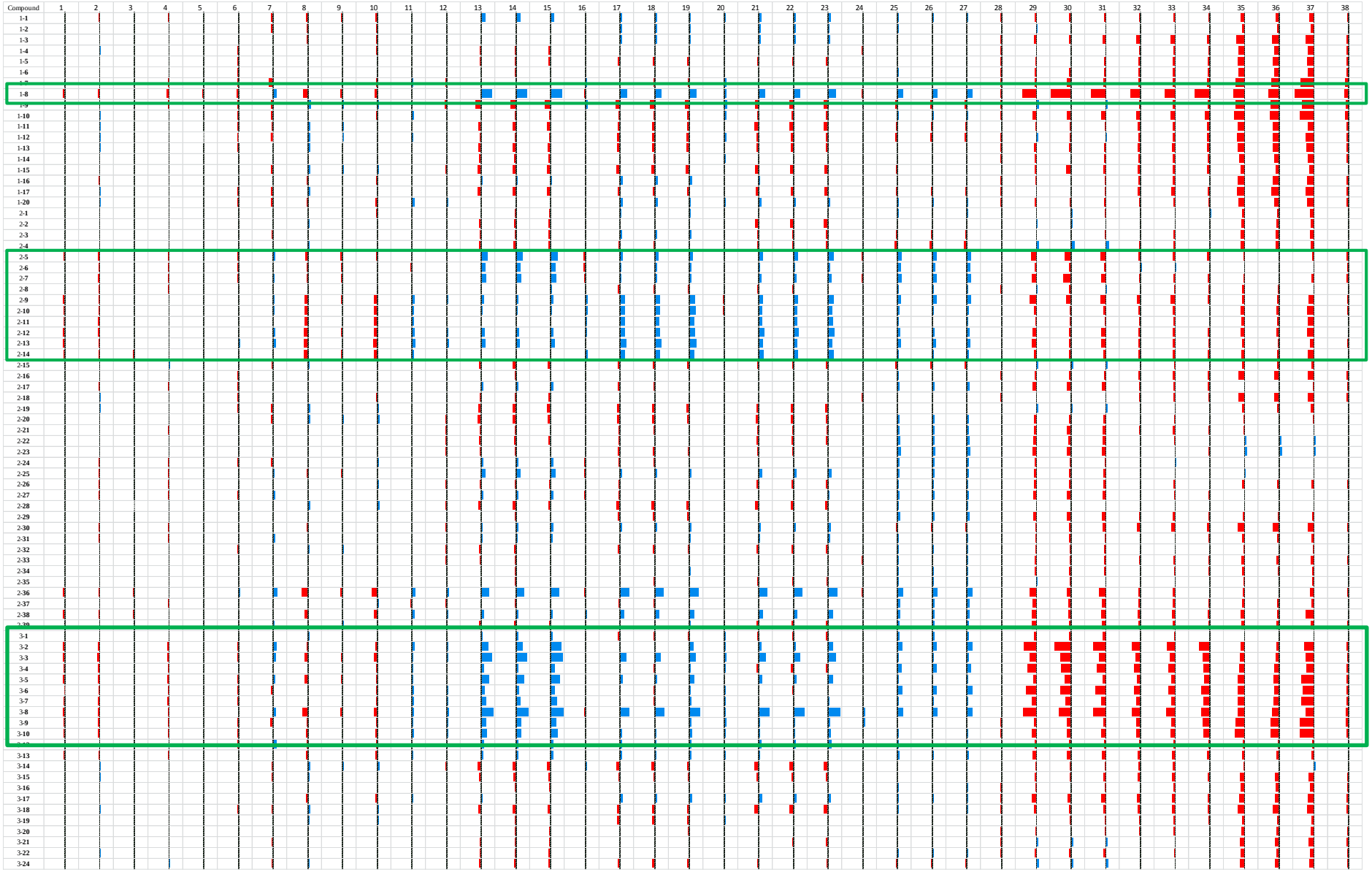
Compound
1 2 3 4 5 6 7 8 9 10 11 12 13 14 15 16 17 18 19 20 21 22 23 24 25 26 27 28 29 30 31 32 33 34 35 36 37 38
1-1
1-2
1-3
1-4
1-5
1-6
1-8
1-10
1-11
1-12
1-13
1-14
1-15
1-16
1-17
1-20
2-1
2-2
2-3
2-4
2-5
2-6
2-7
2-8
2-9
2-10
2-11
2-12
2-13
2-14
2-15
2-16
2-17
2-18
2-19
2-20
2-21
2-22
2-23
2-24
2-25
2-26
2-27
2-28
2-29
2-30
2-31
2-32
2-33
2-34
2-35
2-36
2-37
2-38
3-1
3-2
3-3
3-4
3-5
3-6
3-7
3-8
3-9
3-10
3-13
3-14
3-15
3-16
3-17
3-18
3-19
3-20
3-21
3-22
3-24

(Continued)

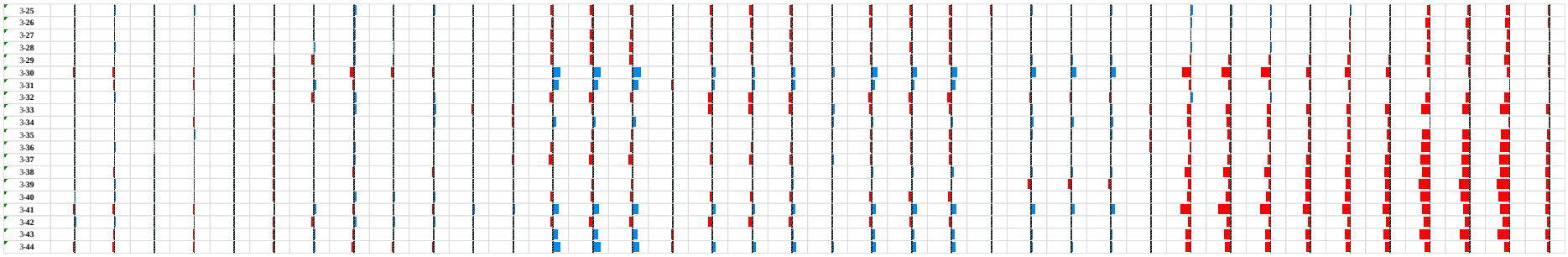

Figure 5.8 Bar chart depicting the cytological profile of metabolites from J. splendens (1-**1** to 1-**22**), G. superba (2-**1** to 2-**39**) and A. villosum (3-**1** to 3-**44**) at 10 µM on 38 parameters based on the log2 ratio of compound and vehicle (DMSO). Red shows a decrease versus vehicle and blue shows an increase versus vehicle. Individual compounds are presented on the y-axis with individual features on the x-axis. 1. Nucleus area (µm²) 2. Nucleus morphology width (µm) 3. Nucleus morphology length (µm) 4. Nucleus morphology ratio width to length 5. Nucleus morphology roundness 6. Nucleus marker texture index 7. Nucleus marker intensity 8. Cell area (µm²) 9. Cell width (µm) 10. Cell length (µm) 11. Cell ratio width to length 12. Cell roundness 13. α-Tubulin marker intensity in the cytoplasm 14. α-Tubulin marker intensity in outer region of cytoplasm 15. α-Tubulin marker intensity in inner region of cytoplasm 16. α-Tubulin marker texture index 17. Mitochondria marker intensity in the cytoplasm 18. Mitochondria marker intensity in outer region of cytoplasm 19. Mitochondria marker intensity in inner region of the cytoplasm 20. Mitochondria marker texture index 21. LC3b marker intensity in the cytoplasm 22. LC3b marker intensity in the outer region of the cytoplasm 23. LC3b marker intensity in inner region of cytoplasm 24. LC3b marker texture index 25. Lysosome marker intensity mean 26. Lysosome marker intensity outer region mean 27 Lysosome marker intensity inner region mean 28. Lysosome marker texture index. 29. Number of EEA1 marker spots in cytoplasm 30. Number of EEA1 marker spots in inner region of cytoplasm 31. Number of EEA1 marker spots in outer region of cytoplasm 32. Number of EEA1 marker spots per Area of cytoplasm 33. EEA1 marker intensity in outer region of cytoplasm 34 EEA1 marker intensity in inner region of cytoplasm 35. EEA1 marker intensity in the cytoplasm 36. Number of EEA1 marker spots per area of outer region 37 Number of EEA1 marker spots per Area of inner region of cytoplasm 38. EEA1 marker texture index. A number of identified structural classes which had significant phenotypic perturbation on hONS cells were shown in the three green rectangles.

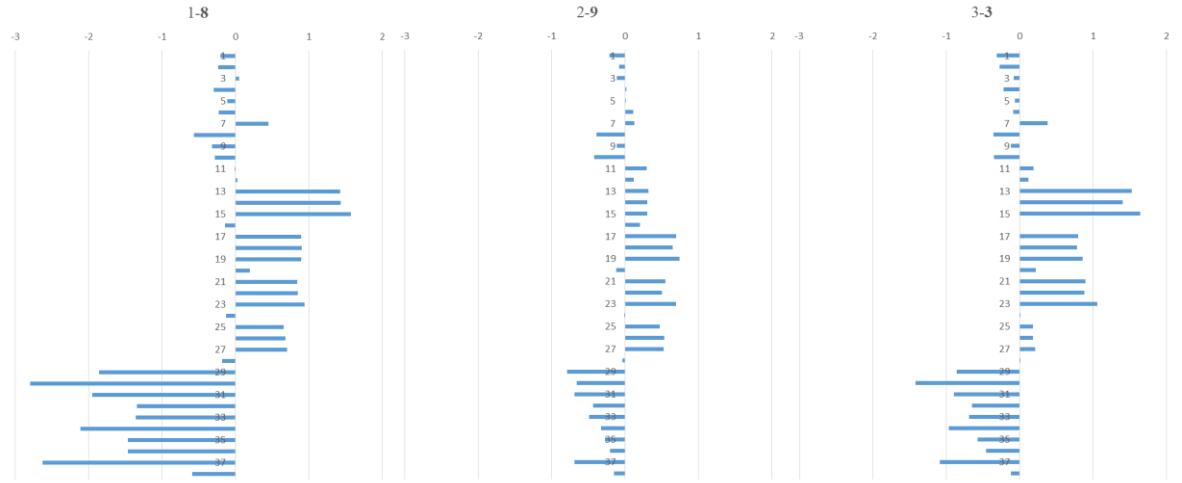

Figure 5.9 Bar chart depicting the cytological profiles of three individual metabolites jaspamycin (1-**8**) from *J. splendens*, colchicine (2-**9**) from *G. superba* L. and 9-demethyltubulosine N^5-oxide (3-**3**) from *A. villosum* at 10 μM on 38 parameters on the basis of the $\log_2$ ratio of compound and vehicle (DMSO), respectively. Individual parameters are presented on the y-axis with $\log_2$ values on the x-axis. The 38 parameters are the same as shown in Figure 8.

5.5 Identification of ideal chemical probes

Three series of secondary metabolites (1-**8**, 2-**5** to 2-**14** and 3-**1** to 3-**11** from three biota samples, respectively) had strong or moderate perturbation on the hONS cell model of PD. They are distributed in those active fractions identified by the initial HTS assay in all cases. More interestingly, the physicochemical properties of all of the identified anti-PD compounds obey Lipinski's rule of five and the analysis of the physicochemical properties (MW, log *P*, HBA and HBD) of the 22 identified chemical probes is shown in Figure 5.10a to 5.10d. As shown also in Figure 5.11a to 5.11d, these identified compounds fall into similar physicochemical space, following PCA analysis, as occupied by the anti-PD compounds. Herein, the three series of natural products are identified as ideal anti-PD chemical probes.

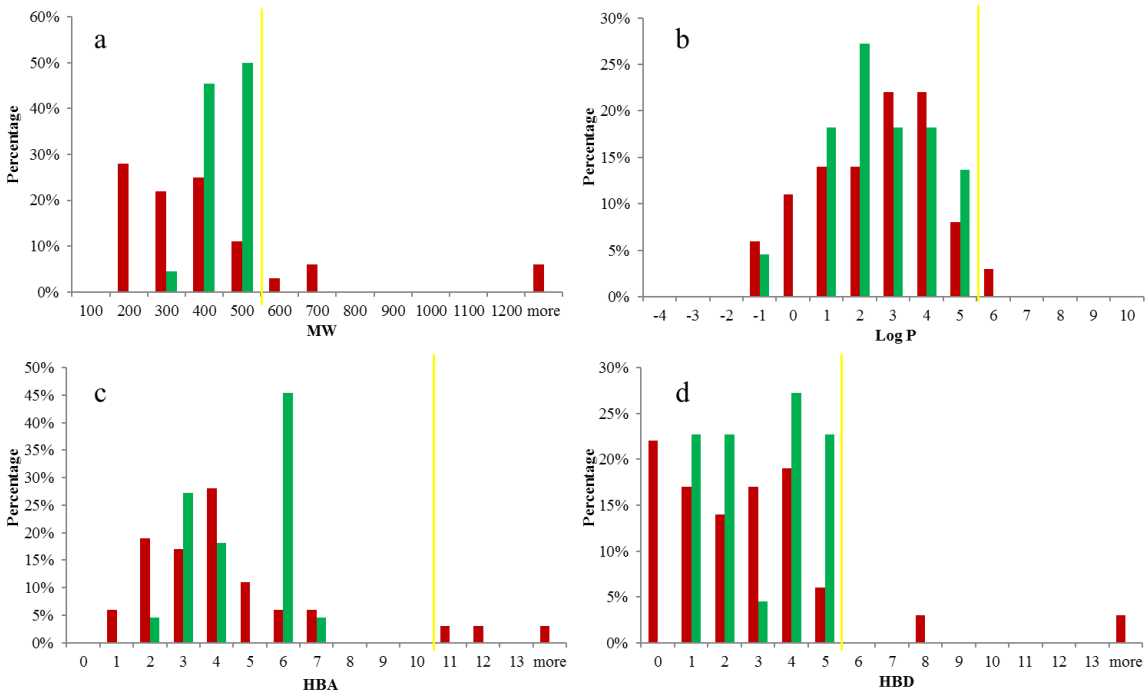

Figure 5.10 Bar chart depicting the cytological profilesof anti-PD compounds (dark red) and 22 identified natural product chemical probes (green): (a) molecular weight (MW), (b) calculated log *P*, (c) hydrogen bond acceptors (HBA), (d) hydrogen bond donors (HBD). In each case the yellow line indicates the maximum desirable value for oral bioavailability defined by Ro5: MW < 500 Da; log *P* < 5, HBA < 10 and HBD < 5.

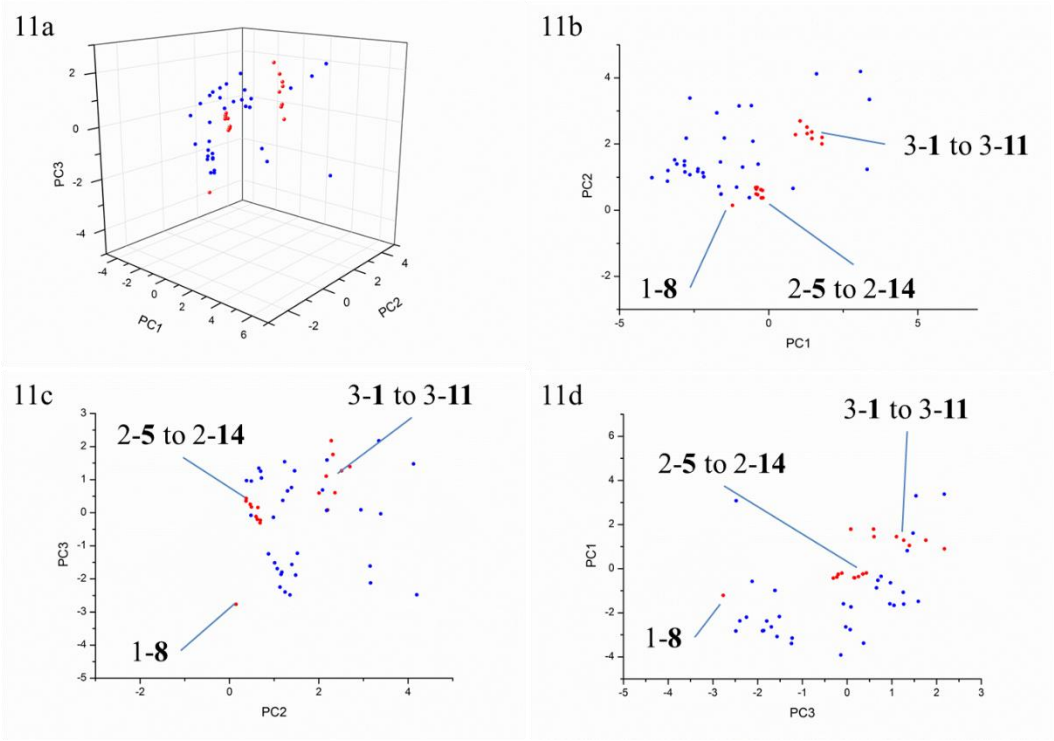

Figure 5.11 Bar chart depicting the cytological profiles chemical probes (red dots) in ChemGPS-NP chemical space defined by the first three principle components PC1, PC2 and PC3. (a-d) 3D and 2D plots comparison of the physicochemical space of anti-PD compounds and 22 identified anti-PD natural product chemical probes.

5.6. Conclusions

Natural products have been a major resource of new drugs and chemical probes due to their diverse structures and specific biological activities. Our investigation concentrated on natural product chemical probes which had significant effects on hONS cells derived from a PD patient. The results demonstrated that the initial biota selection of the Nature Bank library based on physicochemical profiling can translate into isolation of natural products with desirable physicochemical properties. The combined Lipinski's rule-of-five, ChemGPS-NP analysis and phenotypic profiling can be employed as a beneficial strategy for the selection of ideal chemical probes for further investigation on Parkinson's disease. In conclusion, by a combined strategy using cytological profiling, Ro5 and ChemGPS analysis, three series of natural products were identified as ideal chemical probes for further investigation of Parkinson's disease. They also can be used as lead compounds for future PD-drug development.

Significance is that the three series of compounds have different phenotypes. Jaspamycin had much more significant negative effects on EEA1 related markers compared with the other two types of compounds. Colchicine analogues presented lighter effects on α-tubulin related markers while tubulosine analogues showed weaker effects on lysosome related markers. This allows interrogation of different mechanisms.

One difficulty, the valley of death, in the CNS area is the lack of predictive animal models. Importantly, clinical trial failures in CNS tend to occur later in the clinical development process, when resource demands and costs are at their highest. This has resulted in huge attrition in the clinic. Bapineuzumab, investigated by Pfizer, is a humanized N-terminal–specific anti-Aβ monoclonal antibody in clinical development for the treatment of Alzheimer's disease. In preclinical studies, the murine form of the antibody (3D6) was shown

to bind to fibrillar, oligomeric, and monomeric forms of Aβ, reduce the amount of Aβ in the brain, and improve memory in transgenic mice that overproduced Aβ. Phase III trials were discontinued after the first two completed trials showed no treatment effect on either cognitive or functional outcomes. Bapineuzumab engaged its target but had no benefit. The side effects included vascular brain edemas and hydrops of sulci. Solanezumab is another monoclonal antibody investigated by Eli Lilly as a neuro-protector for patients with Alzheimer's disease. It was also failed in Phase III trials due to no significant benefit.

The high risk and low approval rates of drugs targeting neuropsychiatric diseases such as Alzheimer's, Parkinson's, depression, anxiety, schizophrenia and stroke have sent billions of dollars down the drain in recent years. The costs and risks of developing compounds for CNS and pain disorders continues to rise, while the rate of success continues to decline. The extortionate CNS R&D losses of recent years are due to the fact that the majority of neuropsychiatric leads (80%) fail in the pricey Phase III stage of clinical trials. Reasons for the neuro-failures are numerous, ranging from stricter FDA regulations for CNS disorders to insufficient understanding of mechanisms underlying brain disease. Clinical trials involving disorders of the brain are notoriously difficult to set up and run. The matter is further exacerbated by relatively poor diagnosis techniques. Another common hindrance in CNS trials is the Placebo Effect.

Despite the drawbacks, Big Pharma cannot afford to quit CNS. Neurological disorders significantly outnumber diseases in other therapeutic areas, inflict higher treatment and loss of productivity costs than cancer, cardiovascular disease and diabetes put together and are growing in incidence faster than any other disease class. To exacerbate the problem, ageing populations have never before borne so much impact on the global total. Despite varying

strategies, almost all Big Pharma players are keeping one foot sturdily in the door when it comes to neuro-pharmaceutical development.

Reliable CNS targets are lacking. Virtually all CNS disorders beg for novel, more target-specific medications. Most neuro-pharmaceuticals on the market today have come about serendipitously, through observation that certain drugs improved certain symptoms, rather than through research tailored to the disease. In fact, an overwhelming majority of brain medications have widely unknown mechanisms of action, despite having been discovered as early as the 1940s. And nearly all CNS treatments today treat symptoms, rather than modify the disease. The reason for this is that many CNS drugs target very general neurotransmitters in the brain. In order to introduce truly innovative treatments on the neuro-market, basic neuroscience must catch up with the growing global demand for precise therapeutic targets.

Attrition in the clinic is also associated with lack of diagnostic markers. Roche is the world leader in cancer treatments. Three monoclonal antibodies based anti-cancer drugs from Roche, including Avastin, Rituxan and Herceptin, listed in the 2014 10-best-selling drugs worldwide. Precise diagnosis is the key to successful treatment. Biomarkers enable doctors to determine which cancer type a patient has more quickly and specifically. Take Herceptin, the breast cancer drug, for example, it transformed the percentage of cured HER2 patients from 20% to 70%. Roche is also working to identify tumour markers that will detect tumour cells long before the first symptoms become apparent. The understanding of the molecular mechanisms of tumour development and how tumours spread helps Roche to target the processes that lead to cancer.

The benefit of our lead probes is that they have different effects on patient derived cells. The use of patient-derived cells and phenotypic analysis provides diagnostic tools for

evaluation of drug effects in the CNS. In part the value of our probes is to move to a better model for CNS disease, especially on Parkinson's disease.

5.7 References

(1) Rasool, M.; Malik, A.; Qureshi, M. S.; Manan, A.; Pushparaj, P. N.; Asif, M.; Qazi, M. H.; Qazi, A. M.; Kamal, M. A.; Gan, S. H. *Evid. Based Complement. Alternat. Med.* **2014**, *2014*.

(2) Instant JChem, version 15.10.26.10; ChemAxon Kft: Budapest, Hungary, 2015.

(3) Rosén, J.; Lövgren, A.; Kogej, T.; Muresan, S.; Gottfries, J.; Backlund, A. *J. Comput. Aided Mol. Des.* **2009**, *23*, 253-259.

(4) Tang, C.; Ye, Y.; Feng, Y.; Quinn, R. J. *Nat. Prod. Rep.* **2016**, *33*, 6-25.

(5) Larsson, J.; Gottfries, J.; Muresan, S.; Backlund, A. *J. Nat. Prod.* **2007**, *70*, 789-794.